UNIVERSITY OF LATVIA

ANETE OGRIŅA

MOLECULAR SOLUTIONS FOR PLANT VIRUS – LIKE PARTICLES BASED VACCINE GENERATION

DOCTORAL THESIS

Submitted for the degree of Doctor of Biology,

Subfield: Molecular Biology

Rīga, 2024

This work of doctoral thesis was carried out at the Latvian Biomedical Research and Study Centre from year 2018 to 2023.

This work has been supported by the project "Strengthening of the Capacity of Doctoral Studies at the University of Latvia within the Framework of the New Doctoral Model", identification No. 8.2.2.0/20/I/006.

The form of this thesis is a collection of research papers in biology, subfield – molecular biology.

Supervisor: Dr. biol. Andris Zeltiņš;

Advisor: Dr. biol. Ina Baļķe.

Reviewers:

1) Professor, Dr. biol. Kaspars Tārs, University of Latvia;
2) Professor, Dr. biol. Uldis Kalnenieks, University of Latvia;
3) Professor, Dr. med. John Foerster, The University of Dundee.

The thesis will be defended at the public session of the Doctoral Committee of Biology, University of Latvia, on 19th of February at Latvian Biomedical Research and Study Centre, Rātsupītes street 1- k1, Rīga.

The thesis is available at the Library of the University of Latvia, Kalpaka blvd. 4.

Chairman of the Doctoral Committee /_____/ Prof., Dr. biol. Jānis Kloviņš /

Secretary of the Doctoral Committee /_____/ Dr. biol. Vita Rovīte /

ABSTRACT

The development of subunit vaccines with genetic engineering methods significantly facilitates the process of vaccine construction, as it allows placing a large number of antigen molecules on the surface of virus-like particles (VLP). Such approach provides the important multiplicity vaccines require, which is important in triggering strong immune responses. VLPs are self-assembling protein structures consisting of the outer layer of the virus that mimics the natural configuration of the virus, but does not contain its own genome, which is responsible for the viral replication and infection. The high similarity to native virus allows VLPs to elicit humoral and cell-mediated immune responses, exhibiting B cell activity and high-titer antibody production enhanced by exposed, structured and repetitive amino acid motifs on the surface of VLPs. These properties make VLPs an ideal vaccine candidate.

The use of plant VLPs in the creation of vaccines has several positive features - plant VLPs can be used as one carrier in different vaccines, since the mammalians do not have pre-existing immunity against these viruses. Nowadays, the immunological properties of only some plant VLPs are understood and defined, therefore, for the successful use of these objects in vaccinology, it is necessary to construct and test new plant VLPs, which would be possible to compare with each other, drawing conclusions about their immunological activity in the mammalian body.

In the course of the research, several bacterial platforms based on plant VLPs were created for the evaluation of antigen presentation capabilities by comparing different antigen-containing plant VLP candidates (from the genera *Bromovirus, Potyvirus and Tymovirus*) with different morphological forms (filaments and icosahedrons), trying to evaluate the most immunologically successful form of antigen presentation. First, various variants of plant VLPs with distinct morphological forms were generated using different antigen incorporation methods, which included genetic, chemical, enzymatic, and physical approaches. Second, modified plant VLPs were constructed, incorporating the major cat allergen Fel d 1 as a model antigen. Various methods of antigen presentation on the VLP surface were then tested in murine models. Immunological data were then obtained by immunizing the mice and assessing various parameters, including total antibody titer, antibody subclass distribution, the avidity or presence of specific antibodies, and, in some cases, the dispersion flow of these VLPs in the lymph nodes. These studies have successfully confirmed the significant potential of plant VLPs in the development of new vaccines.

KOPSAVILKUMS

Subvienību vakcīnu attīstība ar ģenētiskās inženierijas metodēm būtiski atvieglo vakcīnu konstruēšanas procesu, jo ļauj izvietot uz vīrusveidīgo daļiņu (VLP) virsmas lielu skaitu antigēna molekulu, nodrošinot vakcīnām nozīmīgo multiplicitāti, kas savukārt ir nozīmīga spēcīgās imunūnatbildes izraisīšanā. VLP ir pašsavākties spējīgas proteīnu struktūras, kas sastāv no vīrusa ārējā apvalka, kas ir identiska vīrusa dabiskajai uzbūvei, bet nesatur savu genomu, kas atbildīgs par spēju replicēties un inficēt saimniekorganismu. Lielā līdzība ar dabīgajiem vīrusiem ļauj VLP uzrādīt humorālo un šūnu radīto imūno atbildi, uzrādot B šūnu aktivitāti un augsta titra antivielu ražošanu, ko pastiprina uz VLP virsmas eksponēti, strukturēti un atkārtoti aminoskābju motīvi. Šīs īpašības padara VLP par ideālu vakcīnu kandidātu.

Augu VLP izmantošanai vakcīnu veidošanā ir vairākas pozitīvas iezīmes – augu VLP var izmantojot vienu nesēju dažādās vakcīnās, jo zīdītāju organismā nav iepriekš eksistējošas imunitātes pret šiem vīrusiem. Mūsdienās tikai dažu augu VLP imunoloģiskās īpašības ir izprastas un definētas, līdz ar to veiksmīgai šo objektu izmantošanai vakcinoloģijā nepieciešams konstruēt un pārbaudīt jaunas augu VLP, ko būtu iespējams savstarpēji salīdzināt, izdarot secinājumus par to imunoloģisko aktivitāti zīdītāju organismā.

Pētījuma gaitā tika izveidotas vairākas uz augu VLP balstītas baktēriju platformas antigēnu prezentācijas spēju novērtēšanai, salīdzinot dažādus antigēnu saturošus augu VLP kandidātus (no *Bromovirus*, *Potyvirus* un *Tymovirus* ģintīm) ar dažādām morfoloģiskām formām (filamentiem un ikosaedriem), mēģinot novērtēt imunoloģiski veiksmīgāko antigēna prezentācijas veidu. Pirmkārt, tika izveidoti vairāki augu VLP varianti ar atšķirīgām morfoloģiskām formām, izmantojot dažādus antigēnu ievietošanas paņēmienus, kas ietvēra ģenētiskās, ķīmiskās, enzimātiskās un fizikālās metodes. Otrkārt, tika izveidoti modificēti augu VLP, ievietojot galveno kaķu alergēnu Fel d 1 kā modeļa antigēnu uz VLP virsmas, tālāk pārbaudot to imunogenitāti peļu modeļos. Pēc tam imunoloģiskie dati tika iegūti, imunizējot peles un novērtējot dažādus parametrus, tostarp kopējo antivielu titru, antivielu apakšklašu sadalījumu, aviditāti vai specifisko antivielu klātbūtni un dažos gadījumos šo VLP ieplūšanas ātrumu limfmezglos. Šie pētījumi ir veiksmīgi apstiprinājuši augu VLP nozīmīgo potenciālu jaunu vakcīnu izstrādē.

TABLE OF CONTENTS

ABBREVIATIONS

AA – amino acid
AIT – antigen-based immunotherapy
APC – antigen presenting cells
ATP – adenosine triphosphate
BaMV - Bamboo mosaic virus
BELV - Bermuda grass etched line virus
BBMV – broad bean mottle virus
BHK – hamster kidney cells
BMV – brome mottle virus
Bp – base pair
BSA – bovine serum albumin
BYMV - bean yellow mosaic virus
CCMV – cowpea chlorotic mottle virus
CIYVV - clover yellow vein virus
CMV – cucumber mosaic virus
cDNA – complementary DNA
CP – coat protein
cryo-EM – cryogenic electron microscopy
CsCl – caesium chloride
CTL - cytotoxic T – cell
DC – dendritic cells
DMV – Dulcamara mottle virus
DNA – deoxyribonucleic acid
dsDNA – double stranded DNA
DTT – dithiothreitol
DYMoY - desmodium yellow mottle virus
E. coli – Escherichia coli
EDTA – ethylenediaminetetraacetic acid F
EMV – eggplant mosaic virus
FDA – food and drug administration
Feld1 – major cat allergen
GBS - group B-streptococcus
gdDOTA - gadolinium tetra-aza cyclododecane tetraacetic acid
Gln - glutamine
HBsAg – Hepatitis B surface antigen
HBV - Hepatitis B virus
HPV – human papilloma virus
ICTV – international committee on Taxonomy of Viruses
Ig - immunoglobulin
IPTG – isopropyl β-D-1-thiogalactopyranoside
JGMV - Johnsongrass mosaic virus
Kb – kilobase
kDa – kilodalton
Lys - lysine
MaMV - malva mosaic virus
MHC – major histocompatibility complex
MP – movement protein
MS – mass spectrometry
MRFV - Maize rayado fino virus
mRNA – messenger RNA
nt – nucleotide
NTr – non-coding regions
OBDV - Oat blue dwarf virus
ORF – open reading frame
PapMV - papaya mosaic virus
PCR – polymerase chain reaction
PEG – polyethylenglycol
PhMV – physalis mottle virus

PIPO – pretty interesting polyvirus ORF

PSS - polymer polystyrene sulfonate

PVA – potato virus A

PVM – potato virus M

PVY – potato virus Y

PVX – potato virus X

PWV - passion-fruit woodiness virus

RdRp – RNA dependent RNA polymerase

RNA – ribonucleic acid

RT – room temperature

s.c. - subcutaneous

SCS - subcapsular sinus

SDS-PAGE – sodium dodecyl sulfate polyacrylamide gel electrophoresis

sgRNA – subgenomic RNA

SMPH - succinimidyl-6-(β-maleimidopropionamido) hexanoate

SpA - Staphylococcus aureus protein A

SpyC – SpyCatcher

SpyT - SpyTag

SS – salt stable

ssRNA – single stranded RNA

SYNZIP (SZ) – synthetic zipper

TEM – transmission electron microscopy

TFA – trifluoroacetic acid

TLR – toll-like receptor

TMV – tobacco mosaic virus

Tris-NTA - tris-nitrilotriacetic acid

TT – tetanus toxoid

TuMV – turnip mosaic virus

TyMV – turnip yellow mottle virus

UTR – untranslated region

Val - valine

VLP – virus-like particles

VPg – viral protein genome-linked

WMV - watermelon mosaic virus

INTRODUCTION

One of the greatest medical achievements of the 20th century is undoubtedly the invention of vaccination, which protects about six million people a year from the lethality of diseases caused by bacteria and viruses (Andre *et.al.*,2008). Prior to the development of recombinant vaccine technologies, vaccines were produced from the viral or bacterial pathogens using chemical or physical pathogen inactivation. However, this application is associated with numerous safety flaws - with the possibility of weakened pathogens turning into disease instead of protecting against it (Zeltins, 2016). Over the past three decades, virus – like particles (VLPs) have become a widely used technology (Zeltins, 2013) and are currently the most successful recombinant vaccine platforms, emerging as a leader in vaccine development due to their safety, immunogenicity, and manufacturing advantages. The fact that VLPs exhibit a particulate structure with densely presented viral structural proteins on their surface makes them an appealing choice for displaying foreign epitopes. Consequently, a few vaccines built on VLP platforms have obtained approval for human usage and have enjoyed substantial success in both clinical and economic terms (Chen & Lai, 2013). There are only few licensed VLP vaccines and just one is approved for human use with a foreign epitope – malaria epitope Pfs25 fused with carrier Hepatitis B surface antigen (HBsAg) (RTS, S vaccine) (Balke & Zeltins, 2020).

VLPs are self-assembling protein structures consisting of a viral outer layer that mimics the natural repetitive three-dimensional architecture of corresponding viruses but do not contain their genomes, which is responsible for the ability to replicate and infect host cells. The high similarity to native virus enables VLPs to exhibit both humoral and cell-mediated immune responses (Liu *et.al.*, 2012), for example by exhibiting B cell activity and high-titer antibody production enhanced by exposed, structured and repetitive amino acid motifs on the surface of VLPs (Bachmann & Zinkernagel, 1997). In addition, nanometer-sized VLPs can be uptaken by antigen-presenting cells and degraded, leading to T cell activation (Bachmann & Dyer, 2004). These properties make VLPs as ideal candidates for vaccines, which can also be used in various novel biomaterials, drug delivery systems, and gene therapy processes (Zeltins, 2013).

The immunological properties of only some plant VLPs are understood and defined, therefore it is necessary to construct, test and compare new plant VLPs with different morphology, drawing conclusions about their immunological activity in the mammalian body. Accordingly, the ability to

supplement these VLPs with T cell-stimulating epitopes and enhance the induced immune response is a very useful feature in the development of vaccine efficacy, which could also be found in other plant VLPs. Therefore, there is a need to construct new plant VLPs with immunologically active and defined functions that could serve as a stable vaccine platform or as a vaccine adjuvant.

This work provides a huge experimental basis for the creation of new, universal and immunologically known plant VLP platforms, which could further be used in the development of new vaccines by adding specific antigens for the treatment of infections and other diseases, such as cancer, autoimmune diseases and allergies. The obtained data would also allow to conclude on the immunogenicity of plant VLPs in animal models, where the effect of T cell epitopes and structural fragments of VLPs on the immune system response would be tested.

The aim of this study was to construct new plant VLP candidates from the genera *Bromovirus*, *Potyvirus* and *Tymovirus* containing two antigens (tetanus toxoid and Fel d 1) with different morphological forms (filaments and icosahedrons) and evaluate their immunological potential in mice.

According to the aim of the work several work tasks were proposed:

1. Construct antigen-containing plant VLPs from the genera *Bromovirus*, *Potyvirus* and *Tymovirus* and perform their characterization and morphological assessment with various genetic, chemical, enzymatic and physical methods;
2. Perform immunization in mice models and evaluate VLP immunogenicity and draining kinetics or ability to induce antibodies against introduced Fel d 1 antigen, focusing on different antigen presentation strategies;
3. Evaluate and analyze the obtained results, explaining the positive and limiting factors of each established vaccine platform based on their immunological results.

1. LITERATURE OVERVIEW

1.1. Plant virus – like particles (VLPs)

1.1.1. Description of Bromoviridae family

Bromovirus is a family of plant viruses with tri – partite, positive – sense single stranded RNA (ss (+) RNA) genomes of about 8 kb in size. Genomic RNAs are packaged in separate virions which may also vary in morphology (spherical or bacilliform) and they are transmitted between hosts mechanically, in/on pollen by insect vectors. The members of the family are responsible for major disease epidemics in fruit, vegetable, and fodder crops such as tomato, cucurbits, bananas, fruit trees, and alfalfa. Bromovirus family consists of 6 genera and 36 species by the time of 2020 (ICTV 2020) including *Alfamovirus* and *Cucumovirus* which are transmitted by aphids. Two other genera *Anulavirus* and *Ilarvirus* are transmitted by thrips or pollen but members of *Bromovirus* by beetles. Transmission route for members of the genus *Oleavirus* is not yet known. Three of mentioned - *Alfamovirus, Bromovirus* and *Cucumovirus* - are widely used in VLP nanotechnologies (Bujarski, 2021).

1.1.1.1. Genome organization of *Bromovirus* genus

Bromovirus genome is segmented, consisting of three genomic RNAs (gRNA; gRNA1; gRNA2; gRNA3) and one subgenomic RNA (sgRNA4) (Figure (fig.) 1). Each of gRNAs are packed in its own capsid. Virion with the smallest gRNA (gRNA3) also contains a sgRNA4, which is transcribed from the gRNA3 3 'end and codes for coat protein gene (*CP*). All four gRNAs possess the CAP structure at 5 ' end and 3' untranslated regions (UTR) which resemble the structure of tRNA (King *et.al.*, 2012).

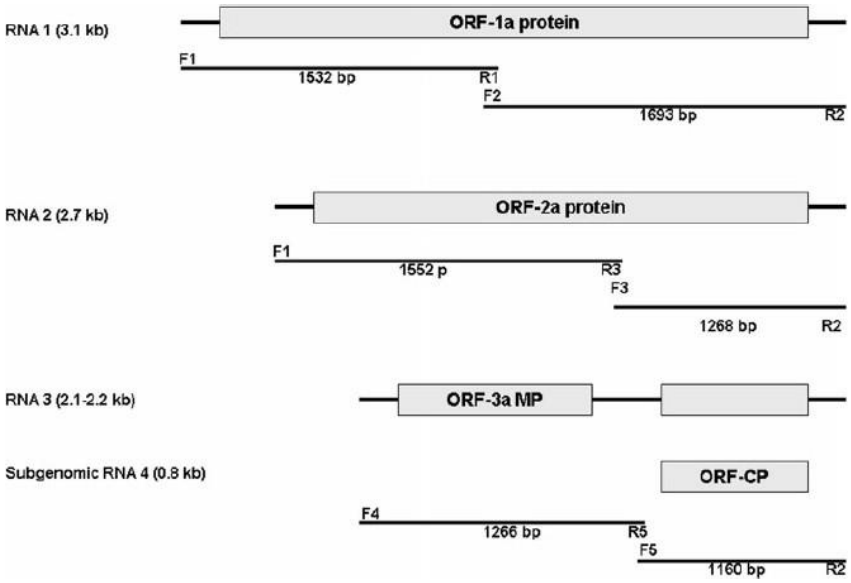

Figure 1. Shematic representation of CCMV genome organization (Ali *et.al.*, 2011).

For bromoviruses, RNA replication functions are provided by proteins encoded by gRNA1 and gRNA2 which are packed into separate particles. gRNA1 and gRNA2 are monocistronic, encoding the 1a (958 aa, gRNA1) and 2a (94 kDa, gRNA2) proteins respectively. 1a contains methyltransferase and helicase motifs, while 2a contains an RNA-dependent RNA polymerase (RdRp) motif that ensures viral RNA replication (Kroner *et al.*, 1990; Traynor *et al.*, 1991). Heterologous combinations of CCMV gRNA1 and gRNA2 do not assure viral gRNA replication, possibly due to impaired ability of 1a and 2a proteins to recognize cis-terminal activating signals which serve as initiate factors for (+) RNA synthesis (Speir *et al.*, 1995).

gRNA3 is dicistronic, encoding 3a or movement protein (MP, 32 kDa), which is involved in cell-to-cell transmission of the virus, and CP, which is translated from sgRNA4 (King *et al.*, 2012). Bromovirus gRNA3 contains an intercistronic oligo-A sequence identified in CCMV, Brome Mottle Virus (BMV) and Broad Bean Mottle Virus (BBMV; Khan & Dijkstra, 2006). In BMV, this 16 - 22 nt long sequence is located 20 nt before the 5' end of sgRNA4. After performing CCMV secondary structure analysis it was determined that the oligo-A sequence allows the synthesis of sgRNA4 from gRNA3 (Wyatt & Kuhn, 1980). To determine the size and location of the CCMV gRNA3 oligo–A sequence, 22 randomly selected full-length cDNA clones were sequenced by Zhao et.al. in 1995. The CCMV oligo-A sequence was located 18 nt before the 5' end of sgRNA4 (Zhao *et al.*, 1995) and varied in size from 34 to 55 nt. Although the location of the CCMV oligo-A sequence matches the one described in BMV, it was much shorter (Alison *et al.*, 1988).

In 1972 Bancroft & Flack combined all BMV gRNAs into a single fraction (gRNA1, gRNA2 and gRNA3) and inoculated it into *Chenopodium hybridum* and found that all three RNAs replicated together, causing lesions in the plant. These results were also confirmed in 1988 by Alison and colleagues with *in vitro* experiments with BMV and CCMV gRNA, where combining CCMV gRNA1 and gRNA2 with BMV gRNA3, also managed to cause local damage in infected plants (Bancroft & Flack, 1972; Alison *et.al.*, 1988). All three virions are required for successful infection of the plant (Zlotnik, *et.al*, 2000).

Experiments with CCMV wild-type CP and N-terminal mutant by Schneider and colleagues in 1997 found that full-length CP is required for CCMV virion formation, but systemic infection of the virus is ensured by the first two-thirds of the carboxyl-terminal end of CP. This indicates that the systemic movement of CCMV through the plant does not require virion formation, but that the viral RNA enters plants in an unencapsidated form. It is possible that the carboxyl-terminal end of the CCMV capsid either physically protects the gRNA during viral movement or actively interacts with host factors and other viral proteins during systemic viral infection (Schneider *et al.*, 1997).

1.1.1.2. Cowpea chlorotic mottle virus (CCMV)

Cowpea Chlorotic Mottle Virus (CCMV) is an icosahedral ss (+) RNA plant-infecting virus belonging to the *Bromoviridae* family (Fox *et.al.*, 1998). The structure of CCMV was determined in 1995 by X-ray crystallography at 3.2 Å resolution (Fig. 2), which revealed several aspects previously not observed in other plant viruses. The size of the virus is 28 nm and its determined structure led to the conclusion that the basic unit of virus self-assembly is non-covalent CP dimers. These dimers form hexamers (trimers of dimers) and the T=3 symmetry of the virus is achieved by connecting non-covalent dimers, viral RNA and divalent cations (Speir *et.al.*, 1995).

A) 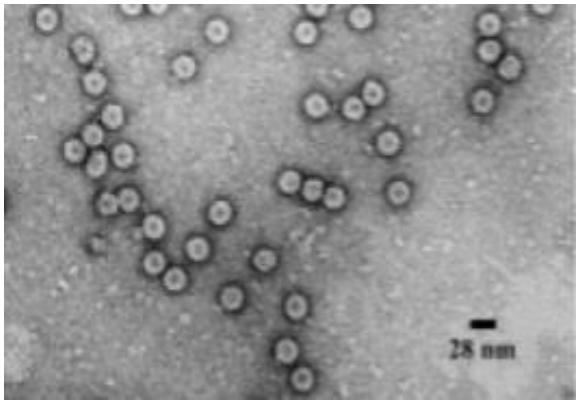

B) 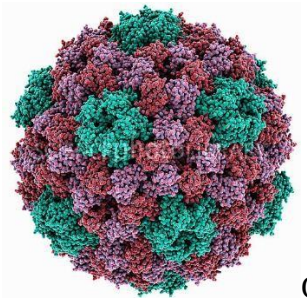 C) 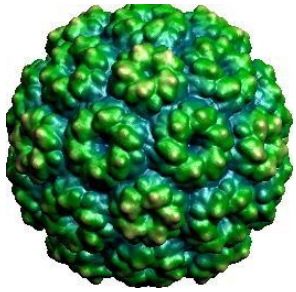

Figure 2. CCMV capsid. A) Electron microscopy image of CCMV (Lavelle *et.al.,* 2007); B, C - Native CCMV crystal structure. B) Science Photo; search CCMV (https://www.sciencephoto.com/); C) Protein Data Bank; file 1CWP).

CCMV is an intriguing subject of study due to its relatively simple and symmetric structure and the fact that it possesses several properties that make it highly attractive for research. One such property is its ability to self-assemble *in vitro*. By combining the capsid protein with RNA under specific pH and ionic strength conditions, infectious viruses can be spontaneously formed, which are indistinguishable from those found in infected plants (Fox *et.al.*, 1998). Additionally, under different conditions, the capsid protein alone can self-assemble into empty capsids that are structurally identical to the full capsids (Fox *et.al.,* 1998). This allows for a comparison between the properties of empty and full capsids, enabling researchers to assess the impact of protein-RNA interactions on the elasticity and strength of the capsid (Michel *et.al.*, 2006).

Furthermore, CCMV capsids have the remarkable ability to assemble around various anionic polymers without external assistance (Douglas & Young, 1998). This unique characteristic has sparked interest in utilizing CCMV as nanocontainers, opening up possibilities for applications in nanotechnology. In summary, CCMV's self-assembly capabilities make it a compelling target for scientific investigation. Its properties offer valuable insights into the protein-RNA interaction within capsids and hold potential for innovative nanocontainer applications (Michel *et.al.,* 2006).

By sequencing the entire CCMV genome in 1988 Allison and colleagues, discovered three CCMV strains (T, M1, R), although only the gRNA3 sequence has been determined for the CCMV-M strain. The symptoms caused by these strains are different - the CCMV-T strain causes systemic infection in cowpea, but the CCMV-M strain produces only pale green leaf spots (Allison *et.al.*, 1988). In 2002, de Assis Filho conducted a study to identify the symptom-causing region in the CCMV

genome. Generation of pseudorecombinants from CCMV-T and CCMV-M strains by exchange of their gRNA3 fragments and direct mutagenesis of the CP gene revealed that 151st aa residue of the CP gene is responsible for the disease phenotype in cowpea. Analysis of the structure revealed that it is located in an α-helix structure and ensures virion stability and ion attraction. These results suggest that it is indeed the aa at position 151 that causes the phenotypic expression, and not the nucleotide sequence of gRNA3 (de Assis Filho *et.al.*, 2002).

In 2008, Ali and Rossinck described two new CCMV isolates, Car1 and Car2, which were isolated from a naturally occurring mixed infection of CCMV and Cucumber mosaic virus (CMV) in cowpea (*Vigna unguiculata*). When cowpea plants were infected separately with both isolates, it was found that CCMV-Car1 caused severe mosaic chlorosis spot infection, while CCMV-Car2 caused only dull spotting on plant leaves. Phylogenetic analyzes comparing gRNA1 showed that the CCMV-Car2 isolate is similar to the previously mentioned CCMV-R strain, and that CCMV-Car1 is distantly similar to all CCMV strains. The sequence similarity of the two isolates was 99.3% for gRNA2 and gRNA3, but 94.6% for gRNA1 alone, which explains the different course of infection (Ali & Roossinck, 2008; Ali *et.al.*, 2011).

1.1.1.3. Structure of CCMV capsids

The overall shape of the CCMV virion resembles that of a truncated icosahedron, with three chemically identical gene products referred to as icosahedral asymmetric subunits, labeled A, B, and C. The CCMV CP subunits assemble into an icosahedral capsid structure through a combination of hydrophobic interactions, hydrogen bonding, and electrostatic interactions where the CCMV capsid is composed of 180 identical CP subunits (12 pentameric and 20 hexameric) arranged in a T=3 quasi-symmetry (Fig. 3) (Speir *et.al.*, 1995).

The CCMV CP is made up of 190 aa residues and exhibits a structural arrangement consisting of an eight β – barrel core arranged in a cylindrical shape (residues 52 - 176) with the N-terminal end (1 - 51 aa residues) and the C-terminal end (176 - 190 aa residues) each pointing in its own direction. These β - strands are numbered from A to H and are arranged in an anti-parallel fashion and connected by loops of varying length as seen below (Fig. 3). Two short α-helices located at the top and bottom of the barrel refers to amino – terminal (N – terminus) streches from residues 1 to 51 while the carboxyl – terminus (C – terminus) extends from residues 176 to 190 (Zhao *et.al.*, 1995).

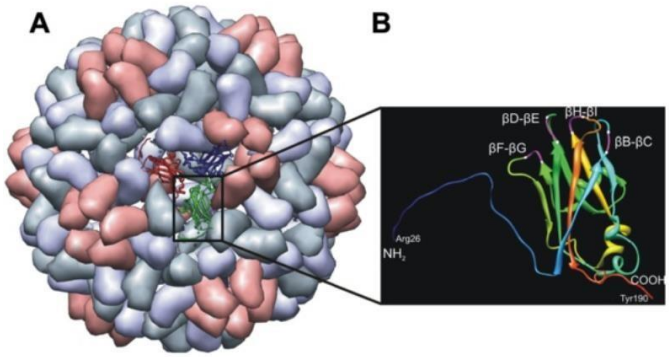

Figure 3. Schematical presentation of a CCMV virion and the coat protein subunit (Hassani – Mehraban *et.al.*, 2015).

The N-terminal domain contains a helix-turn-helix motif, carries a significant positive charge and first 26 aa project into the interior of the capsid, establishing an electrostatic interaction with the viral RNA and are essential for RNA packaging, while 27 - 35 aa form a β-hexamer that stabilizes hexameric capsomers (Speir *et.al.*, 1995). Furthermore, 44 - 51 aa of N terminal end serve as a support element for the C -terminal end (Smith, *et.al.*, 2000), which is also located inside the capsid (Vriend *et.al.*, 1986). The C-terminal domain aligns tangentialy with the capsid structure, fitting in between the N – terminus and the β – barrel structure of adjacent CP subunits, thus playing a stabilizing role in dimeric interactions (Vriend *et.al.*, 1986).

An initial proposal suggested that the early stage of virion formation involved the arrangement of six dimers, which formed a stable hexamer structure. This β-hexamer structure serves as a base for subsequent steps, including the addition of more dimers, the binding of divalent metal cations, and the encapsidation of viral RNA. These factors induced protein shell curvature, leading to the formation of pentamers and the recruitment of additional hexamers, ultimately resulting in the formation of the T-3 icosahedral virion (Johnson and Speir, 1997). This assembly model emphasized the significant role played by the β-hexamer structure in initiating virion assembly. However, later study on CCMV capsid assembly challenged this initial proposal by suggesting that nucleation occurs through the formation of a pentamer, rather than a hexamer of dimers (Zlotnick *et al.*, 2000). Overall, the structure of the CCMV CP subunit and the capsid it forms play a critical role in the virus life cycle, including protecting the viral genome, mediating host cell entry, and facilitating RNA replication and assembly.

1.1.1.4. Salt – stable CCMV CP

In order to successfully use VLPs as platforms for recombinant vaccines, it is necessary to achieve their stability at the pH of circulating mammalian body fluids. The pH value of mammalian blood and blood plasma is strictly regulated between 7.37 – 7.43, which is essential for body fluid homeostasis, as many metabolic processes in the body are particularly sensitive to changes in H+ ion concentration (Atherton, 2009). Likewise, the chemical coupling method using the succinimidyl-6-(β-maleimidopropionamido) hexanoate (SMPH) linker, which would be necessary for the covalent attachment of the antigen on the VLP surface, would need to be performed at pH 7-9 according to the standard protocol, but must not be lower than pH 6.5 (https://www.thermofisher.com/order/catalog/product/22363). Since the stability of CCMV at this pH is not optimal, a solution was needed for the future use of VLPs in the vaccinology industry.

In order to eliminate application deficiencies Bancroft and colleagues in 1973, analyzing the aa sequence of CCMV CP, found that the replacement of one aa from lysine (K) to arginine (R) results in salt stable (SS) CCMV, which does not dissociate at high pH (pH 7.5) and high ionic strength (1M NaCl), retaining 70% infectivity (Bancroft *et.al.,* 1973). Further studies confirmed the substitution of a single aa at position 42, which can be achieved by site-specific mutagenesis (K42R) in the native capsid protein of the virus (Fox *et.al.,* 1996).

1.1.1.5. Self – assembly of CCMV CP

One of the life cycles of icosahedral viruses such as CCMV is organized by protein-protein and protein-nucleic acid interactions (Bancroft & Hiebert, 1967; Allison *et.al.,* 1988), therefore structural changes in viral capsids are critical for capsid self-assembly and disassembly, as well as in the process of release of packaged nucleic acid (Speir *et.al.,* 2006). CCMV is one of the most stable viral self-assembling systems - it is the first icosahedral virus assembled *in vitro* from purified viral components (Bancroft & Hiebert, 1967) and is able to self-assemble into VLPs without the presence of RNA (Speir *et al.,* 1995; Lavelle *et al.,* 2009, Schoonen *et.al.,* 2017). The initial study on CCMV self-assembly by Adolph & Butler in 1974 suggested that CCMV can adopt different morphological forms depending on the pH and ionic strength conditions. These forms included multi-shells, tubes, or even hexagonal nets of CP subunits (Adolph & Butler, 1974). Pronounced structural changes appear by changing the H+ concentration (pH), ionic strength and divalent cation concentration of the medium, which results in the formation of a “swollen” - 10% larger CCMV capsid formation

(Bancroft & Hiebert, 1967). Without the presence of divalent cations, CCMV particles are stable at a pH 6.0 or less and an ionic strength up to 0.2, but when the pH is increased to 7.0 and an ionic strength up to 0.4, the capsid dissociates into protein dimers. If the pH is raised above 7.0 at low ionic strength, the particles immediately transition into the "swollen" form (Speir *et.al.,* 2006). Although the optimal stability of CCMV is between pH 4.8 (Lavelle *et.al.,* 2007) – 6.0 (Speir *et.al.,* 2006). In 2007, Lavelle and colleagues showed that CCMV VLPs with their packaged RNA are stable even at pH 7.5, unlike CCMV VLPs without nucleic acid, but as a side effect a reduction in the number of capsids was observed (Lavelle *et.al.,* 2007).

The CCMV capsid exists in two different structural forms (Bancroft & Hiebert, 1967; Speir *et al.,* 1995; Johnson & Speir, 1997) - the native structure of the wild-type capsid with or without RNA, stable at pH 5.0, with an average diameter of 28 nm and with an average inner diameter of 21 nm, but when the pH is raised to the basic side (pH 7.0), the average radius size of the capsid increases by forming swollen particles but the "empty" capsid remains unstable and dissociates. Although wild-type CCMV is unstable at pH 7.0, its SS mutant variant remains stable at high pH (Fox *et al.,* 1996). This property is used to encapsulate inorganic materials, negatively charged polymers and enzymes by adding these molecules to the culture medium in the process of protein dimer assembly (Schoonen, *et.al.,* 2017). VLPs are predominantly composed of 90 CP dimers forming T=3 symmetry, although T=1 and pseudo T=2 formation can also be observed (Tang *et al.,* 2006).

CCMV CP has been widely used as an efficient object in nanoparticle studies (Michel *et al.,* 2006; Klug *et al.,* 2006) because its structure serves as an excellent model for studying *in vitro* particle self-assembly process by varying buffer conditions (Bancroft, 1970). As the first 26 aa residues of CCMV CP are important for interaction with gRNA (Speir *et al.,* 1995), these structures ensure that the capsid swells in response to the electrostatic repulsion between the negatively charged aa residues in the center and the three-fold axis, which causes the opening of the pore formed by three CP subunits. Functionally, the appearance of pores during the increase in CCMV capsid size is critical for capsid disassembly and genome release in the host cell (Gibbons & Klug, 2008).

Studies on the effects of environmental pH revealed that increasing environmental pH alters the mechanical response of CCMV even before the capsid structure has begun to change. Experiments with "empty" wild-type CCMV in their native state, at pH 5.0, revealed that the structure is relatively stable, but with a tendency for disruption (Michel *et al.,* 2006; Klug *et al.,* 2006). Experiments carried out with an 'empty' capsid at pH 6.0 showed that the capsid is three times 'looser' and remains flexible

even when 'punched with holes' (Michel *et al.,* 2006). The capsid at pH 6.0 is not appreciably different from the native capsid, thus ruling out the possibility of mechanical changes in capsid geometry (Gibbons & Klug, 2008).

1.1.1.6. CCMV CP applications in nanotechnology

CCMV is one of the most stable viral self – assembling systems known and it is the first icosahedral virus assembled *in vitro* using purified viral components (Bancroft & Hiebert, 1967). Several studies have shown that CCMV can package various heterologous RNAs (Cadena – Nava *et.al.,* 2012) as well as form empty particles (Adolph & Butler, 1976; Lavelle *et.al.,* 2009). Since the disassembly and assembly of CCMV is easily manipulated by changing the pH, these results suggest that the successful encapsulation of substances for therapeutic purposes into the CCMV capsid could be relevant (Douglas & Young, 1998).

In 2008 Hu and colleagues reported the encapsulation of the anionic polymer polystyrene sulfonate (PSS) into the CCMV capsid, choosing five different polymer sizes in a range of 408-3441 kDa that CCMV could incorporate into its capsid. The results indicated that the incorporation of elements other than self-RNA depends on the size of the polymer and the preferred size of the CCMV capsid protein in which its serf-assembly are not disturbed. It was found that if the size of the polymer increased, the T value of the icosahedral virus also increased (from T3 to T7), suggesting the high structural plasticity of the CCMV capsid (Hu *et.al.,* 2008). Furthermore, in other study by Valimaki *et.al.* in 2021 CCMV CP was conjugated to heparin – specific binding protein which allowed to encapsulate anticoagulant drug heparin in CCMV VLPs serving for possible heparin antidote applications (Valimaki *et.al.,* 2021).

The properties of CCMV can also be used in the development of antibacterial treatments, as Suci and colleagues did in 2007, modifying the virion to destroy *Staphylococcus aureus* biofilm formation, for example on the surfaces of implanted prostheses. The modified virus with the attached dye fluorescein or the aforementioned contrast agent gadolinium tetra-aza cyclododecane tetraacetic acid (GdDOTA) penetrated the biofilm and attached to the SpA protein on the surface of *S. aureus*, which made it possible to identify the locations of the biofilm-causing bacteria. These results lead to the conclusion that it is possible to treat the infections caused by bacteria in well-defined areas by packaging various substances in the CCMV capsid (Suci *et al.,* 2007).

The CCMV viral capsid can also be used for gene therapy purposes serving as a carrier for modified mammalian viral RNA packed inside the particle, as explored by Azizgolshani and

colleagues in 2013. They engineered a defective Sindbis virus-derived RNA (SINV-RNA) that would produce eYFP (enhanced yellow fluorescent protein) and packaged it into the CCMV capsid. Subsequently, after VLP transfection into hamster kidney cells (BHK) RNA release and transgene expression was observed, suggesting that CCMV might be a successful gene therapy platform (Azizgolshani *et.al.,* 2013). Furthermore, a recent paper by Lam & Steinmetz in 2019 revealed that siRNA (small interfering RNA) loaded CCMV VLPs targeting gene knockdown were able to silence FOXA1 gene – a therapeutic target linked to breast or prostate cancer (Lam & Steinmetz, 2019).

CCMV viral capsids can also serve as a visual contrasting agents in diagnostics. In 2007, Liepold and colleagues created a modified CCMV capsid in which a 9 aa residue metal ion-binding peptide derived from the Ca2+ ion-binding protein calmodulin was inserted into the N-terminal end of the CCMV CP gene, creating a CCMV-Cal complex. Then, GdDOTA, which is used in magnetic resonance imaging, was added to the endogenously available lysine residues of CCMV CP. It was concluded that CCMV binds the widely used counteragents in magnetic resonance - Gd3+ ions, which are produced by dissociation of GdDOTA and are toxic in their free form, but when bound to the CCMV-Cal complex (CCMV-Cal-Gd) are safe and form a high-resolution contrast agent (Liepold *et. al.,* 2007).

Studies of using CCMV as VLP carrier for vaccine development have been described in various papers by generating vaccine protypes against influenza A virus, Foot and Mouth Disease virus (FMD) (Hassani – Mehraban *et.al.,* 2015) and against group B-streptococcus (GBS) capsular polysaccharide type III polysaccharide (Pomwised *et.al.,* 2016). Furthermore, recent COVID – 19 pandemics accelerated the development of CCMV VLP platform as a novel vaccine platform for SARS-CoV-2 epitope presentation suggesting CCMV CP as an attractive vaccine carrier for further clinical evaluation (Almendarez – Rodriguez *et.al.,* 2022).

1.1.2. Description of Potyviridae family

Potyviridae is a family of viruses that belongs to the order *Patatavirales* and is one of the largest families of plant viruses. It includes many economically important pathogens that affect a wide range of plants, including crops, ornamentals, and weeds (Wylie *et al.*, 2017). Members of the *Potyviridae* family are single-stranded RNA viruses that possess a positive-sense RNA genome which is encapsidated within a protein coat (King *et al.,* 2012). All members of this family are characterized by their flexuous filamentous particles with helical symmetry (Khan & Dijkstra, 2006), measuring approximately 650 to 900 nanometers in length. Particle lengths of members of some of the six genera

differ – members of the genera *Potyvirus, Ipomovirus, Macluravirus, Rymovirus, Tritimovirus, Brambyvirus* and the unassigned viruses are monopartite with particle modal lengths of 650 – 900 nm, but members of the genus *Bymovirus* are bipartite with particles of two modal lengths of 250 – 300 nm and 500 – 600 nm (King *et.al.,* 2012).

The genomic RNAs of potyvirids contain a single open reading frame (ORF) that codes for a major polyprotein, which is proteolytically processed by virus – encoded proteinases (Revers & Garcia, 2015). The coded RNA has a 5' – terminal genome – linked 24 kDa protein (VPg) and a 3' poly (A) tail (Riechmann *et.al.,* 1992). In both potyviruses and bymoviruses the central and carboxy-terminal regions of polyproteins share a conserved organization and are responsible for encoding the mature viral proteins P3-6K1-CI-6K2-VPg-NiaPro-Nib-CP (Fig.4.) while the processing of this particular part of the polyprotein is accomplished by the 70 kDa proteinase NiaPro (Revers & Garcia, 2015) with ATFase and helicase activity and forming cytoplasmic cylindrical inclusion bodies (CI) characteristic of the family *Potyviridae* (Roberts *et.al.,* 1998). One intriguing feature universally found in this genomic region is the presence of a short ORF, known as "pretty interesting potyvirus ORF" or PIPO. Remarkably, this ORF is nestled within the P3-encoding region but in a different reading frame from the polyprotein sequence. The PIPO ORF is utilized to produce the P3N–PIPO protein through a +1 frameshift, which occurs at a specific location defined by a GA6 sequence (Chung *et.al.,* 2008).

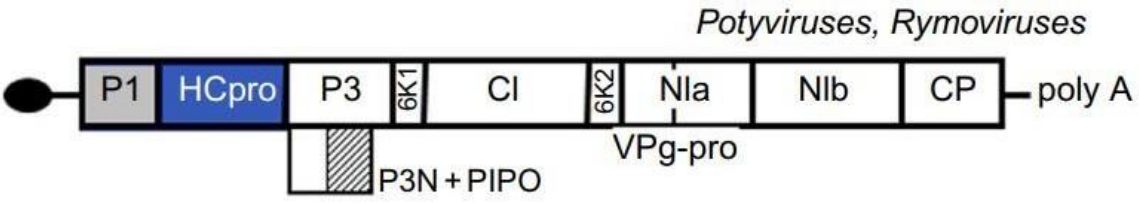

Figure 4. Schematic representation of *Potyvirus* and *Rymovirus* genera. The long open reading frame is represented as a box divided in final products by black lines. PIPO ORF is indicated as a striped area below the P3 region. The terminal protein (VPg) is represented as a black ellipse (Revers & Garcia, 2015).

In a study involving six different potyviruses (bean yellow mosaic virus (BYMV), clover yellow vein virus (CIYVV), Johnson grass mosaic virus (JGMV), passion-fruit woodiness virus (PWV), potato virus Y (PVY), and watermelon mosaic virus II (WMV-2), researchers conducted mild proteolysis using trypsin on viral particles. This process revealed that the N- and C-terminal potyviral regions of CPs are exposed on the surfaces of these particles (Shukla *et.al.,* 1988). The potyviral CPs

goes beyond its primary function of protecting the viral genome; it plays a multifaceted role throughout the entire viral life cycle. Notably, it actively participates in viral transmission through aphids, aids in genome replication and translation, and facilitates both cell-to-cell and long-distance movement of the virus. This protein's remarkable multitasking capabilities underscore its significance in orchestrating various essential processes at different stages of the viral life cycle (Kezar *et.al.*, 2019).

Potyviridae viruses are known for their high genetic diversity and ability to infect a broad spectrum of hosts. They can infect over 200 plant families and more than 1,000 plant species. These viruses are typically transmitted through aphids and other insect vectors, as well as by seed, vegetative propagation, and mechanical means (Roossinck *et.al.*, 2015). Upon infecting a host plant, Potyviridae viruses cause a variety of symptoms that can include stunting, mosaic patterns on leaves, yellowing, necrosis, and reduced yield. The severity of symptoms varies depending on the virus-host interaction and environmental conditions. Some *Potyviridae* viruses are known to cause devastating diseases in economically important crops, leading to significant yield losses (Visser *et.al.*, 2012).

Control strategies for *Potyviridae* viruses involve the use of virus-free planting material, insect vector control, and integrated pest management practices. Plant breeders also work on developing resistant cultivars to combat these viruses. Additionally, strict phytosanitary measures and quarantine regulations help prevent the introduction and spread of these viruses across different regions (Valkonen, 2007).

1.1.2.1. Description of Potato Virus Y (PVY)

One of the most well-known and economically important viruses in the *Potyviridae* family is Potato virus Y (PVY), which affects various Solanaceous plants, particularly potatoes. PVY can cause significant losses in potato production and poses a threat to agricultural productivity, affecting the quality and yield of potatoes (Kerlan & Moury, 2008). PVY was first described in 1930s as the causal agent of a serious disease in potato (Smith, 1931) and stands as a highly significant viral pathogen for potato crops globally, transmitted primarily by aphids (Kerlan & Moury, 2008).

PVY is a nonenveloped virus with filamentous, flexuous rod-shaped virions, approximately 600 - 900 nm long and 11–12 nm in diameter. These virions possess helical symmetry with an axial canal of 2–3 nm in diameter. The virus contains about 6% nucleic acid and a VPg, but no lipids or other components. The PVY genome consists of a single-stranded, positive-sense RNA molecule, approximately 3.1–3.2 million Da in size, with a polyadenosine sequence at the 3' terminus. PVY is a

complex virus that undergoes autoproteolytic cleavage to produce essential proteins responsible for its replication, assembly, and pathogenicity in potato and other host plants (Kerlan & Moury, 2008).

The PVY RNA is around 9700 nucleotides long, excluding the poly(A) tail. Like other members of the Potyvirus genus, PVY expresses its single open reading frame as a large polyprotein (comprising 3061–3063 amino acids) that is autoproteolytically cleaved to yield ten functional proteins: P1, HC-Pro, P3, 6K1, CI, 6K2, VPg, NIaPro, NIb, and CP. The genome also contains two noncoding regions, 5'NTr (184 nt) and 3'NTr (ranging from 326 to 333 nt). The CP (29.95 kDa), comprising 267 aa residues, consists of a core region (218 aa) that is highly conserved in Potyvirus members. It also has two surface-exposed N-terminal (300 aa) and C-terminal (19 aa) regions, which are not essential for virus assembly and infectivity maintenance (Kerlan & Moury, 2008).

The capsid, composed of approximately 2000 of CP units, assembles in a helical arrangement around the viral ssRNA, forming 680 – 900 nm long filaments. Recent cryoelectron microscopy analysis by Kezar *et.al.* in 2019 revealed several previously unknown facts about PVY CP. Various interactions between CP-CP and CP-ssRNA contribute to the flexibility and stability of PVY filaments, ensuring the virus's long-term infectivity, which is crucial for its economic significance. The research highlights the structural plasticity of the PVY CP, which plays multiple roles during different stages of infection. Besides protecting the viral genome, the CP is involved in viral transmission by aphids, genome replication, translation, cell-to-cell movement, and long-distance spread of the virus. Previous studies have indicated the assembly's location near the 5' end of genomic RNA, and other viral and host factors play essential roles in virion formation. Proteins like HcPro and VPg are involved in virion stabilization and RNA replication, further contributing to PVY's intricate life cycle (Kezar *et.al.*, 2019).

The three atomic structures reveal a consistent left-handed helical organization of monomers. These monomers consist of a globular core characterized by seven α-helices and one or two β-hairpins (Fig. 5). Additionally, the N- and C-terminal arms of the monomers do not exhibit any significant secondary structures. This structural similarity suggests a common underlying architecture for the monomers, which play a crucial role in the assembly and function of the viral particle (Kezar *et.al.*, 2019; Martinez-Turino & Garcia, 2020). The surface exposed N-terminal region of the PVY CP, spanning from Val^{44} to Gln^{77}, plays a crucial role in the compactness of the capsid by acting as a clip that connects neighboring core subunits. Unlike previous assumptions that both termini are exposed on the surface (Shukla *et.al.*, 1988; Anindya & Savithri, 2003), the C – terminal end of the PVY coat

protein is positioned within the inner lumen of the viral filament and are entirely shielded from the external environment (Fig.5) (Kezar *et.al.*, 2019). Furthermore, apart from its role in genome encapsidation, the CP protein's N- and C-terminal domains have been identified as essential components for facilitating interactions between CP subunits during the initial stages of virus assembly (Anindya & Savithi, 2003). The deletion of up to 60 C-terminal residues does not hinder VLP assembly, while removing 49 N-terminal residues, including a few from the N-arm of the core, prevents VLP formation (Kezar *et al.*, 2019).

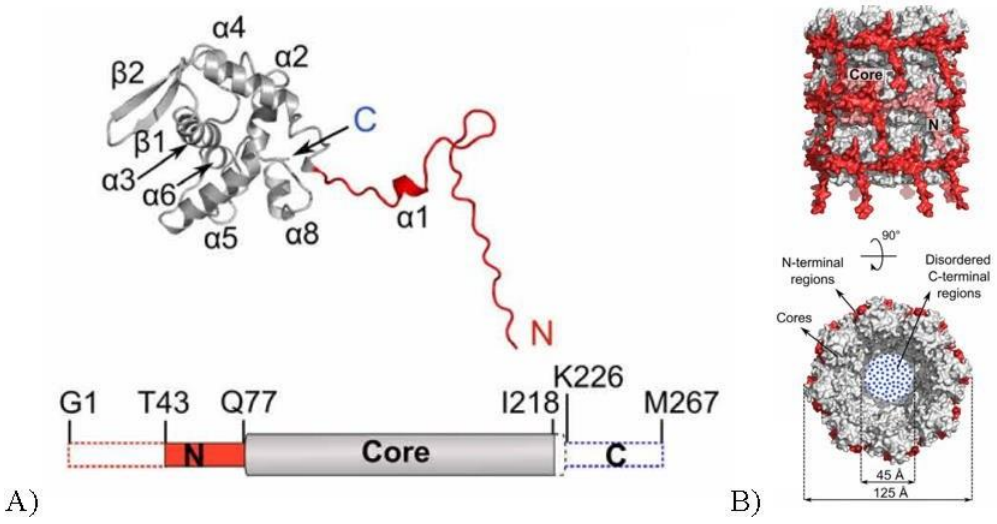

Figure 5. Structural features of PVY VLP. A) Structure of PVY CP (N – terminal region, red; core; grey). Bottom: A linear representation of CP, using the same colors as in the model above. B) Side and top views of the VLP filament; the colors as in (A). Position of on CP unit (pink) is shown in the filament (Kezar *et.al.*, 2019).

The structure of PVY protein rods bears some similarity to the stacked-disk rods formed by the tobacco mosaic virus (TMV) protein. In the initial research by McDonald *et al.*, it was observed that individual building blocks, or monomers, separated from PVY virions, have the capability to reform into elongated VLPs *in vitro* even in the absence of RNA (McDonald *et al.*, 1976). These reassembled structures, referred to as "stacked-ring particles," exhibited distinct characteristics that set them apart from the stacked-disk rods formed by TMV CP self-assembly and the helical potyviral particles. Interestingly, when these stacked-ring particles were exposed to viral RNA, they transformed into short helical rods that closely resembled the natural virions. This observation led researchers to propose that the stacked-ring particles might serve as transitional forms during the assembly of virions (McDonald & Bancroft, 1977; Shukla & Ward, 1989).

When the CP of potyviruses is expressed independently, devoid of any other viral components, it has the ability to spontaneously arrange into VLPs of varying lengths. This phenomenon has been observed in different *in vivo* heterologous systems and has been documented in various studies (Edwards *et al.,* 1994; Hammond *et al.,* 1998; Jagadish *et al.,* 1991). Interestingly, the specific architecture of these VLPs depends on the particular type of potyviral CP being examined. For instance, CP from virus like Potato virus Y (PVY) (Kezar *et al.,* 2019) have been observed to form already mentioned structures "stacked-ring particles." Furthermore, several studies suggest that potyviral VLPs are largely RNA – free (Cuesta *et.al.,* 2019; Kezar *et.al.,* 2019).

1.1.2.2. Description of Potyviral VLPs as an antigen presenting tools

Potyviral capsids have been effectively utilized for antigen presentation purposes through two main strategies. Firstly, this has been accomplished by generating VLPs using chimeric CPs expressed in different host systems. Second approach involves infecting plants with mutant viruses that include the foreign peptide coding sequence fused to the CP gene. The potyviral CPs exhibit remarkable adaptability when it comes to incorporating relatively large peptides and presenting them on the surface of VLPs (Martinez-Turino & Garcia, 2020).

In line with this strategy, hybrid potyvirus VLPs have been engineered and expressed in *E. coli* system, for example, using modified versions of Johnsongrass mosaic virus (JGMV) CP where modified CP variants feature foreign sequences inserted into their N- and/or C-terminal regions (Saini & Vrati, 2003; Choudhury *et.al.,* 2009). Likewise, in a similar fashion, the N-terminal region of PVY CP has been utilized for incorporation of Hepatitis B virus preS1 epitope and the complete rubredoxin protein from *Pyrococcus furiosus* into PVY CP, using *E. coli* as the expression system and resulting in chimeric VLPs (Fig. 6; Kalnciema *et.al.,* 2012). Furthermore, chimeric Pepper vein banding virus (PVBV) particles were genetically engineered to contain the B domain from Staphylococcus aureus protein A (SpA) at the N - terminus of its CP and were successfully used as a potential diagnostic and therapeutic nanocarriers while presenting much higher affinity toward IgGs than SpA itself (Sabharwal *et.al.,* 2020).

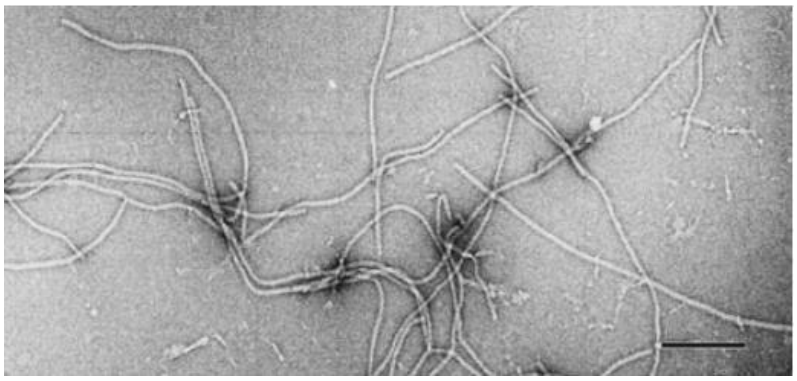

Figure 6. Electron micrographs of PVY CP-derived VLPs. Purified VLPs formed from PVY CP after expression of the PvyCP gene. Bar 100 nm. (Kalnciema *et.al.*, 2012).

Employing an alternative approach for expression in plants, a vector based on Potato virus X (PVX) was utilized for two following studies. Within this framework, specific peptides E7 and L2 originating from Human papillomavirus (HPV) type 16 fused to the either N- or C-termini of Potato virus A (PVA) CP were expressed in plant *Nicotiana benthamiana* and *Brassica rapa* through Agro*bacterium tumefaciens* mediated inoculation. As a result of these manipulations, VLPs carrying these fused peptides were successfully synthesized within these plant species and therefore showed the versatile capability of this system for peptide presentation on VLPs (Cerovska *et.al.*, 2008; Hoffmeisterova *et.al.*, 2008). Additionally, a recent study conducted by Pazos-Castro *et al.* in 2022 demonstrated that VLPs derived from Turnip mosaic virus (TuMV) exhibit promising potential as valuable assets in nanoparticle applications for allergen-specific immunotherapy (AIT). Particularly, when the food allergen Pru p 3 was incorporated into the genetic fusion with TuMV CP, which was expressed in *Nicotiana benthamiana*, these VLPs exhibited notable potential in reducing some serological markers associated with allergic responses in mice without any potential of toxicity (Pazos – Castro *et.al.*, 2022).

1.1.3. Description of Tymoviridae family

The Tymoviridae family comprises three genera: *Tymovirus*, *Marafivirus*, and *Maculavirus*. Tymoviruses and maculaviruses primarily target dicotyledonous plants, whereas marafiviruses have a preference for infecting Poaceae family plants. Members of this family share certain characteristics - their non – enveloped isometric particles are roughly 30 nm in diameter, having a round shape with distinct surface features and these particles cluster into pentamers and hexamers of coat protein subunits. Purified virus preparations reveal two sedimenting components: non-infectious protein shells (T) that may contain small RNA portions (mainly subgenomic coat protein mRNA), and

infectious nucleoproteins (B) that carry the virus's genetic material. The members of *Tymoviridae* family possess a positive-sense, single-stranded RNA genome with an unusually high cytidine content (ranging from 32% to around 50%). This RNA is capped at the 5' terminus and contains a very large ORF encoding replication-related proteins. The replication strategy likely involves post-translational proteolytic cleavage of the polypeptide encoded by ORF1, performed by a virus-encoded protease (Martelli *et.al.,* 2002).

The capsid of tymoviruses is made up of 20 hexameric and 12 pentameric subunits arranged in a T=3 icosahedron and the RNA seems to exhibit a degree of organization, possibly adopting an icosahedral pattern within the core of the protein shell (Fig. 7). The virus particles' CP consists of distinct protein compositions based on the virus type. For instance, tymoviruses contain a single protein species weighing 20 kDa, maculaviruses possess CPs around 24.5–25 kDa, and marafiviruses Oat blue dwarf virus (OBDV) and Maize rayado fino virus (MRFV) exhibit a major protein of 21–21.5 kDa along with a minor protein of 24.4–25 kDa. In contrast, other marafivirus Bermuda grass etched line virus (BELV) have CP composed of a single protein weighing approximately 21 kDa. Infected cells contain distinct cytopathic structures that are believed to be sites of RNA replication (Martelli *et.al.,* 2002).

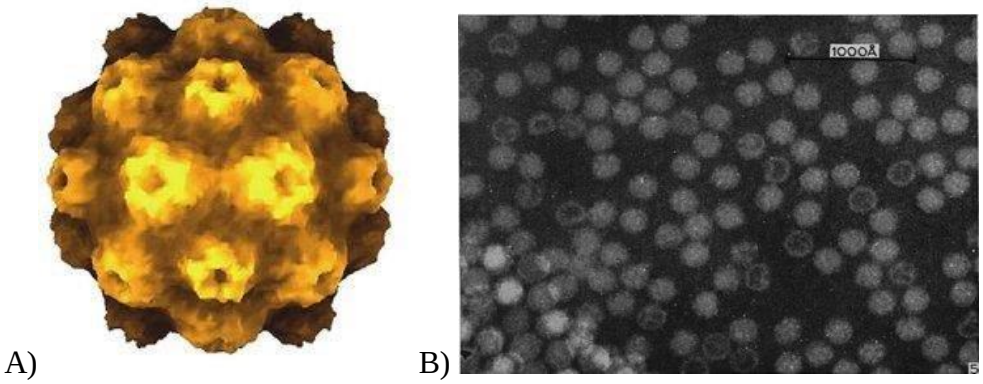

Figure 7. The capsid of TYMV. A) Atomic rendering of a virion of turnip yellow mosaic virus (TYMV) (Canady *et al.,* 1996). B) Negative contrast electron micrograph of TYMV stained with 1% phosphotungstic acid. Biochem. Biophys. Acta., 34, p103. The bar represents 100 nm. (Brenner & Horne, 1959).

1.1.3.1. Description of *Tymovirus* genus

Plant viruses within the *Tymovirus* genus are characterized as monopartite, linear, positive-sense single-stranded RNA (ssRNA) viruses which exhibit a T=3 icosahedral symmetry (King *et.al.,*

2012). These viruses have 30-nanometer-sized virus particles that are constructed from a single 20 kDa CP. Among the 28 species categorized in this genus, only 11 of them have been identified to be transmitted by beetle vectors which highlights the specificity of transmission (King et.al., 2012). All members of the genus are mechanically transmissible and a few (turnip yellow mosaic virus (TYMV), eggplant mosaic virus (EMV) and Dulcamara mottle virus (DMV)) are transmitted through seeds (King *et.al.,* 2012). Vectors responsible for transmission primarily include flea beetles and weevils, although certain leaf beetles have also been recognized as vectors for these tymoviruses (Koch *et.al.*, 2020).

The genomic RNA, ranging from 6.0 to 6.7 kb in size, features three distinct ORFs (Fig. 8). The 5' terminus has a methylated nucleotide cap, the 3' end has a tRNA-like structure accepting valine in TYMV. The first ORF, ORF1, encodes a substantial 206 kDa protein with conserved sequence motifs including methytransferase, papain-like protease, helicase, and RNA polymerase. The 3' ends of the large ORF1 contain a 16 nt sequence known as "tymobox" (GAGUCUGAAUUGCUUC) which plays the role of a promoter for subgenomic RNA. Notably, the C termini of these extensive polypeptides exhibit a high level of conservation. ORF2 substantially overlaps ORF1 and is responsible for encoding a 69 kDa proline-rich protein. While this protein is not crucial for replication, it plays a pivotal role in facilitating cell-to-cell movement (Martelli *et.al.,* 2002; King *et.al.,* 2012). Both RNAs possess a tRNA-like region of 36 nt at the 3' end with pseudoknot structure that plays a crucial role for efficient transcription of RNA – dependent RNA polymerase (RdRp) (Khan & Dijkstra, 2006). ORF3 is responsible for encoding the viral CP (20 kDa), which is brought into expression through a subgenomic RNA (King *et.al.,* 2012).

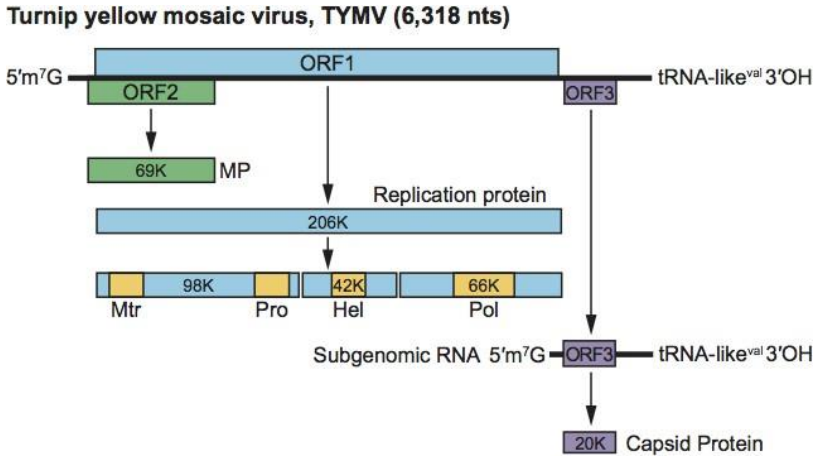

Figure 8. Organization and expression of the genome of turnip yellow mosaic virus (TYMV). Mtr, methyltransferase; Pro, papain-like protease; Hel, helicase; Pol, polymerase (RdRp) (King *et.al.*, 2012).

Tymovirus virions exhibit a remarkable stability, forming approximately 29 nm T=3 icosahedral structures composed of 180 units of the single CP. This arrangement comprises 12 pentamers and 20 hexamers, creating distinct vertices with fivefold and sixfold symmetry. The stability of these structures is primarily maintained by hydrophobic interactions between protein subunits, contributing to the formation of robust shells that seem to lack RNA content. These empty or nearly empty capsids make up around one-third of the particles present in infected tissues. They are easily identifiable through internal staining in negative-contrast EM and are characterized by sedimentation as the 'top component' at 45–55S in CsCl density gradients. These structures can be distinguished from the 'bottom component', which comprises infectious virions with a density of 110–120S and containing the genomic RNA (Hammond & Abrahamian, 2021).

1.1.3.2. Tymovirus capsids as potential platforms for antigen presentation

A total of just three crystal structures of tymoviruses have been examined in detail: turnip yellow mosaic virus (TYMV, Canady *et.al.*, 1996), physalis mottle virus (PhMV, Krishna *et.al.*, 1999) and desmodium yellow mottle virus (DYMoY, Larson *et.al.*, 2000). Among these, TYMV stands out as a pioneer in the field of structural exploration, meaning that electron micrographs of TYMV were published by Cosslett and Markham as far back as 1948. Particularly, TYMV and PhMV have undergone thorough examination to elucidate the significance of the N- and C-terminal regions in the assembly of tymovirus – like particles. This exploration has involved manipulations such as deletion experiments, substitution of amino acid residues, and the introduction of foreign amino acid sequences at the terminal ends of their CPs (Pumpens & Pushko, 2022).

Numerous studies underline the potential utility of tymovirus virus-like particles as effective scaffolds for antigen presentation. This potential is rooted in the distinctive protein capsid arrangement, characterized by three chemically identical coat protein subunits (A, B, C). These subunits occupy distinct microenvironments and adopt slightly varied conformations as the A subunits form pentameric capsomeres, while the B and C subunits create hexameric capsomeres. (Canady *et al.*,1996; van Roon *et al.,* 2004; Larson *et al.* 2005; Barnhill *et al.,* 2007). Numerous investigations involving N-terminal deletions of the tymoviral CP genes have consistently demonstrated that the first 26 amino acids are not essential for capsid assembly. This has been established not only for TYMV (Barnhill *et al.,* 2007; Powell, 2012) but also for PhMV (Sastri *et al.,* 1997; Sastri *et al.,* 1999) and even tomato blistering mosaic virus (ToBMV; Vasques *et.al.,* 2019) suggesting this as prospective sites for epitope displaying. Interestingly, Hayden *et.al.* in 1998 concluded that the N – terminus of the TYMV CP was not exposed at the surface of the virion. Furthermore, there exists a lot of evidence showing the successful integration of CP N-terminal fusions, with some extensions spanning up to 66 aa for PhMV (Hema *et.al.,* 2007; Chandran *et.al.,* 2009; Shahana *et.al.,* 2015; Sahithi *et.al.,* 2019) or shorter model sequences for TYMV (Shin *et al.,* 2013; Shin *et al.,* 2018).

Relatively controversial results were obtained when tymoviral C- terminal modification were performed. Barnhill's study indicated that approximately 90 to 120 carboxyl groups of TYMV could potentially reside on the surface, as they were accessible for chemical modification approaches (Barnhill *et.al.,* 2007) although majority of C – terminal end alterations including aa deletions, replacements or peptide insertions led to reduced yields and the formation of less stable capsids both for TYMV (Shin *et.al.,* 2013; Shin *et.al.,* 2018) or for PhMV (Sastri *et.al.,* 1997; 1999). Contrasting outcomes emerged when the C-terminal end of TYMV underwent extension with a 5 aa sequence (Bransom *et al.,* 1995) or a 10-amino acid poly-histidine tag (Tan *et al.,* 2021a) which were the first successfully engineered C-terminally modified TYMV chimeric VLPs within the *E. coli* system, with no severe impact on capsid assembly.

2.1. Antigens

2.1.1. Tetanus toxoid

Antigenic structures that can be recognized and bind to either immune cells (T or B lymphocytes), free molecules (antibodies) or cell – surface proteins like major histocompatibility complex (MHC) are characterized as epitopes (Konstantinou, 2017). Epitope based vaccines stimulate humoral and cellular immune responses using B – cell and T – cell epitopes but the low

immunogenicity of single – epitope peptides has led to the idea of designing constructs with multiple epitopes (Parvizpour *et.al.,* 2020). As studies have shown that insertion of protein segments into specific regions of VLPs does not interfere with the self-assembly process of the virus (Pushko *et al.*, 2013), addition of epitopes to nanoparticle structures like VLPs which makes them highly immunogenic should be considered when constructing a vaccine (Bachmann & Jennings, 2010).

VLPs are able to induce cytotoxic T – cell (CTL) responses in the absence of infections or replication as they are the key lymphocytes for viral clearance for many viral or bacterial infections (Ruedl *et.al.,* 2005). T lymphocytes are known to recognize MHC molecules displayed on antigen presenting cells (APCs) that have bound peptide epitopes derived from intracellular processing of antigens. However, this process depends on whether the epitope meets three requirements – if it produces the necessary fragment in sufficient quantity, whether it is attached to the MHC molecule and whether T cells are able to recognize this complex (Panina-Bordignon *et al.,* 1989).

Tetanus toxin (TT) epitope, one of the causative agents of tetanus is derived from the toxin of the bacterium *Clostridium tetani* (aa 830-844). It represents the helper peptide (aa: QYIKANSKFIGITE), which binds to MHC class II molecules as a nonspecific vaccine adjuvant. It boosts the immune response by increasing the response of T cells (Alexander *et.al.,* 1994). In 1989, Panina-Bordignon and colleagues analyzed the response of memory T cells to three tetanus toxoid peptides - p2 (aa 830-844), p4 (aa 1237-1284), p30 (aa 947-967) and accordingly analyzed the effect of human MHC class II polymorphism on antigen recognition. The study demonstrated that two of the three TT epitopes (p2 and p30) are immunogenic and are recognized by a large number of MHC class II molecules (Panina-Bordignon *et al.*, 1989).

In humans, the preexisting immune response to TT is largely based on previous tetanus vaccination. TT epitopes are widely used in the development of vaccines against infectious agents and tumors. The TT epitope has been added to several vaccine platforms as an additional T cell stimulating factor in human cancer therapy studies (Lund *et.al.,* 2003; Laubreton *et.al.,* 2016; Mohsen *et.al.*, 2019), against infections (Xu – Amano *et.al.,* 1993; Kovacs – Nolan & Mine, 2006; Wen *et.al.*, 2014), chronic inflammatory conditions (Zeltins *et.al.*, 2017) or even as a part of contraceptive vaccine in mice (Kaumaya *et.al.*, 1993).

2.1.2. Major cat allergen Fel d 1

Cats rank as the primary contributors of indoor airborne allergens following house dust mites. There's a notable and concerning increase in global cases of cat allergies, presenting a significant public health challenge (Bonnet *el.al.,* 2018). The major cat allergen, Fel d 1, is a globular protein of the secretoglobin family. Cats produce this allergen abundantly across various anatomical regions, including the salivary, lacrimal, and sebaceous glands in the facial area, as well as the skin and anal sacs and secretion of Fel d 1 is regulated by androgens (Bienboire – Frosini, *et.al.,* 2020).

Structurally, Fel d 1 is a tetrameric glycoprotein of a size of 35-38 kDa. It comprises two heterodimers, each formed from two polypeptide chains encoded by distinct genes, and connected by three disulfide bridges (Fig. 9). The first chain consists of 70 amino acids, while the second chain comprises either 90 or 92 amino acids (Bonnet *et.al.,* 2018). In the past, the production of recombinant Fel d 1 (rFel d 1) posed challenges due to the distinct genetic origins of its two constituent chains. Efforts to properly refold these chains, preserving their original disulfide linkages and maintaining stability, were unsuccessful. As an innovative solution, some researchers proposed a modified rFel d 1 design, in which chain 1 was connected to chain 2 through a flexible peptide linker of the (GGGGS)n sequence. This strategic arrangement effectively reduced steric hindrance between the fused components. The use of these small amino acids in the linker imparted flexibility, enabling mobility of the connected functional domains (Vailes *et.al.,* 2002).

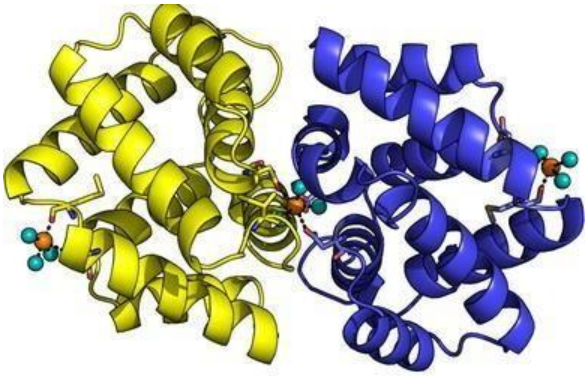

Figure 9. Fel d 1 crystallographic structure highlighting the location of the calcium ions. Chain 1 in yellow; chain 2 in blue. (Ligabue-Braun *et.al.,* 2015).

Individuals sensitive to cat allergens commonly manage their allergic reactions using antihistamines and corticosteroids. Another potential solution is AIT, the approach capable of modifying the disease course. However, AIT comes with the potential drawback of triggering severe

adverse reactions and demanding a substantial time commitment, often spanning several years. In practice, AIT might necessitate between 30 to 80 injections over the course of three to five years, and even then, its efficacy is notably limited (Thoms *et.al.,* 2020). Recently, an alternative strategy for reducing the levels of allergenic Fel d 1 protein in cats involving active immunization has been developed. The goal was to prompt the cat's own immune system to generate antibodies against Fel d 1. As part of this effort, researchers had been working on a feline vaccine designed to address cat allergies in humans which centers around a synthetically produced Fel d 1 protein, which is chemically coupled to a VLPs originating from the CMV (Zeltins *et.al.,* 2017).

Until now, the Fel-CMV vaccine (marketed as HypoCatTM) has undergone testing in 70 cats, demonstrating excellent tolerance both in the short term and over a two-year span, with no reported side effects. Moreover, the vaccination triggered robust production of neutralizing anti-Fel d 1 IgG antibodies, resulting in reduced levels of the active allergen in tears from study cats (Thoms *et.al.*, 2019). Moreover, a study conducted by Thoms et al. in 2020 revealed that administering HypoCatTM to cats led to an early and distinct expansion in the time available for petting before allergic symptoms reached a predetermined threshold. This positive outcome remained consistent and observable over the entire duration of the study (Thoms *et al.,* 2020). Despite the encouraging outcomes, a commercially accessible vaccine is not yet available in the market therefore the necessity to persist in exploring alternative approaches remains unchanged.

3.1. Antigen presenting platforms based on VLPs

3.1.1. Mophology of virus – like particles and its impact on the immune response

VLP vaccines belong to a category of subunit vaccines that are built from self-assembling capsid proteins derived from viruses (Al-Barwani *et.al.,* 2014). VLPs acquire their precise geometric structure from the originating virus, composed of a recurring arrangement of viral structural proteins. Their shapes can range from icosahedral to spherical or rod-shaped, with dimensions influenced by the characteristics of the original virus. VLPs can be generated with differing degrees of intricate structural patterns (Donaldson *et.al.,* 2014).

Vaccines containing VLPs possess the ability to trigger both the cellular and antibody-based components of the immune system therefore it's crucial that they reach lymphoid organs to initiate the activation of defensive T and B cell responses (Al-Barwani *et.al.,* 2014; Bachmann & Zabel, 2016). The humoral immune system is crucial for generating antibodies that can neutralize toxins and pathogens. On the other hand, a cell-mediated cytotoxic immune response plays a critical role in

eliminating intracellular pathogens (like viruses and bacteria) and abnormal cells such as those found in cancer. Both responses of the immune system rely on the recognition of antigens, which begins with the uptake of target antigens by specialized antigen-presenting cells (APCs). These cells process the antigens and display immune epitopes on MHC molecules, initiating immune responses (Manolova *et.al.,* 2008).

VLPs benefit this process by having a repetitive capsid structure that enhances internalization, processing, and presentation of antigens by various types of APCs like B cells, macrophages, and dendritic cells (DCs). The method of administration and the specific characteristics of VLPs can influence which populations of APCs internalize the particles most effectively. Notably, the size of the VLP plays a significant role, as particles larger than 200 nm require APCs to transport them to lymph nodes to facilitate antigen presentation to immune effector cells (Manolova *et.al.,* 2008; Al-Barwani *et.al.,* 2014). Soluble proteins and particles smaller than 200 nm can easily flow and effectively pass through openings in the lymphatic vessel walls. On the other hand, proteins or particles larger than 70 kDa or exceeding 5 nm are too sizable to enter the conduits directly. They require active transportation from the subcapsular sinus (SCS) to the B cell follicles located within the lymph node. This transport involves a range of cell types, including myeloid cells like SCS macrophages and B cells. These cells capture antigens from their surroundings and then transfer them into the B cell follicles found within lymph nodes and the spleen (Bachmann & Zabel, 2016).

Differing from soluble proteins and smaller particles, VLPs of larger dimensions, ranging from 200 to 500 nm, adopt an entirely distinct journey to reach lymphoid organs. These larger particles are unable to enter the lymphatic system independently due to the size limitations of the vessel wall pores. Consequently, they require assistance through cell-mediated transport, involving macrophages and DCs. This transport process begins from the point of entry or injection into the lymphatic system, enabling these particles to eventually reach lymph nodes in a form associated with cells. A challenge arises because dendritic cells (DCs) typically break down the antigens they internalize, potentially altering their original antigenic structure. As a result, it remains unclear how larger particles manage to activate B cells in lymphoid organs. Taken together, majority of viral particles, especially VLPs, possess the optimal size for effectively reaching the B cell follicles within lymph nodes (Manolova *et.al.,* 2008; Bachmann & Zabel, 2016).

Plant viruses typically possess uncomplicated and robust capsid structures. These capsids are constructed from numerous identical protein subunits, either just one type or a few types, organized

in patterns exhibiting either icosahedral or helical symmetry (Lomonossoff & Evans, 2014). While more than 50% of plant viruses exist in filamentous forms, it's worth highlighting that since 1986, when the first recombinant human vaccine against Hepatitis B virus (HBV) was approved for prophylactic therapy, all five of the VLP vaccines currently licensed by the FDA exhibit an icosahedral structure (hepatitis B, A, E virus, human papillomavirus, malaria vaccines) (Pumpens & Pushko, 2022). On the contrary, in-depth investigations conducted by Steinmetz group proposed that filamentous plant virus-like particles PVX possess a set of invaluable characteristics (Shukla *et.al.*, 2013; 2014; Le *et.al.*, 2017). These particles demonstrate a remarkable ability to evade phagocytosis, resulting in their prolonged circulation within the body. Furthermore, they showcase enhanced margination and extravasation, which in turn facilitate their precise accumulation at tumor sites (Toy *et.al.*, 2014; Kinnear *et.al.*, 2017; Le *et.al.*, 2019). A comprehensive review published by Balke & Zeltins in 2020 distinctly illustrates the successful utilization of numerous filamentous plant virus-like particles as effective platforms for vaccines. These particles have found application in two main domains: combating infectious diseases (such as papaya mosaic virus - PapMV; Laliberte-Gagne *et al.*, 2021; PVX - Lico *et al.*, 2009; Bamboo mosaic virus - BaMV; Chen *et al.*, 2012) and serving as tools for cancer prophylactic therapy (like Tobacco mosaic virus - TMV; McCormick *et al.*, 2006; malva mosaic virus - MaMV; Hanafi *et al.*, 2010, and others).

3.1.2. Antigen incorporation methods in vaccine generation process

The practical utilization of native and engineered viral nanoparticles in specific nanotechnological contexts is feasible only in some cases, such as immunizations or certain physical applications. Mostly, viral particles in their original form act as foundational building blocks that require subsequent modification processes to improve them according to desired properties for subsequent applications. In this context, the principles using genetic, physical, chemical and enzymatic modifications can be employed to create virus-like particles possessing the desired characteristics (Zeltins, 2016).

Initially, the adaptation of virus particle surfaces began with genetic modifications of the CP which was originally motivated by the goal of incorporating antigenic peptides into the particles, leading to modified entities called chimaeras, which held potential as innovative subunit vaccines (Lomonossoff & Evans, 2014). Using genetic methods enables the alteration of amino acids within viral coats and the integration of peptides and entire proteins into precise locations within the virus structure (Zeltins, 2016). Genetic techniques are commonly employed to modify or add extra amino

acids in order to achieve desired characteristics in selected nanoparticles. In specific scenarios, when aiming to efficiently generate VLPs from a different host organism, it becomes essential to change the amino acids within the CP structure (Balke & Zeltins, 2019). If the chosen VLPs lack essential amino acids at specific positions, these can be introduced through direct modifications of the target gene via mutagenesis. Additionally, the incorporation of diverse amino acids or even foreign peptide sequences into VLP structures is a widely recognized strategy. This approach has been extensively utilized in the generation of new vaccine candidates, giving insights from studies involving bacterial, plant, mammalian, or bacteriophage display techniques (Zeltins, 2016).

In the process of vaccine development, the integration of protein domains with immunological activity, and occasionally even complete proteins, into VLP structures, is captivating due to the high similarity in spatial arrangement to the native components of pathogens. Nevertheless, incorporating larger amino acid sequences into VLP structures, especially in comparison to viral structural proteins, rises a challenge when considering a direct fusion approach. Directly fusing such extensive antigens onto the VLP surface is complicated, especially when antigen sizes are comparable to, or even surpass, those of viral CPs. As a solution, a variety of construction strategies have been proposed to accommodate larger antigens onto the surface of plant-derived VLPs. An alternative approach involves creating mosaic VLPs, which consist of a combination of unmodified CPs and CPs fused with foreign protein domains within a single viral particle or VLP (Zeltins, 2016; Balke & Zeltins, 2019).

VLP CPs can also undergo chemical or enzymatic modifications through bioconjugation methods. The presence of amine groups on the capsid exterior provides well-defined sites for undergoing chemical alterations (Yildiz *et.al.,* 2011). The outer surfaces of the capsid feature numerous amino acids that can be specifically targeted (lysine, cysteine, aspartate, and glutamate), enabling the attachment of a wide panel of molecules like antibodies, peptides, proteins, oligonucleotides, carbohydrates, fluorescent agents, and drugs which can be achieved through diverse methods including covalent coupling (Fig. 10), click chemistry, and the copper (I)-catalyzed azide-alkyne [3 + 2] cycloaddition reaction (Zhang *et.al.,* 2018). Lysine residues exposed on the surface of VLPs, which are readily available, are widely favored as prime sites for the attachment and linking of various functional molecules (Zeltins, 2018). However, certain chemical modification conditions may not align with the preservation of the virus structure. As a result, process optimization to identify the optimal reaction environment, adjusting factors such as pH, ionic strength, temperature, and the inclusion of additives, is necessary (Balke & Zeltins, 2019).

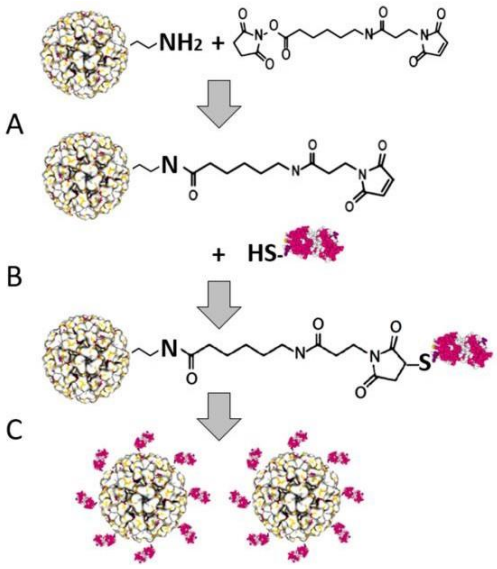

Figure 10. lllustration of the process of antigen integration into the structure of a plant virus through chemical coupling. A) The primary amines present in exposed lysine residues engage with a heterobifunctional crosslinking agent known as SMPH (succinimidyl-6-[(β-maleimidopropionamido) hexanoate]), forming a durable amide bond. B) Subsequently, in the following stage, the thiol group within the antigen structure containing cysteine selectively reacts with the maleimide derivative. C) This results in the decoration of VLPs with multiple antigen molecules (Balke & Zeltins, 2019).

Two recently developed systems that utilize transpeptidase and isopeptidase reactions are considered as enzymatic approach for synthesis of antigen – VLP conjugates. First, the Sortase A-mediated epitope coupling system employs a bacterial transpeptidase to form an amide bond between a VLP and a desired peptide (Obeng *et.al.,* 2023). The other, Spy-Catcher system, originating from the *Streptococcus pyogenes* bacterium, uses peptides capable of spontaneously forming isopeptide bonds (Balke & Zeltins, 2019). Antigens linked with Spy-Tag form covalent bonds with Spy-Catcher-VLPs and can ensure immunoprotection against infectious diseases (Brune & Howarth, 2018; Tan *et.al.,* 2021b; Lampinen *et.al.,* 2023).

Various physical techniques can facilitate the integration of peptides and protein domains into VLP-based nanoparticles. Among these, the interaction between streptavidin and biotin stands out as one of the most robust protein-molecule complexes found in nature. This approach has demonstrated straightforward incorporation of diverse antigens, including larger proteins that surpass the size limitations of genetically introduced antigens (Fredsgaard *et.al.,* 2021). It has also been successfully employed as a platform for generating malaria antigen VAR2CSA vaccine (Thrane *et.al.,* 2015).

Moreover, the robust binding of antigens to the VLP carrier has been demonstrated using alternative noncovalent complexes, such as strong electrostatic interactions facilitated by surface-exposed polyhistidine tags and the formation of multivalent tris-nitrilotriacetic acid (trisNTA) complexes (Koho *et al.*, 2015). Some other methods include extensively studied coiled-coil motifs (Utterstrom *et.al.*, 2021) that can be introduced into plant VLP structures for encapsulation purposes (Ecoil/Kcoil; Minten *et.al.*, 2009) or as a tool for polymeric display of proteins (leucine zipper peptide; Craig *et.al.*, 2012) with promising biomedical and nanotechnological applications.

2. METHODS

2.1. Cloning experiments

2.1.1. Round-shaped and Rod-shaped $CCMV_{TT}$-VLPs cloning, expression and production

A cloned copy of the CCMV coat protein gene (wt *CP)* was used in PCR mutagenesis for insertion of the coding sequence of tetanus toxoid epitope in 5'- and 3'- terminal ends of the CP gene. To replace the original amino acids at the N-terminus and C- terminus of CCMV CP against the TT epitope sequence, two step PCR mutagenesis for each construct was performed. The corresponding PCR fragments were then subcloned into pet42-CCMV-wt plasmid resulting in plasmids pET42-CCMV-Ntt830 and pET42-CCMV-Ctt830.

All plasmids were replicated in *E. coli* strain XL1-Blue. To avoid PCR errors, several CP gene-containing pET42 plasmid clones were sequenced using a BigDye cycle sequencing kit and an ABI Prism 3100 Genetic analyzer (Applied Biosystems, Carlsbad, USA). After sequencing, the plasmid clones without sequence errors were chosen for further experiments. To obtain "salt-stable" CCMV VLPs, the replacement of lysine against arginine in position 42 (K42R) was necessary using additional PCR mutagenesis. Plasmids were replicated in *E. coli* strain XL1-Blue and sequenced as previously described. For more detailed information see paper No. 1 (Zinkhan *et.al.*, 2021.)

2.1.2. PVY CP cloning experiments

Direct fusion and mosaic system: The recombinant sequence of Feld1 was described elsewhere (Zeltins *et.al.,* 2017). For further subcloning, we introduced additional sites in the *Feld1* gene by PCR mutagenesis following by similar expression methodology as previously described.

pTZ-Feld1 plasmid was subcloned into the already constructed plasmid pET-PVY-CP-NG4S (Kalnciema *et.al.,* 2012) resulting in pET-PVY-NG4S-Feld1 (direct fusion). For mosaic particle construction, the *PVY-CP* gene was amplified by PCR mutagenesis. The obtained PVY *CP* DNA fragment was ligated into the pETDuet-1 (Novagen, USA) vector. Furthermore, the fragment from pET-PVY-CP-NG4S was ligated into the pETDuet plasmid, which already contains the PVY *CP* gene resulting in expression vector containing two *PVY CP* genes. Finally, the *Feld1* gene was introduced into the pETDuet-derived plasmid, resulting in expression vector for mosaic VLPs.

SpyT/SpyC system: The sequence of the *SpyCatcher* gene was obtained from GenBank (JQ478411.1) and the coding DNAs for full-size and truncated variants of the *SpyCatcher* gene were

received as a product of commercial gene synthesis. We refer to two tested SpyCatcher domains as SpyCatcher2 (*SpyC2*; full-size gene) and SpyCatcher3 (*SpyC3*; truncated version).

To obtain both *SpyCatcher* genes convenient for subcloning, we used PCR mutagenesis for either *SpyC2* sequence and the *SpyC3* sequence following the usual expression methodology. Corresponding fragments from pTZ-SpyC2 and pTZ-SpyC3 were subcloned into the pET-RSFDuet-1 plasmid. For construction of *Feld1* antigen-SpyCather fusions, pTZ-Feld1 was subcloned into pRSF-Duet-SpyC2 and pRSF-Duet-SpyC3.

The coding sequence for *SpyTag* (*SpyT*) was introduced into the PVY *CP–NG4S* gene by PCR mutagenesis. The fragment from a pTZ plasmid clone containing the *SpyTag* sequence was subcloned into the pET-PVY-CP-NG4S vector.

To achieve covalent binding between the protein partners SpyCatcher and SpyTag directly in recombinant *E. coli*, we subcloned both coding sequences (pRSF-Duet-SpyC2-Feld1 and pRSF-Duet-SpyC3-Feld1) into the expression plasmid using the expression vector pET-PVY-NG4S-SpyT as a vector plasmid, resulting in two expression vectors containing SpyC2-Feld1 and SpyC3-Feld1. For more detailed information see paper No. 2 (Ogrina *et.al.,* 2022.)

2.1.3. EMV CP cloning experiments

Direct fusion and mosaic system: The sequence of the EMV *CP* gene (wtEMV; GenBank Accession Number: NC_001480.1) was obtained as a product of gene synthesis (plasmid pUC57-EMV; BioCat, Heidelberg, Germany). The wtEMV *CP* gene was subcloned into the *E. coli* expression vector pET42a(+) (Novagen, Madison, WI, USA). For the EMV *CP* gene, we introduced a flexible linker $(GGGGS)_3$ and *Bam*HI site coding sequences at the 3′-terminus. The EMV CP 3′-terminal fragment and corresponding additional sequences were amplified in PCR mutagenesis following the same expression scheme as previously.

The *Fel d 1* gene used in this study has been described previously (Zeltins *et al.,* 2017). For the construction of the EMV-Feld1 direct fusion and mosaic system PCR mutagenesis was performed. The *Fel d 1* sequence was excised from pTZ-Feld1-Bam-Xho and ligated into the linearized vector pET42-EMV-CG4S. The correct clone of the direct fusion plasmid was selected by digestion analysis.

For the mosaic system, we introduced flanking *Psc*I and *Sal*I restriction enzyme sites into the EMV CP gene by PCR mutagenesis. After usual expression scheme, the corresponding EMV-Psc fragment was excised from pTZ-EMV-Psc and ligated into the pETDuet-1 (Novagen, Madison, WI, USA) vector under the first T7 promoter. A correct clone of the resulting pETDu-EMV was found

after restriction analysis. The plasmid pETDu-EMV was further used for subcloning of the EMV-CG4S-Feld1 gene from the pET42-EMV-CG4S-Feld1 vector under the second T7. The plasmid clone encoding proteins in the mosaic system (pETDu-mEMV-CG4S-Feld1) was selected by digestion analysis.

Ecoil/Kcoil system: The coding sequences of coiled-coil peptides E (Ecoil) and K (Kcoil) were obtained from overlapping oligonucleotides in PCRs without a template. The *Ecoil* coding sequence was introduced after the $(GGGGS)_3$ linker-coding sequence into the vector pET42-EMV-CG4S. For the Kcoil expression vector, the Kcoil coding sequence was also obtained by PCR. The PCR product was cloned into the pTZ57 vector, sequenced, and introduced into the pACYCDuet-1 vector. Next, the Feld1 sequence was introduced into the resulting vector pACYCDu-Kcoil(3x). Both Ecoil- and Kcoil-containing plasmids were sequenced and used for coexpression of EMV-CG4S-Ecoil(3x) and Kcoil(3x)-Feld1 proteins.

SYNZIP18/17 system: The corresponding sequences for the synthetic zipper pair *SYNZIP (SZ) 17* and *18* were obtained from published supplementary material by *Reinke et al., 2010* and purchased as a gene synthesis product in plasmid pUC57 (BioCat, Germany). SZ17 was subcloned into the commercial vector plasmid pRSFDuet-1 (Novagen, USA) with the kanamycin resistance, and SZ18 was subcloned into pET-Duet1 (Novagen, USA) with the ampicillin resistance gene.

For the Feld1 antigen–SYNZIP 17 fusion, the pTZ-Feld1-Bam-Xho plasmid was subcloned into pRSF-Duet-SZ17 after partial restriction enzyme treatment. Additionally, the sequence coding for Feld1-6xHis-tag from plasmid pET42-Feld1-C6H (Zeltins *et al.,* 2017) was introduced into the constructed pRSF-SZ17-Feld1 sequence by subcloning.

To obtain the EMV *CP–SYNZIP 18* fusion construct, the previously mentioned EMV *CP*-containing plasmid for direct fusion pET42-EMV-CG4S was subcloned into the pET-Duet-SZ18 plasmid. For more detailed information see paper No. 3 (Ogrina *et.al.,* 2023.)

2.2. Expression and Purification of VLPs

Expression of VLPs and antigens: To obtain CCMV, PVY and EMV VLPs or Feld1 antigen proteins each construction was transformed and expressed in *E. coli* C2566 cells (New England Biolabs, Ipswich, USA). For coiled-coil partners (EMV-Ecoil/Kcoil-Feld1 and EMV-SZ18/SZ17-Feld1), two expression strategies were used. First, EMV-CG4S-SZ18- and EMV-CG4S-Ecoil-containing plasmids as well as plasmids SZ17-Feld1-C6H and Kcoil-Feld1 were expressed separately by directly transforming them into *E. coli* C2566 cells (New England, USA). Second, coexpression

of EMV-Ecoil/Kcoil-Feld1 and EMV–SZ18/SZ17–Feld1 plasmids in *E. coli* C2566 cells was performed.

After expression, the highest yield producing clones for the target protein were cultivated in 2TY medium with the addition of the corresponding antibiotic (kanamycin, 25 mg/L; ampicillin, 100 mg/L; chloramphenicol, 25 mg/L). Flasks with cells were cultivated using incubation shaker (200 rev/min; Infors, Switzerland) at 30 °C until the OD reached 0.8–1.0. After induction with 0.2 mM IPTG, cells were further cultivated at 20 °C for 18 h, collected by low-speed centrifugation (8,228 × *g*, 5 min, 5 °C, Eppendorf 5804R, Germany) and kept frozen at -70 °C until use.

Purification of VLPs and antigens:

Sonification: After thawing on ice, all biomasses were suspended in their respective buffers (see papers nr. 1 - 3) and disrupted by ultrasonic treatment. Insoluble proteins and cell debris were removed by centrifugation (15,557 × g, 10 min at 5°C). All steps involved in the expression of VLP were monitored by SDS-PAGE using 12.5% gels.

PEG precipitation: Soluble proteins of CCMV-SS, CCMV-Ntt830-SS and wtEMV after sonification were precipitated two or three times using a mixture of PEG 8,000 (8%) and NaCl (0.15 M), collected by centrifugation and dissolved in respective buffers.

His – tag column: Separately expressed SZ17-Feld1-C6H and rFeld1-C6H for chemical coupling and ELISA analysis were purified on a His–tag column and dialyzed against PBS overnight at +4°C.

Sucrose gradient: Kcoil-Feld1 protein and all VLPs except CCMV-SS, CCMV-Ntt830-SS and wtEMV were separated from cellular proteins by ultracentrifugation in a sucrose gradient (20–60% sucrose in their respective buffers). Fractions containing CP proteins were either combined and dialyzed against 100 volumes of respective buffer to remove the sucrose in a 12–14 kDa Spectra/Por 4 dialysis membrane (Spectrum Laboratories, Canada).

Gelfiltration: Kcoil-Feld1 protein after purification in a sucrose gradient was dialyzed against 100 volumes of 1x PBS followed by purification with gelfiltration on a Äkta Pure 25 XK 16/70 Superdex200 column (GE Healthcare, USA).

Sucrose cushions: After purification or precipitation, all VLPs were further purified using ultracentrifugation through the 30% sucrose “cushion” in their respective buffers supplemented with 0.5% TX-100 (Optima L–100XP; Type70Ti rotor, Beckman, USA; 183,960 × *g*, 4 h, 4 °C). Pellets were then dissolved in their respective buffers and, if necessary, concentrated using an Amicon Ultra–15, 100 K filtration unit (Merck–Millipore, USA), keeping the final VLP products stored at 4 °C.

All steps for the expression and purification of VLPs or antigens were monitored by SDS–PAGE using 12.5% gels, Western blot (WB) and agarose gel analysis. The concentration of proteins was estimated using a Qubit fluorometer (Thermo Fisher Scientific, USA) with a Qubit™ Protein Assay Kit (Thermo Fisher Scientific, USA) in accordance with the manufacturer's recommendations. Concentrated VLP solutions were stored at 4°C.

For more detailed information see papers No. 1 -3.

2.3. Binding of coiled – coil partners *in vitro*

After purification, separately expressed coiled–coil pairs EMV-CG4S-Ecoil and Kcoil-Feld1 or EMV-CG4S-SZ18 and SZ17-Feld1-C6H were mixed together in a 1:1 ratio according to their concentrations in a volume of 100 µL and incubated for 1 h at room temperature (RT). EMV-SZ18/SZ17-Feld1-C6H was purified using a His-tag column as previously described and dialyzed against 100 volumes of 1x PBS. All steps from the binding process were analyzed in SDS–PAGE and agarose gels and examined under TEM as well (paper No. 3; Suppl. Figs. 9, 11).

2.4. Chemical Coupling of PVY or EMV CP VLPs and Fel d 1

rFeld1 was purified using a His-tag column as described previously (Zeltins *et.al.*, 2017). The purified rFeld1 was conjugated to PVY CP VLPs or EMV CP VLPs using the crosslinker SMPH; Thermo Fisher Scientific, USA). A 5-fold molar excess of SMPH to PVY VLPs and a 3-fold molar excess of SMPH to EMV VLPs was used for the reaction at 23 °C for 1 h. Unreacted SMPH was removed by washing step with 1× PBS four times (4 × 6 min) at 3,214 × g (5,000 rpm) and 5 °C. The antigen prior to chemical conjugation was treated with a 10-fold molar excess of mild reducing agent tris (2-carboxyethyl) phosphine (TCEP; Sigma–Aldrich, USA) for 10 min at room temperature (RT). The coupling was performed by adding 4- fold molar excess of rFeld1 to the SMPH-derivatized PVY VLPs or a 2-fold molar excess of rFel d 1 to the SMPH-derivatized wtEMV VLPs at 23°C for 2-3 h by shaking at 1400 rpm/min on a DSG Titertek (Flow Laboratories, UK). Unbound rFeld1 was removed. All stages of coupling were analyzed by SDS–PAGE and the integrity of VLPs was confirmed by TEM. For more detailed information see papers No. 2 -3.

2.5. Transmission Electron Microscopy (TEM)

Purified VLP samples (1 mg/ml) were adsorbed on carbon formvar-coated copper grids and were negatively stained with 0.5% uranyl acetate aqueous solution. The grids were examined using a JEM-1230 electron microscope (JEOL, Tokyo, Japan) at an accelerating voltage of 100 kV. At least five pictures were captured per sample.

2.6. Mass Spectrometry for $CCMV_{TT}$ CP VLPs

CCMV VLPs (1 mg/ml) were diluted with a 3-hydroxypicolinic acid matrix solution and were spotted onto an MTP AnchorChip 400/384TF. Matrix assisted laser desorption/ionization (MALDI)-TOF MS analysis was carried out on an Autoflex MS (Bruker Scientific, Billerica, Massachusetts). The protein molecular mass (MM) calibration standard II (22.3–66.5 kDa; Bruker, Billerica, Massachusetts) was used for mass determination.

2.7. Immunology experiments:

2.7.1. Western Blot (WB) Analysis for PVY CP and EMV CP constructions

For WB analysis, protein samples were separated by SDS–PAGE and transferred to an Amersham Protran 0.45 µm nitrocellulose membrane (GE Healthcare, Piscataway, USA) using a semidry apparatus with parameters of 250 V, 45 A, and 45 min. Membranes were blocked in a PBS solution containing 1% alkali–soluble casein (Merck-Millipore, USA) and incubated overnight (ON) at 4°C in anti-PVY, anti-EMV or anti-Feld1 Ab-containing solutions (diluted 1:1000 in PBS with 1% alkali–soluble casein) obtained from mice that were immunized prior the experiment. The membrane was washed with TBS buffer for 15 min and incubated at RT for 3 h with horseradish peroxidase-conjugated anti-mouse IgG (Sigma–Aldrich, USA). The membrane was washed with TBS for 15 min two times. The signal bands were developed by incubating the membrane in TBS buffer supplemented with peroxidase substrates (0.002% *o*-dianisidine and 0.03% hydrogen peroxide). For more detailed information see papers No. 2 -3.

2.7.2. Mice vaccination regimen

For CCMV experiments: Wild type 8 – 12 weeks old female C57BL/6 mice (Harlan) were vaccinated s.c. with 15 µg Round or Rod-shaped $CCMV_{TT}$-VLPs in 100µl PBS on day 0. Mice were boosted with a similar dose on day 14. Serum samples were collected on days 0, 7, 14, 21, 28 and 35. Experiments were conducted in accordance with the Swiss Animal Act (455.109.1 – September 2008, 5^{th}) of University of Bern.

For PVY CP and EMV CP experiments: 6 – 8 weeks old female BALB/c mice (5 per group) were purchased from Laboratory Animal Centre, University of Tartu (Estonia). 50 µg of each PVY CP VLPs and 30 µg of total protein of each EMV CP VLPs were diluted in 300 µl of sterile PBS and used for s.c. injection in mice without adjuvant on Day 0. Mice received similar booster dosage on Days 14 and 28. One 100 µl serum sample from each mouse were collected each week on Days 0, 7, 14, 28. Final bleeding was performed on Day 42. The experimental protocol was approved by the

Animal Protection Ethical Committee of the Latvian Food and Veterinary Service (permission No. 89).

2.7.3. The enzyme-linked immunosorbent assay (ELISA)

The plates (96–well; Nunc Immuno MaxiSorp, Rochester, NY, Thermo Fisher Scientific, USA) were coated with purified samples (Round and Rod-shaped $CCMV_{TT}$-VLPs, PVY CP, EMV CP, rFeld1) in 50 mM sodium carbonate buffer (pH 9.6) overnight at 4 °C. Plates were washed with PBS-Tween and blocked using 100µl PBS-Casein or BSA in PBS for 1 - 2h. 100 µL of serially diluted mouse sera were added to the wells and incubated for 1 h at 37 °C. After washing with PBS-Tween three times, goat anti-mouse IgG conjugated to Horseradish Peroxidase (HRP) (Jackson ImmunoResearch, West Grove, Pennsylvania) was added 1/1000 for Round and Rod-shaped $CCMV_{TT}$-VLP samples or mouse IgG conjugated to horseradish peroxidase (dilution 1: 10,000; Sigma–Aldrich, USA; 1 h, 37 °C) was added to PVY CP and EMV CP VLP mice samples. Plates were developed and the absorbance measurements were performed at 450 nm for CCMV VLPs or 492 nm for PVY CP and EMV CP VLPs. Titers were calculated as OD50 values (CCMV VLPs) or as the highest absorbance values that exceeded three–fold of the negative control (nonimmunized mouse serum (PVY CP and EMV CP VLPs).

Monoclonal antibody ELISA: Monoclonal Feld1 antibody ELISA tests replaced the immunized mouse sera with two commercially available Feld1 mAbs according to manufacturers' guidelines (MA-3E4 and MA–6F9, Indoor Biotechnologies, UK). Nonimmunized mouse serum was used as a negative control and titer calculations were performed as described in papers No. 2 – 3.

Subclass specific ELISA for CCMV VLPs: IgG subclasses were measured from day 21 sera using the same ELISA protocol with the following secondary Abs: goat anti-mouse IgG1-HRP and goat anti-mouse IgG2a-HRP (1:1000) (Thermo Fischer Scientific, Waltham, Massachusetts), goat anti-mouse IgG2c-HRP (Southern Biotech, Birmingham, Alabama) 1:4000, rat anti-mouse IgG3-biotin (Becton, Dickinson, Franklin Lakes, New Jersey) 1:2000 followed by streptavidin-HRP (Dako, Glostrup, Denmark) 1:1000 incubated at 37°C for 1h. IgA was measured using day 35 sera (immunization at day 0, boost at day 14). IgG was depleted using Dynabeads™ Protein G (Thermo Fischer Scientific, Waltham, Massachusetts). For IgA detection, goat anti mouse IgA conjugated to HRP was used (SouthernBiotech, Birmingham, Alabama) 1/4000. For more detailed information see paper No. 1 (Zinkhan *et.al.*, 2021).

Subclass specific ELISA for PVY CP and EMV CP VLPs: For IgG1 and IgG2a detection, sera obtained from Day 42 following the manufacturer's protocol (mouse mAb antibody isotyping reagent ISO2-1KT kit; Sigma–Aldrich, USA) was used. For secondary Abs, a peroxidase conjugate of monoclonal anti-goat/sheep IgG Abs (Sigma–Aldrich, USA) was used. For more detailed information see papers No. 2 – 3.

Avidity ELISA

To determine the avidity of IgG Abs, two sets of plates were prepared. Both were coated with 10 µg/mL of either PVY CP VLPs or EMV CP VLPs and Feld1-C6H-CG. After serum incubation, one set of plates was washed three times for 5 min with 50 µl/well of a solution containing 7 M urea in PBS supplemented with 0.05% Tween-20. The other set was washed with the same amount of PBS with 0.05% Tween-20. The rest of the procedure was identical to that described above.

ELISA for Native Fel d 1

Sample of nFeld1 (Indoor Biotechnology, UK) in a concentration of 10 µg/mL in 50 mM sodium carbonate buffer (pH 9.6, 100 µl per well), were coated on 96-well ELISA plates (Nunc Immuno MaxiSorp, Rochester, NY, Thermo Fisher Scientific, USA) and stored at 4°C ON. After blocking and washing steps, serially diluted mouse sera (5 µl from each PVY CP or EMV CP VLP sample) were added to the plates and incubated at 37°C for 1 h. The rest of the procedure was identical to that described above. For more detailed information see papers No. 2 – 3.

2.8. Measuring IFN- γ in mouse serum

Serum from Round or Rod-shaped $CCMV_{TT}$-VLPs vaccinated mice was collected on day 14 for measuring IFN- γ. ELISA MAX™ Deluxe Set Mouse IFN-γ (Biolegend, San Diego, California) was performed according to manufacturer's instructions. Serum was used undiluted and concentration was interpolated to a standard curve of the sets standard sample.

2.9. Trafficking of Round and Rod-shaped $CCMV_{TT}$-VLPs to draining lymph nodes

Round or Rod-shaped $CCMV_{TT}$-VLPs were labelled with AF488 as per manufacturer's instructions (Thermo Fischer Scientific, Waltham, Massachusetts) and stored at -20. Wild type C57BL/6 mice (8-12 weeks, Harlan) were injected with 10µg of the VLPs in the footpad under isoflurane anesthesia. Popliteal lymph nodes (LNs) were collected 3h and 24h following footpad injection. LNs were treated with collagenase D (Roche, Basel, Switzerland) and DNase I (Boehringer,

Ingelheim am Rheih, Germany) in DMEM medium containing 5% FBS and 1% Strep/Penicillin for 37°C. L were smashed using 70µm cell strainers, RBC were lysed with ACK buffer. Cells were stained with Fc blocker and then with anti-CD11b, CD11c, CD45R/220, CD8 and F4/80 (all from Biolegend, San Diego, California).

2.10. Immunofluorescence

$CCMV_{TT}$-VLPs were labelled with AF488 as described previously. C57BL/6 mice were injected with 10µg of the VLPs in the footpad and popliteal LNs collected as previously above. LNs were then embedded in Tissue-Tek optimum cutting temperature compound (Sakura). Cryostat sections (7µm in thickness) on Superforst/Plus glass slides (Thermo Fischer Scientific, Waltham, Massachusetts) were air-dried and then fixed. After rehydration, sections were blocked with 1% (w/v) BSA (Sigma Aldrich, St. Louis, Missouri) and 1% (v/v) normal mouse serum. Immunofluorescence labeling was done with Abs diluted in PBS containing 0.1% (w/v) BSA and 1% (v/v) normal mouse serum. Sections were washed 3 times 1x PBS after every labeling step. LN staining: macrophages were detected using a primary antibody against CD11b (1/1000, rat anti mouse CD11b conjugated with PE; BD Biosciences, San Jose, California), B-cell follicles were identified using rat anti mouse B220 Alexa F647 (1/1000; BD Biosciences, San Jose, California). Images were acquired on an Axioplan microscope using an AxioCam MRn (Zeiss).

2.11. Histology of lymph node

$CCMV_{TT}$-VLPs were labelled with AF488 as previously described. C57BL/6 mice were injected with 10µg of the VLPs in the footpad and popliteal LNs collected as previously above. LNs were fixed with 4% paraformaldehyde solution (Sigma Aldrich, St. Louis, Missouri). Of each group, 2 - 4 murine LNs were histologically examined by a board-certified veterinary pathologist (SdB). Of each LN, a full cross section, stained with Hematoxylin and Eosin (HE), was assessed for any histopathological changes.

2.12. Statistical analysis

Data were analyzed and presented as mean ± SEM using GraphPad PRISM 8 and 9. Comparison between the groups was performed using Student's *t*-test or one-way ANOVA test. *P*-values $^{****}P < 0.0001$; $^{***}P < 0.001$; $^{**}P < 0.01$; $^{*}P < 0.05$.

3. RESULTS

3.1. The impact of size on particle drainage dynamics and antibody response

3.1.1. Construction and characterization of round – and rod- shaped CCMV$_{TT}$ VLPs

CCMV VLPs originating from the plant *Bromovirus* genus adopt a configuration of T=3 icosahedral particles. CCMV-VLPs can easily be expressed in the *E. coli* system, encapsulating nucleic acid during the synthesis phase. For the enhancement of VLP stability, we implemented a mutation renowned for its pH fluctuation-resistant properties (SS mutation). This alteration includes the substitution of lysine with arginine at position 42 of the CP gene (Fox *et.al.,* 1996). Subsequently, we engineered CCMV-SS VLPs by integrating a potent T cell stimulatory epitope sourced from the tetanus toxin (TT) (830-843) in the N – terminal end of CCMV-SS CP. The outcome of this engineering effort led to the creation of N-terminal CCMV$_{TT}$ VLPs – icosahedral structures (termed as round-VLPs) adhering to a symmetry of T=3, measuring 30 nm in diameter, similar to their parental VLPs. Noteworthy, the incorporation of TT at the C-terminus of CCMV CP resulted in elongated rod-shaped VLPs varying in length (approximately 1 µm) and ~30 nm in width (termed as rod-VLPs), showing the profound impact of epitope positioning on the morphology of the CCMV$_{TT}$ VLPs.

Both types of VLPs were synthesized within an *E. coli* system. As VLPs encapsulate ssRNA derived from *E. coli*, the quantification of packed RNA was achieved through measurement at 260 nm and validated by employing the agarose gel visualization technique. However, the efficiency of this method was notably reduced for the rod-shaped VLPs, given their substantial size during migration through the gel. Employing mass spectrometry and SDS-PAGE analysis, we determined the molecular weight of CP monomers to approximate 21.8 (round-CCMV$_{TT}$) and 21.9 kDa (rod-CCMV$_{TT}$), respectively. In contrast, the original CCMV-SS VLPs are assembled from CPs with an approximate weight of 20.2 kDa.

3.1.2. Round - and rod – shaped CCMV$_{TT}$ drainage kinetics and interaction with cells in draining lymph node

To explore the impact of size on the lymphatic trafficking of the modified VLPs, we conducted an evaluation of the accumulation and interactions of both round-shaped and rod-shaped CCMV$_{TT}$ VLPs within murine popliteal lymph nodes (LNs). This examination took place at two time points: 3 hours and 24 hours post-injection into the footpads of mice. Subsequently, flow cytometric analysis and cryosections of the popliteal LNs were performed. Our findings confirm that, at the 3h mark

following injection, the round-shaped CCMV$_{TT}$ VLPs exhibit an improved efficacy in migrating towards secondary lymphoid organs. This migration aims to engage professional APCs—such as lymphoid-derived DCs, conventional DCs, and macrophage-derived cells—alongside B cells, facilitating their activation and interaction. By the 24h point following footpad injection, the difference in interaction between round and rod-shaped CCMV$_{TT}$ VLPs with DCs or macrophages reduced. Even the rod-shaped CCMV$_{TT}$ VLPs, though larger, were detectable in the popliteal draining LNs. Although, after 24h, we observed that round-shaped CCMV$_{TT}$ VLPs had penetrated deeper into the LNs. Moreover, the interaction of round-shaped CCMV$_{TT}$ VLPs with B cells, marked by increased MHCII expression, demonstrated a significant rise in comparison to the rod-shaped CCMV$_{TT}$ VLPs.

3.1.3. Humoral immune response against round- and rod- shaped CCMV$_{TT}$ VLPs

Our study reveals that a single initial injection of round-shaped CCMV$_{TT}$ VLPs effectively elicited a substantial titer of specific antibodies already at day 7. This response was subsequently enhanced by a booster injection on the day 14. In contrast, the rod-shaped CCMV$_{TT}$ VLPs initiated a specific antibody response only after the day 14 booster, and this response remained notably lower compared to the response induced by the round-shaped CCMV$_{TT}$ VLPs. In contrast to the rod-shaped VLPs, the round-shaped CCMV$_{TT}$ VLPs triggered a remarkable rise of over 100 times in systemic IgG and IgA levels. For the purpose of cross-reactivity studies, sera collected from both round- and rod-shaped CCMV$_{TT}$ VLP vaccinated mice were tested using ELISA, where the plates were coated with VLPs of the opposite shape. The results revealed that sera derived from round-shaped CCMV$_{TT}$ VLPs exhibited a notably higher efficiency in recognizing rod-shaped VLPs, even following just a single immunization.

Furthermore, round-shaped CCMV$_{TT}$ VLPs can also direct the generated T cell response towards Th1 polarization. Comparatively, round-shaped VLPs outperformed rod-shaped ones in facilitating class-switching. When using round-shaped CCMV$_{TT}$ VLPs for vaccination, the increase in the ratio between Th1 (IgG2a/c, IgG3) and Th2 (IgG1) associated IgG subclasses was notably increased.

3.1.4. Germinal center formation

Since the presence of an antigen reservoir sustained on follicular DCs is crucial for maintaining B cell stimulation within germinal centers (GCs), we examined GC formation in spleens treated with both types of VLPs, 12 days after a single s.c. dose. Notably, the formation of GCs was considerably

more robust in mice vaccinated with round-shaped $CCMV_{TT}$ VLPs compared to those vaccinated with rod-shaped $CCMV_{TT}$ VLPs, whether assessed by the overall count of GCs or the quantification of their spatial distribution (GCs/mm²).

Journal of Controlled Release 331 (2021) 296–308

Contents lists available at ScienceDirect

Journal of Controlled Release

journal homepage: www.elsevier.com/locate/jconrel

The impact of size on particle drainage dynamics and antibody response

Simon Zinkhan [a,1], Anete Ogrina [b,1], Ina Balke [b], Gunta Resevica [b], Andris Zeltins [b], Simone de Brot [c], Cyrill Lipp [a], Xinyue Chang [a], Lisha Zha [d], Monique Vogel [a], Martin F. Bachmann [a,e], Mona O. Mohsen [a,f,*]

[a] Department of BioMedical Research, University of Bern, Bern, Switzerland; Department of Immunology RIA, University Hospital Bern, Bern, Switzerland
[b] Latvian Biomedical Research & Study Centre, Ratsupites iela 1, Riga, LV 1067, Latvia
[c] COMPATH, Institute of Animal Pathology, University of Bern, Bern, Switzerland
[d] International Immunology Center, Anhui Agricultural University, Hefei, Anhui, China
[e] Jenner Institute, Nuffield Department of Medicine, University of Oxford, UK
[f] Interim Translational Research Institute "iTRI", National Center for Cancer Care & Research Doha, Qatar

ARTICLE INFO

Keywords:
Virus-like particles
Cowpea chlorotic mottle virus
Humoral immune response

ABSTRACT

Vaccine-induced immune response can be greatly enhanced by mimicking pathogen properties. The size and the repetitive geometric shape of virus-like particles (VLPs) influence their immunogenicity by facilitating drainage to secondary lymphoid organs and enhancing interaction with and activation of B cells and innate humoral immune components. VLPs derived from the plant Bromovirus genus, specifically cowpea chlorotic mottle virus (CCMV), are $T = 3$ icosahedral particles. (T) is the triangulation number that refers to the number and arrangements of the subunits (pentamers and hexamers) of the VLPs. CCMV-VLPs can be easily expressed in an *E. coli* host system and package ssRNA during the expression process. Recently, we have engineered CCMV-VLPs by incorporating the universal tetanus toxin (TT) epitope at the N-terminus. The modified $CCMV_{TT}$-VLPs successfully form icosahedral particles $T = 3$, with a diameter of ~30 nm analogous to the parental VLPs. Interestingly, incorporating TT epitope at the C-terminus of $CCMV_{TT}$-VLPs results in the formation of Rod-shaped VLPs, ~1 μm in length and ~ 30 nm in width. In this study, we have investigated the draining kinetics and immunogenicity of both engineered forms (termed as Round-shaped $CCMV_{TT}$-VLPs and Rod-shaped $CCMV_{TT}$-VLPs) as potential B cell immunogens using different in vitro and in vivo assays. Our results reveal that Round-shaped $CCMV_{TT}$-VLPs are more efficient in draining to secondary lymphoid organs to charge professional antigen-presenting cells as well as B cells. Furthermore, compared to Rod-shaped $CCMV_{TT}$-VLPs, Round-shaped $CCMV_{TT}$-VLPs led to more than 100-fold increased systemic IgG and IgA responses accompanied by prominent formation of splenic germinal centers. Round-shaped $CCMV_{TT}$-VLPs could also polarize the induced T cell response toward Th1. To our knowledge, this is the first study investigating and comparing the draining kinetics and immunogenicity of one and the same VLP monomer forming nano-sized icosahedra or rods in the micrometer size.

1. Introduction

In 1956, Crick and Watson have stated that "it is a striking fact that almost all small viruses are rods or spheres", "These shells are constructed from a large number of identical protein molecules, of small or moderate size, packed together in a regular manner" [1]. The main reason for this arrangement is the small genome of viruses, especially RNA viruses. Many virus capsids are made up of multiple copies of a single coat protein (CP) arranged in an icosahedral or a helical-shaped geometry [2,3]. The icosahedral structure of viruses is more prevalent than the helical-shaped one.

Virus-like particles (VLPs) are one of the traditional vaccine platforms that emerged few decades ago and have made large strides in the field of vaccinology. The continuous interest in VLPs is due to several reasons including: being a safe platform as they lack replicating genetic materials, their immunogenicity which is largely due to antigen

* Corresponding author at: Department of BioMedical Research, University of Bern, Bern, Switzerland.
E-mail address: mona.mohsen@dbmr.unibe.ch (M.O. Mohsen).
[1] Both authors contributed equally to this study.

https://doi.org/10.1016/j.jconrel.2021.01.012
Received 24 July 2020; Received in revised form 5 January 2021; Accepted 8 January 2021
Available online 12 January 2021

organization and repetitiveness viewed as potent pathogen-associated structural pattern (PASP) similar to pathogen-associated molecular patterns (PAMPs) [4–7], which are usually specific for pathogens, repetitive and rigid surfaces are also specific for pathogens, hence the term PASP. VLPs are further useful tools, as different epitopes may be displayed on their surface. In addition VLPs have favorable sizes ranging between 20 and 200 nm [4]. Such size allows VLPs to rapidly and efficiently filter and drain through the lymphatic system and gain access to lymphoid follicles [4,8–10]. The approved VLP-based vaccines currently in the market mostly exhibit an icosahedral surface geometry based on the quasi-equivalence concept described by Caspar and Klug in 1962 and expressed as *Triangulation number (T)* [11,12]. Triangulation refers to the number and arrangements of the subunits (pentamers and hexamers) of the coat protein of a virus or a VLP. It usually serves as a rough indicator of size. For example, human papilloma viruses (HPVs) are $T = 7$ of ~60 nm in size [13], while hepatitis E virus (HEV) VLPs are $T = 1$ of ~25 nm [14]. The different generations of hepatitis B virus (HBV) vaccines show highly organized sub-viral particles (SVPs) of ~20-25 nm [15]. In addition, the arrangement of CPs of VLPs in helical or rod-shape geometry is also possible; tobacco-mosaic virus (TMV) is a well characterized representative of this category. Virions of TMV are ~300 nm in length and ~ 18 nm in width [16,17]. TMV-VLPs have been investigated as a promising platform in nanotechnology [18] and as a vaccine platform as well [19]. Nevertheless, knowledge is scarce regarding TMV-VLPs drainage dynamics. Icosahedral VLPs can be manipulated by inserting few mutations to form rod-shaped VLP. For example, VLPs derived from the bacteriophage Qβ can assemble in a rod-shaped particle following the mutation of five amino acid (a.a.) residues in the FG loop of its CP [20].

It is known that the repetitive surface geometry of icosahedral VLPs enhances optimal induction of B cell response via cross-linking of B cell receptors (BCRs) [21,22]. Previously, we have shown that displaying epitopes on icosahedral $T = 3$ VLPs such as bacteriophage Qβ or plant-derived $CuMV_{TT}$ VLPs result in high specific IgG antibody (Ab) titers as well as neutralizing Abs [23–28]. Some studies have revealed that a vaccine based on rod-shaped tobacco-mosaic (TMV)-VLPs could also serve as an effective platform to display different epitopes capable of eliciting an immune response against different pathogens [29,30].

Cowpea chlorotic mottle virus (CCMV) is a Bromovirus naturally infecting plants and therefore is non-infectious to humans. The infected plants develop yellow spots on their leaves, hence the name chlorotic [31]. The virus is an icosahedron $T = 3$ of ~28 nm in diameter, consisting of 180 CPs of identical amino-acid sequence. The coat protein can adopt multiple quasi-equivalent forms referred to as the coat subunits A, B and C forming either hexamers (alternating subunits B and C) or pentamers (subunit A). The resulting virus particle consists of 12 pentamers and 20 hexamers [32]. Previously, it has been shown that icosahedral CCMV can be converted into rod-shaped particles after a disassembly/reassembly process [33].

In this study, we have demonstrated that CCMV-derived VLPs of different morphology (icosahedral or rod-shaped structure) can be obtained directly from recombinant *E. coli* cells. We specifically manipulated CCMV-VLPs by inserting the universal tetanus toxin (TT) epitope at the C or N-terminus to form icosahedral VLPs in the nanometer scale or rod-shaped VLPs with sizes in the micron range. Such intervention allowed us to study the impact of particle-size on drainage dynamics and magnitude of induced immune response using VLPs based on essentially the same VLP-monomer. Our results demonstrate for the first time that VLPs in the nm size range are vastly more immunogenic than micron-sized particles.

2. Materials and methods

2.1. Round-shaped and Rod-shaped $CCMV_{TT}$-VLPs cloning, expression and production

Cloning of CCMV-CP with induced tetanus toxin epitope for expression: A cloned copy of the CCMV coat protein gene (wt *CP*) was obtained from Dr. Alain Tissot (Zürich) and used in PCR mutagenesis for insertion of the coding sequence of tetanus toxin epitope (TT830–843; QYIKANSFIGITE) in 5′- and 3′- terminal ends of the CP gene. To replace the original amino acids at the N-terminus of CCMV CP with the TT epitope sequence, the pET42-CCMVwt plasmid was used as a template for PCR amplification and mutagenesis. *NdeI* site at the 5'end of the CCMVwt gene was used for cloning corresponding PCR products. To introduce the tetanus toxin epitope coding sequence into the CCMV-wt gene, two step PCR mutagenesis was necessary. For the first step amplification the following primers were used for N terminal PCR: CC_N83_d24F (5'ATACATATGGGCCAGTATATTAAGGCCAACTC CAAATTTATCGGGATTACCGA 3′) and CC_N83R (5′ AGTTAAC TTCCCTGTACCGACTGTTTCGGTAATCCCGATAAATTTGGAGTTG 3′).

For the second round the PCR products from the first round were diluted 1:50 and re-amplified with primers CC_N83_d24F and CC_AgeR (5′ ACTTCGATACGCTGTAACCGGTCCA 3′).

For C terminal insertion of TT epitope, the following primers were used: CC_C83F (5′ TGACGACTCTTTCACTCCGGTCTATGGCCAGTA-TATTAAGGCCAACTCC 3′) and CC_C83R (5′ TTACTCGA-GAAGCTTATTACTCGGTAATCCCGATAAATTTGGAGTTG 3′). Second round of the PCR was performed as describe above using primers CC_C83R (5′ TTACTCGAGAAGCTTATTACTCGGTAATCCCGA-TAAATTTGGAGTTG 3′) and CC_SacIIF (5′ CCCTTGAA-CAACTCGCCGCGGA 3′).

The corresponding PCR fragments were analyzed in a 0.8% agarose gel and then purified using the *GeneJet Gel Extraction* kit (Thermo Fischer Scientific, Waltham, Massachusetts). Then the 5′ terminal end PCR product and plasmid pET42-CCMVwt were digested with enzymes *NdeI* and *BshTI* (Thermo Fischer Scientific, Waltham, Massachusetts) and ligated, resulting in plasmid pET42-CCMV-Ntt830. The 3'terminal end PCR product and plasmid pET42-CCMVwt were digested with enzymes *Cfr42I* and *XhoI* (Thermo Fischer Scientific, Waltham, Massachusetts) and ligated, resulting in plasmid pET42-CCMV-Ctt830.

E.coli XL1-Blue cells were used as a host for cloning and plasmid amplification. To avoid PCR errors several CP gene-containing pET42 plasmid clones were sequenced using the BigDye cycle sequencing kit and an ABI Prism 3100 Genetic analyser (Applied Biosystems, Foster City, California). After sequencing, the plasmid clones without sequence errors were chosen for further experiments.

Cloning of CCMV-SS-CP with induced tetanus toxin epitope for expression: To obtain "salt-stable" CCMV VLPs, the replacement of lysine against arginine in position 42 (K42R) was necessary. For CCMVwt-SS the following primers were used: CCP_salt_AgeI_R (5′ TGTAACCGGTCCATGCTTTAATAGCGCGGCCTT 3′) and CCM_NdeF (5′ ATACATATGTCTACAGTCGGTACAGGG 3′). For CCMV-Ntt830-SS the following primers were used: CC_N83_d24F and CC_salt_AgeI_R. The corresponding PCR products were cloned into the pTZ57R/T vector (Thermo Fischer Scientific, Waltham, Massachusetts). *E. coli* XL1-Blue cells were used as a host for cloning and plasmid amplification. To avoid RT-PCR errors, several CP gene-containing pTZ57 plasmid clones were sequenced using the BigDye cycle sequencing kit and an ABI Prism 3100 Genetic analyser (Applied Biosystems, Foster City, California). After sequencing, corresponding DNA fragments without sequence errors were subcloned into the *NdeI/AgeI* sites of pET42-CCMVwt and pET42-CCMV-Ntt830 expression vectors, resulting in the expression plasmids pET42-CCMV-SS and pET42-CCMV-Ntt830-SS. For generating the C terminal tetanus toxin CCMV-SS construct the corresponding *NdeI/BsrGI*-fragment from pET42-CCMV-SS was subcloned into pET-CCMV-Ctt830, generating the expression vector pET42-CCMV-Ctt830-SS.

Expression and purification of CCMV-SS VLPs: To obtain all salt stable CCMV CP VLPs, each construct was transformed and expressed in *E. coli* C2566 cells (New England Biolabs, Ipswich, USA). After selection of clones with the highest expression levels of the target protein, *E. coli* cultures were grown in 2xTY medium containing kanamycin (25 mg/l) on a rotary shaker (200 rev/min; Infors, Bottmingen, Switzerland) at 30 °C to an OD600 of 0.8–1.0. Then, expression was induced with 0.2 mM Isopropyl-β-D-thiogalactopyranoside (IPTG), and the medium was supplemented with 5 mM $MgCl_2$ and 2 mM $CaCl_2$. Incubation was continued on the rotary shaker at 20 °C for 18 h. The resulting biomass was collected by low-speed centrifugation and was frozen at -70 °C. After thawing on ice, the cells were suspended in buffer containing 15 mM sodium phosphate pH 7.5 supplemented with 150 mM NaCl (buffer A) with additional 0.5 mM urea, 1 mM PMSF, 5 mM mercapto-ethanol, and were disrupted by ultrasonic treatment. Insoluble proteins and cell debris were removed by centrifugation (13,000 rpm, 30 min at 5 °C). All steps involved in the expression of VLP were monitored by SDS-PAGE using 12.5% gels.

CCMV-SS and CCMV-Ctt830-SS VLPs were separated from cellular proteins by ultracentrifugation (SW28 rotor, Beckman, Indianapolis, Indiana; at 25,000 rpm, 6 h, 5 °C) in a sucrose gradient (20–60% sucrose in buffer A, without mercapto-ethanol and urea, supplemented with 0.5% Triton X-100). The content of gradient tubes was divided into six fractions, starting at the bottom of the gradient, and the fractions were analyzed by SDS-PAGE. Fractions containing CCMV-SS CP proteins were combined and dialyzed against 100 volumes of buffer A to remove the sucrose. If necessary, samples were concentrated using an Amicon Ultra-15 centrifugal device (Millipore, Cork, Ireland).

However, soluble proteins of CCMV-Ntt830-SS were precipitated using a mixture of PEG 8,000 (8%) and NaCl (0.15 M), collected by centrifugation and dissolved in buffer A. PEG/NaCl precipitation was repeated for CCMV-Ntt830-SS. After solubilisation or dialysis (in case of CCMV-SS), all CCMV CP preparations were purified two times using an ultracentrifuge and 30% sucrose cushion – first with additional 0.5% Triton X-100 and the second time without Triton X-100 (4 h, 50 000 rpm, 4 °C; Type 70Ti rotor, Beckman, Indianapolis, Indiana) and the pellet was then dissolved in buffer A. If necessary, samples were concentrated using an Amicon Ultra-15 centrifugal device (Millipore, Cork, Ireland). To obtain pure preparations of CCMV-CPs for subsequent electron microscopy (EM) analysis, stability and immunological studies, the sucrose gradient, dialysis, and concentration steps were repeated.

All steps involved in the expression and purification of VLP were monitored by SDS-PAGE (using 12.5% gels). The concentration of purified CCMV–CPs were estimated using the QuBit fluorometer in accordance with manufacturer's recommendations (ThermoFisher Scientific, Waltham, Massachusetts). Concentrated VLP solutions were stored at +4 °C.

2.2. Electron microscopy

Purified Round-shaped or Rod-shaped $CCMV_{TT}$-VLPs proteins (1 mg/ml) were adsorbed on carbon formvar-coated copper grids and were negatively stained with 0.5% uranyl acetate aqueous solution. The grids were examined using a JEM-1230 electron microscope (JEOL, Tokyo, Japan) at an accelerating voltage of 100 kV.

2.3. Mass spectrometry

Wild type $CCMV_{TT}$-VLPs, Round- or Rod-shaped $CCMV_{TT}$-VLPs (1 mg/ml in buffer A) were diluted with a 2,5-Dihydroxyacetophenone (2,5-DHAPI) matrix solution and were spotted onto an MTP AnchorChip 400/384TF. Matrix assisted laser desorption/ionization (MALDI)-TOF MS analysis was carried out on an Autoflex MS (Bruker Scientific, Billerica, Massachusetts). The protein molecular mass (MM) calibration standard II (22.3–66.5 kDa; Bruker, Billerica, Massachusetts) was used for mass determination.

2.4. SDS-Page and gel electrophoresis

SDS-Page: 6 μg of Round- or Rod-shaped $CCMV_{TT}$-VLPs were mixed with 2× mercaptoethanol and heated at 95 °C for 3 min and then loaded into Any kD Mini-PROTEAN TGX precast protein gels (BIO-RAD, Hercules, California). Gel was run for 35 min at 180 V. As reference Page Ruler™ Prestained Protein Ladder was used (Thermo Fisher Scientific, Waltham, Massachusetts). Gel electrophoresis: 10 μg of Round- or Rod-shaped $CCMV_{TT}$-VLPs were loaded on a 1% agarose gel. Nucleic acids were visualized using Cybr Safe DNA Gel Stain (Life Technologies, Carlsbad, California). 5 μl Quick-Load Purple 1 kb DNA ladder (New England Biolabs, Ipswich, Massachusetts) was used as reference. Gel was run for 30 min at 100 V.

2.5. Mice

Wild type C57BL/6J mice were purchased from Harlan. All in vivo experiments were performed using 8–12 weeks old female mice. All animal procedures were conducted in accordance with the Swiss Animal Act (455.109.1 – September 2008, 5th).

2.6. Vaccination regimen

Wild type C57BL/6J mice (8–12 weeks, Harlan) were vaccinated subcutaneously (s.c.) with 15 μg Round- or Rod-shaped $CCMV_{TT}$-VLPs in 100 μl PBS on day 0. Mice were boosted with an identical dose on day 14. Serum samples were collected on days 0, 7, 14, 21, 28 and 35.

2.7. The enzyme-linked immunosorbent assay (ELISA)

For determination of total IgG antibody titers against Round- and Rod-shaped $CCMV_{TT}$-VLPs in sera of immunized mice, ELISA plates (Nunc Immuno MaxiSorp, Rochester, NY) were coated over night with Round- or Rod-shaped $CCMV_{TT}$-VLPs, respectively. Plates were washed with PBS-0.01%Tween and blocked using 100 μl PBS-Casein 0.15% for 2h. *Sera* from immunized mice were diluted 1/20 initially and a 1/3 dilution chain was performed. Plates were incubated for 1 h at 37 °C. After washing with PBS-0.01%Tween, goat anti-mouse IgG conjugated to Horseradish Peroxidase (HRP) (Jackson ImmunoResearch, West Grove, Pennsylvania) was added 1/1000 and incubated for 1 h at 37 °C. Plates were developed and OD 450 reading was performed.

IgG subclasses were measured from day 21 sera using the same ELISA protocol with the following secondary Abs: rat anti-mouse IgG1-HRP (BD Biosciences, San Jose, California) 1:1000, goat anti-mouse IgG2b-HRP (Thermo Fischer Scientific, Waltham, Massachusetts) 1:1000, goat anti-mouse IgG2c-HRP (Southern Biotech, Birmingham, Alabama) 1:4000, rat anti-mouse IgG3-biotin (Becton, Dickinson, Franklin Lakes, New Jersey) 1:2000 followed by streptavidin-HRP (Dako, Glostrup, Denmark) 1:1000 incubated at 37 °C for 1 h.

IgA was measured using day 35 sera. IgG was depleted using Dynabeads™ Protein G (Thermo Fischer Scientific, Waltham, Massachusetts). Serum was diluted 1/20 in PBS-Casein 0.15%. 25 μl beads were used per sample. Manufacturer's protocol was followed until step 3. of "Bind Antibody". Supernatant was added to ELISA plates and a 1/3 serial dilution was performed. For IgA detection, goat anti mouse IgA conjugated to HRP was used (Thermo Fisher Scientific, Waltham, Massachusetts) 1/4000.

For OD50 calculations, if a sample did not reach the threshold a value of 1 was appointed.

2.8. Measuring IFN- γ in mouse serum

Wild type C57BL/6J mice (8–12 weeks, Harlan) were vaccinated with 15 μg Round or Rod-shaped $CCMV_{TT}$-VLPs on day 0 and boosted on day 14. Serum from vaccinated mice was collected for measuring IFN- γ. ELISA MAX™ Deluxe Set Mouse IFN-γ (Biolegend, San Diego, California)

was performed according to manufacturer's instructions. Serum was used undiluted and concentration was interpolated to a standard curve of the sets standard sample.

2.9. Trafficking of Round- and Rod-shaped $CCMV_{TT}$-VLPs to draining lymph nodes

Round- or Rod-shaped $CCMV_{TT}$-VLPs were labelled with AF488 as per manufacturer's instructions (Thermo Fischer Scientific, Waltham, Massachusetts) and stored at −20 °C. Wild type C57BL/6J mice (8–12 weeks, Harlan) were injected with 10 μg of the VLPs in the footpad under isoflurane anesthesia. Popliteal LNs were collected 3 h and 24 h following footpad injection. Lymph nodes were treated with collagenase D (Roche, Basel, Switzerland) and DNase I (Boehringer, Ingelheim am Rhein, Germany) in DMEM medium containing 5% FBS and 1% Strep/Penicillin for 30 min at 37 °C. Lymph nodes were smashed using 70 μm cell strainers, RBCs were lysed with ACK buffer. Cells were stained with Fc block CD16/CD32 (FRC/4G8) and then with 7-AAD viability staining solution (Thermo Fisher Scientific, Waltham, Massachusetts) 1/500, anti-CD8 PE clone 53–6.7 (BD Biosciences, San Jose, California), anti-CD11c APC clone HL3 (BD Biosciences, San Jose, California), anti-CD11b PE-Cy7 clone M1/70 (Thermo Fisher Scientific, Waltham, Massachusetts), anti-F4/80 PE clone BM8 (Thermo Fisher Scientific, Waltham, Massachusetts), anti-CD19 APC-H7 clone 1D3 (BD Biosciences, San Jose, California), anti-CD45R/B220 PE-Cy7 clone RA3-6B2 and MHC-II PE clone M5/114.15.2 (Thermo Fisher Scientific, Waltham, Massachusetts) in different mixtures (gating strategy shown in Supplementary Fig. 1). Fluorescence labelled cells were recorded using a BD FACSCanto™ Flow Cytometer (BD Biosciences, San Jose, California).

2.10. Immunofluorescence

Round- or Rod-shaped $CCMV_{TT}$-VLPs were labelled with AF488 as per manufacturer's instructions (Thermo Fischer Scientific, Waltham, Massachusetts) and stored at −20 °C. Wild type C57BL/6J mice (8–12 weeks, Harlan) were injected with 10 μg of the VLPs in the footpad under isoflurane anesthesia. Popliteal LNs were collected 3 h and 24 h following footpad injection and embedded in Tissue-Tek optimum cutting temperature compound (Sakura, Torrance, California) without prior fixation. Cryostat sections (7 μm in thickness) on Superforst/Plus glass slides (Thermo Fischer Scientific, Waltham, Massachusetts) were air-dried overnight and then fixed for 10 min in ice-cold 100% acetone (PanReac, Barcelona, Spain). After rehydration (5 min in 1× PBS), sections were blocked with 1% (w/v) BSA (Sigma Aldrich, St. Louis, Missouri) and 1% (v/v) normal mouse serum. Immunofluorescence labeling was done with Abs diluted in PBS containing 0.1% (w/v) BSA and 1% (v/v) normal mouse serum. Sections were washed 3 times for 5 min in 1× PBS after every labeling step. LN staining: macrophages were detected using a primary antibody against CD11b (1/1000, rat anti mouse CD11b conjugated with PE; BD Biosciences, San Jose, California), B cell follicles were identified using rat anti mouse CD45/B220 Alexa F647 (1/1000; BD Biosciences, San Jose, California). Images were acquired on an Axioplan microscope using an AxioCam MRn (Zeiss).

2.11. Histology of lymph node

Round- or Rod-shaped $CCMV_{TT}$-VLPs were labelled with AF488 as per manufacturer's instructions (Thermo Fischer Scientific, Waltham, Massachusetts) and stored at −20. Wild type C57BL/6J mice (8–12 weeks, Harlan) were injected with 10 μg of the VLPs in the footpad under isoflurane anesthesia. Popliteal LNs were collected 3 h and 24 h following footpad injection and fixed with 4% paraformaldehyde solution (Sigma Aldrich, St. Louis, Missouri). Of each group, two to four murine popliteal LNs were histologically examined by a board-certified veterinary pathologist (SdB). Of each LN, a full cross section, stained with Hematoxylin and Eosin (HE), was assessed for any histopathological changes.

2.12. Statistical analysis

Data were analyzed and presented as mean ± SEM using GraphPad PRISM 8. Comparison between the groups was performed using the Mann-Whitney test. *p*-values are given as exact values.

3. Results

3.1. Directional insertion of tetanus toxin (TT) epitope in the N or C-terminus results in Round- or Rod-shaped $CCMV_{TT}$-VLPs

In a first step, we engineered CCMV-VLPs derived from a non-human pathogenic plant virus by incorporating a powerful T cell stimulatory epitope derived from tetanus toxin (TT) (830–843) at the N or C-terminus of CCMV-VLPs. The TT epitope was genetically fused to the capsid protein (CP) of CCMV-VLPs as has been previously described for our newly developed platform derived from cucumber-mosaic virus-like particles ($CuMV_{TT}$-VLPs) [34]. The introduced TT epitope is considered a universal epitope in humans as it is recognized by essentially all individuals. Since all individuals have been immunized against TT, memory Th cells may be able to help B cells to generate protective IgG even under more challenging conditions such as in aged populations [34]. CCMV-VLPs with insertion of TT epitope at the N-terminus retain their self-assembly as an icosahedron similar to the native virus. In contrast, insertion of TT epitope at the C-terminal end led to formation of Rod-shaped particles. Both Round- and Rod-shaped CCMV-VLPs forms carry a lysine to arginine mutation at residue 42 [35]. This mutation renders the VLPs less sensitive to pH and salt concentration (Ogrina, Balke, Zeltins; unpublished), which is an advantage in in vivo environments. Therefore, the engineered VLPs in this study are salt-stable (SS). The shape and integrity of the cloned VLPs were confirmed via electron microscopy which shows a size of ~30 nm in diameter for CCMV-Ntt-SS (Fig. 1a). The size of the $CCMV_{TT}$-Ctt-SS greatly varies in length but can reach up to more than 1 μm, with a width of about 30 nm. Fig. 1b shows a magnified image of $CCMV_{TT}$-Ctt-SS VLPs for easy comparison of their width with the icosahedral $CCMV_{TT}$-Ntt-SS VLPs in Fig. 1a. To reach a rather homogenous population, we performed sucrose gradient separation to focus on the long rods (Fig. 1c). For simplification we refer to the two forms of engineered $CCMV_{TT}$ in this paper as Round-shaped $CCMV_{TT}$-VLPs (CCMV-Ntt-SS) and Rod-shaped $CCMV_{TT}$-VLPs (CCMV-Ctt-SS).

To further characterize the two forms of $CCMV_{TT}$, we performed mass spectrometry (MS). MS data revealed a molecular weight for the CP monomers of Round- and Rod-shaped $CCMV_{TT}$-VLPs of roughly 21.8 and 21.9 kDa, respectively (Fig. 1d). The original CCMV-SS (salt-stable CCMV without TT insertion) is formed by CPs of roughly 20.2 kDa. Considering the weight of the TT 830–843 epitope of 1.611 kDa the obtained data are consistent with a fusion of the CCMV-SS CP to this epitope. Reducing SDS-page experiments confirmed these findings and showed bands for Round- and Rod-shaped $CCMV_{TT}$-VLPs of equal height at the appropriate position (Fig. 1e).

Both engineered $CCMV_{TT}$-VLPs were produced in an *E. coli* system. The VLPs packaged ssRNA derived from *E. coli* spontaneously, which serves as a potent TLR7/8 ligand. The concentration of RNA in both Round- and Rod-shaped $CCMV_{TT}$-VLPs was similar when measured at 260 nm. The RNA content of the Round-shaped $CCMV_{TT}$-VLPs could also be visualized by agarose gel electrophoresis, however this was less efficient for the Rod-shaped $CCMV_{TT}$-VLPs due to its large size which do not allow the particles to migrate through the gel. The agarose gel was also stained with Coomassie blue, staining the protein shell of VLPs (Fig. 1f and Supplementary Fig. 2).

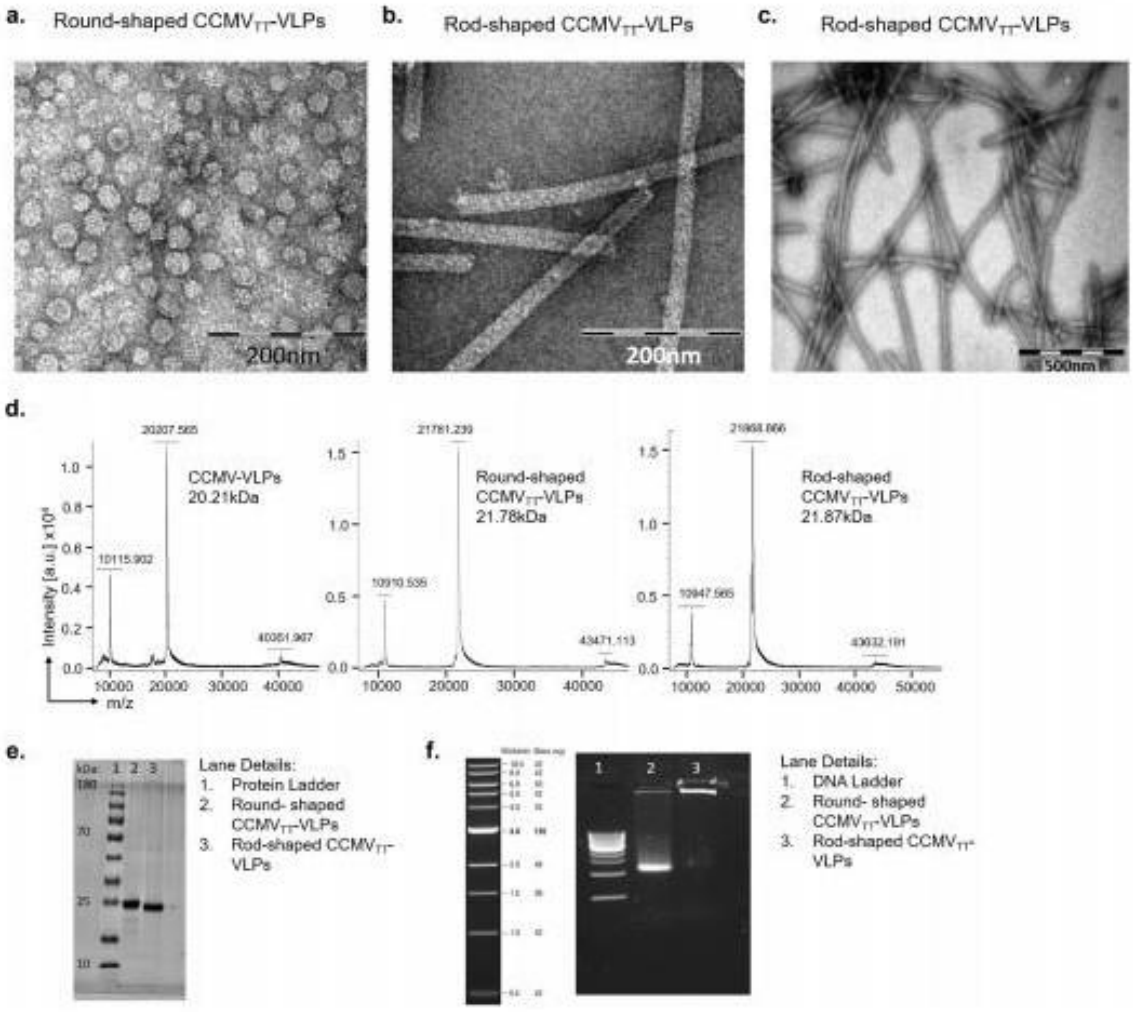

Fig. 1. *Directional insertion of tetanus toxin (TT) epitope in the N or C-terminus results in Round- or Rod-shaped CCMV$_{TT}$-VLPs. a*, EM of Round-shaped and b./c. Rod-shaped CCMV$_{TT}$-VLPs, adsorbed on carbon grids and negatively stained with uranyl acetate solution, scale bars 200 nm (Round) and 200 nm/500 nm (Rod). Round-shaped CCMV$_{TT}$-VLPs are ~30 nm in diameter, Rod-shaped CCMV$_{TT}$-VLPs are ~1 μm in length and ~ 30 nm in width. d, Mass spectrometry data, from left to right: wild type CCMV-VLPs, Round-shaped CCMV$_{TT}$-VLPs and Rod-shaped CCMV$_{TT}$-VLPs. *e*, Reducing SDS-Page stained with Coomassie-blue stain, lane 1: protein marker, lane 2: Round-shaped CCMV$_{TT}$-VLPs, lane 3: Rod-shaped CCMV$_{TT}$-VLPs. *f*, Agarose gel stained with SYBR safe, lane 1: DNA ladder, lane 2: Round-shaped CCMV$_{TT}$-VLPs, lane 3: Rod-shaped CCMV$_{TT}$-VLPs. (For interpretation of the references to color in this figure legend, the reader is referred to the web version of this article.)

3.2. *Round-shaped CCMV$_{TT}$-VLPs exhibit faster draining kinetics and interaction with cells in draining lymph nodes compared to Rod-shaped CCMV$_{TT}$-VLPs*

To test the role of size in lymphatic trafficking of the engineered VLPs, we assessed and visualized the accumulation and interaction of Round- or Rod-shaped CCMV$_{TT}$-VLPs in murine popliteal lymph nodes (LNs) 3 h and 24 h after injection in mouse footpads. To this end, Round- and Rod-shaped CCMV$_{TT}$-VLPs were labelled with AF488 and 10 μg of either VLPs were injected s.c. in the mouse footpad. The popliteal LN in each group was collected 3 h or 24 h following injection and processed as explained in the method section. We have studied the following cells for their ability to interact with CCMV$_{TT}$-VLPs: lymphoid-derived dendritic cells (DCs) characterized by CD8$^+$CD11c$^+$, conventional DCs (cDCs) characterized by CD8$^-$CD11c$^+$, macrophage-derived cells characterized by CD11b$^+$ and macrophages characterized by CD11b$^+$F4/80$^+$ as well as B cells identified by CD19$^+$ or more generally by CD45R/B220$^+$. Lymphoid-derived DCs or cDCs (Fig. 2a and b) did not show a significant increase in the interaction with Round- compared to Rod-shaped CCMV$_{TT}$-VLPs at 3 h. However, macrophages CD11b$^+$F4/80$^+$ (Fig. 2c), macrophage-derived cells CD11b$^+$ (Fig. 2d and h-top) as well as B cells CD19$^+$ (Fig. 2.e, f and h-middle) or CD45R/B220$^+$ (Fig. 2.g and h-bottom) were more efficient in interacting with Round-shaped CCMV$_{TT}$-VLPs than with the Rod-shaped ones at 3 h. Such findings confirm previous studies highlighting the ability of nanoparticles ranging from 20 to 200 nm to directly drain to the LNs [36,37].

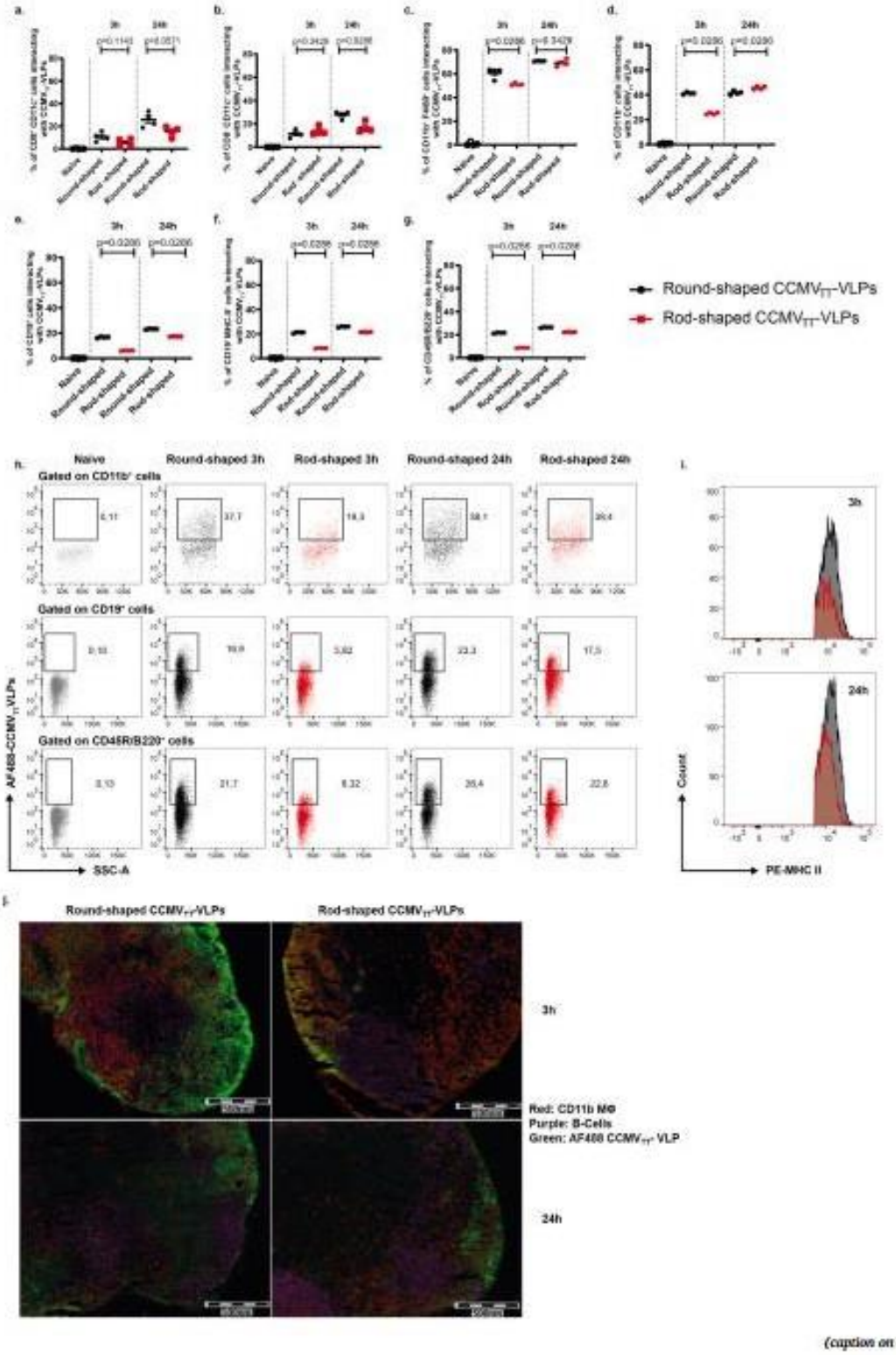

(caption on next page)

Fig. 2. *Round-shaped CCMV$_{TT}$-VLPs exhibit faster draining kinetics and interaction with cells in draining lymph nodes than Rod-shaped CCMV$_{TT}$-VLPs.* Percentage of different cell populations positive for AF488 labelled Round- and Rod-shaped CCMV$_{TT}$-VLPs in murine popliteal LNs 3 h and 24 h post injection in footpad: *a*, CD8$^+$CD11c$^+$ cells; *b*, CD8$^-$CD11c$^+$ cells; *c*, CD11b$^+$F4/80$^+$ cells; *d*, CD11b$^+$ cells. *e*, CD19$^+$ cells; *f*, CD19$^+$MHCII$^+$ cells and *g*, CD45R/B220$^+$ cells. *h*, Representative FACS plots showing the percentage of cells positive for AF488 labelled Round- and Rod-shaped CCMV$_{TT}$-VLPs in CD11b$^+$(top), CD19$^+$ (middle) and CD45R/B220$^+$ (bottom) cell populations in popliteal LNs 3 h and 24 h post injection in mouse footpads. *i*, Representative histogram counts of MHC-II expression gated on CD19$^+$ cells interacting with AF488 Round- (black color) and Rod-shaped CCMV$_{TT}$-VLPs (red color) at 3 h and 24 h post injection in mouse footpads. *j*, Immunofluorescence of popliteal LNs 3 h and 24 h post vaccination with Round- or Rod-shaped CCMV$_{TT}$-VLPs labelled with AF488, cytosections were treated with Abs detecting CD11b$^+$ cells (red color) and CD45/B220$^+$ cells (purple color). Mean ± SEM, 4 mice per group, one representative of 2 similar experiments is shown. (For interpretation of the references to color in this figure legend, the reader is referred to the web version of this article.)

Nevertheless, the Rod-shaped CCMV$_{TT}$-VLPs were also detectable in the popliteal draining LN 3 h post injection in the footpad, despite their micron-size. This could be due to the fact that the width of these rods is ~30 nm, similar to the diameter of the Round-shaped CCMV$_{TT}$-VLPs enabling their draining through the lymphatic vessels. Twenty-four hours following the injection in the footpad, there was no significant difference in the interaction between Round- or Rod-shaped CCMV$_{TT}$-VLPs with cDCs or macrophages. However, other subsets of macrophage-derived cells characterized by CD11b$^+$ were more efficient in interacting with Rod-shaped CCMV$_{TT}$-VLPs, further studies are required to characterize these subsets. B cells still showed a significantly increased interaction with the Round-shaped CCMV$_{TT}$-VLPs compared to the Rod-shaped ones. CD19$^+$ B cells interacting with Round-shaped CCMV$_{TT}$-VLPs showed a higher expression of MHC-II at 3 and 24 h (Fig. 2i). Additionally, we have calculated the percentage of CD11c$^+$, CD11b$^+$ F4/80$^+$, CD11b$^+$ and CD19$^+$ cell populations in the pool of total cells interacting with AF488 Round- or Rod-shaped CCMV$_{TT}$-VLPs in the popliteal LN 3 h after injection in the mouse footpad. The CD19$^+$ B cell

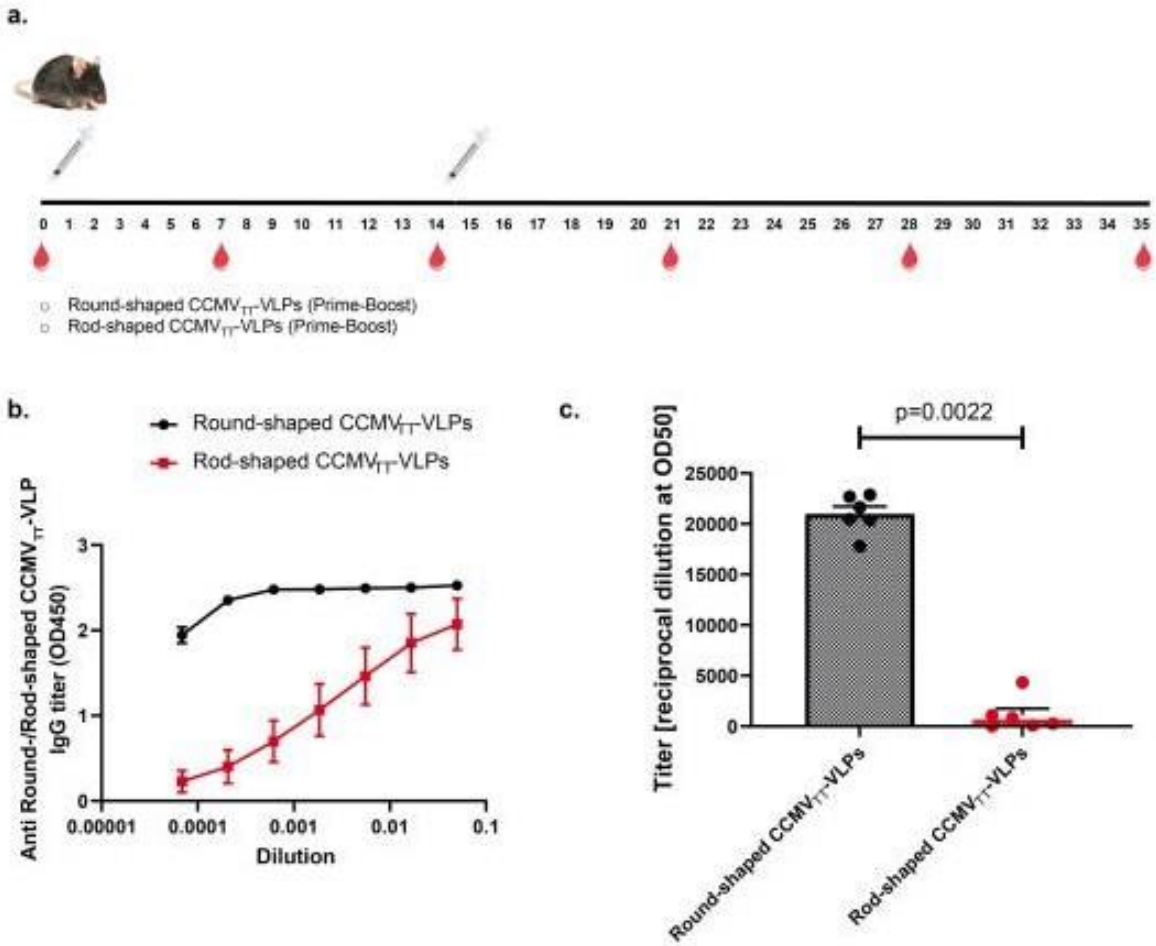

Fig. 3. *Round-shaped CCMV$_{TT}$-VLPs are more potent at inducing IgG antibodies than Rod-shaped CCMV$_{TT}$-VLPs.* *a*, Vaccination regimen and bleeding time-points. *b*, IgG titer of Round- and Rod-shaped CCMV$_{TT}$-VLP immunized mice measured in day 21 mice sera using OD450nm. ELISA plates were coated with Round-shaped CCMV$_{TT}$-VLPs for detecting IgG Abs in mice vaccinated with Round-shaped CCMV$_{TT}$-VLPs. ELISA plates were coated with Rod-shaped CCMV$_{TT}$-VLPs for detecting IgG Abs in mice vaccinated with Rod-shaped CCMV$_{TT}$-VLPs. *c*, OD50 titers of total IgG of Round- or Rod-shaped CCMV$_{TT}$-VLP immunized mice in day 21 sera given as reciprocal dilution values of data depicted. Mean ± SEM, 6 mice per group, one representative of 2 similar experiments is shown.

population contributes most to this pool (Supplementary Fig. 3).

We next followed the arrival of the labelled $CCMV_{TT}$-VLPs to the draining LNs by fluorescence microscopy of cryosections obtained from excised popliteal LNs at 3 h and 24 h following injection in the mouse footpad. The sections were co-stained with macrophage-derived cells and B cell markers, $CD11b^+$ and $CD45/B220^+$, respectively. The results demonstrate that AF488 Round-shaped $CCMV_{TT}$-VLPs accumulated in large numbers in the subcapsular sinus area (SCS), the cortex and the medullary sinus (MS) of the popliteal LNs 3 h post injection (Fig. 2j). $CD11b^+$ cells were prominent 3 h following injection with Round-shaped $CCMV_{TT}$-VLPs at the SCS and MS. Rod-shaped $CCMV_{TT}$-VLPs were less visible in the popliteal LN 3 h post injection in the footpad and their presence was confined to the SCS with scarce VLPs in the cortex. Twenty-four hours post injection, Round-shaped $CCMV_{TT}$-VLPs were found deeper in the popliteal LN. Whereas, this observation was less obvious for the Rod-shaped $CCMV_{TT}$-VLPs. B cells were detectable 3 h and 24 h post injection of the VLPs in the mouse footpads. As the accumulation of Round-shaped $CCMV_{TT}$-VLPs was prominent 3 h post injection in the footpad, the B cell signal was less noticeable. Twenty-four hours later the accumulation of B cells was pronounced at the SCS and the cortical area of the LN upon injection of both types of $CCMV_{TT}$-VLPs.

3.3. Round-shaped $CCMV_{TT}$-VLPs are more potent at inducing IgG antibodies than Rod-shaped $CCMV_{TT}$-VLPs

In a next step, we have assessed the humoral immune response induced by both engineered Round- and Rod-shaped $CCMV_{TT}$-VLPs. It is important to keep in mind that it is usually difficult to compare different sized particles for their immunogenicity as for spheres, the surface is proportional to radius $(r)^2$, while the weight will be proportional to $(r)^3$. Hence the weight of the injected particles grows much more rapidly than the surface, rendering a comparison difficult. In contrast, for rods, both the surface and weight are proportional to the length of the rod, rendering this comparison more appropriate.

Hence, C57BL/6J mice were vaccinated subcutaneously (s.c.) with 15 μg of Round- or Rod-shaped $CCMV_{TT}$-VLPs on day 0 and boosted once on day 14 as illustrated in Fig. 3a. Serum was collected on day 0 before vaccination and subsequently on days 7, 14, 21, 28 and 35. Total specific IgG response against Round- or Rod-shaped $CCMV_{TT}$-VLPs was assessed by ELISA. The Round-shaped $CCMV_{TT}$-VLPs were very potent at inducing specific IgG responses 7 days following the administration of the first dose. These responses were enhanced dramatically on days 14, 21, 28 and 35. On the contrary, vaccination with Rod-shaped $CCMV_{TT}$-VLPs led to low specific IgG titers after the first dose which have been increasing significantly only following boost on day 14 (Supplementary Fig. 4a and b). However, even following the boost specific IgG titers remained higher for Round-shaped $CCMV_{TT}$-VLP immunized mice, as shown for day 21 serum in Fig. 3b and c.

Even though subunits of both VLPs were almost identical, in order to test the cross-reactivity of both Round- and Rod-shaped $CCMV_{TT}$-VLPs, we have tested the collected sera in ELISA coated with the opposite VLP shape. Specifically, sera from mice vaccinated with Round-shaped $CCMV_{TT}$-VLPs were tested by ELISA on plates coated with Rod-shaped $CCMV_{TT}$-VLPs and vice versa. Our results showed that sera from mice vaccinated with Round-shaped $CCMV_{TT}$-VLPs are capable of recognizing the Rod-shaped $CCMV_{TT}$-VLPs after a single dose on day 7. The response was enhanced on days 14, 21, 28 and 35. However, sera from mice vaccinated with Rod-shaped $CCMV_{TT}$-VLPs could only significantly recognize the Round-shaped $CCMV_{TT}$-VLPs after boosting (Supplementary Fig. 4c and d). This indicates the same epitope(s) to be responsible for induction of humoral immune responses in both constructs, despite of different assembly of coat proteins and possible small differences in secondary/tertiary structure. In a next step, we have produced Rod-shaped $CCMV_{TT}$-VLPs exhibiting variation in lengths including smaller fragmented pieces of less than ~1 μm in length (By ways of using polyethylene glycol precipitation instead of sucrose gradient centrifugation for purification, as described for Round-shaped $CCMV_{TT}$-VLPs in the methods section; Supplementary Fig. 5a). The results showed that specific anti-IgG response against the Rod-shaped $CCMV_{TT}$-VLPs was enhanced substantially, indicating that indeed the rod-length limited the magnitude of the immune response (Supplementary Fig. 6a). In all other experiments presented in this paper the more homogeneous (~1 μm) long Rod-shaped $CCMV_{TT}$-VLPs were used.

3.4. Rod-shaped $CCMV_{TT}$-VLPs induce reduced switching to IgG2b/IgG2c in comparison to the Round-shaped $CCMV_{TT}$-VLPs

The C57BL/6J murine IgG family consists of four major subclasses IgG1, IgG2b, IgG2c and IgG3. Each unique subclass is implicated in distinct effector functions during humoral immune responses. VLPs and other nanoparticles induce a humoral response dominated by IgG1 in the absence of packaged RNA or DNA in mice [29,38,39]. Isotype switching to the protective IgG2 subtype is strictly TLR dependent. Thus, VLPs packaged with prokaryotic ssRNA during *E. coli* production induce a humoral immune response dominated with IgG2 subclasses [40,41]. Based on these grounds, we were interested in characterizing the different IgG subclasses in mice sera vaccinated with Round- or Rod-shaped $CCMV_{TT}$-VLPs, respectively. As explained earlier the engineered Round- and Rod-shaped $CCMV_{TT}$-VLPs package the same quantity of ssRNA. Therefore, TLR7/8 ligand effect can be eliminated as a confounding variable and the difference in the induced IgG subclasses can be correlated to the size of the VLPs. Our analysis revealed that Round-shaped $CCMV_{TT}$-VLPs significantly enhanced all IgG subclasses compared to the Rod-shaped ones. The difference, however, was most striking for TLR7/8 related subclasses IgG2b/c and IgG3 (Fig. 4a). By performing OD50 analysis we compared the titers (given as reciprocal dilution values) in both groups as depicted in Fig. 4b. Titers are significantly higher ($p. < 0.01$ for IgG1, IgG2b and IgG2c) ($p. < 0.05$ for IgG3) post immunization with Round-shaped $CCMV_{TT}$-VLPs. The ratio between Th1 and Th2 associated IgG subclasses was calculated next and it became evident that Th1 contribution is more pronounced with Round-shaped $CCMV_{TT}$-VLPs (Fig. 4c).

3.5. Systemic IgA response depends on size of VLPs

Previous studies have shown that s.c. injection of VLPs packaging RNA leads to a strong serum IgA in a Th-cell independent manner [40]. In addition, our previous findings revealed that systemic IgA response is heavily dependent on TLR7/8 in B cells [42]. The role of the size of VLPs packaging similar contents of RNA has not been investigated before, therefore we carried out an experiment to investigate this matter. Our findings indicate that Round-shaped $CCMV_{TT}$-VLPs could induce significantly higher ($p. < 0.01$) isotype switching to IgA when compared to the Rod-shaped ones (Fig. 5a and b). To rule out differences in type I Th cell induction, we have also measured IFN-γ in the serum of vaccinated mice on day 21; the results showed no significant difference ($p. > 0.9999$) between both groups (Fig. 5c). More specifically, factoring in the LOD (limit of detection) of the INF-γ detection kit of 4 ng/ml, we conclude, that neither Round- nor Rod-shaped $CCMV_{TT}$-VLPs are capable of inducing strong INF-γ responses.

3.6. Germinal center formation is prominent following a single dose of Round-shaped $CCMV_{TT}$-VLPs

Antigen reservoir persisting on follicular dendritic cells (fDCs) is essential for germinal centers (GC) to keep B cells stimulated and to generate a strong and long-lived antibody response. We therefore studied the formation of GCs in the spleens of mice vaccinated with Round- and Rod-shaped $CCMV_{TT}$-VLPs 12 days following a single s.c. dose of the engineered VLPs. Results showed that the formation of GCs in mice vaccinated with Round-shaped $CCMV_{TT}$-VLPs was significantly

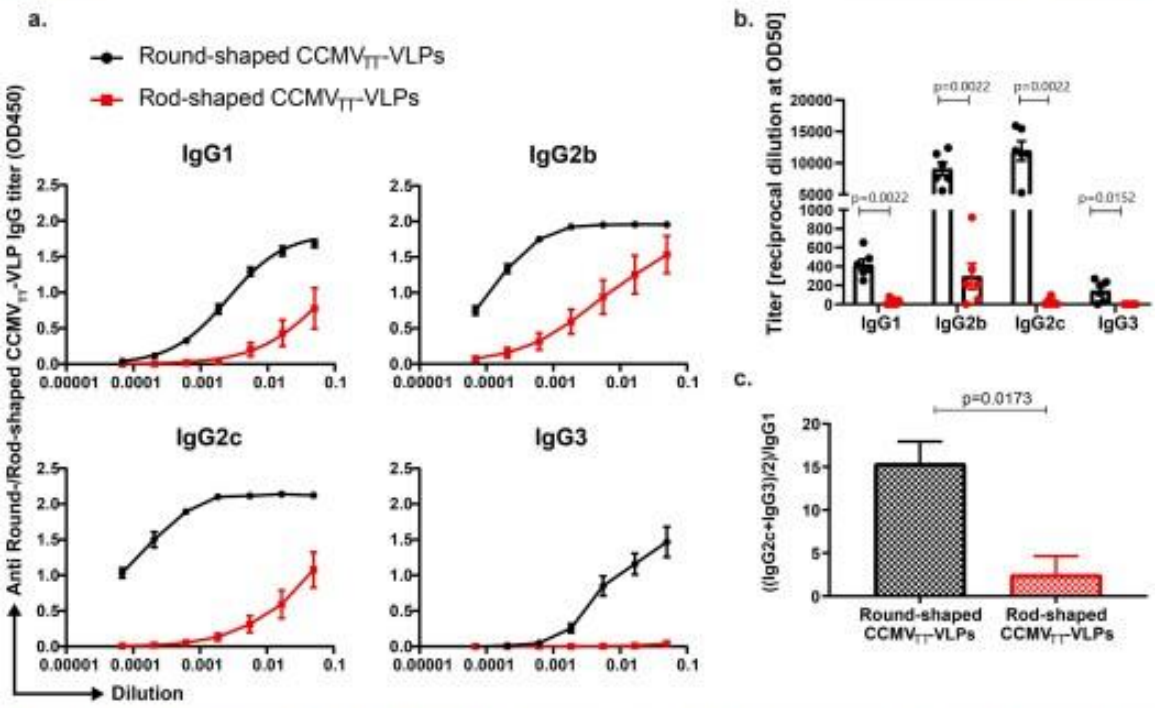

Fig. 4. *Rod-shaped CCMV$_{TT}$-VLPs induce reduced switching to IgG2c/IgG2b in comparison to the Round-shaped CCMV$_{TT}$-VLPs.* a, Anti-Round- and Rod-shaped CCMV$_{TT}$-VLP specific IgG1, IgG2b, IgG2c and IgG3 titers measured in day 21 mice sera using OD450nm. ELISA plates were coated with Round-shaped CCMV$_{TT}$-VLPs for detecting IgG subclasses in mice vaccinated with Round-shaped CCMV$_{TT}$-VLPs. ELISA plates were coated with Rod-shaped CCMV$_{TT}$-VLPs for detecting IgG subclasses in mice vaccinated with Rod-shaped CCMV$_{TT}$-VLPs. *b*, Anti-Round- and Rod-shaped CCMV$_{TT}$-VLP specific IgG1, IgG2b, IgG2c and IgG3 titers measured in day 21 mice sera using OD50 calculation of data depicted in *a*. *c*, Th1/Th2 ratio in Round- and Rod-shaped CCMV$_{TT}$-VLP immunized mice depicted as ((IgG2c + IgG3)/2)/IgG1 of OD50 values shown in *b*. Mean ± SEM, 6 mice per group, one representative of 2 similar experiments is shown.

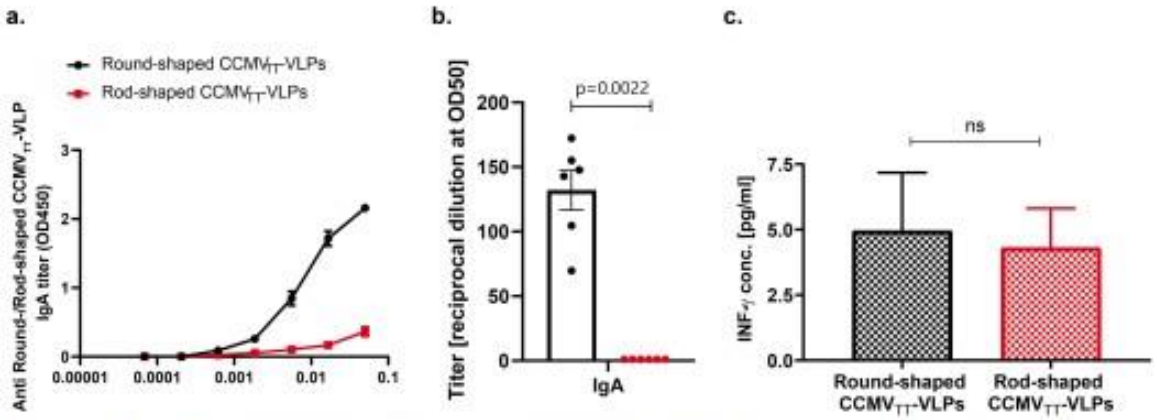

Fig. 5. *Systemic IgA response depends on size of VLPs.* a, Anti-Round- and Rod-shaped CCMV$_{TT}$-VLP specific IgA titers measured in day 35 serum from mice vaccinated with Round- and Rod-shaped CCMV$_{TT}$-VLPs using OD450nm. ELISA plates were coated with Round-shaped CCMV$_{TT}$-VLPs for detecting IgA Abs in mice vaccinated with Round-shaped CCMV$_{TT}$-VLPs. ELISA plates were coated with Rod-shaped CCMV$_{TT}$-VLPs for detecting IgA Abs in mice vaccinated with Rod-shaped CCMV$_{TT}$-VLPs. *b*, Anti-Round- and Rod-shaped CCMV$_{TT}$-VLP specific IgA titers measured in day 35 mice sera using OD50 calculations of data depicted in *a*. *c*, Concentration of IFN-γ measured in day 14 serum from mice vaccinated with Round- and Rod-shaped CCMV$_{TT}$-VLPs. Mean ± SEM, 6 mice per group, one representative of 2 similar experiments is shown.

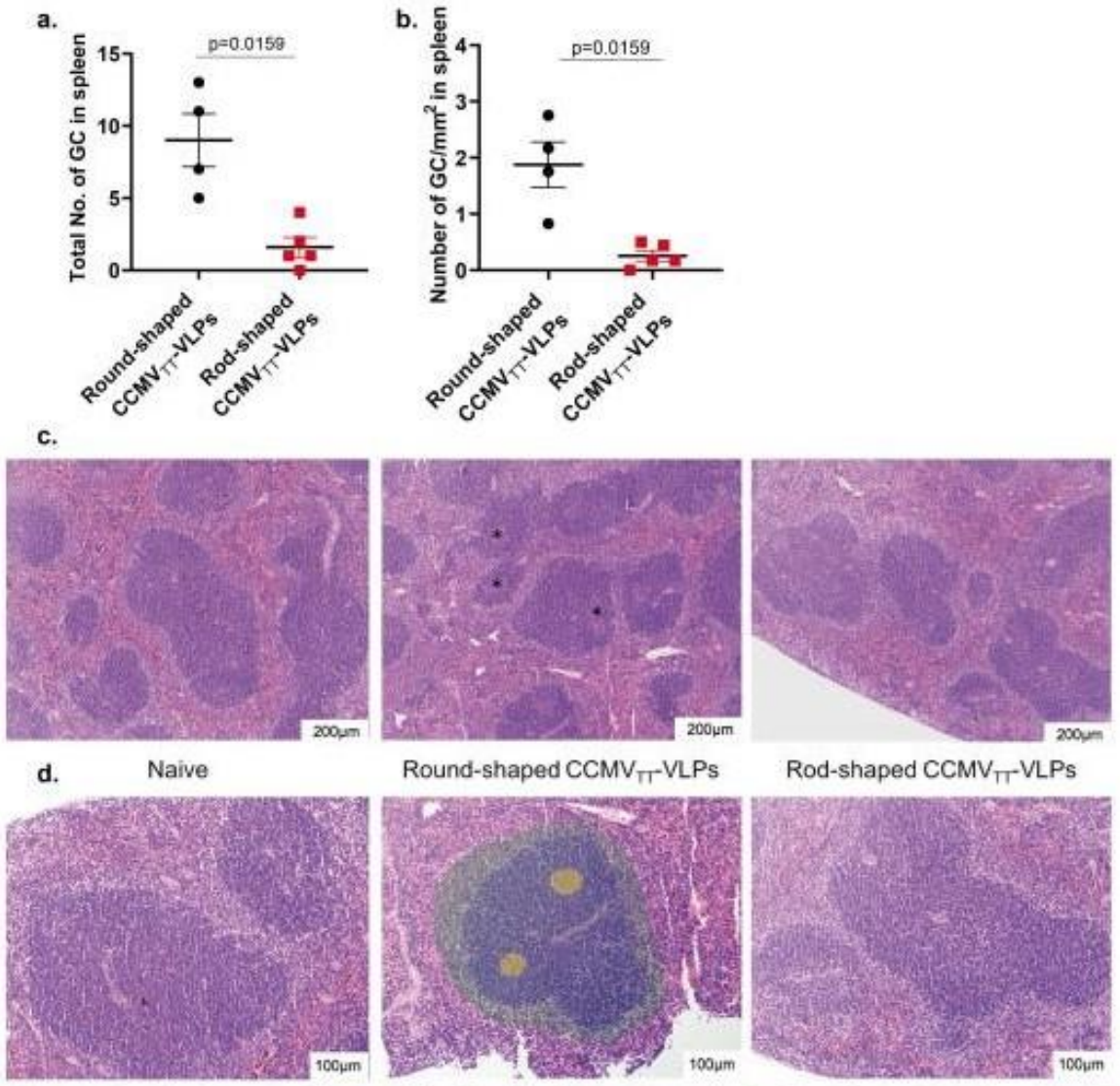

Fig. 6. *Germinal center formation is prominent following a single dose of Round-shaped CCMV$_{TT}$-VLPs.* a, Total number of germinal centers (GCs) in the examined splenic tissue fragments of mice vaccinated with a single dose of 15 µg of Round- or Rod-shaped CCMV$_{TT}$-VLPs. b, Number of GCs/mm^2 in spleen of mice vaccinated with a single dose of 15 µg of Round- or Rod-shaped CCMV$_{TT}$-VLPs. c, Histology of HE stained murine spleens, 10× objective. From the left: naïve spleen, lymph follicles lack evident GC formation; spleen of mice vaccinated with Round-shaped CCMV$_{TT}$-VLPs, lymph follicle present multifocal GC formation (*); last spleen of mice vaccinated with Rod-shaped CCMV$_{TT}$-VLPs, lymph follicle lack visible GCs. d, Higher magnification of c., 20× objective. From the left: naïve spleen, lymph follicles present with densely arranged lymphocytes without evident GC formation; spleen of mice vaccinated with Round-shaped CCMV$_{TT}$-VLPs, GCs (*) are visible within the lymph follicles, GCs and surrounding follicular and perifollicular zones are highlighted with colors (GCs (yellow), mantle zone (blue) and marginal zone (green)); last spleen of mice vaccinated with Rod-shaped CCMV$_{TT}$-VLPs, lymph follicles present with densely arranged lymphocytes without evident GC formation. Mean ± SEM, 2 splenic tissue fragments were analyzed from naïve group, 4 from Round-shaped CCMV$_{TT}$-VLPs group and 5 from Rod-shaped CCMV$_{TT}$-VLPs group. (For interpretation of the references to color in this figure legend, the reader is referred to the web version of this article.)

higher than in Rod-shaped CCMV$_{TT}$-VLP vaccinated mice when measuring the total number of GCs ($p. = 0.0159$) or the number of GCs/mm^2 ($p. = 0.0159$) (Fig. 6a and b). Histological examination of Hematoxylin and Eosin (HE) stained splenic tissue indicated the presence of multiple GCs within the lymphoid follicles upon vaccination with Round-shaped CCMV$_{TT}$-VLPs. On the other hand, mice vaccinated with Rod-shaped CCMV$_{TT}$-VLPs revealed only rare GC formation. Spleens from naïve C57BL/6J mice were used as a control (Fig. 6c and d). The examined spleens in mice vaccinated with Round- or Rod-shaped CCMV$_{TT}$-VLPs were free of any relevant degenerative or necrotic histopathological changes.

4. Discussion

In the current study we have engineered VLPs with nearly identical primary sequence but fundamentally different structural properties; one forming round icosahedrons with a diameter of around 30 nm while the other formed rods of about −1 μm. To this end, we inserted a universal tetanus toxin (TT) epitope at the N or C-terminus of cowpea chlorotic mottle virus (CCMV)-VLPs. The insertion of TT epitope at the N-terminus did not interfere with the original parental structure and resulted in icosahedral particles $T = 3$; named in this study as Round-shaped $CCMV_{TT}$-VLPs. However, inserting TT epitope at the C-terminus of CCMV-VLPs caused the formation of Rod-shaped $CCMV_{TT}$-VLPs of −1 μm in length and − 30 nm in width. As both engineered VLPs were expressed in *E. coli*, they packaged a similar quantity of ssRNA serving as TLR7/8 agonists recognized by PRRs (pattern recognition receptors) for effective stimulation of the innate immune system. This allowed us to study the impact of size on drainage dynamics and the magnitude of the induced immune responses with one and the same VLP monomer while excluding the effect of TLR7/8 ligands. As mentioned above, both the surface and mass of rods are proportional to the diameter and length, allowing to vary the surface exposed to B cells with a proportional change in mass.

B cell activation by antigens is a critical step for effective initiation of the adaptive immune response [7]. Particulate antigens like VLPs can be passively or actively transported in association with e.g. dendritic cells to the lymphoid organs following injection. The passive transportation is based on their ability to drain freely through the pores of the lymphatic vessels 200 nm in diameter [43] as VLPs have an ideal size of −30-50 nm.

Our previous studies have shown that icosahedral VLPs such as bacteriophage Qβ-VLPs and VLPs derived from cucumber-mosaic virus ($CuMV_{TT}$-VLPs) can freely reach the draining LN in less than a minute, both having a size of −30 nm [9,10,44]. By contrast, particulate antigens larger than 500 nm cannot efficiently enter the lymphatic capillaries [45,46]. Instead, they need to be actively transported via specialized cells [47]. To visualize the trafficking kinetics of the engineered Round- and Rod-shaped $CCMV_{TT}$-VLPs (−30 nm and − 1 μm) respectively, they were labelled with AF488 and injected in mouse footpads. Flow cytometric analysis and cryosections of the popliteal LNs 3 h and 24 h post injection were performed. The results demonstrate an increase in the drainage of the Round-shaped $CCMV_{TT}$-VLPs 3 h following injection in mice footpad via the lymphatic vessels, which have pores of −200 [43]. Nevertheless, in lower amounts Rod-shaped $CCMV_{TT}$-VLPs have also been detected in the draining popliteal LN 3 h post injection in the mouse footpad. This observation could be explained by the fact that Rod-shaped $CCMV_{TT}$-VLPs exhibit a width of −30 nm which might allow them to drain into the lymphatic capillaries despite their length. Indeed, if spheres of >500 nm size are used for injection, these spheres required 24 h to arrive in LNs and fully depend on cellular transport [36].

Different subsets of cells, including APCs, interacted with Round- or Rod-shaped $CCMV_{TT}$-VLPs upon injection in mouse footpads. There was no difference in the interaction between lymphoid-derived or conventional DCs with both shapes of $CCMV_{TT}$-VLPs 3 h post injection with increased interaction of Round- compared to Rod-shaped VLPs after 24 h. Macrophages, other macrophage-derived cells as well as B cells were more efficient in interacting with Round-shaped $CCMV_{TT}$-VLPs compared to the Rod-shaped ones. The subcapsular sinus macrophages are considered the frontline cells to capture pathogens in the draining LN and retain them from entering the LN parenchyma. Afterwards they relay the antigen to B cells for efficient priming and induction of humoral immune responses [48]. Yolanda et al. proposed a model for particulate-antigen acquisition by B cells. The model suggests that particulate antigens firstly accumulate in the macrophage-niche area in the SCS of the draining LN followed by a still unknown filtration process of the antigens to the follicle. Next, non-antigen specific B cells carry particles via binding of antigens to complement receptor from the SCS to be deposited on follicular dendritic cells (FDCs) [44]. Our fluorescent microscopy cryosections could demonstrate such findings as Round-shaped $CCMV_{TT}$-VLPs were more efficient in draining to the popliteal LNs 3 h post injection in the mouse footpad where macrophages could also be abundantly observed. 24 h later the Round-shaped $CCMV_{TT}$-VLPs could be detected deeper in the LN. The interaction of the Round-shaped $CCMV_{TT}$-VLPs with B cells with increased MHC-II expression was significantly higher ($p. = 0.0286$) when compared to the Rod-shaped $CCMV_{TT}$-VLPs, both at 3 h and 24 h post injection in the footpad as shown using FACS analysis. This is consistent with our previous observation that Round-shaped VLPs bind to B cells in a complement and CD21-dependent manner [49] and may suggest an impaired ability of B cells to bind Rod-shaped $CCMV_{TT}$-VLPs.

The repetitive surface geometry of VLPs enhance their cross-linking to B cells and ability to activate complement [7]. $T = 3$ VLPs are capable of cross-linking up to 180 BCRs resulting in a strong humoral immune response. $T = 3$ VLPs may be favorable over $T = 1$ as the later can cross-link maximally −60 BCRs which is at the threshold for an optimal immune response [50]. However, data are scarce regarding Rod-shaped VLPs and their ability to activate B cells. In this study, we show that a single priming injection of Round-shaped $CCMV_{TT}$-VLPs was efficient at inducing a high specific Ab titer which was further enhanced upon boosting on day 14. On the contrary, the Rod-shaped $CCMV_{TT}$-VLPs could only induce a specific Ab response following boosting on day 14 which remained much reduced compared to the Round-shaped VLP induced response. These results were confirmed by the significantly increased formation of total no. of GCs ($p. = 0.0159$) as well as no. of GCs/mm^2 ($p. = 0.0159$) in spleens 12 days following vaccination with Round-shaped $CCMV_{TT}$-VLPs.

When testing the sera from vaccinated mice against the opposite engineered VLPs, Round-shaped $CCMV_{TT}$-VLPs were also more efficient in inducing IgG antibodies recognizing the Rod-shaped VLPs even after a single dose. These data indicate that icosahedral VLPs are capable of inducing specific Ab directed against other forms of the same VLPs in an efficient manner and that 30 nm sized round VLPs are far superior over 1 μm sized rods.

To achieve successful IgG class-switching and memory formation in B cells, co-delivery of innate immune stimuli is crucial [21]. It has been shown that class-switching to IgG2a/c and IgG2b is dependent on simultaneous engagement of BCR and TLR9 after immunization with particulate antigens [51,52]. Furthermore, TLR7 engagement with different RNA types influenced the outcome of the humoral immune response to VLP immunization. Bacterial RNA pointed the immune response toward IgG2 production, whereas eukaryotic RNA induced responses favored higher IgG1 titers [53]. IgG1 is associated with Th2 responses, whereas IgG2a/c and IgG3 is associated with Th1 responses even though TLR-signaling in B cells is key for IgG subclass induction. The obtained data reveal that Round-shaped $CCMV_{TT}$-VLPs were more efficient than the Rod-shaped VLPs at inducing class-switching. Furthermore, the ratio between Th1 and Th2 associated IgG subclasses was more significantly increased ($p. = 0.0173$) when vaccinating with Round-shaped $CCMV_{TT}$-VLPs. As class switching to IgG2a/b as well as IgA is driven by TLR7/8 signaling in B cells, these results suggest that it is easier for B cells to interact with and process particles of −30 nm size rather than micron-sized structures.

Similar to IgG2a responses, VLPs packaged with RNA lead to a strong systemic IgA response. We have shown previously that serum IgA responses are Th cell independent [40] and require TLR7/8 or 9 to induce a systemic response [42]. Here, we show that the systemic IgA response measured on day 21 using a s.c. prime-boost regimen was much higher in mice vaccinated with Round-shaped $CCMV_{TT}$-VLPs than in mice vaccinated with Rod-shaped $CCMV_{TT}$-VLPs ($p. = 0.0022$).

It has previously been shown that particle-drainage trafficking into B cell and T cell areas of the lymph node is heavily dependent on the size of the particles. Indeed, particles smaller 200 nm usually freely enter the

lymphatic system via fenestrated lymph vessels while larger particles need to be transported by e.g. dendritic cells. This results in small particles reaching subcapsular sinuses within minutes while larger particles (>200 nm) typically reach lymph nodes after 24 h and mainly reach T cell zones as this is the region dendritic cells typically target. Despite the clearness of these results a direct impact on B cell responses has been difficult to assess; mainly because B cells respond to antigens on surfaces and the surface of the particle grows proportionally to the square of the radius (r^2) while volume/weight is proportional to r^3. Hence, to compare particles with 10-fold different radius, 10-fold increased dose (weight) of the larger particle must be injected for compensation of differences in the surface. Consequently, direct comparison of B cell responses induced by small and large particles becomes impossible. This is, however, a very important point, as adjuvant may vary in size between nanometers and micrometers. In the current study, we used rods versus icosahedra built up by essentially the same monomer. As both the surface and the weight of rods is proportional to the length of the rod, B cell responses by Rod- and Round-shaped VLPs are more directly comparable. We find that Round-shaped VLPs are more immunogenic for B cells by orders of magnitude, highlighting that VLPs of a size smaller than 200 nm are optimal for induction of B cell responses. In a next study, we will address the importance of rod size on B cell receptor and TLR7/8 stimulation and will also determine whether rods of homogenously small size are equally immunogenic as round VLPs.

Authors' contributions

Design of experiments, acquisition of data, interpretation of data and analysis of data: SZ, AO, SdB, CL, XC, MFB and MOM; VLP design, expression and production: AO, IB, GR and AZ; H&E stains and IF microscopy: SdB, CL, XC; Writing and revision of manuscript: SZ, MOM, AO, MFB, MV and AZ; Technical and material support: LZ, Study supervision: MOM and MFB. All authors read and approved the final manuscript.

Declaration of Competing Interest

The authors declare no competing interests

Acknowledgment

This work was supported by Qatar National Research Fund (PDRA4-0118-18002), the Swiss National Science Foundation (SNF 310030_185114 and SNF 310030_179165) and by Latvian Science Council (Grant No. lzp-2019/1-0131).

Appendix A. Supplementary data

Supplementary data to this article can be found online at https://doi.org/10.1016/j.jconrel.2021.01.012.

References

[1] F.H. Crick, J.D. Watson, Structure of small viruses, Nature 177 (4506) (Mar 10 1956) 473–475, https://doi.org/10.1038/177473a0.
[2] D.L. Caspar, Movement and self-control in protein assemblies. Quasi-equivalence revisited, Biophys. J. 32 (1) (Oct 1980) 103–138, https://doi.org/10.1016/S0006-3495(80)84929-0.
[3] J. Luoten, Essential Human Virology, 2017, p. 344.
[4] A.C. Gomes, M. Mohsen, M.F. Bachmann, Harnessing Nanoparticles for Immunomodulation and Vaccines, Vaccines (Basel) 5 (1) (Feb 14 2017), https://doi.org/10.3390/vaccines5010006.
[5] M.O. Mohsen, A.C. Gomes, M. Vogel, M.F. Bachmann, Interaction of Viral Capsid-Derived Virus-Like Particles (VLPs) with the Innate Immune System, Vaccines (Basel) 6 (3) (Jul 2 2018), https://doi.org/10.3390/vaccines6030037.
[6] M.F. Bachmann, U.H. Rohrer, T.M. Kundig, K. Burki, H. Hengartner, R. M. Zinkernagel, The influence of antigen organization on B cell responsiveness, Science 262 (5138) (Nov 26 1993) 1448–1451, https://doi.org/10.1126/science.8248784.
[7] M.F. Bachmann, G.T. Jennings, Vaccine delivery: a matter of size, geometry, kinetics and molecular patterns, Nat Rev Immunol 10 (11) (Nov 2010) 787–796, https://doi.org/10.1038/nri2868.
[8] J.E. Gretz, C.C. Norbury, A.O. Anderson, A.E. Proudfoot, S. Shaw, Lymph-borne chemokines and other low molecular weight molecules reach high endothelial venules via specialized conduits while a functional barrier limits access to the lymphocyte microenvironments in lymph node cortex, J Exp Med 192 (10) (Nov 20 2000) 1425–1440, https://doi.org/10.1084/jem.192.10.1425.
[9] M.O. Mohsen, et al., Delivering adjuvants and antigens in separate nanoparticles eliminates the need of physical linkage for effective vaccination, J. Control. Release 251 (Apr 10 2017) 92–100, https://doi.org/10.1016/j.jconrel.2017.02.031.
[10] M.O. Mohsen, et al., Correction to: Vaccination with nanoparticles combined with micro-adjuvants protects against cancer, J Immunother Cancer 7 (1) (May 23 2019) 137, https://doi.org/10.1186/s40425-019-0616-y.
[11] D.L. Caspar, A. Klug, Physical principles in the construction of regular viruses, Cold Spring Harb. Symp. Quant. Biol. 27 (1962) 1–24, https://doi.org/10.1101/sqb.1962.027.001.005.
[12] M.O. Mohsen, G. Augusto, M.F. Bachmann, The 3Ds in virus-like particle based-vaccines: "Design, Delivery and Dynamics", Immunol Rev (May 30) (2020) https://doi.org/10.1111/imr.12863.
[13] J.W. Wang, R.B. Roden, Virus-like particles for the prevention of human papillomavirus-associated malignancies, Expert Rev Vaccines 12 (2) (Feb 2013) 129–141, https://doi.org/10.1586/erv.12.151.
[14] T.S. Guu, et al., Structure of the hepatitis E virus-like particle suggests mechanisms for virus assembly and receptor binding (in eng), Proc Natl Acad Sci U S A 106 (31) (Aug 4 2009) 12992–12997, https://doi.org/10.1073/pnas.0904848106.
[15] J.K. Ho, B. Jeevan-Raj, H.J. Netter, Hepatitis B Virus (HBV) Subviral Particles as Protective Vaccines and Vaccine Platforms (in eng), Viruses 12 (2) (Jan 21 2020), https://doi.org/10.3390/v12020126.
[16] M.L. Chapman, Advances in Protein Chemistry, 2003, pp. 1–253.
[17] P. Ge, Z.H. Zhou, Hydrogen-bonding networks and RNA bases revealed by cryo electron microscopy suggest a triggering mechanism for calcium switches, Proceedings of the National Academy of Sciences 108 (23) (2011) 9637, https://doi.org/10.1073/pnas.1018104108.
[18] Y. Zhang, Y.X. Dong, J.H. Zhou, X. Li, F. Wang, Application of Plant Viruses as a Biotemplate for Nanomaterial Fabrication (in English), Molecules 23 (9) (Sep 2018), https://doi.org/10.3390/molecules23092311. doi: ARTN 2311.
[19] I. Balke, A. Zeltins, Recent Advances in the Use of Plant Virus-Like Particles as Vaccines (in English), Viruses-Basel 12 (3) (Mar 2020), https://doi.org/10.3390/v12030270. doi: ARTN 270.
[20] I. Cielens, et al., Mutilation of RNA phage Qbeta virus-like particles: from icosahedrons to rods, FEBS Lett 482 (3) (Oct 6 2000) 261–264, https://doi.org/10.1016/s0014-5793(00)02061-5.
[21] G.T. Jennings, M.F. Bachmann, The coming of age of virus-like particle vaccines in: Biological Chemistry Volume 389 Issue 5 (2008), in: Biological Chemistry, Volume 389: Issue 5, ed, 2008.
[22] G.T. Jennings, M.F. Bachmann, Immunodrugs: Therapeutic VLP-Based Vaccines for Chronic Diseases, in: Annual Review of Pharmacology and Toxicology vol. 49, 2009, pp. 303–326, ed: Annual Reviews.
[23] G. Cabral-Miranda, et al., Zika Virus-Derived E-DIII Protein Displayed on Immunologically Optimized VLPs Induces Neutralizing Antibodies without Causing Enhancement of Dengue Virus Infection, Vaccines (Basel) 7 (3) (Jul 23 2019), https://doi.org/10.3390/vaccines7030072.
[24] F. Olomski, et al., Interleukin 31 in insect bite hypersensitivity-alleviating clinical symptoms by active vaccination against itch, Allergy 75 (4) (Apr 2020) 862–871, https://doi.org/10.1111/all.14145.
[25] A. Fettelschoss-Gabriel, et al., Active vaccination against interleukin-5 as long-term treatment for insect-bite hypersensitivity in horses, Allergy 74 (3) (Mar 2019) 572–582, https://doi.org/10.1111/all.13689.
[26] F. Thoms, et al., Immunization of cats to induce neutralizing antibodies against Fel d 1, the major feline allergen in human subjects, J. Allergy Clin. Immunol. 144 (1) (Jul 2019) 195–203, https://doi.org/10.1016/j.jaci.2019.01.050.
[27] F. Storni, et al., Vaccine against peanut allergy based on engineered virus-like particles displaying single major peanut allergens, J Allergy Clin Immunol 145 (4) (Apr 2020), https://doi.org/10.1016/j.jaci.2019.12.007, 1240–1253 e3.
[28] G. Cabral-Miranda, et al., DOPS Adjuvant Confers Enhanced Protection against Malaria for VLP-TRAP Based Vaccines (in eng), Diseases (Basel, Switzerland) 6 (4) (2018) 107, https://doi.org/10.3390/diseases6040107.
[29] G.P. Pogue, J.A. Lindbo, S.J. Garger, W.P. Fitzmaurice, Making an ally from an enemy: plant virology and the new agriculture, Annu. Rev. Phytopathol. 40 (2002) 45–74, https://doi.org/10.1146/annurev.phyto.40.021102.150133.
[30] M.L. Smith, et al., Modified tobacco mosaic virus particles as scaffolds for display of protein antigens for vaccine applications, Virology 348 (2) (May 10 2006) 475–488, https://doi.org/10.1016/j.virol.2005.12.039.
[31] A. Hassani-Mehraban, S. Creutzburg, L. van Heereveld, R. Kormelink, Feasibility of Cowpea chlorotic mottle virus-like particles as scaffold for epitope presentations (in English), Bmc Biotechnol 15 (Aug 27 2015), https://doi.org/10.1186/s12896-015-0180-6. doi: ARTN 80.
[32] J.A. Speir, S. Munshi, G. Wang, T.S. Baker, J.E. Johnson, Structures of the native and swollen forms of cowpea chlorotic mottle virus determined by X-ray crystallography and cryo-electron microscopy, Structure 3 (1995) 63–78, ed.
[33] K.W. Adolph, P.J. Butler, Studies on the assembly of a spherical plant virus. I. States of aggregation of the isolated protein (in eng), Journal of molecular biology 88 (2) (Sep 15 1974) 327–341, https://doi.org/10.1016/0022-2836(74)90485-9.
[34] A. Zeltins, et al., Incorporation of tetanus-epitope into virus-like particles achieves vaccine responses even in older recipients in models of psoriasis, Alzheimer's and

cat allergy, NPJ Vaccines 2 (2017) 30, https://doi.org/10.1038/s41541-017-0030-8.
[35] J.M. Fox, X. Zhao, J.A. Speir, M.J. Young, Analysis of a salt stable mutant of cowpea chlorotic mottle virus, in: Virology vol. 222, ed: Academic Press Inc, 1996, pp. 115–122.
[36] V. Manolova, A. Flace, M. Bauer, K. Schwarz, P. Saudan, M.F. Bachmann, Nanoparticles target distinct dendritic cell populations according to their size (in English), European Journal of Immunology 38 (5) (May 2008) 1404–1413, https://doi.org/10.1002/eji.200737984.
[37] L. Kahari, et al., Transcytosis route mediates rapid delivery of intact antibodies to draining lymph nodes, J Clin Invest 129 (8) (Jun 24 2019) 3086–3102, https://doi.org/10.1172/JCI125740.
[38] G.T. Jennings, M.F. Bachmann, The coming of age of virus-like particle vaccines, Biol. Chem. 389 (5) (May 2008) 521–536, https://doi.org/10.1515/bc.2008.064.
[39] C. G. A, E.S. Roesti, A. El-Turabi, M.F. Bachmann, Type of RNA Packed in VLPs Impacts IgG Class Switching-Implications for an Influenza Vaccine Design, Vaccines (Basel) 7 (2) (Jun 4 2019), https://doi.org/10.3390/vaccines7020047.
[40] J. Bessa, M.F. Bachmann, T cell-dependent and -independent IgA responses: role of TLR signalling, Immunol. Investig. 39 (4–5) (2010) 407–428, https://doi.org/10.3109/08820131003663357.
[41] A. Jegerlehner, P. Maurer, J. Bessa, H.J. Hinton, M. Kopf, M.F. Bachmann, TLR9 signaling in B cells determines class switch recombination to IgG2a, J Immunol 178 (4) (Feb 15 2007) 2415–2420, https://doi.org/10.4049/jimmunol.178.4.2415.
[42] J. Bessa, et al., Alveolar macrophages and lung dendritic cells sense RNA and drive mucosal IgA responses, J Immunol 183 (6) (Sep 15 2009) 3788–3799, https://doi.org/10.4049/jimmunol.0804004.
[43] Y.A.P.P. Khudyakov, viral nanotechnology, Taylor and Francis Group LLC, 2016.
[44] Y.R. Carrasco, F.D. Batista, B cells acquire particulate antigen in a macrophage-rich area at the boundary between the follicle and the subcapsular sinus of the lymph node, Immunity 27 (1) (Jul 2007) 160–171, https://doi.org/10.1016/j.immuni.2007.06.007.
[45] S.T. Reddy, et al., Exploiting lymphatic transport and complement activation in nanoparticle vaccines, Nat. Biotechnol. 25 (10) (Oct 2007) 1159–1164, https://doi.org/10.1038/nbt1332.
[46] D.A. Berk, M.A. Swartz, A.J. Leu, R.K. Jain, Transport in lymphatic capillaries. II. Microscopic velocity measurement with fluorescence photobleaching, Am. J. Phys. 270 (1 Pt 2) (Jan 1996) H330–H337, https://doi.org/10.1152/ajpheart.1996.270.1.H330.
[47] V. Manolova, A. Flace, M. Bauer, K. Schwarz, P. Saudan, M.F. Bachmann, Nanoparticles target distinct dendritic cell populations according to their size, Eur. J. Immunol. 38 (5) (May 2008) 1404–1413, https://doi.org/10.1002/eji.200737984.
[48] D.A.P. Louie, S. Liao, Lymph Node Subcapsular Sinus Macrophages as the Frontline of Lymphatic Immune Defense (in English), Frontiers in Immunology 10 (Feb 28 2019), https://doi.org/10.3389/fimmu.2019.00347. doi: ARTN 347.
[49] M.O. Mohsen, D.E. Speiser, A. Knuth, M.F. Bachmann, Virus-like particles for vaccination against cancer, Wiley Interdiscip Rev Nanomed Nanobiotechnol 12 (1) (Jan 2020) e1579, https://doi.org/10.1002/wnan.1579.
[50] A. Jegerlehner, T. Storni, G. Lipowsky, M. Schmid, P. Pumpens, M.F. Bachmann, Regulation of IgG antibody responses by epitope density and CD21-mediated costimulation, Eur. J. Immunol. 32 (11) (Nov 2002) 3305–3314, https://doi.org/10.1002/1521-4141(200211)32:11<3305::AID-IMMU3305>3.0.CO;2-J.
[51] J. Eckl-Dorna, F.D. Batista, BCR-mediated uptake of antigen linked to TLR9 ligand stimulates B-cell proliferation and antigen-specific plasma cell formation, Blood 113 (17) (Apr 23 2009) 3969–3977, https://doi.org/10.1182/blood-2008-10-185421.
[52] B. Hou, et al., Selective utilization of toll-like receptor and MyD88 signaling in B cells for enhancement of the antiviral germinal center response, in: Immunity vol. 34, 2011, pp. 375–384, ed: NIH Public Access.
[53] A.C. Gomes, E.S. Roesti, A. El-Turabi, M.F. Bachmann, Type of RNA packed in VLPs impacts IgG class switching—implications for an influenza vaccine design, in: Vaccines vol. 7, 2019 ed: MDPI AG.

3.2. Comparison of bacterial expression systems based on potato virus Y- like particles for vaccine generation

3.2.1. Construction and characterization of PVY CP Feld1 constructs

In the VLP vaccine development, there exist various techniques for antigen incorporation including genetic, enzymatic, chemical, and physical methods. Our prior findings with filamentous plant-derived VLPs have demonstrated their capacity to host large protein domains on their surface, either through N- or C-terminal fusion, while maintaining VLP integrity (Kalnciema *et.al.,* 2012). This study outlines the development and comparison of simple *E. coli*-based platforms for displaying antigens, producing vaccines derived from PVY VLPs.

We established four distinct systems involving the major cat allergen, Feld1. These approaches included direct fusion with the CP of the plant virus potato virus Y (PVY), mosaic PVY VLPs, and two coexpression variants with the SpyTag/SpyCatcher (full size – SpyC3 and truncated - SpyC2) system. These coexpression systems enabled both expression and conjugation to occur directly in *E. coli* cells, simplifying the procedure by combining VLP production, antigen synthesis, and purification into a single step. All the PVY-Feld1 versions we created showed strong expression and remained soluble, resulting in PVY-like filamentous particles in various sizes ranging from 400 – 800 nm for direct fusion and mosaic system, 200 – 400 nm for PVY-SpyT/SpyC2 or 3 - Feld1 conjugate protein VLPs. The output of all constructed VLPs varied between 10 – 12 mg/g biomass.

We detected the presence of nucleic acids in purified VLP samples through NAG electrophoresis with ethidium bromide staining. Our observation revealed that all vaccine variations displayed visible nucleic acid signals, with both of SpyT/SpyC constructs exhibiting the most pronounced signals. As anticipated, filamentous VLPs, due to their substantial size, were unable to migrate effectively within the agarose gel, resulting in bands forming within the gel pockets.

The successful incorporation of Feld1 was affirmed through WB and ELISA analyses employing two commercially available Fel d 1 monoclonal antibodies. Assuming that direct fusion results in 100% incorporation of the Feld1 antigen, densitometric analysis of SDS-PAGE gel showed an approximate 63% incorporation for mosaic VLPs and approximately 65-71% for PVY - SpyT/SpyC2 and 3 – Feld1 VLPs.

3.2.2. Chemical coupling of PVY CP VLP with Feld1

For the chemical coupling, PVY and rFeld1 components were separately purified. Following purification, PVY CP samples were combined with 5xSMPH, while rFeld1 was mixed with the

reducing agent TCEP. After the reaction, any unreacted SMPH was removed. A four-fold molar excess of rFeld1 was then added to modified PVY-VLPs, and an unreacted rFeld1 was removed. SDS-PAGE analysis verified a 24% incorporation of rFeld1 into PVY CP particles through chemical coupling, denoted as cPVY-Feld1. TEM imaging showed the formation of slightly shorter PVY-like filamentous VLPs with sizes ranging from 100 to 200 nm. Notably, cPVY-Feld1 VLPs exhibited minimal packed nucleic acid, as observed in NAG.

3.2.3. Immunological evaluation of PVY-Feld1 vaccines

To determine the most promising PVY-Feld1 candidate among the five variants (direct fusion, mosaic, SpyT/SpyC2, SpyT/SpyC3, or cPVY-Feld1) for potential vaccine development, we conducted murine experiments which aimed to detect antigen-specific total IgGs and assess their specificity, along with IgG subclasses, using ELISA on Balb/c mice sera collected on day 42. We administered s.c. injections of 50 µg for each of five vaccine variants on day 0, without the use of adjuvants. Subsequent booster doses were administered on days 14 and 28, with blood samples collected on days 7, 14, 28, and 42.

All vaccine variants elicited notable levels of anti-Feld1 antibodies, which were detectable as early as day 7. Particularly noteworthy were the antibodies generated by cPVY-Feld1, displaying the highest titers and highest specificity in terms of antigen-antibody binding avidity (36%), as observed in sera collected on day 42.

In the context of conferring protection against infections, Th1 cells play a pivotal role by promoting antibody production primarily within the IgG2a subclass (Jegerlehner *et.al.*, 2007). This response is highly effective against a broad range of viral and bacterial pathogens. However, across all variants, the majority of produced Ab's belonged to the IgG1 subclass, indicating a switching towards a Th2-type response. Notably, the PVY-SpyT/SpyC3-Feld1 vaccine variant displayed the lowest IgG1/IgG2a ratio, suggesting a potential balance between Th1 and Th2 responses.

3.2.4. Native Fel d 1 recognition

To assess the potential vaccine efficacy among the developed variants in real-life scenarios, we investigated the ability of sera obtained from vaccinated mice to recognize the commercially accessible native Feld1 (nFel d 1) antigen sourced from cats. The outcomes mirrored those acquired using rFeld1, with the cPVY-Feld1 variant once again demonstrating the highest titers. This outcome strongly suggests that the Ab's generated in response to immunization with this particular variant exhibit robust specificity towards nFel d 1.

vaccines

MDPI

Article

Comparison of Bacterial Expression Systems Based on Potato Virus Y-like Particles for Vaccine Generation

Anete Ogrina [1], Dace Skrastina [1], Ina Balke [1], Ieva Kalnciema [1], Juris Jansons [1], Martin F. Bachmann [2] and Andris Zeltins [1,*]

[1] Plant Virology Laboratory, Latvian Biomedical Research and Study Centre, LV-1067 Riga, Latvia; anete.ogrina@biomed.lu.lv (A.O.); daceskr@biomed.lu.lv (D.S.); inab@biomed.lu.lv (I.B.); ieva.kalnciema@biomed.lu.lv (I.K.); jansons@biomed.lu.lv (J.J.)

[2] Department of BioMedical Research, University of Bern, 3008 Bern, Switzerland; martin.bachmann@dbmr.unibe.ch

* Correspondence: anze@biomed.lu.lv

Abstract: Plant-based virus-like particle (VLP) vaccines have been studied for years, demonstrating their potential as antigen-presenting platforms. In this paper, we describe the development of, and compare between, simple *Escherichia coli*-based antigen display platforms for the generation of potato virus Y (PVY) VLP-derived vaccines, thus allowing the production of vaccines from a single bacterial cell culture. We constructed four systems with the major cat allergen Fel d 1; namely, direct fusion with plant virus PVY coat protein (CP), mosaic PVY VLPs, and two coexpression variants of conjugates (SpyTag/SpyCatcher) allowing coexpression and conjugation directly in *E. coli* cells. For control experiments, we included PVY VLPs chemically coupled with Fel d 1. All constructed PVY–Fel d 1 variants were well expressed and soluble, formed PVY-like filamentous particles, and were recognized by monoclonal Fel d 1 antibodies. Our results indicate that all vaccine variants induced high titers of anti-Fel d 1 antibodies in murine models. Mice that were immunized with the chemically coupled Fel d 1 antigen exhibited the highest antibody titers and antibody–antigen interaction specificity, as detected by binding avidity and recognition of native Fel d 1. IgG1 subclass antibodies were found to be the dominant IgG class against PVY–Fel d 1. PVY CP-derived VLPs represent an efficient platform for the comparison of various antigen presentation systems to help evaluate different vaccine designs.

Keywords: virus-like particles; *E. coli*; expression; potato virus Y; Fel d 1

Citation: Ogrina, A.; Skrastina, D.; Balke, I.; Kalnciema, I.; Jansons, J.; Bachmann, M.F.; Zeltins, A. Comparison of Bacterial Expression Systems Based on Potato Virus Y-like Particles for Vaccine Generation. *Vaccines* 2022, 10, 485. https://doi.org/10.3390/vaccines10040485

Academic Editors: Kamil Kuca, Jakub D. Rybka and Tomasz Pniewski

Received: 25 February 2022
Accepted: 20 March 2022
Published: 22 March 2022

1. Introduction

One of the greatest vaccination challenges is the generation of long-lasting and protective immune responses against various pathogens including bacterial or viral infections, as well as against autoimmune and cancer-related illnesses. Vaccine construction strategies using icosahedral or filamentous plant-based virus-like particles (VLPs) are increasingly harnessed and have been proven to be excellent platforms for antigen presentation [1].

VLPs are self-assembling competent protein structures with identical or highly related overall structures to their corresponding native viruses, representing ideal building blocks to create a variety of new nanomaterials for different purposes, including the active ingredients of different vaccines. One of the most important VLP properties is the ability to mimic viral infection and induce strong immune responses in mammalian organisms, the effects of which are comparable to those induced by native infectious viruses. Plant virus-derived VLPs are viral particles that are noninfectious in mammals, and are very stable, easy to produce, and relatively simply engineered by introducing different antigens at high density on the VLP surface [2], resulting in an effective immune response [3]. Several excellent review articles about VLP immunological properties, including plant virus-derived vaccines, have recently been published [4–7].

In VLP vaccine construction, several approaches may be considered, including genetic, enzymatic, chemical, and physical processes [1]. In some cases, these methods can be combined. Genetic modifications include techniques that allow the introduction of coding sequences of antigenic peptides or even whole antigens in virus *CP* genes, resulting in N-, C-, or internal fusions of antigens (Figure 1A). When CP fusion with a chosen antigen affects VLP formation due to antigen size or biochemical properties, mosaic VLPs can be constructed to reduce steric hindrance. As shown in a recent paper, mosaic VLPs are formed as a result of a coexpression of antigen-containing and unmodified *CP* genes, leading to VLPs containing antigen fusion and unmodified viral CPs (Figure 1B) [8].

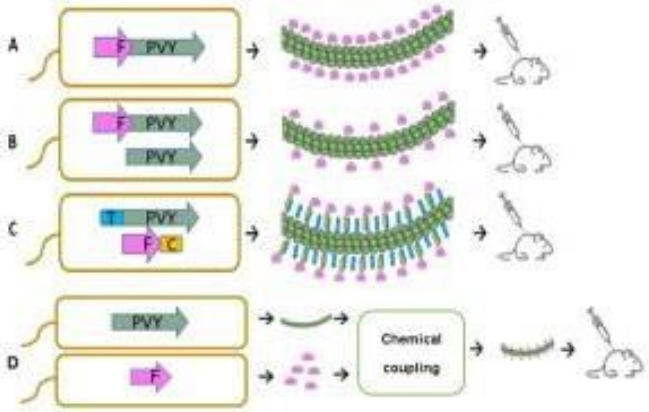

Figure 1. Principal schemes of vaccine production processes using *E. coli* expression systems; (A)—direct antigen fusion to the coat protein (CP) of filamentous PVY VLPs; (B)—coexpression of antigen-containing PVY CP and unmodified PVY CP for the production of mosaic VLPs; (C)—coexpression of vaccine components, allowing the formation of VLP–antigen conjugates directly in *E. coli* cells. F—Feld1 protein; (D)—chemical coupling of PVY VLPs and Fel d 1 protein. PVY—PVY coat protein; T—SpyTag; C—SpyCatcher.

Chemical and enzymatic approaches are broadly used for the introduction of antigens into the structure of carrier VLPs. VLPs and the chosen antigen are expressed and purified separately, and are linked using chemical crosslinking agents or enzymes such as transpeptidase or isopeptidase. Chemical or enzymatic approaches in VLP vaccine construction have several advantages, such as no size or structural limits for the antigen of choice and no influence on the antigen incorporation process on VLP assembly [1]. A recently developed efficient enzymatic system is based on spontaneous isopeptide bond formation between two conjugate partners, SpyTag (13 amino acids, AAs) and SpyCatcher (138 AAs), originating from the *Streptococcus pyogenes* protein CnaB2 [9,10]. This system allows the introduction of chosen antigens into the VLP structure by recombinantly attaching each partner to components of interest [11–13]; therefore, this approach may simplify the vaccine production process (Figure 1C) [14].

The main cat allergen from *Feline domesticus*, Fel d 1, is responsible for most allergies caused by cats worldwide, and cat allergies remain a major problem despite several new treatment approaches [15]. Our previous studies have confirmed that Fel d 1 is a very efficient model antigen for vaccine concept representation due to its well described features, such as a high protein production rate and immunogenicity [16,17]. It has previously been tested as a part of a conjugate vaccine using icosahedral plant VLPs derived from a cucumber mosaic virus (CMV) as a VLP carrier, resulting in strong immune responses, including a high-level production of neutralizing antibodies (nAbs) against Fel d 1 in Fel d 1-sensitized mice [16] and cats [17]. In this case, we used the strategy of covalent coupling where the Fel d 1 antigen was chemically conjugated to CMV VLPs, resulting in highly

immunogenic particles that induced stronger antibody (Ab) responses than free Fel d 1 or Fel d 1 mixed with VLPs (Figure 1D) [16].

Our previous results using filamentous VLPs, derived from potato virus Y (PVY) as a vaccine carrier for the hepatitis B viral (HBV) preS1 epitope, demonstrated a strong anti-preS1 immune response, even in the absence of adjuvants [18]. Furthermore, PVY VLPs contain several surface exposed lysins that have been used for the successful chemical coupling of milbemycin A3/A4 derivatives [19]. These data suggest the potential use of PVY VLPs as a new antigen-displaying platform. Our recent study revealed that icosahedral plant-based VLPs are more efficient at producing higher immune responses and draining kinetics to secondary lymphoid organs than filaments of the same genetic background [20]. However, considering the results of our previous studies on filamentous PVY VLPs, we decided to test different vaccine designs based on these VLPs.

In this study, we selected Fel d 1 as a model antigen for the comparison of three vaccine construction strategies. We demonstrate that PVY CP-derived VLPs can be engineered for antigen incorporation, resulting in simple *E. coli*-based antigen display platforms, and allowing the production of vaccines from a single bacterial production strain. There are several systems with the major cat allergen Fel d 1, namely; direct fusion with plant virus PVY CPs (Figure 1A), mosaic VLPs (Figure 1B), and two coexpression variants of VLP–antigen conjugates using Spy-Tag and Spy-Catcher systems (Figure 1C) which were constructed and tested in an *E. coli* expression system for VLP formation. The VLPs were characterized and used for immunological studies. In addition, recombinant Fel d 1 (rFel d 1) was chemically coupled to PVY VLPs and used as a control for immunization experiments (Figure 1D). These results can be used to evaluate the most eligible vaccine development process based on filamentous plant VLPs

2. Materials and Methods

2.1. Cloning of the Fel d 1 Gene with a G4S Linker at the 5′ End of the PVY CP Gene

The recombinant sequence of Fel d 1, which has an additional 15 aa linker sequence of $(GGGGS)_3$ genetically fused between two Fel d 1 chains for more flexibility, has been described previously [16]. For further subcloning, we introduced flanking *Nco*I and *Bam*HI sites in the *Fel d 1* gene by PCR mutagenesis using primers Fel_NcoF (5′-ACC ATGGGAAATGACGAAATTTGTCCGGCAGTTAAACGT-3′) and Fel_BamR (5′-GGATCCA CGACCCAGGGT ATTCAGTTTCAGA-3′), following the recommended manual for Taq DNA polymerase usage (Thermo Fisher Scientific, Waltham, MA, USA), and adjusting the annealing temperature to 50 °C for 45 s. The corresponding PCR product was then analyzed in a 0.8% agarose gel. After purification with a GeneJet Gel Extraction kit (Thermo Fisher Scientific, USA), the PCR product was ligated into the pTZ57R/T plasmid (Thermo Fisher Scientific, USA), which was later transformed into *E. coli* XL1 Blue cells (Novagen, Madison, WI, USA) for plasmid amplification. Three plasmid clones containing inserts were sequenced using a BigDye cycle sequencing kit (Thermo Fisher Scientific, USA) and an ABI Prism 3100 genetic analyzer (Applied Biosystems, Bedford, MA, USA) for sequence identity. A plasmid clone, pTZ-Fel d 1, without PCR errors was used for further subcloning.

2.2. Cloning of the PVY CP–NG4S Direct Fusion and Mosaic System with Fel d 1

The plasmid pET-PVY-CP-NG4S was constructed previously [18] and used for insertion of the Fel d 1 antigen coding sequence. The *Nco*I/*Bam*HI fragment from pTZ-Fel d 1 was subcloned into the same sites of pET-PVY-NG4S, resulting in the expression plasmid pET-PVY-NG4S-Fel d 1 (direct fusion; for plasmid map see Supplementary Figure S1).

For mosaic particle construction, the *PVY-CP* gene was amplified by PCR as previously described, using the primers PVY-NdeF (5′-ACATATGGGAAATGACACAATCGATGCA-3′) and PVY-XhoR (5′-ACTCGAGTTACATGTTCTTCACTCCAAGTAGAGTATGCA-3′).

The corresponding PCR product was then ligated into the pTZ57R/T plasmid (Thermo Fisher Scientific, USA) and transformed into *E. coli* XL1 Blue cells (Novagen, USA). Three plasmid clones containing the insert were sequenced using a BigDye cycle sequencing

kit (Thermo Fisher Scientific, USA) and an ABI Prism 3100 genetic analyzer (Applied Biosystems, USA) for identification of the plasmid clone without sequence errors. The obtained PVY *CP* DNA fragment containing the flanking *Nde*I and *Xho*I sites was then ligated into the pETDuet-1 (Novagen, USA) vector cut with the same restriction enzymes. Furthermore, the *Nco*I/*Hind*III fragment from pET-PVY-CP-NG4S was ligated into the pETDuet plasmid, which already contained the PVY–CP gene. The resulting expression vector contained two *PVY CP* genes, the first of which had *Nco*I/*Bam*HI sites for antigen subcloning and a flexible Gly-Ser linker. Finally, the *Fel d 1* gene was introduced into the pETDuet-derived plasmid, resulting in an expression vector for the production of mosaic VLPs (Supplementary Figure S2).

2.3. Cloning of Covalently Binding Protein Partners SpyCatcher and SpyTag

The sequence of the *SpyCatcher* gene was obtained from GenBank (JQ478411.1) [9]. The coding DNAs for full-size and truncated variants of the *SpyCatcher* gene were received as a product of commercial gene synthesis. We refer to the two tested SpyCatcher domains as SpyCatcher2 (*SpyC2*; full-size gene) and SpyCatcher3 (*SpyC3*; truncated version) [21].

To obtain both *SpyCatcher* genes with the additional *Nde*I and *Xho*I restriction sites convenient for subcloning, we used PCR mutagenesis as previously described, with the primers SpyC2_NdeF (5′-ACATATGGTTGATACCCTGAGCGGTCT-3′) and SpyC_XhoR (5′-GTAAAGCAACCAAAGGTGATGCACATATTGGATCCGGTACTAGTTAATAAGCTTC TCGAGT-3′) for the *SpyC2* sequence, and SpyC3_NdeF (5′-ACATATGAGCGATAGCGCAA CCCACATCAAATTCAG-3′) and SpyC_XhoR for the *SpyC3* sequence. Both corresponding PCR products were then analyzed in a 0.8% agarose gel. After purification with a GeneJet Gel Extraction kit (Thermo Fisher Scientific, USA), PCR products were ligated into the pTZ57R/T plasmid (Thermo Fisher Scientific, USA). After transformation of *E. coli* XL1 Blue cells and plasmid DNA isolation, three plasmid clones from each variant were sequenced using a BigDye cycle sequencing kit (Thermo Fisher Scientific, USA) and an ABI Prism 3100 genetic analyzer (Applied Biosystems, USA) for identification of plasmid clones without PCR errors. Correct clones for *SpyC2* and *SpyC3* were then used for further subcloning into the commercial vector plasmid pRSF-Duet1 (Novagen, USA). Using the introduced restriction sites *NdeI*/*XhoI*, corresponding fragments from pTZ-SpyC2 and pTZ-SpyC3 were subcloned into the pET-RSFDuet-1 plasmid, resulting in plasmids pRSF-Duet-SpyC2 and pRSF-Duet-SpyC3.

For construction of Fel d 1 antigen–SpyCatcher fusions, pTZ-Fel d 1 was digested with *Bam*HI/*Xho*I, and the corresponding fragment was ligated into pRSF-Duet-SpyC2 and pRSF-Duet-SpyC3.

As previously described, the coding sequence for *SpyTag* (*SpyT*) was introduced into the PVY *CP*–*NG4S* gene by PCR mutagenesis using the primers pet_BglF (5′-GATCGAGATC TCGATCCCGCGAA-3′) and PVY_SpTBamR (5′-GGATCCTTTGGTCGGTTT ATACGCATC CACCATCACAATATGCGCGTCATTTCCCATGGTATATCTCCTTCT-3′). The corresponding PCR product after purification with a GeneJet Gel Extraction kit (Thermo Fisher Scientific, USA) was ligated into the pTZ57R/T plasmid (Thermo Fisher Scientific, USA). *E. coli* XL1 Blue cells were used for plasmid amplification, resulting in the plasmid pET-PVY-NG4S-SpyT. To avoid PCR errors, three plasmid clones were selected for sequencing and analysis using a BigDye cycle sequencing kit (Thermo Fisher Scientific, USA) and an ABI Prism 3100 genetic analyzer (Applied Biosystems, USA). Furthermore, the *Bgl*II/*Bam*HI fragment from a pTZ plasmid clone containing the *SpyTag* sequence was subcloned into the pET-PVY-CP-NG4S vector, resulting in an expression vector coding for the *PVY* gene containing a coding sequence for SpyTag (SpyT).

To achieve covalent binding directly between the protein partners SpyCatcher and SpyTag in recombinant *E. coli*, we subcloned both coding sequences into one expression plasmid using the expression vector pET-PVY-NG4S-SpyT as a vector plasmid. Corresponding *Hind*III/*Blp*I fragments from pRSF-Duet-SpyC2-Fel d 1 and pRSF-Duet-SpyC3-Fel d 1 were subcloned into pET-PVY-NG4S-SpyT, resulting in two expression vectors, pET-PVY-

NG4S-SpyT-SpyC2-Fel d 1 (Supplementary Figure S3) and pET-PVY-NG4S-SpyT-SpyC3-Fel d 1, respectively (Supplementary Figure S4).

2.4. Expression and Purification of PVY VLPs and PVY Containing Fel d 1 VLPs

E. coli C2566 cells (New England Biolabs, Ipswich, MA, USA) were transformed with PVY *CP*-containing plasmids, which were then expressed and purified as previously described [18]. The same transformation was performed for each construct containing the *Fel d 1* antigen. The clones with the highest expression levels of the target protein were selected afterwards, and *E. coli* cultures were grown in a 2TY medium (1.6% tryptone, 1.0% yeast extract, 0.5% NaCl) containing a corresponding antibiotic ((kanamycin (25 mg/L) or ampicillin (50 mg/L)) on a rotary shaker (200 rev/min; Infors, Bottmingen, Switzerland) at 30 °C to an OD600 of 0.8–1.0. Then, 0.2 mM isopropyl β-d-1-thiogalactopyranoside (IPTG) and 5 mM $MgCl_2$ were added to induce the cell cultures. Cells were grown on a rotary shaker at 20 °C for 18 h and collected by low-speed centrifugation. The resulting biomass was kept frozen at −70 °C. After thawing on ice, the biomasses containing wild-type (wPVY), mosaic PVY VLPs containing a NG4S-linker (mPVY), direct fusion (PVY-NG4S-Fel d 1), and mosaic VLPs containing the Fel d 1 protein (mPVY-NG4S-Fel d 1), were suspended in a 1× PBS buffer containing 5 mM β-mercaptoethanol (β-ME) and 0.5% TX-100 (buffer A), and were disrupted by ultrasonic treatment. For PVY-NG4S-SpyT/SpyC2-Fel d 1 and PVY-NG4S-SpyT/SpyC3-Fel d 1, the biomass was suspended in a 20 mM TRIS pH 7.0 buffer supplemented with 150 mM NaCl (buffer B) and an additional 5 mM β-ME and 0.5% TX-100, and was disrupted by ultrasonic treatment. Insoluble proteins and cell debris were removed by centrifugation (15,557× *g*, 10 min at 5 °C).

All PVY VLPs were separated from cellular proteins using ultracentrifugation (Optima L—100XP; SW32 rotor, Beckman, USA; at 106,559× *g* (25,000 rpm), 6 h, 18 °C) in a sucrose gradient (20–60% sucrose in buffer A (wPVY, mPVY, PVY-NG4S-Fel d 1, and mPVY-NG4S-Fel d 1)) or in buffer B ((PVY-NG4S-SpyT/SpyC2-Fel d 1 and PVY-NG4S-SpyT/SpyC3-Fel d 1) without β-ME and TX-100). The gradient was divided into six fractions and prepared by carefully filling 6 mL of each solution, one at a time, in descending order (60–20%) with a long needle syringe in tubes (36 mL, for SW—32 rotor, Beckman, Brea, CA, USA), and overlapping the sample on top of all layers. After centrifugation, all fractions were collected in reverse order, starting with the 60% sucrose fraction, and then analyzed by SDS–PAGE. Fractions containing proteins of interest (PVY CP or CP–Fel d 1) were pooled and dialyzed to remove sucrose against 100 volumes of buffer A or B in a 12–14 kDa Spectra/Por 4 dialysis membrane (Spectrum Laboratories, Calgary, Canada). If necessary, the samples were concentrated using an Amicon Ultra-15 100 K filtration unit (Merck–Millipore, St. Louis, MO, USA).

All steps for the expression and purification of VLPs were monitored by SDS–PAGE using 12.5% gels, Western blot (WB), and agarose gel analysis. The concentrations of the proteins were estimated using a Qubit™ fluorometer (Thermo Fisher Scientific, USA) with a Qubit™ Protein Assay Kit (Thermo Fisher Scientific, USA), in accordance with the manufacturer's recommendations. Concentrated VLP solutions were stored at 4 °C.

2.5. Transmission Electron Microscopy (TEM)

The visualization of purified PVY CP-derived VLPs was done with uranyl acetate negative staining. First, 5 µL of the sample (1 mg/mL) was absorbed on carbon formvar-coated 300 Mesh Copper grids (Agar Scientific, Stansted, UK; 2 grids per sample were prepared) and incubated for 3 min. The grids were then washed with 1 mM ethylenediaminetetraacetic acid (EDTA) and negatively stained with 0.5% uranyl acetate aqueous solution. The grids were analyzed with a JEM-1230 electron microscope (JEOL, Tokyo, Japan) at an accelerating voltage of 100 kV and a minimum of five electrograph pictures were made per sample.

2.6. Chemical Coupling of PVY CP VLPs and Fel d 1

rFel d 1 was purified using a His-tag column as described previously [16]. The purified rFel d 1 was conjugated to PVY CP VLPs using the crosslinker succinimidyl-6-(β-maleimidopropionamido) hexanoate (SMPH; Thermo Fisher Scientific, USA). A 5-fold molar excess of SMPH to PVY VLPs was used for the reaction at 23 °C for 1 h. Unreacted SMPH was removed by an Amicon Ultra-15 50 K centrifugal filter (Merck–Millipore, USA); VLPs were further washed with 1× PBS four times (4 × 6 min) at 3214× *g* (5000 rpm) and 5 °C. The antigen prior to chemical conjugation was treated with a 10-fold molar excess of mild reducing agent tris (2-carboxyethyl) phosphine (TCEP; Sigma–Aldrich, Burlington, MA, USA) for 10 min at room temperature (RT). The coupling was performed by adding a 4-fold molar excess of rFel d 1 to the SMPH-derivatized PVY VLPs at 23 °C for 3 h by shaking at 1400 rpm/min on a DSG Titertek (Flow Laboratories, Oldham, UK). Unbound rFel d 1 was removed using an Amicon Ultra–15 100 K centrifugal filter (Merck–Millipore, USA). All stages of coupling were analyzed by SDS–PAGE and the integrity of VLPs was confirmed by TEM.

2.7. Immunological Studies

2.7.1. Western Blot (WB) Analysis

For WB analysis, protein samples were separated by SDS–PAGE and transferred to an Amersham Protran 0.45 µm nitrocellulose membrane (GE Healthcare, Piscataway, NJ, USA) using a semidry apparatus with parameters of 250 V, 45 A, and 45 min. After blocking the membrane in a PBS solution containing a 1% alkali–soluble casein (Merck–Millipore, USA), the membrane was incubated overnight (ON) at 4 °C in anti-PVY or anti-Fel d 1 Ab-containing solutions (diluted at 1:1000 in PBS with 1% alkali–soluble casein) obtained from mice that were immunized with PVY CP VLPs [18] or a recombinant antigen (rFel d 1) [16]. The membrane was washed with a TBS buffer (150 mM NaCl; 10 mM Tris pH 7.5) for 15 min and then incubated at RT for 3 h with horseradish peroxidase-conjugated anti-mouse IgG (Sigma–Aldrich, USA) that was diluted at 1:1000 in PBS, supplemented with 1% alkali–soluble casein. The membrane was washed with TBS for 15 min two times. The signal bands were developed by incubating the membrane in a TBS buffer supplemented with peroxidase substrates (0.002% *o*-dianisidine and 0.03% hydrogen peroxide).

2.7.2. Mouse Vaccination

For immunogenicity testing, 6–8 weeks old female BALB/c mice (5 per group) were purchased from Laboratory Animal Centre, University of Tartu (Estonia). A volume of 50 µg of each VLP (direct, mosaic, SpyT/SpyC2, SpyT/SpyC3, and chemically coupled) were diluted in 300 µL of sterile PBS and used for subcutaneous injection in mice without adjuvant on Day 0. Mice received a similar booster dosage on Days 14 and 28. One 100 µL serum sample from each mouse was collected each week on Days 7, 14, 28 and 42. The experimental protocol was approved by the Animal Protection Ethical Committee of the Latvian Food and Veterinary Service (permission no. 89).

2.7.3. The Enzyme-Linked Immunosorbent Assay (ELISA)

For total IgG Ab titer determination against Fel d 1 and PVY CP in sera of immunized mice, purified samples of rFel d 1 and PVY VLPs in a concentration of 10 µg/mL in 50 mM sodium carbonate buffer (pH 9.6, 100 µL per well) were coated on 96-well ELISA plates (Nunc Immuno MaxiSorp, Thermo Fisher Scientific, Rochester, NY, USA), and stored at 4 °C ON. The next day, blocking with 1% BSA in PBS at 37 °C for 1 h was performed, and serially diluted mouse sera were added to the plates and incubated at 37 °C for 1 h. Afterwards, plates were washed three times with PBS containing 0.05% Tween-20. A volume of 100 µL of horseradish peroxidase, labelled anti-mouse Ab (Sigma–Aldrich, USA), was added at a 1:10,000 dilution per well. After incubation at 37 °C for 1 h, plates were washed again, and the *o*-phenylenediamine dihydrochloride (OPD) (Sigma–Aldrich, USA) substrate was added for color development. Optical absorbance was measured with a

Labsystems 352 Multiscan MS microplate reader (Sweden) at 492 nm. The endpoint titers were calculated at the highest serum dilution, resulting in an absorbance value exceeding three-fold that of the negative control (serum obtained from nonimmunized mice).

For monoclonal Fel d 1 Ab ELISA tests, two sets of plates were coated with 10 µg/mL of each variant PVY–Fel d 1 VLPs at 4 °C ON. After blocking with 1% BSA in PBS at 37 °C for 1 h, serial dilutions of two types of Fel d 1 monoclonal Abs (mAb) against chain 1 (MA-3E4 and MA-6F9; Indoor Biotechnologies, Cardiff, UK) were added to the plates and incubated at 37 °C for 1 h, and then washed three times with PBS containing 0.05% Tween-20. The rest of the procedure was identical to that described above.

For the detection of IgG1 and IgG2a subclasses, isotype-specific ELISA was performed for the detection of anti-PVY and anti-Fel d 1 Ab, using mouse mAb isotyping reagent ISO2 (Sigma–Aldrich, USA) as secondary Abs, using the peroxidase conjugate of monoclonal anti-goat/sheep IgG Abs (Sigma–Aldrich, USA). The endpoint titers were calculated as stated above.

2.7.4. Avidity ELISA

To determine the avidity of IgG Abs, two sets of plates were prepared. Both were coated with 10 µg/mL PVY CP VLPs and Fel d 1-C6H-CG. After serum incubation, one set of plates was washed three times for 5 min with a 50 µL/well of a solution containing 7 M urea in PBS supplemented with 0.05% Tween-20. The other set was washed with the same amount of PBS with 0.05% Tween-20. Between washing steps, all the plates were washed with PBS, with 0.01% Tween-20 as usual. The rest of the procedure was identical to that described above.

2.7.5. ELISA for Native Fel d 1

To test whether the Abs induced by PVY–Fel d 1 VLP variants can recognize the native Fel d 1 (nFel d 1) protein, a sample of nFel d 1 (Indoor Biotechnology, UK) in a concentration of 10 µg/mL in a 50 mM sodium carbonate buffer (pH 9.6, 100 µL per well), was used to coat 96-well ELISA plates (Nunc Immuno MaxiSorp, Thermo Fisher Scientific, Rochester, NY, USA) and stored at 4 °C ON. To further the blocking, 1% BSA in PBS at 37 °C for 1 h was performed, and serially diluted mouse sera (5 µL from each sample) were added to the plates and incubated at 37 °C for 1 h. Afterwards, the plates were washed three times with PBS containing 0.05% Tween-20. A volume of 100 µL of horseradish peroxidase labelled anti-mouse Ab (Sigma–Aldrich, USA) was added at a 1:10,000 dilution per well. After incubation at 37 °C for 1 h, plates were washed again, and the *o*-phenylenediamine dihydrochloride (OPD) (Sigma–Aldrich, USA) substrate was added for color development. Optical absorbance was measured with a Labsystems 352 Multiscan MS microplate reader (Sweden) at 492 nm. The endpoint titers were calculated as the highest serum dilution that resulted in an absorbance value exceeding three-fold that of the negative control (serum obtained from nonimmunized mice).

3. Results and Discussion

3.1. Construction and Characterization of PVY CP VLPs Containing Fel d 1

Our previous studies revealed that some filamentous plant VLPs (PVY, potato virus M (PVM)) can accommodate comparably large protein domains on their surface as N– or C–terminal fusions without influencing VLP self-assembly [18,22]. First, we constructed direct fusions from a previously described PVY *CP* sequence with an introduced Gly-Ser linker [18] between *CP* and antigen sequences to reduce the influence of foreign sequences, which may interfere with VLP formation, further purification, and identification. The *Fel d 1* coding sequence was introduced in the N–terminal part of PVY–NG4S-CP, and expressed directly in *E. coli* cells (see plasmid map in Supplementary Figure S1).

To construct the mosaic system, we incorporated the wPVY *CP* and PVY *CP-NG4S-Fel d 1* genes into the expression vector pET-Duet1, allowing the formation of mosaic particles (mPVY-NG4S-Fel d 1) after expression in *E. coli*. The protein size of PVY-NG4S-Fel d 1 is

~55 kDa (Figure 2A; track 4). For mosaic VLPs, we identified two protein bands—wPVY with a size of ~35 kDa and PVY-NG4S-Fel d 1 with a size of ~55 kDa—after SDS–PAGE analysis, as expected (Figure 2A; track 5). The TEM results confirmed that the expression of both systems resulted in similar filamentous VLPs with an average size of 400–800 nm (Figure 2D,E), similar to what was previously described [18], suggesting that VLPs can tolerate Fel d 1 insertion without significantly interfering with their structure. Assuming that direct fusion leads to 100% incorporation of the Fel d 1 antigen, densitometric analysis of SDS–PAGE gels revealed approximately 63% Fel d 1 incorporation in the mosaic particles. The output of VLPs varied between 11 and 12 mg/g biomass.

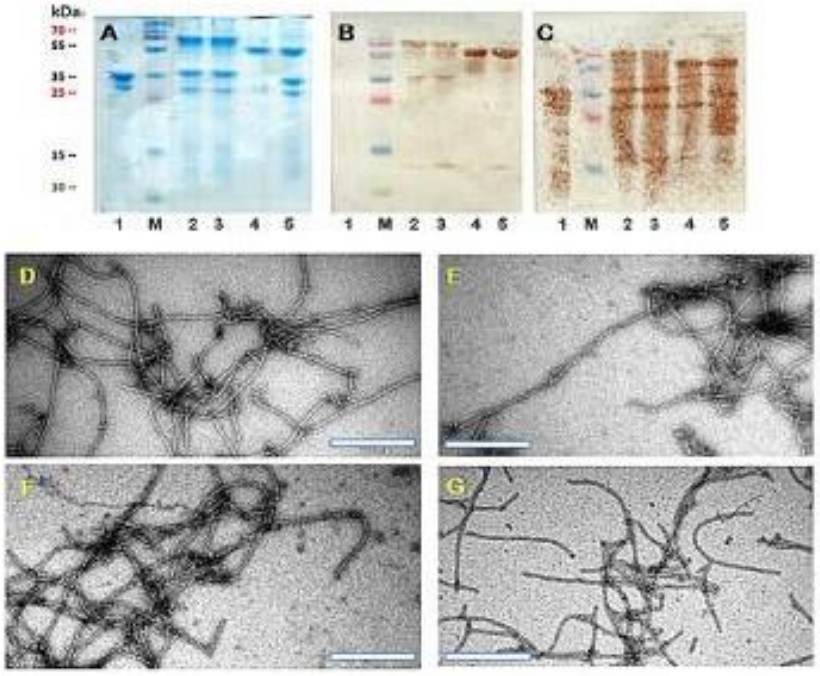

Figure 2. Characterization of PVY CP VLPs with the Fel d 1 antigen. (A) Coomassie-stained SDS–PAGE gel of PVY–Fel d 1 vaccine variants at a concentration of 2 mg/mL; (B) the same samples as in (A) analyzed by Western blot using anti-Fel d 1 antibodies; (C) the same samples as (A) analyzed by Western blot using anti-PVY antibodies. Electron micrographs of negatively stained VLPs; (D) direct fusion of PVY-NG4S-Fel d 1; (E) mosaic PVY-NG4S-Fel d 1; (F) PVY-SpyT/SpyC2-Fel d 1; (G) PVY-SpyT/SpyC3-Fel d 1, scale bars 500 nm. M—PageRulerTM Plus Prestained Protein Ladder, 10 to 250 kDa (Thermo Fisher Scientific, USA), 1—PVY-NG4S-PVY (mosaic; control); 2—PVY-SpyT-SpyC2-Fel d 1; 3—PVY-SpyT-SpyC3-Fel d 1; 4—PVY-NG4S-Fel d 1; 5—PVY-NG4S-Fel d 1 PVY-(mosaic).

Several previously developed SpyTag/SpyCatcher-based platforms involved individually purified components which were then linked together in a separate process [10,23,24]. However, there are examples of the reaction between SpyTag- and SpyCatcher-containing proteins forming covalent bonds directly in the cells of recombinant bacteria or even in plants [23,25].

To test whether SpyTag-containing PVY VLPs can directly form a conjugate with a SpyCatcher–Fel d 1 protein in the same bacterial cell, we first genetically introduced PVY *CP-NG4S* with a *SpyTag* sequence using PCR mutagenesis and expressed it in *E. coli* strain C2566. The majority of the protein was soluble and well expressed, with a size of ~35 kDa (Figure 3B). TEM also confirmed PVY-like VLP formation in various sizes ranging from 200–1000 nm (Figure 3A). In a second step, two SpyCatcher peptide sequences (full size

SpyC2 and N–terminally truncated *SpyC3*) [14] were genetically fused with *Fel d 1* and then used for further subcloning. To introduce *SpyTag/SpyCatcher* partner sequences into one expression system, we used the commercial vector plasmid pRSF-Duet, which has two *T7* promoters and multiple cloning sites, one for each genetically fused *PVY-NG4S-SpyTag/SpyCatcher-Fel d 1* partner.

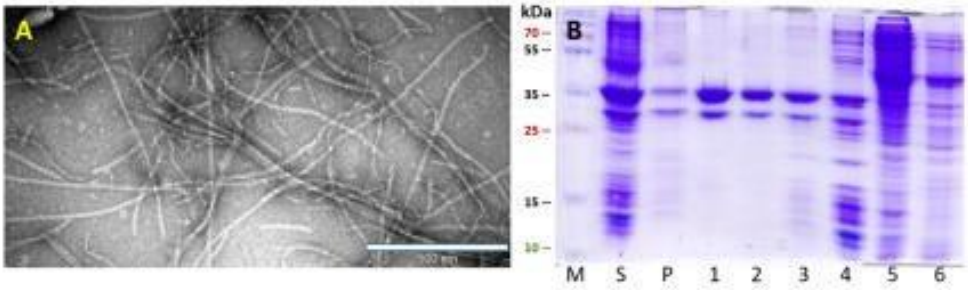

Figure 3. PVY-NG4S-SpyT analysis. (**A**) Electron micrographs of negatively stained VLPs; (**B**) Coomassie-stained SDS–PAGE. M—PageRulerTM Plus Prestained Protein Ladder (Thermo Fisher Scientific). S—soluble proteins in cell lysate; P—insoluble proteins in cell lysate; 1–6—sucrose gradient fractions (60–0% sucrose).

Both expression vectors pRSFDu-PVY-NG4S-SpyT/SpyC2-Fel d 1 and pRSFDu-PVY-NG4S-SpyT/SpyC3-Fel d 1 were used for *E. coli* C2566 transformation. Cloned genes were expressed, and the corresponding VLPs after purification were analyzed using SDS–PAGE gels. The analysis confirmed that SpyTag- and SpyCatcher-derived proteins form conjugates directly in *E. coli* cells. The expected size of conjugated PVY-SpyT/SpyC proteins containing the Fel d 1 antigen was ~70 kDa (Figure 2A; track 2, 3), while the band ~35 kDa corresponds to overlapping antigen-free PVY-NG4S-SpyT (32.6 kDa) and free SpyC2–Fel d 1 (31.3 kDa) or SpyC3–Fel d 1 (29.2 kDa; see Figure 2 and plasmid maps in Supplementary File). The output of VLPs was approximately 10 mg/g biomass.

The morphology of filamentous VLPs was confirmed by TEM (Figure 2F,G), revealing shorter VLP particle formation with sizes ranging from 200–400 nm. Additionally, densitometric analysis revealed approximately 65% Fel d 1 incorporation for PVY-NG4S-SpyT/SpyC2-Fel d 1 and 71% for PVY-NG4S-SpyT/SpyC3-Fel d 1. These results demonstrate that both SpyCatcher versions (full size and truncated) have similar conjugation efficiency, as observed in previous studies [14].

Native filamentous plant viruses contain a comparably low proportion of encapsidated nucleic acids. We previously observed a low nucleic acid content for filamentous VLPs derived from plant viruses [22]. Considering the importance of bacterial nucleic acids in stimulating the immune response, we attempted to identify DNA/RNA in purified VLP samples. Native agarose gel (NAG) analysis of VLP variants after ethidium bromide staining suggested that only four vaccine variants contained visible signals of nucleic acids (Figure 4). Packaged RNA was hardly noticeable for wPVY and cPVY–Fel d 1 VLPs. In contrast, PVY-NG4S-SpyT/SpyC2-Fel d 1 and PVY-NG4S-SpyT/SpyC3-Fel d 1 VLPs contained clearly detectable nucleic acid signals. As shown in Figure 4, a large portion of filamentous VLPs cannot enter the agarose gel due to their large size, and therefore, they appear as bands in NAG pockets.

To further characterize vaccine candidates, we performed WB analysis using an Ab against both Fel d 1 and carrier PVY VLPs. Mosaic VLPs consisting of NG4S-containing and unmodified PVY CPs were used as a control for both analyses. As expected after WB analysis, mPVY did not react with anti-Fel d 1 Abs (Figure 2B). In contrast, all four Fel d 1-containing vaccine prototypes revealed the presence of Fel d 1 in WB analysis by reacting with anti-Fel d 1 Abs (Figure 2B). The WB signals overlapped with the corresponding bands identified in SDS–PAGE: ~70 kDa for PVY–Fel d 1 conjugates and ~35 kDa for

free Fel d 1. We also observed a slight degradation of the Fel d 1 protein, resulting in an ~13 kDa degradation product in samples containing both SpyCatcher variants and mosaic VLPs. WB analysis using anti-PVY Abs demonstrated proteolytic degradation of the VLP carrier (Figure 2C). We also noted similar results in our previous experiments [18], where the formation of truncated PVY CP derivatives appeared, possibly due to proteolytic processing by *E. coli* trypsin-like enzymes.

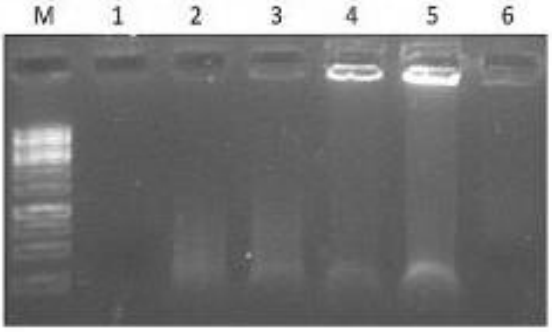

Figure 4. Agarose gel analysis of PVY–Fel d 1 vaccine variants at a concentration of 1.5 mg/mL. M—GeneRuler 1 kb DNA ladder (Thermo Fisher Scientific, USA); 1—wPVY (wild-type; control); 2—PVY-NG4S-Fel d 1 (direct fusion); 3—PVY-NG4S-Fel d 1-PVY (mosaic fusion); 4—PVY-SpyT-SpyC2-Fel d 1; 5—PVY-SpyT-SpyC3-Fel d 1; 6—cPVY–Fel d 1 (chemically coupled). A 0.8% native agarose gel stained with ethidium bromide was used for analysis.

3.2. *Chemical Coupling of PVY CP with Fel d 1*

For the chemically coupled PVY–Fel d 1 (cPVY–Fel d 1) variant, the two principal components, the PVY CP and the antigen, were expressed separately. First, we purified unmodified PVY VLPs using PEG8000/NaCl precipitation and ultracentrifugation in a sucrose gradient, as previously described [18]. Fractions containing PVY CPs were purified, as described in Materials and Methods, for further use. The concentration of PVY CP VLPs was measured using a Qubit™ Protein Assay Kit (Thermo Fisher Scientific, USA), and the samples were analyzed by SDS–PAGE (Figure 5B), confirming the correct size of ~35 kDa. The sample was then mixed with 5× SMPH for derivatization and incubated for 1 h. Unreacted SMPH was removed by buffer exchange on Amicon-Ultra-15 50 K filtration units (Merck–Millipore, USA).

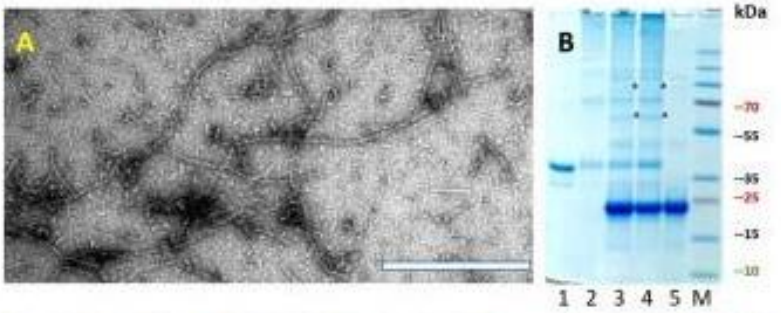

Figure 5. Chemically coupled PVY–Fel d 1 analysis. (A) Electron micrographs of negatively stained cPVY–Fel d 1, scale bar 500 nm; (B) Coomassie-stained SDS–PAGE gel. 1—PVY; 2—PVY after 5× SMPH derivatization and unreacted SMPH removal; 3—PVY coupling with 4 × Fel d 1-C6H-CG; 4—PVY + 4 × Fel d 1-C6H-CG after partial Fel d 1-C6H-CG removal; 5—rFel d 1-C6H-CG treated with 10× TCEP; M—PageRuler™ Plus Prestained Protein Ladder (Thermo Fisher Scientific); *—coupling product of PVY-rFel d 1.

The rFel d 1 protein with a His-tag and C–terminal Cys residue was purified, as described previously, using a Protino Ni-TED 1000 Packed Column (Macherey-Nagel, Bethlehem, PA, USA) [16]. Then, fractions containing the rFel d 1 protein were dialyzed against 1x PBS. Before coupling, rFel d 1 was treated with the reducing agent TCEP, and then, a 4-fold molar excess of rFel d 1 was added to the derivatized PVY–VLP at 23 °C for 2 h. Uncoupled rFel d 1 was removed in Amicon-Ultra-15 100 K filtration units by centrifugation. All stages of chemical coupling were monitored by SDS–PAGE (Figure 5B). Densitometric analysis suggested rFel d 1 incorporation of approximately 24% when calculated from the signal intensities of the unmodified PVY CP and coupling products (Figure 5B; track 4).

Electron microscopy analysis of the final product demonstrated that the PVY-like particles preserved the filamentous VLP structure after the coupling procedure (Figure 5A), although we noticed the presence of much shorter filaments with sizes ranging approximately 100–200 nm. A similar observation about chemical coupling efficiency in rod-shaped nanoparticles was made by Rioux et al. and Therien et al. when analyzing Papaya mosaic virus (PapMV) particle formation after two influenza epitopes (HA11; 9 AA) [26] and (M2e; 26 AA) [27] were coupled to PapPMV CP. TEM revealed that chemical coupling slightly interfered with longer particle formation compared with PapMV WT, suggesting that successful coupling relies on several aspects, such as the size of the chosen epitope, chemical linker, or nanoparticle surface morphology [26,27].

3.3. *Immunological Characterization of the PVY–Fel d 1 Vaccine Candidates*

To characterize the immune stimulation potency of the constructed variants, we performed ELISA to test the antigenicity of VLP-introduced antigens using two commercially available monoclonal Fel d 1 Abs before murine experiments. To elucidate which of the constructed PVY–Fel d 1 variants is the most promising candidate for possible vaccine design, we performed experiments in mice to measure the amount of antigen-specific total IgG as well as IgG subclasses by ELISA. For additional analysis of IgG specificity, avidity ELISAs were performed using sera collected on Day 42. To test whether collected sera from immunized mice were able to recognize a nFel d 1 allergen, we included an ELISA test for total specific IgG Abs.

3.3.1. Monoclonal Antibody ELISA

Before starting in vivo murine experiments, we wanted to characterize the antigenicity of the constructed PVY–Fel d 1 vaccine candidate by measuring recognition with two commercially available Fel d 1 mAbs with ELISA. The nFel d 1 protein consists of two chains (chain-1 and chain-2) [28]; the two chosen commercially available mAbs bind to two different epitopes on the cat *F. domesticus* allergen Fel d 1, both on chain-1 (MA-6F9; MA-3E4; Indoor biotechnologies, UK). For optimal induction of nAbs, it is important that the Fel d 1 incorporated into PVY VLPs is structurally identical to nFel d 1 and is capable of inducing Abs that recognize nFel d 1; therefore, we wanted to establish whether there is a difference in mAb binding to rFel d 1 or nFel d 1. Our results indicated that nFeld1 is equally recognized by both mAbs (Figure 6D) (corresponding to reciprocal titers between 55,000 and 75,000). Surprisingly, MA-3E4 mAbs demonstrated an even higher interaction with the rFel d 1 produced by us (corresponding reciprocal titers for MA-3E4 1:548,000; for MA-6F9 1:158,000).

Similar analysis using these two mAbs was performed for the constructed VLP variants and revealed that both mAbs strongly bound to all PVY–Fel d 1 vaccine variants (Figure 6A,B); MA–3E4 mAbs demonstrated the highest binding to each VLP variant. Although MA–6F9 did not show significant differences in Ab binding to PVY–Fel d 1 vaccine variants, titers against MA–3E4 mAbs were highest for mPVY-NG4S-Fel d 1 (Figure 6C) (corresponding reciprocal titers for MA–6F9 1:130,000; for MA–3E4 1:560,000), indicating that Fel d 1 is well exposed on the surface of these VLPs. PVY-NG4S-SpyT/SpyC2-Fel d 1 and PVY-NG4S-SpyT/SpyC3-Fel d 1 were also capable of binding to MA-3E4 very efficiently (corresponding reciprocal titers for SpyT/SpyC2 1:485,000; for SpyT/SpyC3

1:468 000). Interestingly, the chemically coupled variant produced slightly lower titers for MA–3E4 than other PVY–Fel d 1 vaccine variants (corresponding reciprocal titer 1:330,000).

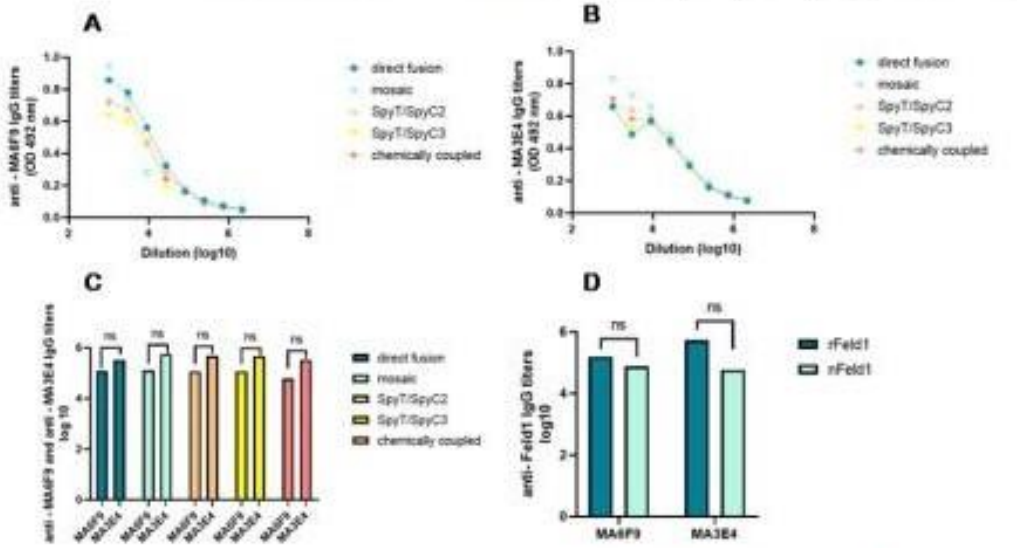

Figure 6. Monoclonal Fel d 1 antibody reaction with displayed Fel d 1 on the surface of vaccine variants. Plates were coated with 10 µg/mL of each VLP. (A)—total IgG titers against Fel d 1 monoclonal antibody MA-6P9 (Indoor Biotechnology, USA); (B)—total IgG titers against Feld1 monoclonal antibody MA-3E4 (Indoor Biotechnology, USA); (C)—comparison of MA-6P9 and MA-3E4 titers of total IgGs against; (D)—comparison of monoclonal antibody MA-6P9 and MA-3E4 titers against recombinant Fel d 1 (rFel d 1) or native Fel d 1 (nFel d 1). (C,D)—Statistical analysis using Student's *t* test in GraphPad Prism 9.0. Vaccine groups $n = 5$. One representative experiment was performed. A value of $p > 0.05$ was considered statistically significant (ns—not significant).

3.3.2. Total Levels of IgG

Subcutaneous immunizations of 6 to 8-weeks old female BALB/c mice were performed on Day 0 with 50 µg of the five PVY–Fel d 1 vaccine candidates PVY-NG4S-Fel d 1, mPVY-NG4S-Fel d 1, PVY-NG4S-SpyT/SpyC2-Fel d 1, PVY-NG4S-SpyT/SpyC3-Fel d 1 and cPVY–Fel d 1 without additional adjuvants. Booster doses were given on Days 14 and 28. Total specific IgG immune responses were detected in sera collected on Days 7, 14, and 28, and a final blood collection was performed on Day 42 for ELISA test analysis. Total IgG levels were measured against the levels of carrier PVY CP as well as rFel d 1 and nFel d 1.

Fel d 1-specific Abs were detected very early after the first dose. IgG titers at Day 7 were highest for PVY-SpyT/SpyC3-Fel d 1 (Figure 7C). The same was observed on Day 14. IgG responses against Fel d 1 were enhanced dramatically on Day 28 after the first boost, which led to IgG levels that showed a minimum of a 5.6-fold increase compared with those detected on Day 14, showing that the highest anti-Fel d 1 titers from Day 28 were obtained from mice injected with cPVY–Fel d 1 (corresponding reciprocal titer 1:11,500).

Each of the IgG response levels against PVY CP and Fel d 1 reached the maximum on the final day (42) after the second boost, demonstrating the highest anti-Fel d 1 titers for cPVY–Fel d 1 (Figure 7A,C) (corresponding reciprocal titer 1:52,938), followed by PVY-SpyT/SpyC3-Fel d 1 (corresponding reciprocal titer 1:36,500). Furthermore, the IgG levels for these two VLPs increased by approximately five-fold after the second boost compared to previously obtained titers, indicating the possibility of a high repetitiveness of antigens on the VLP surface, which has previously been reported to induce high IgG titers [29]. PVY CP-specific Abs were only detectable from Day 28 and were highest against cPVY–Fel d 1

as well as for mPVY-NG4S-Fel d 1 (Figure 7B,D). The obtained results only partly correlate with the data from densitometric analysis of the incorporated Fel d 1 antigen. The immune responses were higher for PVY-SpyT/SpyC3-Fel d 1 (71%) than for PVY-SpyT/SpyC2-Fel d 1 (65%) or mPVY–Fel d 1 (63%), but this could not be considered the main factor because for cPVY–Fel d 1, which had the highest Ab levels, densitometric analysis suggested only 24% Fel d 1 incorporation. Additionally, direct fusion of PVY–Fel d 1 with 100% incorporated Fel d 1 antigen did not result in the highest Ab levels, suggesting that the process of generating an immune response is also influenced by other factors, such as the particle size and RNA content.

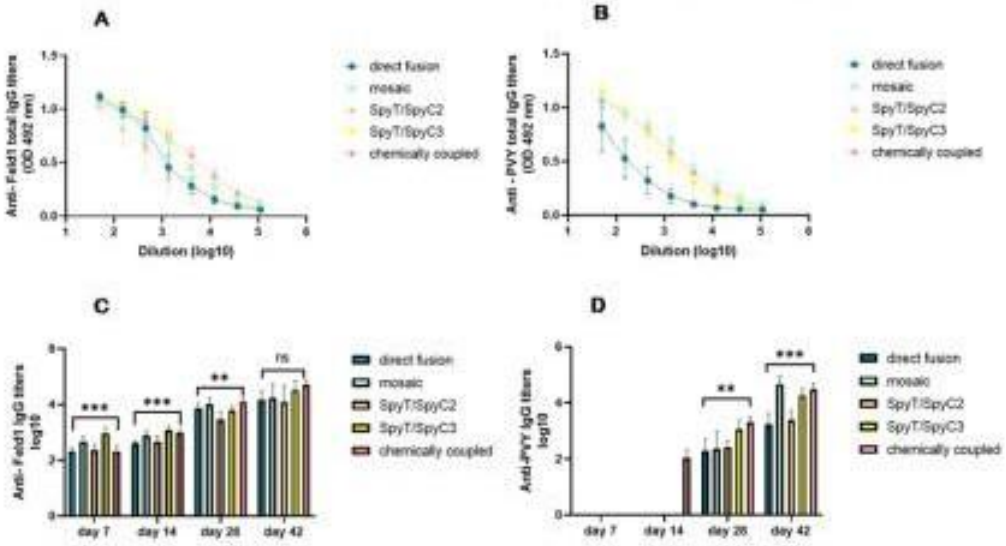

Figure 7. Fel d 1 IgG titer analysis after vaccination with PVY–Fel d 1 vaccine variants. (A)—Fel d 1-specific IgG titers on Day 42 for the groups vaccinated with PVY–Fel d 1 variants measured at OD 492 nm; (B)—PVY CP-specific IgG titers on Day 42 for the groups vaccinated with PVY–Fel d 1 variants measured at OD 492 nm; (C)—Log_{10} values (mean ± SEM) of Feld1-specific IgG titers for the groups vaccinated with PVY–Fel d 1 VLPs on Days 7, 14, 28 and 42; (D)—Log_{10} values (mean ± SEM) of PVY CP-specific IgG for the groups vaccinated with PVY–Fel d 1 VLPs on Days 7, 14, 28 and 42. (C,D)—Statistical analysis using one-way ANOVA in GraphPad Prism 9.0. Vaccine groups $n = 5$. One representative experiment is shown. A value of $p > 0.05$ was considered statistically significant (ns—not significant; ** $p < 0.001$; *** $p < 0.0001$).

To further characterize induced Abs against Fel d 1, we performed an avidity ELISA experiment using sera from Day 42. According to several authors, avidity may be defined as the ability of a polyvalent molecule to form multiple connections of the same kind with ligands tethered to the same surface, or in other words, it characterizes the potential multivalent interaction of an Ab with an antigen [30,31]. Furthermore, polyvalent molecules such as Abs are restricted by the geometry of interaction, meaning that recognition of the surface-bound ligands is linked to topological properties of the surface [31]; therefore, avidity could possibly define the strength and/or number of interactions that determine the quality of produced Abs. As shown for the malaria vaccine, RTS, S, and Ab avidity are a very important factors, which correlates with vaccine efficacy [32].

For avidity tests, most studies rely on ELISA format analysis with different concentrations of chaotropic agents to determine the stability of the antigen–Ab complex. We compared the total IgG levels of two identical plates, where one was washed with 7 M urea while the other was treated as usual. The results indicated that the cPVY–Fel d 1 variant induces Abs with the highest avidity index (AI) values (Figure 8A,B), meaning that 36% of all IgGs were specific and could not be washed away with 7 M urea. PVY–Fel

d 1, mPVY–Fel d 1 and PVY-SpyT/SpyC3-Fel d 1 induced Abs with ~9–12% specificity, whereas variants with the least specific Abs included PVY-SpyT/SpyC2-Fel d 1, which resulted in only ~4% specificity. These findings clearly demonstrate that the method of antigen incorporation in VLPs can influence the structure of the Fel d 1 antigen on the VLP surface and result in the generation of Abs with different specificities.

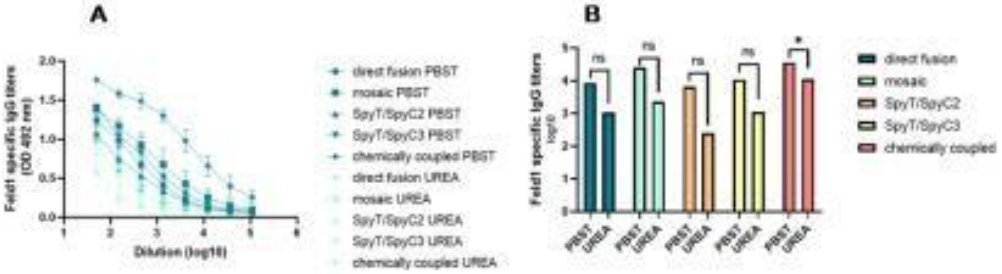

Figure 8. Avidity antibody detection after vaccination with PVY–Fel d 1 variants. (**A**)—Fel d 1-specific IgG titers for the groups vaccinated with PVY–Fel d 1 variants on Day 42 measured at OD_{492}. After serum incubation, one plate was treated with PBS with 0.05% Tween 80, and the other plate was treated with 7 M urea in PBS with 0.05% Tween 80; (**B**)—Log_{10} values (mean ± SEM) of Fel d 1-specific IgG titers (shown in a) for the group vaccinated with PVY–Fel d 1 vaccine variants. Statistical analysis was performed using Student's *t* test in GraphPad Prism 9.0. Vaccine groups $n = 5$. One representative experiment was performed. A value of $p > 0.05$ was considered statistically significant (ns—not significant; * $p < 0.01$).

3.3.3. Subclass Specific Antibody Production

Previously published papers have suggested that several factors, such as the structure and quantity of antigen, as well as the possible route and time period of antigenic stimulation, can affect which IgG subclass of Abs will be produced [33]. The murine IgG family is divided into four major subclasses, namely; IgG1, IgG2a/c, IgG2b and IgG3, elucidating that in particular, the IgG2a subclass is most capable of protecting individuals against an infectious bacterial challenge [34]. It is known that in the absence of nucleic acids that serve as toll-like receptor (TLR) stimulators, nanoparticles such as VLPs induce IgG1-dominated immune responses in mice, whereas the dominating subclass in the presence of nucleic acids becomes a much more protective IgG2a subclass [30]. Furthermore, it has been shown that these two IgG subclasses (IgG2a and IgG1) in mice can define whether the T helper 1 (T_h1) or T helper (T_h2) signaling pathway is dominating, respectively [35]. For protective immunity against infection, T_h1 cells stimulate Ab production toward the IgG2a subclass and are considered the most potent Ab response against most viral and bacterial pathogens [29].

Although it is known that viral infections with live or inactivated viruses are mostly restricted to the IgG2a isotype, several papers have confirmed that immunization with many viral proteins or peptides, often combined with adjuvants, leads to an IgG1 Ab response, especially in the absence of naturally packed nucleic acids [36–39].

Analysis of the induced anti-Fel d 1 Abs revealed an excess of IgG1 over IgG2a in all cases. The highest IgG1 Ab response was produced by mice that were vaccinated with cPVY–Fel d 1 (corresponding reciprocal titer 1:91,000), followed by mPVY–Fel d 1 (corresponding reciprocal titer 1:36,000), whereas PVY-NG4s-SpyT/SpyC3-Fel d 1 produced the highest IgG2a titer (Figure 9A,B) (corresponding reciprocal titer 1:3200) among the groups.

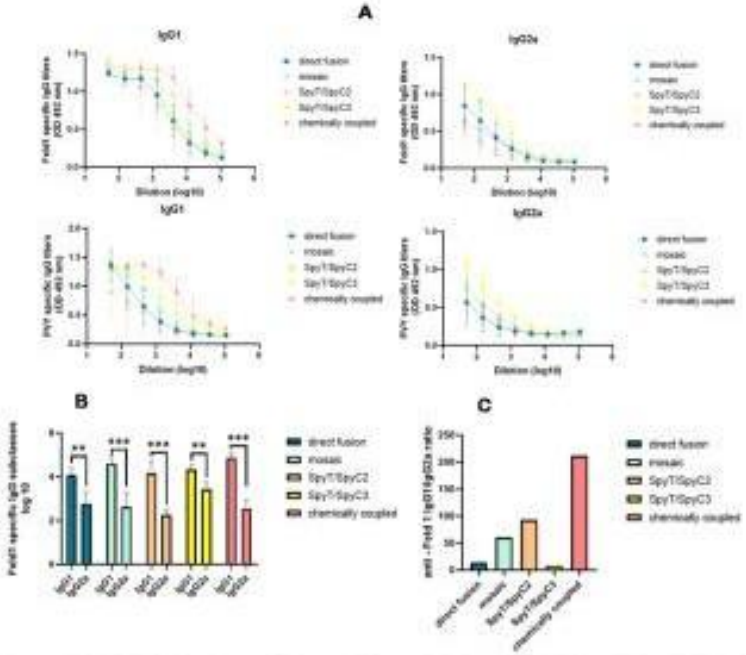

Figure 9. PVY–Fel d 1 variants induce subclass switching by ELISA analysis. (**A**)—Anti–Fel d 1- and anti-PVY CP-specific IgG1 and IgG2a titers measured in Day 42 mouse sera at OD492 nm. ELISA plates were coated with PVY–Fel d 1 variants to detect IgG subclasses in mice vaccinated with PVY–Fel d 1 variants. (**B**)—Log_{10} values of Feld1-specific IgG1 and IgG2a titers measured in Day 42 mouse sera; (**C**)—anti-Fel d 1 IgG1/IgG2a ratio measured from titers used in the experiment shown in (**B**); (**A**,**B**) Statistical analysis using Student's *t* test in GraphPad Prism 9.0. Vaccine groups $n = 5$. One representative experiment is shown. A value of $p > 0.05$ was considered statistically significant (** $p < 0.001$; *** $p < 0.0001$).

Our previous research on filamentous virus PVM VLPs revealed very low amounts of packaged nucleic acids [22]. We obtained similar results in this study, indicating low amounts of nucleic acids within PVY (Figure 4), which may be a reason for the dominance of IgG1 in mice vaccinated with most of the VLP variants. The lowest IgG1/IgG2a ratio value was obtained in sera from mice immunized with PVY-NG4s-SpyT/SpyC3-Fel d 1 (Figure 9C). These results correlate with the nucleic acid content found in VLPs after NAG analysis. However, this effect was not observed in PVY-NG4s-SpyT/SpyC2-Fel d 1-immunized mice.

3.3.4. Native Fel d 1 Recognition

Sensitization through environmental exposure to the main cat allergen, Fel d 1, continues to be one of the main allergy-related problems worldwide [40]. Moreover, our previously obtained data using the main cat allergen Fel d 1 have confirmed it to be a well characterized, easily produced, and efficient model antigen for vaccine design [16]. To evaluate possible vaccine efficiency between constructed variants in vivo, we tested how well-produced sera from vaccinated mice could recognize the commercially available nFel d 1 antigen isolated from cats (Indoor Biotechnologies, USA).

After serum incubation on plates with nFel d 1, and all the additional steps as previously described, ELISA was performed. The results were very similar to those obtained with rFel d 1—the highest absorbance values were for cPVY–Fel d 1 after chemical coupling (Figure 10A,B) (corresponding reciprocal titer 1:25,000), which produced a minimum two-

fold excess compared to that of the following three variants with approximately similar titers—PVY–Fel d 1, mPVY–Fel d 1 and PVY-SpyT/SpyC3-Fel d 1 (corresponding titers approximately 1:9000–10,000). The lowest lgG values were observed for PVY-SpyT/SpyC2-Fel d 1 (corresponding titer 1:3400), again as seen with rFel d 1, suggesting that this variant was not as immunogenic as others, possibly due to its inability to present antigens in a recognizable manner.

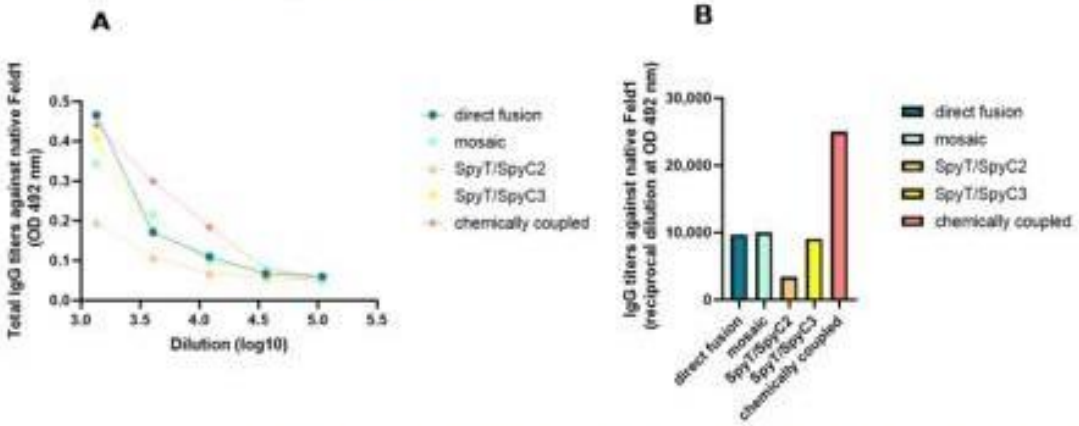

Figure 10. PVY–Fel d 1 variants induced antibodies against Fel d 1 ELISA analysis using native Feld1. (A,B)—Fel d 1-specific IgG titers against native Feld1 for the groups vaccinated with PVY–Fel d 1 vaccine variants on Day 42 measured at OD_{492}. One representative experiment was performed.

These findings strongly correlate with previously obtained data from avidity tests, confirming that cPVY–Fel d 1 produces Abs that are very specific to the VLP surface-exposed Fel d 1 antigen, whereas Abs from PVY-SpyT/SpyC2-Fel d 1 struggled to interact with the presented antigen, resulting in fewer nonspecific Abs. These results clearly demonstrate the effect of the chosen Fel d 1 vaccine design on the immune response and specificity of the elicited Abs.

4. Conclusions

In vaccine manufacturing, production platforms need to be simple. Here, we demonstrate that the Fel d 1 antigen can be introduced genetically into the PVY structure by direct and mosaic fusions as well as enzymatically by SpyTag/SpyCatcher–mediated antigen coupling to the VLP carrier. These processes are performed directly in *E. coli* cells, avoiding multiple separate processes, such as the production and purification of VLPs in one process, antigen production and purification in a second process and the subsequent third process—reaction between both components. We managed to successfully clone and express four PVY CP VLPs containing the genetically fused Fel d 1 antigen directly in *E. coli* cells, resulting in stable PVY-like filamentous VLP production. All obtained constructs were well expressed, soluble, and had Fel d 1 incorporation confirmed by WB and ELISA analysis using mAbs. Chemical coupling of Fel d 1 on surface-exposed lysines of PVY VLPs was also successful, allowing us to compare five different PVY–Fel d 1 vaccine variants in murine models.

A number of plant viruses have been used for new vaccine platform development, exploiting chemical, physical, genetic, and immunological aspects for the best possible outcome [1]. Immunology studies of VLPs as vaccine carriers demonstrate that antigens larger than 200 µm cannot freely enter the lymphatic system due to their time-consuming active uptake mechanism, resulting in fewer total lgG Abs than icosahedral particles ~30 nm in size [20,41,42].

It is known that the immunological features of VLPs depend on repetitive and particulate structures and induction of innate immunity through activation of pathogen-associated

molecular pattern recognition receptors (PAMPs) [3]. A recent study by Pitek et al. [43] observed the interaction between VLPs of different shapes and surface chemistry and plasma proteins, leading to the conclusion that different surface charges attract protein coronas with different compositions. They proposed a mechanism in which nanoparticle–cell interactions are enhanced by additional interactions with the cell surface-mediated corona proteins, which may enhance cell receptor clustering and interactions to promote uptake [43]. As a result, differences in surface charge can significantly influence the Ab titers. The constructed PVY-derived vaccines are differently charged: (1) chemical coupling modifies the Lys residues and decreases the positive charges on the VLP surface; and (2) adding the positively charged SpyTag on the surface of PVY VLPs increases the overall positive charge. These changes may explain the observed differences in our experiments with Ab titers and avidity. Additionally, epitope spacing on the VLP surface can affect the immune response: a 5–10 nm distance between antigen molecules is considered to be optimal to induce the best Ab response [44]. In our experiments, we did not observe a correlation between the percentage of VLP-incorporated Fel d 1 antigens and the immune response, so additional studies are necessary to elucidate the influence of these factors on the quality of Abs.

Interestingly, all of the constructed vaccine variants elicited high Ab production against Fel d 1, the use of cPVY–Fel d 1 resulted in the strongest immune response and highest avidity Ab, suggesting that Fel d 1 antigen attachment on the VLP surface via chemical coupling may be the most effective way to obtain an efficient vaccine against Fel d 1. On the other hand, this result may be explained by the presence of small particles in the cPVY–Fel d 1 VLP sample observed in EM (Figure 5A), therefore such strong immune reactions were elicited because the VLP size was previously proven to be significant in this context [20]. Moreover, Abs against cPVY–Fel d 1 demonstrated the best recognition of nFel d 1, which indicates that Abs generated after immunization by this variant are strongly specific to nFel d 1.

IgG2a subclass Abs are most effective against virus infection in mouse models [39]. However, in our study, the majority of produced Abs were IgG1 subclasses for all variants demonstrating switching toward the T_h2 response. Several authors suggest that isotype switching toward the IgG2a subclass is strongly dependent on TLR ligands such as ssRNAs [39,45] which are naturally packed into VLPs during *E. coli* expression [29]. Therefore, improving TLR stimulation by using T_h1–inducing adjuvants or packed TLR9 stimulators such as CpGs [29,46,47] should be considered.

Although the size and shape of VLPs were confirmed to be important, these factors may not be the only critical parameters. Surprisingly, the obtained results reveal that filamentous PVY–Fel d 1 variants induce similar titers of total IgGs when compared with those of recently published icosahedral Qb-Fel d 1 vaccines [48] or even exceed the IgG levels elicited by VLPs from CMV containing the same Fel d 1 antigen [16].

Our study clearly demonstrates that the chosen expression platform can significantly influence the immune response, and several vaccine variants must be tested to find the best vaccine variant ensuring the highest and most specific immune response. PVY CP-derived VLPs are an efficient platform for comparing various antigen presentation systems that can help to evaluate different vaccine designs. Moreover, PVY VLPs might be used in the future for the development of the vaccine against cat allergy and other clinically significant vaccines.

Supplementary Materials: The following are available online at https://www.mdpi.com/article/10.3390/vaccines10040485/s1, Supplement File: Plasmid maps and amino acid sequences. Figure S1: Description of plasmid pET-PVY-NG4S-Feld1; Figure S2: Description of plasmid pET-PVY-NG4S-Feld1-PVY; Figure S3: Description of plasmid pET-PVY-SpT-SpC2-Feld1; Figure S4: Description of plasmid pET-PVY-SpT-SpC2-Feld1.

Author Contributions: Conceptualization, A.O., M.F.B. and A.Z.; experimental work, A.O., D.S., I.B., I.K. and J.J.; writing—original draft preparation, A.O. and A.Z.; writing—review and editing, A.O.,

I.B., M.F.B. and A.Z.; supervision, A.Z.; funding acquisition, A.Z. All authors have read and agreed to the published version of the manuscript.

Funding: This research was funded by the Latvian Science Council, Grant No. lzp-2019/1-0131.

Institutional Review Board Statement: Not applicable.

Informed Consent Statement: Not applicable.

Data Availability Statement: Not applicable.

Acknowledgments: The authors would like to thank Janis Bogans for his help in the chromatographic purification of the Fel d 1 antigen; Gunta Resevica and Vilija Zeltina are acknowledged for their technical assistance. We acknowledge Mona O. Mohsen from the University of Bern for their help with the statistical analysis.

Conflicts of Interest: The authors declare no conflict of interest. The funders of the study had no role in the design of the study; in the collection, analyses, or interpretation of data; in the writing of the manuscript; or in the decision to publish the results.

References

1. Balke, I.; Zeltins, A. Use of plant viruses and virus-like particles for the creation of novel vaccines. *Adv. Drug Deliv. Rev.* 2019, *145*, 119–129. [CrossRef] [PubMed]
2. Zeltins, A. Viral Nanoparticles: Principles of Construction and Characterization. In *Viral Nanotechnology*; Khudyakov, Y.E., Pumpens, P., Eds.; CRC Press: Boca Raton, FL, USA, 2016; pp. 93–119.
3. Lebel, M.E.; Chartrand, K.; Leclerc, D.; Lamarre, A. Plant Viruses as Nanoparticle-Based Vaccines and Adjuvants. *Vaccines* 2015, *3*, 620–637. [CrossRef] [PubMed]
4. Benne, N.; van Duijn, J.; Kuiper, J.; Jiskoot, W.; Slütter, B. Orchestrating immune responses: How size, shape and rigidity affect the immunogenicity of particulate vaccines. *J. Control. Release* 2016, *234*, 124–134. [CrossRef] [PubMed]
5. Moyer, T.J.; Zmolek, A.C.; Irvine, D.J. Beyond antigens and adjuvants: Formulating future vaccines. *J. Clin. Investig.* 2016, *126*, 799–808. [CrossRef] [PubMed]
6. Citiulo, F.; Crosatti, C.; Cattivelli, L.; Biselli, C. Frontiers in the Standardization of the Plant Platform for High Scale Production of Vaccines. *Plants* 2021, *10*, 1828. [CrossRef]
7. Tariq, H.; Batool, S.; Asif, S.; Ali, M.; Abbasi, B.H. Virus-Like Particles: Revolutionary Platforms for Developing Vaccines against Emerging Infectious Diseases. *Front. Microbiol.* 2022, *12*, 4137. [CrossRef]
8. Mohsen, M.O.; Balke, I.; Zinkhan, S.; Zeltina, V.; Liu, X.; Chang, X.; Krenger, P.S.; Plattner, K.; Gharailoo, Z.; Vogt, A.S.; et al. A scalable and highly immunogenic virus-like particle-based vaccine against SARS-CoV-2. *Allergy* 2022, *77*, 243–257. [CrossRef]
9. Zakeri, B.; Fierer, J.O.; Celik, E.; Chittock, E.C.; Schwarz-Linek, U.; Moy, V.T.; Howarth, M. Peptide tag forming a rapid covalent bond to a protein, through engineering a bacterial adhesin. *Proc. Natl. Acad. Sci. USA* 2012, *109*, E690–E697. [CrossRef]
10. Brune, K.D.; Leneghan, D.; Brian, I.J.; Ishizuka, A.; Bachmann, M.F.; Draper, S.; Biswas, S.; Howarth, M. Plug-and-Display: Decoration of Virus-Like Particles via isopeptide bonds for modular immunization. *Sci. Rep.* 2016, *6*, 19234. [CrossRef]
11. Marini, A.; Zhou, Y.; Li, Y.; Taylor, I.; Leneghan, D.B.; Jin, J.; Zaric, M.; Mekhaiel, D.; Long, C.A.; Miura, K.; et al. A Universal Plug-and-Display Vaccine Carrier Based on HBsAg VLP to Maximize Effective Antibody Response. *Front. Immunol.* 2019, *10*, 2931. [CrossRef]
12. Fredsgaard, L.; Goksøyr, L.; Thrane, S.; Aves, K.-L.; Theander, T.; Sander, A. Head-to-Head Comparison of Modular Vaccines Developed Using Different Capsid Virus-Like Particle Backbones and Antigen Conjugation Systems. *Vaccines* 2021, *9*, 539. [CrossRef] [PubMed]
13. Chevillard, C.; Amen, A.; Besson, S.; Hannani, D.; Bally, I.; Dettling, V.; Gout, E.; Moreau, C.J.; Buisson, M.; Gallet, S.; et al. Elicitation of potent SARS-CoV-2 neutralizing antibody responses through immunization with a versatile adenovirus-inspired multimerization platform. *Mol. Ther.* 2022. [CrossRef] [PubMed]
14. Liu, Z.; Zhou, H.; Wang, W.; Tan, W.; Fu, Y.-X.; Zhu, M. A novel method for synthetic vaccine construction based on protein assembly. *Sci. Rep.* 2014, *4*, 7266. [CrossRef] [PubMed]
15. Bonnet, B.; Messaoudi, K.; Jacomet, F.; Michaud, E.; Fauquert, J.L.; Caillaud, D.; Evrard, B. An update on molecular cat allergens: Fel d 1 and what else? Chapter 1: Fel d 1, the major cat allergen. *Allergy Asthma Clin. Immunol.* 2018, *14*, 14. [CrossRef]
16. Zeltins, A.; West, J.; Zabel, F.; El Turabi, A.; Balke, I.; Haas, S.; Maudrich, M.; Storni, F.; Engeroff, P.; Jennings, G.T.; et al. Incorporation of tetanus-epitope into virus-like particles achieves vaccine responses even in older recipients in models of psoriasis, Alzheimer's and cat allergy. *npj Vaccines* 2017, *2*, 30. [CrossRef]
17. Thoms, F.; Haas, S.; Erhart, A.; Nett, C.S.; Rüfenacht, S.; Graf, N.; Strods, A.; Patil, G.; Leenadevi, T.; Fontaine, M.C.; et al. Immunization of Cats against Fel d 1 Results in Reduced Allergic Symptoms of Owners. *Viruses* 2020, *12*, 288. [CrossRef]
18. Kalnciema, I.; Skrastina, D.; Ose, V.; Pumpens, P.; Zeltins, A. Potato Virus Y-Like Particles as a New Carrier for the Presentation of Foreign Protein Stretches. *Mol. Biotechnol.* 2011, *52*, 129–139. [CrossRef]

19. Zeltins, A.; Turks, M.; Skrastina, D.; Lugiņina, J.; Kalnciema, I.; Balke, I.; Bizdēna, Ē.; Skrivelis, V. Synthesis and Immunological Evaluation of Virus-Like Particle-Milbemycin A3/A4 Conjugates. *Antibiotics* **2017**, *6*, 18. [CrossRef]
20. Zinkhan, S.; Ogrina, A.; Balke, I.; Reseviča, G.; Zeltins, A.; de Brot, S.; Lipp, C.; Chang, X.; Zha, L.; Vogel, M.; et al. The impact of size on particle drainage dynamics and antibody response. *J. Control. Release* **2021**, *331*, 296–308. [CrossRef]
21. Li, L.; Fierer, J.O.; Rapoport, T.A.; Howarth, M. Structural Analysis and Optimization of the Covalent Association between SpyCatcher and a Peptide Tag. *J. Mol. Biol.* **2014**, *426*, 309–317. [CrossRef]
22. Kalnciema, I.; Balke, I.; Skrastina, D.; Ose, V.; Zeltins, A. Potato Virus M-Like Nanoparticles: Construction and Characterization. *Mol. Biotechnol.* **2015**, *57*, 982–992. [CrossRef] [PubMed]
23. Peyret, H.; Ponndorf, D.; Meshcheriakova, Y.; Richardson, J.; Lomonossoff, G.P. Covalent protein display on Hepatitis B core-like particles in plants through the in vivo use of the SpyTag/SpyCatcher system. *Sci. Rep.* **2020**, *10*, 17095. [CrossRef] [PubMed]
24. Li, X.; Pan, C.; Sun, P.; Peng, Z.; Feng, E.; Wu, J.; Wang, H.; Zhu, L. Orthogonal modular biosynthesis of nanoscale conjugate vaccines for vaccination against infection. *Nano Res.* **2021**, *15*, 1645–1653. [CrossRef] [PubMed]
25. Stander, J.; Chabeda, A.; Rybicki, E.P.; Meyers, A.E. A Plant-Produced Virus-Like Particle Displaying Envelope Protein Domain III Elicits an Immune Response Against West Nile Virus in Mice. *Front. Plant Sci.* **2021**, *12*. [CrossRef]
26. Rioux, G.; Babin, C.; Majeau, N.; Leclerc, D. Engineering of Papaya Mosaic Virus (PapMV) Nanoparticles through Fusion of the HA11 Peptide to Several Putative Surface-Exposed Sites. *PLoS ONE* **2012**, *7*, e31925. [CrossRef]
27. Thérien, A.; Bédard, M.; Carignan, D.; Rioux, G.; Gauthier-Landry, L.; Laliberté-Gagné, M.-È.; Bolduc, M.; Savard, P.; Leclerc, D. A versatile papaya mosaic virus (PapMV) vaccine platform based on sortase-mediated antigen coupling. *J. Nanobiotechnol.* **2017**, *15*, 54. [CrossRef]
28. Andersson, T.N.; Ekman, G.J.; Grönlund, H.; Buentke, E.; Eriksson, T.L.J.; Scheynius, A.; Van Hage-Hamsten, M.; Gafvelin, G. A novel adjuvant-allergen complex, CBP-rFel d 1, induces up-regulation of CD86 expression and enhances cytokine release by human dendritic cells in vitro. *Immunology* **2004**, *113*, 253–259. [CrossRef]
29. Jegerlehner, A.; Maurer, P.; Bessa, J.; Hinton, H.J.; Kopf, M.; Bachmann, M.F. TLR9 Signaling in B Cells Determines Class Switch Recombination to IgG2a. *J. Immunol.* **2007**, *178*, 2415–2420. [CrossRef]
30. Klein, J.S.; Bjorkman, P.J. Few and Far Between: How HIV May Be Evading Antibody Avidity. *PLOS Pathog.* **2010**, *6*, e1000908. [CrossRef]
31. Vorup-Jensen, T. On the roles of polyvalent binding in immune recognition: Perspectives in the nanoscience of immunology and the immune response to nanomedicines. *Adv. Drug Deliv. Rev.* **2012**, *64*, 1759–1781. [CrossRef]
32. Dobaño, C.; Sanz, H.; Sorgho, H.; Dosoo, D.; Mpina, M.; Ubillos, I.; Aguilar, R.; Ford, T.; Diez-Padrisa, N.; Williams, N.A.; et al. Concentration and avidity of antibodies to different circumsporozoite epitopes correlate with RTS,S/AS01E malaria vaccine efficacy. *Nat. Commun.* **2019**, *10*, 2174. [CrossRef] [PubMed]
33. Visciano, M.L.; Tagliamonte, M.; Tornesello, M.L.; Buonaguro, F.M.; Buonaguro, L. Effects of adjuvants on IgG subclasses elicited by virus-like Particles. *J. Transl. Med.* **2012**, *10*, 4. [CrossRef] [PubMed]
34. Rostamian, M.; Sohrabi, S.; Kavosifard, H.; Niknam, H.M. Lower levels of IgG1 in comparison with IgG2a are associated with protective immunity against Leishmania tropica infection in BALB/c mice. *J. Microbiol. Immunol. Infect.* **2017**, *50*, 160–166. [CrossRef] [PubMed]
35. Gomes, A.C.; Roesti, E.S.; El-Turabi, A.; Bachmann, M.F. Type of RNA Packed in VLPs Impacts IgG Class Switching—Implications for an Influenza Vaccine Design. *Vaccines* **2019**, *7*, 47. [CrossRef]
36. Huber, V.C.; McKeon, R.M.; Brackin, M.N.; Miller, L.A.; Keating, R.; Brown, S.A.; Makarova, N.; Perez, D.; MacDonald, G.H.; McCullers, J.A. Distinct Contributions of Vaccine-Induced Immunoglobulin G1 (IgG1) and IgG2a Antibodies to Protective Immunity against Influenza. *Clin. Vaccine Immunol.* **2006**, *13*, 981–990. [CrossRef]
37. Snapper, C.M.; Paul, W.E. Interferon-γ and B Cell Stimulatory Factor-1 Reciprocally Regulate Ig Isotype Production. *Science* **1987**, *236*, 944–947. [CrossRef]
38. Hocart, M.J.; MacKenzie, J.S.; Stewart, G.A. The Immunoglobulin G Subclass Responses of Mice to Influenza A Virus: The Effect of Mouse Strain, and the Neutralizing Abilities of Individual Protein A-purified Subclass Antibodies. *J. Gen. Virol.* **1989**, *70*, 2439–2448. [CrossRef]
39. Markine-Goriaynoff, D.; Van Der Logt, J.T.; Truyens, C.; Nguyen, T.D.; Heessen, F.W.A.; Bigaignon, G.; Carlier, Y.; Coutelier, J.-P. IFN-γ-independent IgG2a production in mice infected with viruses and parasites. *Int. Immunol.* **2000**, *12*, 223–230. [CrossRef]
40. Ichikawa, K.; Iwasaki, E.; Baba, M.; Chapman, M. High prevalence of sensitization to cat allergen among Japanese children with asthma, living without cats. *Clin. Exp. Allergy* **1999**, *29*, 754–761. [CrossRef]
41. Reddy, S.T.; Van Der Vlies, A.J.; Simeoni, E.; Angeli, V.; Randolph, G.J.; O'Neil, C.P.; Lee, L.K.; Swartz, M.A.; Hubbell, J.A. Exploiting lymphatic transport and complement activation in nanoparticle vaccines. *Nat. Biotechnol.* **2007**, *25*, 1159–1164. [CrossRef]
42. Caldeira, J.C.; Perrine, M.; Pericle, F.; Cavallo, F. Virus-Like Particles as an Immunogenic Platform for Cancer Vaccines. *Viruses* **2020**, *12*, 488. [CrossRef] [PubMed]
43. Pitek, A.S.; Wen, A.M.; Shukla, S.; Steinmetz, N.F. The Protein Corona of Plant Virus Nanoparticles Influences their Dispersion Properties, Cellular Interactions, and In Vivo Fates. *Small* **2016**, *12*, 1758–1769. [CrossRef] [PubMed]
44. Dintzis, H.M.; Dintzis, R.Z.; Vogelstein, B. Molecular determinants of immunogenicity: The immunon model of immune response. *Proc. Natl. Acad. Sci. USA* **1976**, *73*, 3671–3675. [CrossRef] [PubMed]

45. Guo, C.; Peng, Y.; Lin, L.; Pan, X.; Fang, M.; Zhao, Y.; Bao, K.; Li, R.; Han, J.; Chen, J.; et al. A pathogen-like antigen-based vaccine confers immune protection against SARS-CoV-2 in non-human primates. *Cell Rep. Med.* 2021, *2*, 100448. [CrossRef]
46. Benne, C.; Harmsen, M.; van der Graaff, W.; Verheul, A.; Snippe, H.; Kraaijeveld, C. Influenza virus neutralizing antibodies and IgG isotype profiles after immunization of mice with influenza A subunit vaccine using various adjuvants. *Vaccine* 1997, *15*, 1039–1044. [CrossRef]
47. Gupta, C.L.; Akhtar, S.; Waye, A.; Pandey, N.R.; Pathak, N.; Bajpai, P. Cross talk between Leishmania donovani CpG DNA and Toll-like receptor 9: An immunoinformatics approach. *Biochem. Biophys. Res. Commun.* 2015, *459*, 424–429. [CrossRef]
48. Chang, X.; Krenger, P.; Krueger, C.C.; Zha, L.; Han, J.; Yermanos, A.; Roongta, S.; Mohsen, M.O.; Oxenius, A.; Vogel, M.; et al. TLR7 Signaling shapes and maintains antibody diversity upon virus-like particle immunization. *Front. Immunol.* 2022, *12*, 827256. [CrossRef]

3.3. Bacterial expression systems based on Tymovirus-like particles for the presentation of vaccine antigens

3.3.1. Construction and characterization of EMV CP Feld1 constructs

Within this study, we present several simple *E. coli* expression strategies designed to produce vaccines derived from EMV VLPs. These systems embrace various strategies for antigen incorporation including direct fusion of EMV CP with Feld1 and coexpression of antigen containing EMV CPs unmodified (mosaic) EMV CPs. Additionally, we included two coexpression methods, one involving the synthetic zipper pair 18/17 (SYNZIP; SZ18/17) and the other employing coiled-coil forming peptides E and K (Ecoil/Kcoil), for the simultaneous expression of EMV VLPs and Feld1 antigen.

Initially, to improve flexibility for accommodating antigens on the VLP surface we introduced the G4S linker sequence to the C-terminal of the EMV CP. The resultant VLPs were similar to parental VLPs in size of 30 nm when observed in TEM. Subsequently, we created direct fusion EMV CP VLPs and mosaic VLPs. This involved the incorporation of the Feld1 antigen following the introduction of a G4S linker at the CP's C-terminal end. Furthermore, we explored two physical binding partner strategies in vaccine design. This involved the incorporation of negatively charged partners, Ecoil and SZ18, within the EMV CP gene. These partners formed robust physical complexes with another set of partners: the positively charged pair Kcoil and SZ17, both of which were introduced into Feld1 coding sequence. Subsequently, we coexpressed the two binding partners (EMV-Ecoil/Kcoil-Feld1 and EMV-SZ18/SZ17-Feld1) in *E. coli* cells. To validate the interaction between separately expressed and purified VLPs and Feld1, we carried out *in vitro* binding studies. Remarkably, we observed the successful formation of complexes in both scenarios.

All four vaccine variants (direct, mosaic, Ecoil/Kcoil and SZ18/17) expression in *E. coli* was followed by purification and comprehensive characterization through SDS-PAGE, WB and NAG analysis. Icosahedral VLPs approximately 30 nm in size was confirmed for all VLPs in TEM. Following purification, the yield of VLP types was around 7-8 mg/L for direct and mosaic VLPs and around 50 – 70mg/L for Ecoil/Kcoil and SZ18/17 VLPs. 100% integration of the Feld1 antigen was achieved for direct fusion after SDS-PAGE and WB analysis. For mosaic VLPs, SDS-PAGE image densitometric analysis revealed an incorporation rate of ~46% for the Feld1 antigen and ~56% for the EMV-SZ18/SZ17-Feld1 complex, but only 5.2% for the EMV-Ecoil/Kcoil-Feld1 complex.

3.3.2. Chemical coupling of EMV CP VLP with Feld1

For chemical coupling, both EMV and rFeld1 components were separately purified. EMV CP samples were combined with 3xSMPH, while rFeld1 was mixed with reducing agent TCEP (10-molar excess). After the reaction, any residual unreacted SMPH was eliminated. Further, a two-fold molar excess of rFeld1 was added to modified PVY-VLPs, and any unbound rFeld1 was removed. Verification through SDS-PAGE analysis confirmed the integration of rFeld1 into EMV CP VLPs through chemical coupling (termed as cEMV-Feld1). TEM imaging revealed well-assembled VLPs of T=3 symmetry. However, the quantification of Feld1 incorporation level became challenging due to signal overlap between the EMV CP dimer and the cEMV-Feld1 signal.

3.3.3. Immunological evaluation of EMV-Feld1 vaccines

The most promising EMV-Feld1 candidate for potential vaccine development among the five different variants (direct fusion, mosaic, Ecoil/Kcoil, SZ18/17, or cEMV-Feld1) was determined by series of murine experiments like detecting antigen-specific total IgGs and evaluate their specificity, along with the IgG subclasses, using ELISA method. This analysis was conducted on sera collected on day 42. The vaccination regimen involved subcutaneous injections of 30 µg for each of the five vaccine variants into Balb/c mice on day 0 without adjuvants. Subsequent booster doses were given on days 14 and 28, and blood samples were collected on days 0, 14, 28, and 42.

The assessment of the immunogenicity of the formulated vaccine candidates displayed elevated levels of Feld1-specific antibody production. However, it's noteworthy that a similarly robust immune response against the carrier EMV was also detected. We concluded that cEMV-Feld1 and SZ18/17 emerge as the most effective frameworks for antigen presentation. These platforms exhibited substantial antigenicity against Feld1, and the resulting ab’s displayed an improved specificity (exceeding 50%) for four out of the five vaccine candidates. Moreover, the VLPs formed by EMV-Feld1 demonstrated modest production of the desired protective IgG2a subclass ab’s against Feld1, with IgG1 prevailing as the predominant subclass.

3.3.4. Native Fel d 1 recognition

We assessed the ability of ab’s generated from five EMV-Feld1 variant vaccinations to recognize nFeld1. In this context, the IgG titers against nFeld1 were notably highest for the direct fusion approach, closely followed by SZ18/17. These outcomes align with the measurements of antibody avidity, wherein SZ18/17 yielded the most specific ab’s (68%). Intriguingly, it's worth noting

that the antibody titers against nFeld1 for EMV-Feld1 variants were notably lower when compared to the levels induced by PVY-Feld1 vaccine variants.

frontiers | Frontiers in Microbiology

TYPE Original Research
PUBLISHED 23 March 2023
DOI 10.3389/fmicb.2023.1154990

OPEN ACCESS

EDITED BY
Esther Blanco,
Instituto Nacional de Investigación y Tecnología Agraria y Alimentaria (INIA), Spain

REVIEWED BY
Fabrizio Chiodo,
National Research Council (CNR), Italy
Haiwei Wang,
Harbin Veterinary Research Institute, Chinese Academy of Agricultural Sciences, China

*CORRESPONDENCE
Andris Zeltins
anze@biomed.lu.lv

SPECIALTY SECTION
This article was submitted to Virology, a section of the journal Frontiers in Microbiology

RECEIVED 31 January 2023
ACCEPTED 06 March 2023
PUBLISHED 23 March 2023

CITATION
Ogrina A, Balke I, Kalnciema I, Skrastina D, Jansons J, Bachmann MF and Zeltins A (2023) Bacterial expression systems based on *Tymovirus*-like particles for the presentation of vaccine antigens.
Front. Microbiol. 14:1154990.
doi: 10.3389/fmicb.2023.1154990

Bacterial expression systems based on *Tymovirus*-like particles for the presentation of vaccine antigens

Anete Ogrina[1], Ina Balke[1], Ieva Kalnciema[1], Dace Skrastina[1], Juris Jansons[1], Martin F. Bachmann[2] and Andris Zeltins[1]*

[1]Latvian Biomedical Research and Study Centre, Riga, Latvia, [2]Department of BioMedical Research, University of Bern, Bern, Switzerland

Virus-like particles (VLPs) are virus-derived artificial nanostructures that resemble a native virus-stimulating immune system through highly repetitive surface structures. Improved safety profiles, flexibility in vaccine construction, and the ease of VLP production and purification have highlighted VLPs as attractive candidates for universal vaccine platform generation, although exploration of different types of expression systems for their development is needed. Here, we demonstrate the construction of several simple *Escherichia coli* expression systems for the generation of eggplant mosaic virus (EMV) VLP-derived vaccines. We used different principles of antigen incorporation, including direct fusion of EMV coat protein (CP) with major cat allergen Feld1, coexpression of antigen containing and unmodified (mosaic) EMV CPs, and two coexpression variants of EMV VLPs and antigen using synthetic zipper pair 18/17 (SYNZIP 18/17), and coiled-coil forming peptides E and K (Ecoil/Kcoil). Recombinant Fel d 1 chemically coupled to EMV VLPs was included as control experiments. All EMV-Feld1 variants were expressed in *E. coli*, formed *Tymovirus*-like VLPs, and were used for immunological evaluation in healthy mice. The immunogenicity of these newly developed vaccine candidates demonstrated high titers of Feld1-specific Ab production; however, a comparably high immune response against carrier EMV was also observed. Antibody avidity tests revealed very specific Ab production (more than 50% specificity) for four out of the five vaccine candidates. Native Feld1 recognition and subclass-specific antibody tests suggested that the EMV-SZ18/17-Feld1 complex and chemically coupled EMV-Feld1 vaccines may possess characteristics for further development.

KEYWORDS

eggplant mosaic virus, Fel d 1, virus-like particles, *E. coli*, expression

1. Introduction

Recent outbreaks of infectious diseases have highlighted that traditional vaccination strategies focusing on attenuated or inactivated viruses may face several limitations, including time-consuming and cost-ineffective manufacturing procedures (Tariq et al., 2022). The widespread coronavirus infectious disease-19 (COVID-19) pandemic has encouraged the development of multiple vaccine candidates and their accelerated progress

toward clinical trials, of which mRNA-based technology has shown to be the leading industrial success story. Nevertheless, other technologies for vaccine generation, such as subunit and viral vector vaccines, should not be eliminated in further studies, as their COVID-19 vaccines also provide immunoprotection (Chung et al., 2020).

Immunologically active multivalent structures such as virus-like particles (VLPs) have been extensively studied as new prophylactic and therapeutic vaccine platforms against human or animal infectious agents, cancers and autoimmune diseases (Balke and Zeltins, 2019). VLPs not only have the potential to offer improved safety profiles but can also be manipulated to deliver various antigens and drugs to different targets within tissues and cells by stimulating humoral and cellular immune responses (Nooraei et al., 2021). Furthermore, currently, four VLP-based vaccines against human papilloma virus, malaria and hepatitis B and E viruses are authorized, although many others have entered clinical trials (for review, see Balke and Zeltins, 2019; Nooraei et al., 2021).

A variety of VLPs can be modified to display antigens by using different gene engineering technologies, resulting in recombinant N-, C-, or internal fusions (Frietze et al., 2016). This includes insertion of antigenic sequences onto the VLP surface to achieve optimal epitope presentation without affecting viral morphology (Balke and Zeltins, 2019) since insertions up to 50 aa can easily be tolerated (Lebel et al., 2015) but successful incorporation of proteins of > 300 amino acids in length have been described as well (Walker et al., 2011). A more advanced approach should be considered for placing larger antigens with comparable sizes to the viral coat protein (CP) or antigens with specific biochemical properties. Therefore, mosaic VLPs may overcome these limitations, as they contain unmodified and genetically engineered CPs in the same VLP (Balke and Zeltins, 2019).

Commonly used methods other than molecular cloning are chemical or enzymatic conjugation and physical binding, where foreign antigens are introduced into the structure of VLPs through a specific linkage between two partners (Lebel et al., 2015; Balke and Zeltins, 2019). Chemical coupling of separately purified preassembled carrier VLPs and antigens is achieved by chemical crosslinking agents that modify naturally occurring or engineered surface-exposed lysine residues, creating covalent bonds to the antigen. Several successful examples of vaccines based on chemical coupling against infectious diseases or allergies have been previously published (Zeltins et al., 2017; Gomes et al., 2019; Storni et al., 2019; Rothen et al., 2022). Furthermore, a very efficient enzymatic tool in the vaccine production process based on spontaneous isopeptide bond formation between *Streptococcus pyogenes* bacteria-originated SpyTag/SpyCatcher conjugate partners has recently been described (Ogrina et al., 2022).

Different physical approaches can also be applied in the vaccine construction process for the introduction of peptides or protein domains into VLP structures, which then merge into highly specific, and stable complexes (Balke and Zeltins, 2019). One of many efficient tools that can be used in the construction of vaccines is the artificial complementary coiled-coil-forming oligopeptide pair Ecoil/Kcoil derived from the membrane fusion protein complex SNARE (Litowski and Hodges, 2002; Kumar et al., 2018). The first successful VLP application was heterodimerization using Ecoil/Kcoil demonstrated by Minten et al. (2009) by introducing each binding partner in either CCMV (Cowpea Chlorotic Mottle Virus) or EGFP (enhanced green fluorescent protein), resulting in EGFP-filled capsids. Another option with a similar application was suggested by Reinke et al. (2010) by presenting a set of 23 synthetic coiled-coil pairs (SYNZIPs; SZ). Biophysical characterization of 22 SYNZIP pairs by Thompson et al. (2012) revealed their potential as fusion partners due to the high affinity and specificity between them, which may serve as an attractive protein–protein interaction tool.

Eggplant mosaic virus (EMV) is one of many icosahedral virus species belonging to the *Tymovirus* genus. The members of this genus share many common features, such as size (approximately 30 nm), structural organization, and surface geometry (T = 3 symmetry), possession of positive-sense, single-stranded RNA genome, and dicotyledon plants as preferable plant hosts (Martelli et al., 2002). EMV was first reported in infected Solanaceae family plants in Trinidad (Ferguson, 1951), and the complete genome was sequenced by Osorio-Keese et al. (1989) revealing a genome of 6,330 nt residues organized in three open reading frames (ORFs) (Martelli et al., 2002). *Tymovirus* ORF3 codes for the viral *CP* with a size of approximately 20 kDa, which is translated from a subgenomic RNA (sgRNA; 694 nt) (Khan and Dijkstra, 2006).

Several papers highlight the potential of *Tymovirus* VLPs as efficient scaffolds for antigen presentation due to their protein capsid structure position, which includes three chemically identical CP subunits (A, B, and C) that are each located in a different microenvironment and possess a slightly different conformation, such as pentameric capsomeres (A subunits) and hexameric capsomeres (B and C subunits) (Canady et al., 1996; van Roon et al., 2004; Larson et al., 2005; Barnhill et al., 2007). Furthermore, early Turnip yellow mosaic virus (TYMV) studies demonstrated a different type of viral capsid that lacks viral RNA, resulting in the formation of empty shells ("top component"; Matthews, 1960). Later, the same phenomenon was found in other *Tymovirus* members, namely, Physalis mottle virus (PhMV) (Krishna et al., 1999), or Belladonna mottle virus (BDMV) (Savithri et al., 1987). This feature is useful for packaging and drug delivery by producing empty shells *in vitro* (van Roon et al., 2004; Powell and Dreher, 2022). These empty CP shells could serve as drug delivery vehicles (Kim et al., 2018) as they can be loaded with fluorescent dyes (Michels et al., 1999; Barnhill et al., 2007; Masarapu et al., 2017; Hu et al., 2019), chemotherapy drugs (Hu and Steinmetz, 2020), and mammalian cell penetrating enzymes (Kim et al., 2018).

Turnip yellow mosaic virus crystallization experiments by Canady et al. (1996) demonstrated that the N-terminal 26 amino acids of the CP A subunit are disordered, forming flexible chains (Barnhill et al., 2007), and are not essential for VLP self-assembly even after removing the first 26 amino acids of the N-terminus of the CP, resulting in no interference in either particle formation or infectivity (Powell et al., 2012). The same phenomenon was observed for PhMV CP VLPs expressed in *Escherichia coli* (Sastri et al., 1997, 1999) and for Tomato blistering mosaic virus (ToBMV)-like particles in a baculovirus expression system (Vasques et al., 2019), suggesting the high potential of the N-terminal end position as a possible antigen presentation locus. Taking this into account, several authors have demonstrated successful epitope insertion in the N-terminal ends of PhMV CP expressed in *E. coli* cell cultures (Hema et al., 2007;

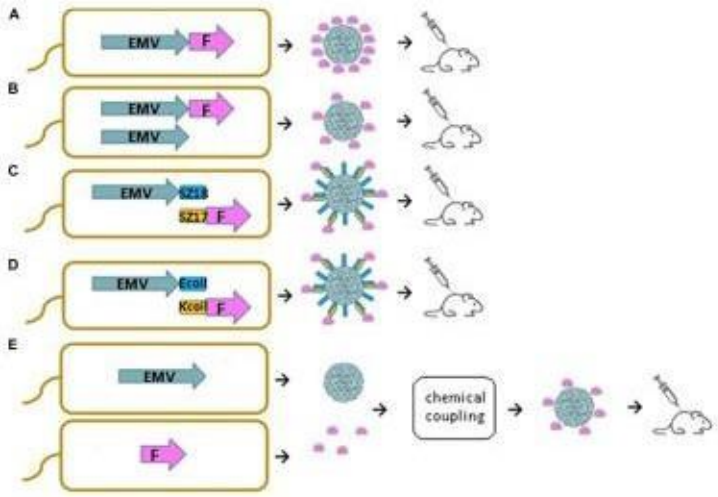

FIGURE 1
Schematic representation of *E. coli* expression systems used to produce EMV-Feld1 VLPs. (A) Direct antigen fusion to the coat protein (CP) of EMV; (B) coexpression of antigen-containing EMV CP and unmodified EMV CP for the production of mosaic VLPs; (C,D) coexpression of vaccine components allowing the formation of VLP-antigen complexes directly in *E. coli* cells; (E) chemical coupling of Feld1 antigen to EMV VLPs. EMV, eggplant mosaic virus; F, Fel d 1 protein; SZ18, synthetic zipper (SZ) 18; SZ17, synthetic zipper (SZ) 17; Ecoil, coiled-coil forming peptide E; Kcoil, coiled-coil forming peptide K.

Chandran et al., 2009; Shahana et al., 2015) or model sequence insertions in TYMV CPs using agroinfiltration in *Nicotiana benthamiana* leaves (Shin et al., 2013, 2018), all resulting in the formation of *Tymovirus*-like particles.

Additionally, a study (Barnhill et al., 2007) revealed that approximately 90–120 carboxyl groups of TYMV CP are exposed on the surface and can be used for chemical modifications. Later, studies of PhMV CP C-terminal end deletions demonstrated its significant role in CP folding and capsid assembly, either by removing 5 and 10 amino acids (Sastri et al., 1997), or even in the case of one residue deletion (Sastri et al., 1999), which resulted in lower yield and unstable capsid formation. Furthermore, short peptide (c-Myc, 10 aa) (Shin et al., 2013), or cysteine residue (Shin et al., 2018) insertion in TYMV CP resulted in disruption of VLP assembly. In contrast, opposite results with no interference in capsid assembly were observed when the C-terminal end of TYMV was extended by a 5 aa sequence (Bransom et al., 1995) or a 10 aa poly-histidine tag (Tan et al., 2021), which were the first reports of successfully produced C-terminally modified TYMV chimeric VLPs in *E. coli*.

The main cat allergen Fel d 1 is one of the identified allergens produced by domestic cats (*Felis domesticus*), causing a severe incidence of allergic respiratory diseases worldwide (Bonnet et al., 2018). Fel d 1 has been extensively studied and served as a model antigen in several of our papers as a part of a conjugate vaccine (Zeltins et al., 2017) or in the form of a fusion protein vaccine (Ogrina et al., 2022), inducing strong immune responses. Although Fel d 1 neutralizing Ab production has been detected in Fel d 1-sensitized mice (Zeltins et al., 2017) and cats (Thoms et al., 2020), there is no commercially available vaccine on the market.

In this study, we demonstrate that new VLPs derived from EMV CP are suitable for the construction of antigen-containing vaccine candidates. Moreover, we show that antigen sequences can be incorporated into the VLP structure using different genetic, chemical, and physical methods. We introduced a flexible 15 aa linker sequence $(GGGGS)_3$ at the C-terminal end of EMV CP by PCR mutagenesis followed by the introduction of the previously described main cat allergen from *F. domesticus* Fel d 1 as a model antigen. We compared four different bacterial expression systems for vaccine generation, such as direct genetic fusion of the antigen with *Tymovirus* EMV CPs (Figure 1A), mosaic VLPs (Figure 1B), and two coexpression variants of EMV VLP and antigen sequences using synthetic zipper pairs 18/17 (SZ18/17) (Figure 1C) and coiled-coil forming peptides E and K (Ecoil/Kcoil) (Figure 1D). All variants were expressed in *E. coli*, formed *Tymovirus*-like VLPs and were used for immunological evaluation in healthy mice individuals. Furthermore, recombinant Fel d 1 (rFeld1) was chemically coupled to EMV CP VLPs and included in mural immunization experiments (Figure 1E) to find the most promising platform for antigen presentation.

2. Materials and methods

2.1. Cloning of EMV *CP*

The sequence of the EMV *CP* gene (wtEMV; GenBank Accession Number: NC_001480.1) was obtained as a product

of gene synthesis (plasmid pUC57-EMV; BioCat, Heidelberg, Germany) with flanking restriction sites *Nde*I and *Xho*I for further subcloning. The wtEMV *CP* gene was excised from the helper plasmid with *Nde*I and *Xho*I restriction enzymes (Thermo Fisher Scientific, Waltham, MA, USA), followed by DNA fragment purification with the GeneJET Gel Extraction Kit (Thermo Fisher Scientific, Waltham, MA, USA) and cloning into the *Nde*I and *Xho*I sites of the *E. coli* expression vector pET42a(+) (Novagen, Madison, WI, USA), resulting in the pET42-EMV expression vector. XL1-Blue Super competent cells (Agilent Technologies, Santa Clara, CA, USA) were used for plasmid preparations. Clones with the corresponding insert were selected by restriction analysis by digestion with *Nde*I and *Xho*I.

2.2. Construction of the EMV direct fusion and mosaic system with Feld1

The *Fel d 1* gene used in this study has been described previously (Zeltins et al., 2017; Ogrina et al., 2022). For the construction of the EMV-Feld1 direct fusion and mosaic system, we introduced *Bam*HI and *Xho*I sites in the Fel d 1 gene by PCR mutagenesis using the primers Feld_BamF (5′ CAG GAT CCG AAA TTT GTC CGG CAG TTA AAC G 3′) and Feld_XhoR (5′ CTC GAG TTA TTA ACG ACC CAG GGT ATT CAG TTT C 3′) and Taq DNA polymerase (Thermo Fisher Scientific, Waltham, MA, USA). PCRs were carried out in a 96-well thermal cycler Veriti (Thermo Fisher Scientific, Waltham, MA, USA). The PCR product was subcloned into the linearized vector pTZ-57 using the InsTAclon PCR Cloning Kit (Thermo Fisher Scientific, Waltham, MA, USA), resulting in pTZ-Feld1-Bam-Xho. PCR fragment-containing clones were selected by digestion analysis using *Bam*HI and *Xho*I restriction enzymes (Thermo Fisher Scientific, Waltham, MA, USA). For all PCR-derived plasmids, three positive clones were sequenced by the Sanger sequencing method using the ABI PRISM BigDye Terminator v3.1 Ready Reaction Cycle Sequencing Kit (Thermo Fisher Scientific, Waltham, MA, USA) and ABI PRISM 3130xl sequencer (Thermo Fisher Scientific, Waltham, MA, USA) with the corresponding primers M13seq-F (5′ GCC AGG GTT TTC CCA GTC ACG A 3′) and/or M13seq-R (5′ GAG CGG ATA ACA ATT TCA CAC AGG 3′). The clone without PCR errors was used for further development of the Fel d 1 expression vector.

For the EMV *CP* gene, we introduced a flexible linker $(GGGGS)_3$ and *Bam*HI site coding sequences at the 3′-terminus. The EMV CP 3′-terminal fragment and corresponding additional sequences were amplified in PCR mutagenesis using long overlapping primers EMV-g4sF (5′ CCA TGG CAA GCT CCG CTT GTC CTC CCC CCT CCT CCA AGC CAA TGG AGG AGG TGG TAG TGG TGG AGG TGG ATC T 3′) and EMV-g4sR (5′ CTC GAG AAG CTT ATT AGG ATC CAC CTC CTC CAG ATC CAC CTC CAC CAC TAC CAC CTC CTC C 3′) without template. A PCR fragment (3′EMV-CG4S) containing clones (pTZ-3′EMV-CG4S) was selected after sequencing several plasmid clones. The *Nco*I/*Xho*I fragment from pTZ-3′EMV-CG4S was further ligated into the pET42-EMV vector digested with the same enzymes, resulting in the pET42-EMV-CG4S vector. The corresponding vector clone was selected by digestion analysis using *Nde*I/*Xho*I restriction enzymes.

The *Fel d 1* sequence was excised from pTZ-Feld1-Bam-Xho with *Bam*HI and *Xho*I restriction enzymes and ligated into the linearized vector pET42-EMV-CG4S at the same sites. The correct clone of the direct fusion plasmid pET42-EMV-CG4S-Feld1 was selected by digestion analysis with *Sty*I (Thermo Fisher Scientific, Waltham, MA, USA) and *Xho*I.

For the mosaic system, we introduced flanking *Psc*I and *Sal*I restriction enzyme sites into the EMV CP gene by PCR mutagenesis using the following primers: EMV-PscF (5′ ACA TGT CTG AAG ACA CAG CAA TCA TCA GAA 3′) and EMV-SalR (5′ GTC GAC TTA TTA ATT GGC TTG GAG GAG GGG GGA 3′). The pTZ-57 plasmid containing the PCR fragment (EMV-Psc) was selected by digestion analysis using *Psc*I and *Sal*I restriction enzymes (Thermo Fisher Scientific, Waltham, MA, USA). After verification by Sanger sequencing, the corresponding EMV-Psc fragment was excised from pTZ-EMV-Psc by *Psc*I and *Sal*I restriction enzymes (Thermo Fisher Scientific, Waltham, MA, USA) and ligated into the pETDuet-1 (Novagen, Madison, WI, USA) vector under the first T7 promoter in the cloning sites *Nco*I (Thermo Fisher Scientific, Waltham, MA, USA) and *Sal*I. A correct clone of the resulting pETDu-EMV was found after restriction analysis using the *Not*I enzyme.

The plasmid pETDu-EMV was further used for subcloning of the EMV-CG4S-Feld1 gene from the pET42-EMV-CG4S-Feld1 vector under the second T7 promoter using *Nde*I and *Xho*I digestion enzymes. The plasmid clone encoding proteins in the mosaic system (pETDu-mEMV-CG4S-Feld1) was selected by digestion analysis with *Nco*I and *Xho*I.

2.3. Cloning of complementary coiled-coil forming peptides *K* and *E*

The coding sequences of coiled-coil peptides E (Ecoil) and K (Kcoil) were obtained from overlapping oligonucleotides in PCRs without a template. The Ecoil coding sequence was amplified using primers Ecoil-BamF (5′ CAG GAT CCG AAA TTG CTG CTC TCG AAA AAG AGA TCG CGG CGC TCG AAA AAG AAA TT 3′) and Ecoil-XhoR (5′ CTC GAG AAG CTT ATT TTT CAA GAG CAG CAA TTT CTT TTT CGA GCG CCG CGA 3′). The *Ecoil* coding sequence was introduced after the $(GGGGS)_3$ linker-coding sequence into the vector pET42-EMV-CG4S using cloning sites *Bam*HI and *Xho*I.

For the Kcoil expression vector, the Kcoil coding sequence was also obtained by PCR using the following oligonucleotides: Kcoil-NcoF (5′ CCA TGG GAA AGA TCG CGG CCC TCA AAG AAA AGA TCG CCG CCC T 3′) and Kcoil-BamR (5′ GGA TCC TTC CTT CAG GGC CGC AAT CTT TTC CTT GAG GGC GGC GAT CTT TTC T 3′). The PCR product was cloned into the pTZ57 vector, and after verifying the sequence, it was introduced into the pACYCDuet-1 vector at the *Nco*I and *Bam*HI sites. Next, the Feld1 sequence was introduced into the resulting vector pACYCDu-Kcoil(3x) between the cloning sites *Bam*HI and *Xho*I. Both Ecoil- and Kcoil-containing plasmids were sequenced and used for coexpression of EMV-CG4S-Ecoil(3x) and Kcoil(3x)-Feld1 proteins.

2.4. Cloning of synthetic coiled-coil anti-parallel zipper pair SYNZIP 17/18

The corresponding sequences for the synthetic zipper pair *SYNZIP (SZ) 17* and *18* were obtained from published Supplementary material by Reinke et al. (2010) and purchased as a gene synthesis product in plasmid pUC57 (BioCat, Germany). For further subcloning, the plasmid pUC57-SZ17 (Amp) contained the introduced restriction sites of *Nco*I and *Hin*dIII, and pUC57-SZ18 (Amp) contained the *Nde*I and *Xho*I restriction sites. For convenient protein coexpression in *E. coli* cells, each SZ pair was subcloned into vector plasmids with different antibiotic resistances. SZ17 was subcloned into the commercial vector plasmid pRSFDuet-1 (Novagen, USA) with the kanamycin resistance gene using previously introduced *NdeI/XhoI* restriction sites, and SZ18 was subcloned into pET-Duet1 (Novagen, USA) with the ampicillin resistance gene using *NcoI/Hin*dIII sites, resulting in plasmids pRSF-Duet-SZ17 and pET-Duet-SZ18.

For the Feld1 antigen-SYNZIP 17 fusion, the pTZ-Feld1-Bam-Xho plasmid was digested with *Bam*HI/*Xho*I and subcloned into the same sites of pRSF-Duet-SZ17 after partial restriction enzyme treatment, resulting in the expression vector pRSF-SZ17-Feld1. Additionally, for convenient protein purification, the 6xHis-tag coding sequence was introduced into the constructed pRSF-SZ17-Feld1 sequence by subcloning the *MscI/XhoI* fragment from plasmid pET42-Feld1-C6H (Zeltins et al., 2017) into pRSF-SZ17-Feld1 digested with the same enzymes. The sequence of the resulting plasmid pRSF-SZ17-Feld1-C6H was verified by sequencing to confirm the introduction of His-tag coding DNA.

To obtain the EMV *CP-SYNZIP 18* fusion construct, the previously mentioned EMV *CP*-containing plasmid for direct fusion pET42-EMV-CG4S was digested with *Bam*HI/*Sph*I, and subcloned into the pET-Duet-SZ18 plasmid cut by the same restriction enzymes, resulting in the expression vector pETDu-EMV-CG4S-SZ18. Several plasmid clones were sequenced to confirm the introduction of the SZ18-EMV sequence.

2.5. Expression and purification of EMV CP VLPs and EMV-Feld1-containing VLPs

First, all constructed expression vectors coding for wtEMV CP, direct fusion (EMV-CG4S-Feld1), and mosaic fusion (mEMV-CG4S-Feld1) were transformed into *E. coli* C2566 cells (New England, USA). For coiled-coil partners, two expression strategies were used. First, EMV-CG4S-SZ18- and EMV-CG4S-Ecoil-containing plasmids as well as plasmids coding for Feld1 expression SZ17-Feld1-C6H and Kcoil-Feld1 were expressed separately by directly transforming them into *E. coli* C2566 cells (New England, USA). Second, coexpression of EMV-Ecoil/Kcoil-Feld1 and EMV-SZ18/SZ17-Feld1 plasmids in *E. coli* C2566 cells was performed. After expression, the highest yield producing clones for the target protein were cultivated in 2TY medium (1,6% tryptone, 1,0% yeast extract, and 0.5% NaCl) with the addition of the corresponding antibiotic (kanamycin for pET42 and pRSF-derivatives, 25 mg/L; ampicillin for pETDuet-1 derivatives, 100 mg/L; and chloramphenicol for pACYCDuet-1 derivatives, 25 mg/L). Cultivation conditions were as previously described (Balke et al., 2018). In brief, flasks with cells were cultivated using an Ecotron HT table-top incubation shaker (200 rev/min; Infors, Switzerland) at 30°C until the OD reached 0.8–1.0. After induction with 0.2 mM isopropyl β-d-1-thiogalactopyranoside (IPTG), cells were further cultivated at 20°C for 18 h, collected by low-speed centrifugation (8,228 × *g*, 5 min, 5°C, Eppendorf 5804R, Germany) and kept frozen at −70°C until use.

The cells containing wtEMV CP were thawed on ice, suspended in 1× PBS and disrupted using an ultrasonic device (Hielscher 200, power 70%, pulse 50%, 16 min) on ice. The same procedure was applied for direct fusion and mosaic EMV-Feld1 using PBS buffer containing 5 mM β-mercaptoethanol (β-ME). For separately expressed EMV-CG4S-Ecoil, EMV-CG4S-SZ18, Kcoil-Feld1, and SZ17-Feld1-C6H for both coexpression pairs EMV-Ecoil/Kcoil-Feld1 and EMV-SZ18/SZ17-Feld1, 1× PBS with an additional 5 mM β-ME and 0.5% TX-100 was used in the cell disruption procedure with the same parameters. The solutions were collected, and cell debris was removed by centrifugation (15,557 × *g*, 10 min, 5°C).

The purification was performed by ultracentrifugation for all constructs except for wtEMV VLPs and SZ17-Feld1-C6H in a sucrose gradient (20–60% sucrose in 1× PBS with additional 0.5% TX-100) as described in our previous paper (Ogrina et al., 2022). After ultracentrifugation, fractions were collected and analyzed by SDS-PAGE to select fractions with EMV-Feld1-containing VLPs or Kcoil-Feld1 protein. VLP samples were then combined and transferred to a new ultracentrifugation tube followed by a second round of ultracentrifugation to sediment the VLPs (Optima L-100XP; Type70Ti rotor, Beckman, USA; 183,960 × *g*, 4 h, 4°C). The pellet was then dissolved in 1× PBS. Soluble wtEMV proteins were purified by polyethylene glycol (PEG) precipitation by adding 8% PEG8000 and 0.3 M NaCl to the cell lysate. After incubation, the VLP precipitate was separated from cellular proteins (15,557 × *g*, 10 min, 5°C), and the pellet was dissolved in 1× PBS. Precipitation was repeated three more times.

After purification or precipitation, all EMV CP VLPs (wtEMV; EMV-Feld1, mEMV-Feld1, EMV-CG4S-Ecoil; EMV-CG4S-SZ18, EMV-SZ18/SZ17-Feld1 and EMV-Ecoil/Kcoil-Feld1) were further purified using ultracentrifugation through the 30% sucrose "cushion" in 1× PBS supplemented with 0.5% TX-100 (Optima L-100XP; Type70Ti rotor, Beckman, USA; 183,960 × *g*, 4 h, 4°C). Pellets were then dissolved in 1× PBS and, if necessary, concentrated using an Amicon Ultra-15, 100 K filtration unit (Merck-Millipore, USA), keeping the final VLP products stored at 4°C.

Kcoil-Feld1 protein after purification in a sucrose gradient (Supplementary Figure 10) was dialyzed against 100 volumes of 1× PBS followed by purification with gel filtration on a ÄKTA Pure 25 XK 16/70 Superdex200 column (GE Healthcare, USA). Purified proteins were eluted with 1× PBS at 1 ml/min, collecting 2 ml per fraction. Separately expressed SZ17-Feld1-C6H was purified on a His-tag column and dialyzed as previously described (Zeltins et al., 2017).

The concentrations of all purified proteins were estimated using a Qubit Protein Assay Kit (Thermo Fisher Scientific, USA) and Qubit 2.0 fluorometer (Thermo Fisher Scientific, USA) according to the manufacturer's recommendations. All steps in the purification/precipitation process were monitored by using 12.5% SDS-PAGE and agarose gels and Western blot (WB) analysis.

2.6. Chemical coupling of wtEMV CP VLPs and rFeld1

rFel d 1 was expressed and purified as previously described (Zeltins et al., 2017). For chemical coupling, the crosslinker succinimidyl-6-(β-maleimidopropionamido)-hexanoate (SMPH; Thermo Fisher Scientific, USA) was used for rFel d 1 conjugation to wtEMV CP VLPs. A threefold molar excess of SMPH to EMV VLPs was used for the reaction at 23°C for 1 h. Unreacted SMPH was removed by an Amicon Ultra-15, 50 K centrifugal filter (Merck-Millipore, USA) washing with 1× PBS four times (4 × 6 min) at 3,214 × *g* (5,000 rpm) and 5°C. The antigen was treated with a 10-fold molar excess of the mild reducing agent tris (2-carboxyethyl) phosphine (TCEP; Sigma-Aldrich, Burlington, MA, USA) for 10 min at 23°C prior to chemical conjugation. The coupling was performed by adding a twofold molar excess of rFel d 1 to the SMPH-derivatized wtEMV VLPs at 23°C for 2 h by shaking at 1,400 rpm/min on a DSG Titertek (Flow Laboratories, Oldham, UK). Free rFel d 1 was removed using an Amicon Ultra-15, 50 K centrifugal filter (Merck-Millipore, USA) by washing with 1× PBS four times (4 × 6 min) at 3,214 × *g* (5,000 rpm) and 5°C. All stages of coupling were monitored by SDS-PAGE and native agarose gel, and the integrity of VLPs was confirmed by transmission electron microscopy (TEM).

2.7. Binding of coiled-coil partners *in vitro*

After purification, separately expressed coiled-coil pairs EMV-CG4S-Ecoil and Kcoil-Feld1 or EMV-CG4S-SZ18 and SZ17-Feld1-C6H were mixed together in a 1:1 ratio according to their concentrations in a volume of 100 μl and incubated for 1 h at room temperature (RT). Additionally, as EMV-SZ18/SZ17-Feld1-C6H contains a 6-histidine tag, it was purified using a His-tag column as previously described and dialyzed against 100 volumes of 1× PBS followed by 12.5% SDS-PAGE, NAG analysis and TEM. All steps from the binding process were analyzed in SDS-PAGE and agarose gels and examined under TEM as well (Supplementary Figures 9, 11). Concentrations of protein samples were measured by a Qubit 2.0 fluorometer (Thermo Fisher Scientific, USA) with a Qubit Protein Assay Kit (Thermo Fisher Scientific, USA) according to the manufacturer's recommendations.

2.8. Transmission electron microscopy

All steps for purified EMV CP VLP visualization in TEM were performed as previously described in our paper (Ogrina et al., 2022). At least five pictures were captured per sample.

2.9. Immunological evaluation of EMV CP-Feld1-containing VLPs

2.9.1. Western blot analysis

Western blot analysis was performed as described in Ogrina et al. (2022). First, samples for EMV-Feld1-containing VLPs were loaded and run on 17-well 1.0 mm Bolt 4–12% Bis-Tris Plus gel (Thermo Fisher Scientific, USA). The corresponding proteins were then transferred onto an Amersham Protran 0.45 μm nitrocellulose membrane (GE Healthcare, Piscataway, USA) for antibody detection using a semidry blotting apparatus (45 mA, 45 min). A membrane was then blocked with 1% alkali-soluble casein (Merck-Millipore, USA) for 1 h at RT followed by incubation overnight at 4°C in anti-EMV and anti-Feld1 polyclonal antibodies (Ab's) (dilution 1: 1,000 in PBS with 1% alkali-soluble casein, in-house produced). After a 15 min washing step with TBS buffer (150 mM NaCl; 10 mM Tris pH 7.5), membranes were incubated for 3 h with horseradish peroxidase-conjugated anti-mouse IgG (Sigma-Aldrich, USA; 1:1,000 in PBS with 1% alkali-soluble casein) at RT. After a repeated washing step with TBS buffer, signals were detected by incubating the membrane in TBS buffer supplemented with peroxidase substrates (0.002% *o* – dianisidine and 0.03% hydrogen peroxide).

2.9.2. Vaccination

Female BALB/c mice (5 per group, 6–8 weeks, Laboratory Animal Centre, University of Tartu, Estonia) were vaccinated subcutaneously (s.c.) with 30 μg of total protein of each VLP (five groups – direct, mosaic, Ecoil/Kcoil, SZ18/SZ17, and chemically coupled) in 300 μl of PBS on Day 0. Mice were boosted on Days 14 and 28 with the same dosage of VLPs. Serum samples from each mouse were collected on Days 0, 14, and 28, and final bleeding was performed on Day 42. All animal-related procedures in this study were approved by the Animal Protection Ethical Committee of the Latvian Food and Veterinary Service (permission No. 89).

2.9.3. Enzyme-linked immunosorbent assay

Enzyme-linked immunosorbent assay (ELISA) tests were performed as described in Ogrina et al. (2022). The plates (96-well; Nunc Immuno MaxiSorp, Rochester, NY, USA, Thermo Fisher Scientific, USA) were coated with 100 μl of 10 μg/ml purified samples (EMV CP or rFeld1) in 50 mM sodium carbonate buffer (pH 9.6) overnight at 4°C. After three washes of the plates with PBS-0.05% Tween-20 solution and blocking with 1% BSA in PBS at 37°C for 1 h, 100 μl of serially diluted mouse sera were added to the wells and incubated for 1 h at 37°C. Then, the washing step was repeated three times, followed by incubation with 100 μl of secondary antibodies (anti-mouse IgG conjugated to horseradish peroxidase, dilution 1: 10,000; Sigma-Aldrich, USA; 1 h, 37°C). Finally, plates were washed once again three times, and the substrate (o-phenylenediamine dihydrochloride, OPD; Sigma-Aldrich, USA) was added for color development. The absorbance measurements were performed using a Labsystems 353 Multiscan MS microplate reader (Sweden) at 492 nm. Final titers were calculated as the highest absorbance values that exceeded threefold of the negative control (non-immunized mouse serum) which was collected from all five immunization groups on Day 0 and pooled (5 μl from each mouse per group).

Monoclonal Feld1 antibody ELISA tests were similarly performed by replacing the immunized mouse sera with two commercially available Feld1 mAbs as described previously according to manufacturers' guidelines (MA-3E4 and MA-6F9, Indoor Biotechnologies, UK; Ogrina et al., 2022). After blocking with 1% BSA in PBS at 37°C for 1 h, serial dilutions of two types

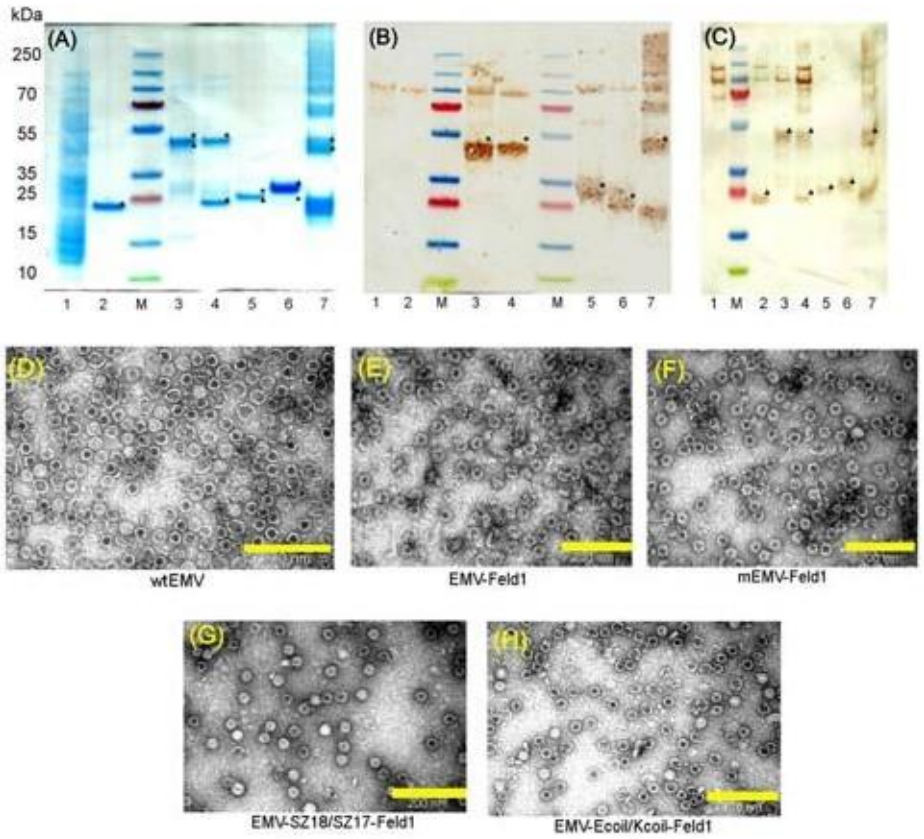

FIGURE 2
Analysis of EMV-derived VLPs containing Feld1 antigen. (A) Coomassie – stained 10 well 1.0 mm Bolt 4–12% Bis-Tris Plus gel (Thermo Fisher Scientific, USA) of EMV-Feld1 vaccine variants at a concentration of 0.7 mg/ml; (B) the same samples as in panel (A) analyzed by Western blot using anti-Feld1 polyclonal antibodies; and (C) the same samples as in panel (A) analyzed by Western blot using anti-EMV polyclonal antibodies. Electron micrographs of negatively stained VLPs: (D) EMV wt; (E) direct fusion EMV-Feld1; (F) mosaic EMV-Feld1; (G) EMV-SZ18/SZ17-Feld1; and (H) EMV-Kcoil/Ecoil-Feld1. Scale bars, 200 nm. M, PageRuler Plus Prestained Ladder, 10–250 kDa (Thermo Fisher Scientific, USA); 1, total cell lysate of *E. coli* C2566 strain (negative control); 2, wtEMV (control); 3, EMV-Feld1; 4, mEMV-Feld1; 5, EMV-SZ18/SZ17-Feld1; 6, EMV-Ecoil/Kcoil-Feld1; 7, wtEMV coupling with 2xFeld1-C6H-CG. Asterisk denotes the relative position of Feld1 protein; triangle denotes the relative position of EMV CP protein.

of mAbs were added to plates and incubated for 1 h 37°C and then washed three times with PBS containing 0.05% Tween-20. The rest of the procedure was the same as to that described above. Non-immunized mouse serum was used as a negative control and titer calculations were performed as described above.

To assess the subclass antibody response (IgG1 and IgG2a), isotype-specific ELISA experiments were performed for both anti-EMV and anti-Feld1 Ab detection for each mouse from sera obtained from Day 42 following the manufacturer's protocol (mouse mAb antibody isotyping reagent ISO2-1KT kit; Sigma-Aldrich, USA). For secondary Abs, a peroxidase conjugate of monoclonal anti-goat/sheep IgG Abs (Sigma-Aldrich, USA) was used, and endpoint titers were calculated as previously described.

2.9.4. Avidity ELISA

Avidity ELISA is performed as previously described ELISA test with one additional washing step and was performed following the protocol described in our previous papers (Mohsen et al., 2021; Ogrina et al., 2022) using sera obtained on Day 42 from each mouse: two sets of plates were coated with 10 μg/ml EMV- or rFeld1-derived proteins. After serum incubation plates were washed separately, one set of plates was washed three times with 50 μl/well of a 7 M urea solution in PBS-0.05% Tween-20 for 5 min, whereas other plates were washed with the same volume of PBS-0.05% Tween-20. For the rest of the washing steps, a solution of PBS-0.01% Tween-20 was used. The following procedure was identical to that reported above.

2.9.5. ELISA for native Feld1

For native Feld1 (nFeld1) – EMV-Feld1 containing VLP variants, all five constructed VLP variants at a concentration of 10 μg/ml in 50 mM sodium carbonate buffer (pH 9.6, 100 μl per well) were coated on ELISA plates and stored at 4°C ON. Final mouse serum samples (5 mice per group) from each of five immunization groups were pooled (5 μl from each mouse), serially diluted, added to the wells, and incubated as previously described. The rest of the ELISA test was performed as described before. The endpoint titers were calculated as stated above.

3. Results

3.1. EMV CP Feld1 VLP construction and characterization

Our previous results demonstrated that a flexible 15 aa long glycine-serine linker sequence [$(GGGGS)_3$; G4S] improved the overall flexibility of the Feld1 antigen dimer (Zeltins et al., 2017) and allowed the folding and VLP assembly of potato virus Y (PVY) CP-antigen fusion (Kalnciema et al., 2012; Ogrina et al., 2022). The usefulness of the G4S linker was previously shown for C-terminal fusions to Tobacco mosaic virus (TMV) CP (Werner et al., 2006). Several prior failed attempts with *Tymovirus* CP C-terminal fusions have been noted (Shin et al., 2013, 2018); therefore, we assumed that adding the G4S linker sequence should facilitate VLP formation after genetic fusion of foreign antigens. We constructed the C-terminally extended EMV CP resulting in EMV-CG4S, which formed intact icosahedral VLPs with a size of ~28–30 nm after expression in *E. coli* and purification (data not shown).

Next, we constructed direct fusion of EMV-CG4S and Feld1 antigen (Supplementary Figure 1) and expressed the fusion protein in *E. coli* cells. In addition, we constructed mosaic VLPs by incorporating unmodified wtEMV *CP* and the newly constructed EMV-CG4S-Feld1 *CP* gene into the pET-Duet expression vector (Supplementary Figure 2). After expression in *E. coli* cells, both EMV-CG4S-Feld1 CPs and mEMV-CG4S-Feld1 CPs were analyzed in SDS-PAGE, confirming an EMV-CG4S-Feld1 protein size of ~50 kDa (Figure 2A, lane 3), but for the mosaic system, two bands were identified – the same of 50 kDa for EMV-CG4S-Feld1 CP and wtEMV CP with a size of ~19.6 kDa (Figure 2A, lane 4), which was exactly the same as the separately expressed wtEMV used for control analysis (Figure 2A, lane 2). Electron microscopy analysis resulted in the identification of *Tymovirus*-like particle formation with a size of approximately 30 nm for both constructed VLP platforms. Unlike wtEMV VLPs (Figure 2D), Feld1-containing particles seemed more heterogeneous, and fragments of partially assembled VLPs were identified for either direct (Figure 2E) or mosaic VLPs (Figure 2F). In the case of direct fusion, each CP subunit is fused to the Feld1 antigen, resulting in 100% incorporation of the Feld1 antigen. The results of densitometric analysis of SDS-PAGE images suggested an approximate 46% Feld1 antigen incorporation in mosaic VLPs. The output of both VLPs after purification was approximately 7–8 mg/L.

To overcome the limiting factors that may arise from genetic fusion, such as incomplete assembly and stability of VLPs, several approaches using chemical and physical methods are available (Balke and Zeltins, 2019). We have previously described a successful strategy of using SpyTag/SpyCatcher for VLP-Feld1 chemical conjugate formation directly in bacterial cells (Ogrina et al., 2022). Here, we tested two binding partners: coiled coil-forming oligopeptide K and E interaction (Kcoil/Ecoil; Litowski and Hodges, 2002) and orthogonal synthetic coiled-coil anti-parallel "zipper" pair SYNZIP17/18 (SZ17/18; Reinke et al., 2010; Thompson et al., 2012), which should form stable physical complexes between protein partners when Kcoil/Ecoil or SYNZYP 17/18 sequences are genetically introduced in target proteins.

First, we constructed two EMV CP genetic fusions encoding DNAs of negatively charged peptides (Ecoil or SZ18, Supplementary Figures 3, 6) were subcloned into the pET42-EMV-CG4S CP plasmid, resulting in two new expression vectors coding for EMV-CG4S-Ecoil and EMV-CG4S-SZ18, which were then expressed separately in the *E. coli* cell strain C2566 to confirm solubility, expression level, and intact VLP formation (Supplementary Figures 8, 10). Further cloning involved the subcloning of the *Feld1* coding sequence into plasmids containing either the positively charged SZ17 or Kcoil sequence (Supplementary Figures 4, 5, 7). Both binding partners were then coexpressed, purified, and used for further characterization by SDS-PAGE, WB, and NAG analysis. To confirm that separately expressed and purified VLPs and Feld1 are capable of interacting, we also expressed each binding partner in the C2566 *E. coli* strain separately, followed by purification and binding. After binding, we observed complex formation after agarose gel analyses (Supplementary Figures 9, 11). The output of VLPs was approximately 77 mg/L for SZ18/17 and 46 mg/L for Ecoil/Kcoil coexpression VLPs.

Molecular mass calculations suggested that the SZ18/17 protein pair has an approximately similar molecular weight at ~25 kDa, which can be seen as overlapping bands in SDS-PAGE (Figure 2A, lane 5), whereas the Ecoil/Kcoil protein pair appears as two distinct bands, where one could be identified as an ~23 kDa band corresponding to the EMV-Ecoil part and a weak signal band at ~ 21.7 kDa for the Feld1-Kcoil part (Figure 2A, lane 6). To confirm that both covalently linked pairs are present in our samples, we performed WB analysis using antibodies against both Fel d 1 and carrier EMV VLPs for all vaccine candidates, where wtEMV was used as a negative control for the Feld1 signal (Figures 2B, C, lane 2). In the case of Fel d 1, we used polyclonal Fel d 1 Abs obtained from our previous experiments with BALB/c mice (Zeltins et al., 2017). WB analysis indicated that both Feld1 and EMV were copurified in the same sucrose-gradient fractions (Figures 2B, C), seen as colored bands at the expected protein sizes when analyzed with corresponding antibodies (anti-Feld1 or anti-EMV). Furthermore, probably due to chosen purification conditions that failed to remove small amounts of host proteins, all of the samples gave additional ~100 kDa bands (Figures 2B, C, lanes 1–6), which were considered the background, as some in-house-produced polyclonal Abs reacted to those proteins as well during previous immunization experiments.

For EMV detection in WB, we used polyclonal Abs from experiments with Balb/C mice immunized with wtEMV-derived VLPs (unpublished) and observed that EMV was present in all samples (Figure 2C). Densitometric analysis of SDS-PAGE

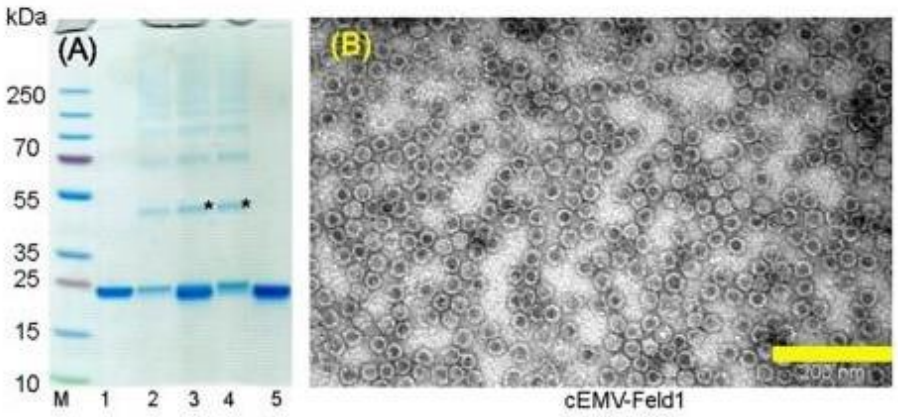

FIGURE 3
Chemically coupled EMV-2xFeld1 analysis. (A) Coomassie – stained 10 well 1.0 mm Bolt 4–12% Bis-Tris Plus gel (Thermo Fisher Scientific, USA). (B) Electron micrographs of negatively stained cEMV-Feld1. M, PageRuler Plus Prestained Ladder, 10–250 kDa (Thermo Fisher Scientific, USA); 1, wtEMV; 2, EMV after 3xSMPH derivatization and unreacted SMPH removal; 3, EMV coupling with Feld1-C6H-CG; 4, EMV + 2xFeld1-C6H-CG after Feld1-C6H-CG removal; 5, Feld1-C6H-CG treated with 10x TCEP. *Coupling product of EMV-rFeld1. Scale bar, 200 nm.

gels suggested 56% Fel d 1 incorporation for EMV-SZ18/SZ17-Feld1 and only 5.2% for EMV-Kcoil/Ecoil-Feld1. Additional TEM analysis demonstrated icosahedral particle formation for both vaccine constructs (Figures 2G, H).

3.2. Chemical coupling of EMV CP with Feld1

Two components (EMV CP VLP and antigen) for chemically coupled EMV-Feld1 (cEMV-Feld1) variant construction were expressed and purified separately. First, we purified unmodified wtEMV VLPs as described in the Materials and Methods and measured the concentration using a Qubit Protein Assay Kit (Thermo Fisher Scientific, USA). The purified sample was analyzed by SDS-PAGE (Figure 2A, lane 2 and Figure 3A, lane 1), and the correct protein size of ~25 kDa was confirmed. TEM was used to visualize VLP formation (Figure 2D). The wtEMV sample was then mixed with SMPH for derivatization and incubated for 1 h, after which unreacted SMPH was removed.

Recombinant Fel d 1 protein with an additional His-tag was purified as previously described (Zeltins et al., 2017; Ogrina et al., 2022) followed by treatment with the reducing agent 10xTCEP to gain access to the cysteine at the COOH terminus of rFeld1. Finally, 2 molar excess of rFeld1-TCEP complex was added to derivatized EMV at 23°C for 2 h, and uncoupled rFeld1 was then removed by ultrafiltration in Amicon Ultra-0.5, 50 K (Merck-Millipore, USA) filtration units. The coupling reaction was monitored in an SDS-PAGE gel (Figure 3A), and the final product was observed by TEM (Figure 3B), representing well-assembled VLPs and preserving the $T = 3$ icosahedral structure. As the dimer of the EMV CP overlaps with the cEMV-Feld1 signal in the SDS-PAGE gel (Figure 3A, lane 4), we could not perform densitometric analysis of Feld1 incorporation, however, we were able to demonstrate the presence of the cEMV-Feld1 conjugate in WB analysis, which suggests that a successful reaction has taken place (Figures 2B, C, lane 7).

3.3. EMV-Feld1 VLP encapsidated nucleic acids and overall charge

Tymoviruses lack strong RNA-protein interactions due to missing specific regions rich in basic residues in CP amino acid composition (Dupin et al., 1985). As described above, during infection, *Tymoviruses* may produce two types of virions—one that contains a single viral genome (approximately 35% of their mass) as well as free "empty" protein shells, while some of those empty VLPs may pack small RNA molecules from their hosts (Gibbs and Mackenzie, 1998). Another interesting aspect of empty particle formation was addressed in a recent paper suggesting that freezing conditions may influence viral RNA migration through pores in *Tymovirus* capsids (Powell and Dreher, 2022). These observations stimulated us to evaluate encapsulated nucleic acids in all constructed EMV-Feld1 VLPs. This is a very important aspect for vaccine generation, as incorporated nucleic acids serve as Toll-like receptor (TLR) ligands and improve the overall immune response (Mohsen et al., 2020).

The TEM results strongly indicated that the majority of EMV VLPs produced in *E. coli* were indeed "empty" despite using different construction strategies, however, the total proportion of "full" particles increased in the case of binding pairs SZ18/SZ17 and Ecoil/Kcoil as well as for chemically coupled EMV-Feld1 VLPs. To explore this further, we performed native agarose gel (NAG) analysis of constructed vaccines with ethidium bromide staining to evaluate whether the results of TEM analysis correlated with their nucleic acid content. We concluded that the signal intensity for physical binding pairs and chemically coupled VLPs was much

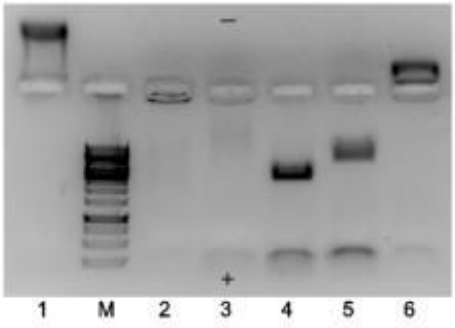

FIGURE 4
Agarose gel analysis of EMV–Feld1 vaccine variants at a concentration of 0.7 mg/mL 1, wtEMV (wild-type; control); M, GeneRuler 1 kb DNA ladder (Thermo Fisher Scientific, USA); 2, EMV-Feld1 (direct fusion VLPs); 3, mEMV-Feld1 (mosaic VLPs); 4, EMV-SZ18/SZ17-Feld1; 5, EMV-Ecoil/Kcoil-Feld1; 6, cEMV-Feld1 (chemically coupled). A 0.8% native agarose gel stained with ethidium bromide was used for analysis. The symbols "+" and "–" denotes the electrode polarity.

stronger than that for direct fusion and mosaic VLPs, as expected (Figure 4, lanes 4, 5, and 6).

Another finding after agarose gel analysis was a different movement of VLPs in the electric field. We observed wtEMV migration toward the negative electrode (Figure 4, lane 1) in the selected buffer system, which can be explained by the calculated isoelectric point of EMV CP (*IEP* = 8.52). The incorporation of Fel d 1 in all VLPs resulted in a reduction in the VLP positive charge due to negatively charged Fel d 1 molecules. Interestingly, direct and mosaic fusion VLPs contained significantly less host RNA than all other vaccine variants (Figure 4, lanes 2 and 3). We also observed that EMV-SZ18/SZ17-Feld1 and EMV-Ecoil/Kcoil-Feld1 VLPs were strongly negatively charged (Figure 4, lanes 4 and 5) and contained large amounts of host nucleic acids.

Our experiments show that a higher nucleic acid content results in VLPs with a higher proportion of "filled" particles. Furthermore, the chosen antigen and nucleic acid content can affect the overall VLP charge. It is known that the surface charge of nanoparticles plays a significant role in the modulation of the immune response, particularly in the activation of dendritic cells (DCs). Moreover, positively charged nanoparticles considerably increase interleukin expression and secretion by DCs compared to negatively charged particles (Fontana et al., 2019).

3.4. Immunological characterization of the EMV-Feld1 vaccine candidates

To gain insight into the immune stimulation properties of the constructed vaccine variants, we performed immunization experiments using murine models. First, before animal immunizations, we evaluated the antigenicity of introduced model antigens on the VLP surface by ELISA using commercially available monoclonal antibodies against Fel d 1 (MA-6F9; MA-3E4; Indoor Biotechnologies, UK). The constructed and purified vaccines were injected into mice, and the formation of total IgG was monitored during repeated vaccination. Additionally, we tested subclass-specific IgG1 and IgG2 Abs and the avidity of Abs obtained from Day 42 to elucidate the proportion of strongly binding antibodies, which correlates with vaccine efficacy, as confirmed in previous studies (Dobano et al., 2019; Rothen et al., 2022). Additionally, the specificity of the generated polyclonal Abs was tested against both recombinant and native Fel d 1 antigen and compared with commercially available mAbs. Immune responses and Ab avidity results are considered important criteria for choosing the most effective VLP variant for further VLP platform development.

3.4.1. Monoclonal antibody ELISA

To characterize the immunogenicity of the constructed EMV-Feld1 vaccine variants, we used two commercially available Fel d 1 mAbs in ELISA experiments as previously described (Ogrina et al., 2022). First, we compared nFel d 1 and rFel d 1 to determine whether rFel d 1 incorporated into VLP structures can be recognized as native. Interestingly, according to the obtained results, rFel d 1 is recognized even better than nFel d 1 by either MA-6F9 or MA-3E4 (Figure 5D), although both mAbs are produced against native Feld 1 allergen. The same finding was detected in our previously performed experiments (Ogrina et al., 2022), but otherwise, no significant differences between mAb titers were identified.

Although both mAbs (MA-3E4; MA-6F9; Indoor Biotechnology, USA) were produced specifically against chain-1 of cat *F. domesticus* allergen Fel d 1 (Schmitz et al., 2009), our recent data with potato virus Y (PVY)-Fel d 1-based vaccines revealed that the binding ability of MA-3E4 mAb was more efficient than MA-6F9 mAb for all produced variants, possibly due to the higher specificity and better access to the corresponding part of the exposed Fel d 1 epitope from chain 1 (Ogrina et al., 2022). The data presented in this experiment also indicated that titers for MA-3E4 mAbs were at least twice as high as those for MA-6F9 for all EMV-Feld1 vaccine variants tested, reaching the maximum for EMV-Feld1 direct fusion (corresponding reciprocal titers for MA-6F9 1: 71,000; for MA-3E4 1: 447,000) (Figures 5A–C) and minimum for EMV-Ecoil/Kcoil-Feld1 (corresponding reciprocal titers for MA-6F9 1: 29,000; for MA-3E4 1: 168,000). Furthermore, both mAbs were also highly specific to mEMV-Feld1 and EMV-SZ18/SZ17-Feld1 (reciprocal titers varying between ~ 1: 350,000 for MA-6F9 and ~ 1: 100,000 for MA-3E4), confirming the presentation of the Fel d 1 epitope on the EMV VLP surface. Overall, these mAb results indicate the most promising VLP vaccine platform with the correct folding of the Fel d 1 epitope after introduction into EMV VLPs.

3.4.2. Total IgG levels

Only some *Tymovirus*-based vaccine studies have emphasized the high potential of the well-described PhMV VLP platforms as effective vaccine candidates either by testing their immunogenicity in sera (Hema et al., 2007; Sahithi et al., 2019) or by performing immunization experiments in guinea pigs and dogs (Chandran et al., 2009) and mice (Shahana et al., 2015; Hu and Steinmetz, 2021). To evaluate the immunological potential of the EMV-based vaccines, total IgG levels against both principal components—antigen Fel d 1 and EMV VLPs of produced chimeric VLP

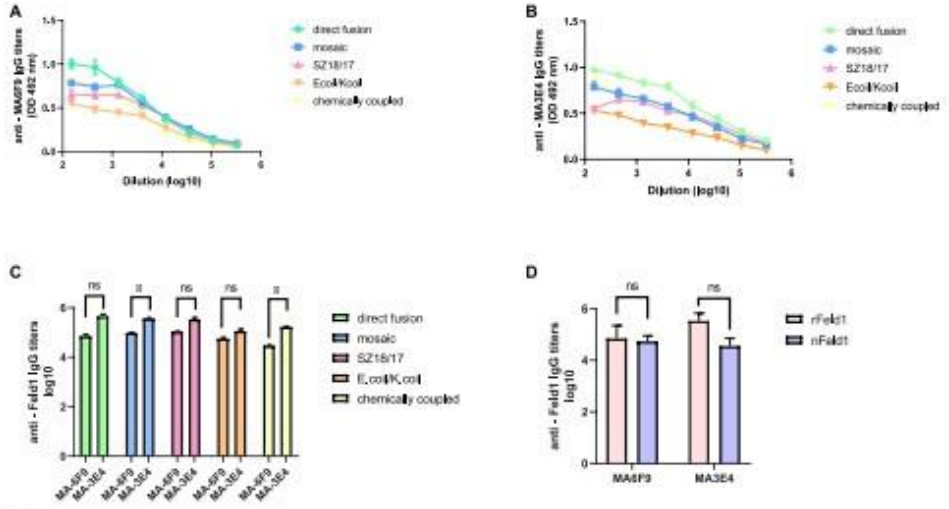

FIGURE 5
Monoclonal Feld1 antibody titers with displayed Feld1 on the surface of vaccine variants. Plates were coated with 10 μg/ml of each VLP. (A) Total IgG titers against Feld1 monoclonal antibody MA-6F9 (Indoor Biotechnologies, UK); (B) total IgG titers against Feld1 monoclonal antibody MA-3E4 (Indoor Biotechnologies, UK); (C) comparison of MA-6F9 and MA-3E4 titers against each vaccine construct; and (D) comparison of monoclonal antibody MA-6F9 and MA-3E4 titers against recombinant Feld1 (rFeld1) or native Feld1 (nFeld1). (C,D) Statistical analysis using Student's *t*-test in GraphPad Prism 8.0. Vaccine groups $n = 5$. Graphs are showing the mean values of single titers. A value of $p > 0.05$ was considered statistically significant (*$p < 0.01$).

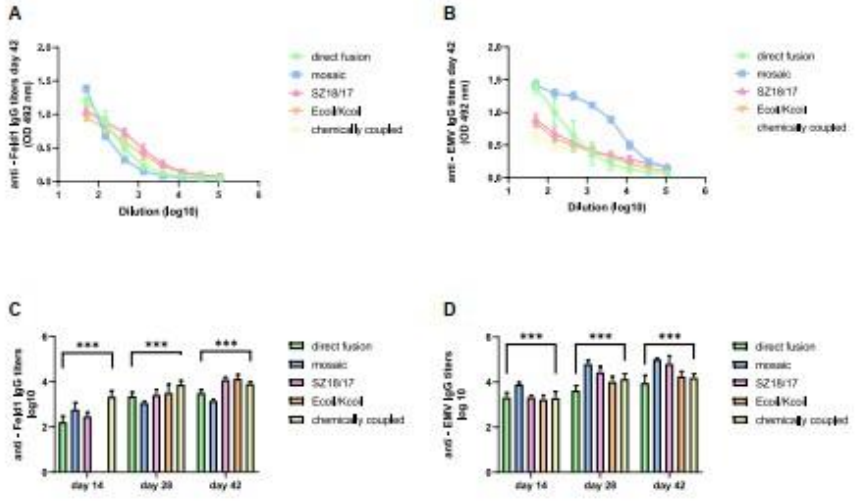

FIGURE 6
IgG titer analysis after vaccination with EMV-Feld1 vaccine variants. (A) Feld 1 specific IgG titers on Day 42 for the groups immunized with EMV-Feld1 variants measured at OD 492 nm; (B) EMV CP-specific IgG titers on Day 42 for the groups immunized with EMV-Feld1 variants measured at OD 492 nm; (C) Log_{10} values (mean ± SEM, $n = 5$) of Feld1-specific IgG titers for the groups vaccinated with EMV-Feld1 VLPs on Days 14, 28, and 42; (D) Log_{10} values (mean ± SEM, $n = 5$) of EMV-specific IgG titers for the groups vaccinated with EMV-Feld1 VLPs on Days 14, 28, and 42. (C,D) Statistical analysis using one-way ANOVA in GraphPad Prism 8.0. Vaccine groups $n = 5$. Graphs are showing the mean values of single titers. A value of $p > 0.05$ was considered statistically significant (***$p < 0.0001$).

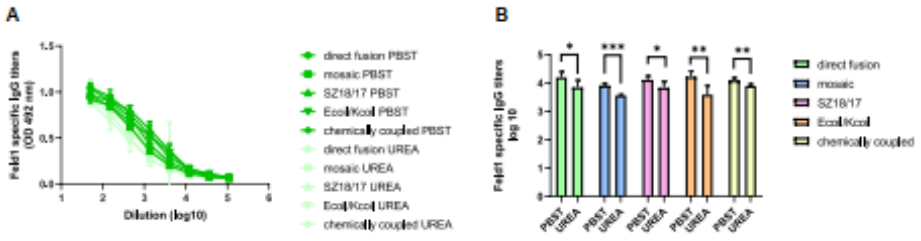

FIGURE 7
Avidity antibody detection after vaccination with EMV-Feld1 vaccine variants. (A) Feld1 specific IgG titers on Day 42 for the groups vaccinated with EMV-Feld1 variants measured with OD_{492} nm. After serum incubation one plate was treated with PBS with 0.05% Tween-80 and the other plate with 7 M UREA in PBS with 0.05% Tween-80; (B) Log_{10} values (mean ± SEM, $n = 5$) of Feld1 specific IgG titers (shown in panel A) for the groups vaccinated with EMV-Feld1 vaccine variants. Statistical analysis using Student's *t*-test in GraphPad Prism 9.0. Vaccine groups $n = 5$. Graphs are showing the mean values of single titers. A value of $p > 0.05$ was considered statistically significant (*$p < 0.01$; **$p < 0.001$; ***$p < 0.0001$).

vaccines—were measured by ELISA analysis in murine sera collected on Days 14, 28, and 42.

First, we noticed that the majority of produced EMV-Feld 1 vaccines induced Fel d 1-specific IgG production on Day 14, reaching the highest titers for the cEMV-Feld1 variant (reciprocal titers 1:2,800; Figure 6C; Supplementary Figure 12), whereas Feld 1-specific antibodies for the Ecoil/Kcoil vaccine were not yet detected (Figure 6C), probably due to the low Feld1 incorporation level discussed previously. Following the booster dosage on Day 14 Fel d 1, the specific IgG titers measured on Day 28 increased by at least 2 times for mEMV-Feld1 (reciprocal titers 1: 2,500; Figure 6C), while a minimum of fourfold excess was detected for the other four vaccine candidates, demonstrating that effective immunostimulation through B-cell activation was accomplished (Bachmann and Jennings, 2010). Furthermore, an additional booster dose dramatically prompted the Feld1-specific antibody response in mice vaccinated with the Ecoil/Kcoil variant (corresponding reciprocal titers 1: 3,900; Figure 6C) as well as for EMV-Feld1 (corresponding reciprocal titers 1: 2,400; Figure 6C), although cEMV-Feld1 once again demonstrated the highest Fel d 1-specific IgG response on Day 42 among all tested. Data presented for the final IgG titers on Day 42 after the second booster showed differences in some results—the most effective Fel d 1-specific antibody elicitors were SZ18/17 and Ecoil/Kcoil vaccine variants (corresponding reciprocal titers approximately 1: 12,000 for both; Figures 6A, C) despite the relatively long delay in anti-Fel d 1 Ab production for the Ecoil/Kcoil variant. Unfortunately, EMV-Feld1 and mEMV-Feld1 did not elicit high IgG levels, as their titers varied between 1:3,400 for direct fusion and 1:1,500 for the mosaic variant even after two booster injections (Figures 6A, C).

Interestingly, all measurements for EMV-specific IgG titers demonstrated a much higher IgG response against VLP carriers than against Feld 1-specific Abs (Figure 6D; Supplementary Figure 12). The same tendency was observed throughout the experiment, meaning that VLPs themselves have a crucial effect on triggering strong immune responses. For instance, of all vaccine constructs tested, titers against EMV were the highest for mEMV-Fel d 1 at every time point measured (Days 14, 28, and 42), reaching 1:68,000 after the first booster (Day 28) and increasing even more after the second on Day 42 (corresponding reciprocal titer 1:102,000; Figures 6B, D). Anti-EMV titers dramatically exceeded anti-Feld1 titers in three out of five groups (EMV-Feld1, mEMV-Feld1, SZ18/17) in vaccinated mouse sera obtained from Day 42 producing 1:12,000 for EMV-Fel d 1 and 1:66,000 for SZ18/17. Interestingly, similar observations were shown by Hu and Steinmetz in 2021 using a PhMV-based cancer vaccine, where anti-PhMV titers were higher than those against the chemically coupled HER (human epidermal growth factor receptor)-2-derived CH401 epitope (Hu and Steinmetz, 2021). This leads to the speculation that some *Tymovirus*-like particles strongly resemble a native virus through particulate virus-like structures and are able to stimulate the immune system more efficiently than surface-exposed Fel d 1 antigen (Mohsen et al., 2017). Here, additional studies are needed.

Our recent study regarding the MERS-coronavirus (CoV) VLP vaccine in murine immunological experiments showed that the production of specific antibodies with a high avidity index successfully provided protection against infectious diseases such as MERS-CoV (Mohsen et al., 2021). As the higher avidity index may correlate with efficient Fel d 1 neutralization, we evaluated the antibody avidity for all five EMV-Feld1 vaccine variants.

We compared two identical ELISA plates in the total IgG detection experiment, where one plate was treated with an additional 7 M UREA washing step and the other plate was treated as usual (Ogrina et al., 2022) to determine Ab binding avidity. The results showed that four out of five vaccine groups produced Abs with very high avidity index (AI) values (Figures 7A, B; Supplementary Figure 13), resulting in over 50% binding specificity represented as a proportion of Abs still bound to antigen after a 7 M UREA washing step. Three of the vaccines with the highest avidity were SZ18/17, cEMV-Feld1, and Ecoil/Kcoil, all reaching 64–68% specificity, whereas mEMV-Feld1 resulted in less specific Ab production (47%), suggesting that the most promising vaccine for future experiments should be chosen from candidates demonstrating the highest AI values.

3.4.3. Subclass specific IgG production

Different approaches should be considered when shaping the most beneficial immune response, as the strategy used for anti-pathogen vaccines can be not as successful against allergies and vice versa (Zepeda-Cervantes et al., 2020). Modern solutions in allergy treatment now include not only widely described allergen-specific IgE-targeted treatments but also novel allergen-specific

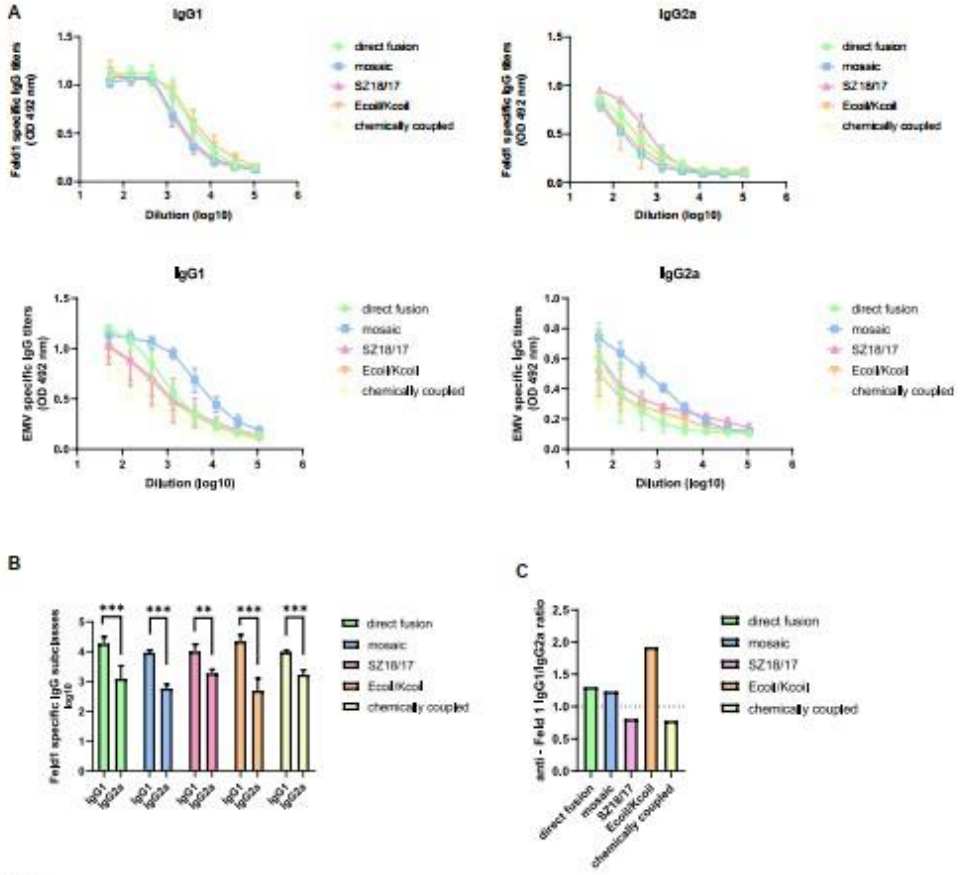

FIGURE 8
Subclass specific antibody detection. (A) Anti-Feld1 and anti-EMV CP specific IgG1 and IgG2a titers measured in Day 42 mice sera using OD 492 nm. ELISA plates were coated with EMV-Feld1 variants for IgG subclass detection in mice sera vaccinated with EMV-Feld1 vaccine variants. (B) Log_{10} values of Feld1 specific IgG1 and IgG2a titers measured in Day 42 mice sera; (C) anti-Feld1 IgG1/IgG2a ratio measured from mean titers used in experiment shown in panel (B). (A,B) Statistical analysis using Student's *t*-test in GraphPad Prism 8.0. Vaccine groups $n = 5$. Graphs are showing the mean values of single titers. A value of $p > 0.05$ was considered statistically significant (**$p < 0.001$; ***$p < 0.0001$).

IgGs, which are possible key effectors for so-called next-generation immunotherapy when allergens are displayed on the VLP surface (Schmitz et al., 2009; Bachmann et al., 2020). A recent paper underlines that specific IgG subclasses play a minor role in allergy-specific immunotherapy (Zinkhan et al., 2022).

It has been emphasized that strong activators of antigen presenting cells (APC) such as VLPs are recognized by so-called pathogen recognition receptors (PRRs) expressed on the surface of antigen-presenting cells (APCs). Specific types of PRRs are TLRs, which are able to recognize various viral or bacterial pathogen-associated molecules. After TLR stimulation, these VLPs are taken up and processed by the most potent APCs, dendritic cells (DCs), leading to their maturation and further proinflammatory responses (Zepeda-Cervantes et al., 2020). Captured antigens are then presented on the surface of mature DCs for T-cell recognition through major histocompatibility complex (MHC) classes I or II and through cross-presentation (Mohsen et al., 2017; Zepeda-Cervantes et al., 2020), which then determine the IgG isotype pattern. In the case of VLP-based vaccines, two mural antibody subclasses (IgG1 and IgG2a) are linked to Th2 and Th1 signaling pathways, each representing different effector functions. Hence, the immune response driven by Th1 is more defensive against viral infections (Nimmerjahn and Ravetch, 2008; Gomes et al., 2019) and may help to control IgE-dependent allergic reactions by regulating allergen-specific IgG production (Bachmann and Kündig, 2017).

To characterize the nature of the generated immune response, we measured IgG1 and IgG2a titers in mouse sera collected on Day 42 against both the Fel d 1 antigen and EMV VLPs. Our obtained data clearly demonstrated IgG1 subclass dominance for all variants tested, producing the highest anti-Feld1 IgG1 titers

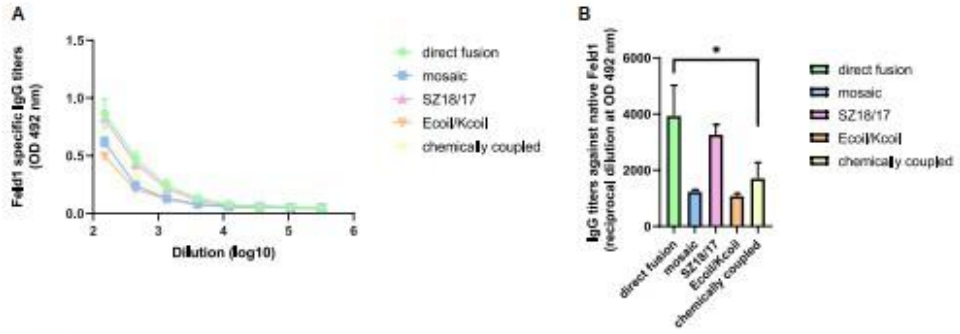

FIGURE 9
Native Feld1-specific antibody detection in EMV-Feld1 vaccinated mice sera. (A,B) Feld1 specific IgG titers (mean ± SEM) against native Feld1 for the groups vaccinated with EMV-Feld1 vaccine variants. Sera obtained from Day 42 and measured at OD 492 nm. (B) Statistical analysis using one-way ANOVA in GraphPad Prism 8.0. Vaccine groups $n = 5$. Graphs are presenting mean of pooled mice titers. A value of $p > 0.05$ was considered statistically significant (*$p < 0.01$).

for Ecoil/Kcoil and EMV-Feld1 (corresponding reciprocal titers 1: 25,000 for Ecoil/Kcoil; 1: 20,500 for EMV-Feld1; Figures 8A, B; Supplementary Figure 14), whereas the highest IgG2a antibody response was approximately similar for three groups of EMV-Feld1, SZ18/17, and cEMV-Feld1, producing titers of 1: 1,700–2,000, respectively (Figures 8A, B). Additionally, the subclass-specific Ab response against carrier EMV was dominated by IgG1 producing the highest titers for mEMV-Feld1 (reciprocal IgG1 titers 1: 56,000; IgG2a titers 1: 5,800; Figures 8A, B).

Furthermore, we also determined that the lowest Feld1 IgG1/IgG2a ratio values were obtained for SZ18/17 and cEMV-Feld1 (ratio values <0.8) (Figure 8C), meaning that these vaccine candidates induce more balanced Th1/Th2 phenotypes when compared with Ecoil/Kcoil (ratio value 1.92) and therefore should be considered the most promising candidates for desired protective immune response generation in anti-allergy treatment procedures.

Virus-like particles induce an immune response dominated by the Th2 pathway producing IgG1 Abs unless TLR ligands such as nucleic acids are present that may achieve isotype switching toward the IgG2a Ab response (Jegerlehner et al., 2007). As IgG1 predominance was also addressed in other studies with VLP-based vaccines (Cai et al., 2019; Hu and Steinmetz, 2021; Ogrina et al., 2022), we assumed that TLR stimulation was not sufficiently effective due to the reduced amount of encapsidated nucleic acids, as observed in NAG analysis. This observation possibly indicates the low activation of TLR7/8 dependent responses (Gomes et al., 2019; Krueger et al., 2019).

3.4.4. Native Fel d 1 recognition

Allergy cases caused by the domestic cat *F. domesticus* arise each year, affecting a large part of the population, as common symptoms such as allergic respiratory diseases negatively affect quality of life (Bonnet et al., 2018). Recent studies in the VLP field have highlighted the optimal strategy for allergy treatment focusing on neutralizing IgG Ab production when challenged with native Fel d 1 allergen (Schmitz et al., 2009; Thoms et al., 2019) or peanut allergy allergens Arah1 and Arah2 (Storni et al., 2019). Therefore, we evaluated the recognition of native Fel d 1 by antibodies obtained after mouse vaccination with all constructed vaccine variants using native Fel d 1 (nFel d 1; Indoor Biotechnology, USA).

The obtained results revealed that titer values for EMV-Feld1 reached almost 1:4,000 and represented the highest IgG titers against nFel d 1 (Figures 9A, B) but were closely followed by SZ18/17 (corresponding reciprocal titers 1:3,300; Figures 9A, B), whereas the lowest anti-Feld1 IgG titers were detected for the Ecoil/Kcoil and mEMV-Feld1 vaccines, which varied by approximately 1:1,000. These results correlate with avidity measurements, where the SZ18/17 variant produced the most specific Abs against Feld1 compared to other vaccine candidates. Interestingly, we have noted that rFeld1 used for cloning experiments and covering ELISA plates is somehow recognized more efficiently than the native form, which was also observed for mAb ELISA experiments. Furthermore, titers against nFel d 1 were significantly lower for EMV-derived Feld1 vaccine constructs than for filamentous Feld1 antigen-containing PVY CP VLPs (Ogrina et al., 2022), meaning that despite the large size of the 200–400 nm filaments of PVY CP VLPs, they could represent the Fel d 1 antigen in a much more recognizable manner, observed as high levels of nFeld1 binding IgGs.

4. Conclusion

The generation of more effective vaccine candidates can improve vaccine manufacturing by avoiding complicated, multistep processes in vaccine construction and purification. As the native spatial structures of recombinant antigens are highly important for eliciting antibodies with neutralizing activity and long-lasting immunity, recombinant VLP vaccines must contain strongly organized and multiple copies of exposed antigen (Balke and Zeltins, 2019). Here, we demonstrated the construction and tests of several simple bacterial expression systems for vaccine generation based on new *Tymovirus*-like particles and different principles of Fel d 1 antigen incorporation, including genetic techniques by introducing the antigen directly into EMV CP or

as a part of a mosaic system with wtEMV CP. Additionally, we showed two physical binding approaches resulting in VLP-antigen complexes using synthetic zipper pairs 18/17 (SZ18/17) and coiled-coil-forming peptides E and K (Ecoil/Kcoil). Both systems were tested *in vitro* after purification of the corresponding proteins and in coexpression directly in *E. coli* cells. These experiments resulted in the formation of stable complexes regardless of the method of epitope incorporation. Here, we have demonstrated that these protein–protein interaction partners allowed the binding of coexpressed antigen to the VLP surface directly in *E. coli* cells during cultivation due to their ability to form highly specific and high affinity interactions with a low dissociation constant ($K_d < 1 \times 10^{-8}$; Reinke et al., 2010; Thompson et al., 2012). The presented systems can be used for the introduction of antigens, resulting in new antigen presentation platforms, as they reduce the influence of expressed antigens on the spatial structure and self-assembly of VLPs.

All four constructed systems were successfully expressed in *E. coli* and purified in the form of antigen-containing VLPs. The presence of EMV CP VLPs and Feld1 antigen for all four vaccine variants was confirmed by SDS-PAGE, WB, and ELISA using mAbs. As the *E. coli* expression systems allow rapid expression and subsequent large-scale, cost-effective manufacturing of recombinant proteins, the constructed vaccines can be a prototype for Feld1 therapeutic vaccines in the future. Chemical coupling of Feld1 to wtEMV CP VLPs was also achieved and therefore included in immunological experiments, resulting in a total of five different EMV-Feld1 vaccine variants tested in murine models.

To our knowledge, this is the first report of successful tymoviral VLP formation after the introduction of long antigen sequences into the C-terminal end of CP. Our experiments suggest that EMV CP VLPs are fully suitable for CP modifications and ensure the necessary VLP morphology. Furthermore, obtained immune responses, antibody avidity, and subclass switching toward the Th1 pathway were the main criteria for choosing the most effective EMV-Feld1 VLP platform. Therefore, we conclude that cEMV-Feld1 and SZ18/17 should be considered the most efficient platforms for antigen presentation, as they possess most of the features needed. All five constructed vaccines elicited high titers of Feld1-specific Abs. Moreover, the obtained antibodies recognized the native Fel d 1 allergen; therefore, our results suggest good potential for SZ18/17 and cEMV-Feld1 vaccine variants as the most promising VLP platforms among all tested.

However, the vaccine's ability to produce comparatively higher titers against carrier EMV is a matter of concern. In the context of emerging vaccination strategies, an ideal vaccine candidate should be universal, meaning that one antigen presentation platform should be adapted for multiple vaccine development. In the case of EMV VLPs, their usage can be limited due to their high immunogenicity against the VLP carrier. Another aspect that should be taken into consideration is that the constructed EMV-Feld1 VLPs produce low levels of protective IgG2a subclass antibodies, which correlates with the reduced nucleic acid signal intensity detected in NAG and the "empty" particle presence observed in TEM.

The induction of optimal B-cell responses depends on immunostimulating characteristics such as repetitive epitope structures spaced 5–10 nm from each other on the VLP exterior and surface charge that can attract the protein corona consisting of absorbed serum proteins and natural antibodies (Blanco et al., 2015). Another factor is the size and morphology of vaccine carriers, suggesting that antigens larger than 200 nm struggle to freely enter the lymphatic system when compared to icosahedral particles with a size of ~30 nm (Mohsen et al., 2017; Zinkhan et al., 2021). As we have previously described similar Fel d 1 epitope presenting strategies based on bacterial expression platforms using filamentous PVY VLPs (Ogrina et al., 2022), the results from this study gave us the opportunity to compare and evaluate icosahedral and filamentous VLPs and speculate which could serve as the most suitable candidate for vaccination purposes. Although both PVY-Feld1 and EMV-Feld1 vaccines elicited approximately similar total Ab levels against Fel d 1 ($\sim 10^4$–10^5), four EMV-Feld1 vaccine candidates stimulated a stronger Th1 immune response and IgG2a subclass production. Furthermore, the avidity of Abs produced was higher for EMV-Feld1 vaccine variants, meaning that ~64–68% of Abs were very specific to surface-exposed Feld1 compared to 36% specificity for the best variant of PVY-Feld1 (Ogrina et al., 2022). On the other hand, better native Fel d 1 recognition was observed for Feld1 presenting PVY filaments; therefore, more comprehensive analysis between both strategies is needed.

Finally, the results of our designed and tested EMV-Feld1 vaccine platforms suggest that the chosen construction strategy can significantly influence the amplitude progress and specificity of the elicited immune responses. Therefore, several antigen incorporation strategies should be elaborated for the generation of each new VLP-based vaccine to find the best variant.

Data availability statement

The original contributions presented in this study are included in the article/Supplementary material, further inquiries can be directed to the corresponding author.

Ethics statement

This animal study was reviewed and approved by the Animal Protection Ethical Committee of the Latvian Food and Veterinary Service (permission no. 89).

Author contributions

AO, MB, and AZ: conceptualization. AO, IB, IK, DS, and JJ: experimental work. AO, IB, and AZ: writing—original draft preparation. AO, IB, MB, and AZ: writing—review and editing. IB and AZ: supervision. AO and AZ: funding acquisition. All authors read and agreed to the published version of the manuscript.

Funding

This research was funded by the project "Strengthening of the Capacity of Doctoral Studies at the University of Latvia within

the Framework of the New Doctoral Model", identification No. 8.2.2.0/20/I/006.

Acknowledgments

We thank Janis Bogans for his help in the chromatographic purification of the Fel d 1 and Kcoil-Feld1 proteins.

Conflict of interest

The authors declare that the research was conducted in the absence of any commercial or financial relationships that could be construed as a potential conflict of interest.

Publisher's note

Supplementary material

The Supplementary Material for this article can be found online at: https://www.frontiersin.org/articles/10.3389/fmicb.2023.1154990/full#supplementary-material

References

Bachmann, M., and Jennings, G. (2010). Vaccine delivery: A matter of size, geometry, kinetics and molecular patterns. *Nat. Rev. Immunol.* 10, 787–796. doi: 10.1038/nri2868

Bachmann, M., and Kündig, T. (2017). Allergen-specific immunotherapy: Is it vaccination against toxins after all? *Allergy* 72, 13–23. doi: 10.1111/all.12890

Bachmann, M., Mohsen, M., Kramer, M., and Heath, M. (2020). Vaccination against allergy: A paradigm shift? *Trends Mol. Med.* 26, 357–368. doi: 10.1016/j.molmed.2020.01.007

Balke, I., Resevica, G., and Zeltins, A. (2018). Isolation and characterization of two distinct types of unmodified spherical plant sobemovirus-like particles for diagnostic and technical uses. *Methods Mol. Biol.* 1776, 19–34. doi: 10.1007/978-1-4939-7808-3_2

Balke, I., and Zeltins, A. (2019). Use of plant viruses and virus-like particles for the creation of novel vaccines. *Adv. Drug Deliv. Rev.* 145, 119–129. doi: 10.1016/j.addr.2018.08.007

Barnhill, H., Reuther, R., Ferguson, P., Dreher, T., and Wang, Q. (2007). Turnip yellow mosaic virus as a chemoaddressable bionanoparticle. *Bioconjug. Chem.* 18, 852–859. doi: 10.1021/bc060391s

Blanco, E., Shen, H., and Ferrari, M. (2015). Principles of nanoparticle design for overcoming biological barriers to drug delivery. *Nat. Biotechnol.* 33, 941–951.

Bonnet, B., Messaoudi, K., Jacomet, F., Michaud, E., Fauquert, J. L., Caillaud, D., et al. (2018). An update on molecular cat allergens: Fel d 1 and what else? Chapter 1: Fel d 1, the major cat allergen. *Allergy Asthma Clin. Immunol.* 14:14. doi: 10.1186/s13223-018-0239-8

Bransom, K., Weiland, J., Tsai, C., and Dreher, T. (1995). Coding density of the turnip yellow mosaic virus genome: Roles of the overlapping coat protein and p206-readthrough coding regions. *Virology* 206, 403–412. doi: 10.1016/s0042-6822(95)80056-5

Cai, H., Shukla, S., Wang, C., Masarapu, H., and Steinmetz, N. (2019). Heterologous prime-boost enhances the antitumor immune response elicited by plant-virus-based cancer vaccine. *J. Am. Chem. Soc.* 141, 6509–6518. doi: 10.1021/jacs.9b01523

Canady, M., Larson, S., Day, J., and McPherson, A. (1996). Crystal structure of turnip yellow mosaic virus. *Nat. Struct. Biol.* 3, 771–781. doi: 10.1038/nsb0996-771

Chandran, D., Shahana, P., Rani, G., Sugumar, P., Shankar, C., and Srinivasan, V. (2009). Display of neutralizing epitopes of Canine parvovirus and a T-cell epitope of the fusion protein of Canine distemper virus on chimeric tymovirus-like particles and its use as a vaccine candidate both against Canine parvo and Canine distemper. *Vaccine* 28, 132–139. doi: 10.1016/j.vaccine.2009.09.093

Chung, Y., Beiss, V., Fiering, S., and Steinmetz, N. (2020). COVID-19 vaccine frontrunners and their nanotechnology design. *ACS Nano* 14, 12522–12537. doi: 10.1021/acsnano.0c07197

Dobaño, C., Sanz, H., Sorgho, H., Dosoo, D., Mpina, M., Ubillos, I., et al. (2019). Concentration and avidity of antibodies to different circumsporozoite epitopes correlate with RTS,S/AS01E malaria vaccine efficacy. *Nat. Commun.* 10:2174. doi: 10.1038/s41467-019-10195-z

Dupin, A., Collot, D., Peter, R., and Witz, J. (1985). Comparisons between the Primary Structure of the coat protein of Turnip Yellow Mottle Virus and Eggplant mosaic virus. *J. Gen. Virol.* 66(Pt 12), 2743–2748. doi: 10.1099/0022-1317-66-12-2571

Ferguson, I. A. C. (1951). Four virus diseases of solanaceous plants in Trinidad. *Plant Dis. Rep.* 35, 102–105.

Fontana, F., Figueiredo, P., and Santos, H. A. (2019). "Advanced nanovaccines for immunotherapy applications: From concept to animal tests," in *Theranostic bionanomaterials*, 1st Edn, eds W. Cui and X. Zhao (Amsterdam: Elsevier), 231–260. doi: 10.1016/B978-0-12-815341-3.00010-9

Frietze, K., Peabody, D., and Chackerian, B. (2016). Engineering virus-like particles as vaccine platforms. *Curr. Opin. Virol.* 18, 44–49. doi: 10.1016/j.coviro.2016.03.001

Gibbs, A., and Mackenzie, A. (1998). Tymovirus isolation and genomic RNA extraction. *Methods Mol. Biol.* 81, 219–224.

Gomes, A., Roesti, E., El-Turabi, A., and Bachmann, M. (2019). Type of RNA packed in VLPs impacts IgG class switching-implications for an influenza vaccine design. *Vaccines* 7:47. doi: 10.3390/vaccines7020047

Hema, M., Nagendrakumar, S., Yamini, R., Chandran, D., Rajendra, L., Thiagarajan, D., et al. (2007). Chimeric tymovirus-like particles displaying foot-and-mouth disease virus non-structural protein epitopes and its use for detection of FMDV-NSP antibodies. *Vaccine* 25, 4784–4794. doi: 10.1016/j.vaccine.2007.04.023

Hu, H., Masarapu, H., Gu, Y., Zhang, Y., Yu, X., and Steinmetz, N. (2019). Physalis mottle virus-like nanoparticles for targeted cancer imaging. *ACS Appl. Mater. Interfaces* 11, 18213–18223. doi: 10.1021/acsami.9b03956

Hu, H., and Steinmetz, N. (2020). Cisplatin prodrug-loaded nanoparticles based on physalis mottle virus for cancer therapy. *Mol. Pharm.* 17, 4629–4636. doi: 10.1021/acs.molpharmaceut.0c00834

Hu, H., and Steinmetz, N. (2021). Development of a virus-like particle-based anti-HER2 breast cancer vaccine. *Cancers* 13:2909. doi: 10.3390/cancers13122909

Jegerlehner, A., Maurer, P., Bessa, J., Hinton, H., Kopf, M., and Bachmann, M. (2007). TLR9 signaling in B cells determines class switch recombination to IgG2a. *J. Immunol.* 178, 2415–2420. doi: 10.4049/jimmunol.178.4.2415

Kalnciema, I., Skrastina, D., Ose, V., Pumpens, P., and Zeltins, A. (2012). Potato virus Y-like particles as a new carrier for the presentation of foreign protein stretches. *Mol. Biotechnol.* 52, 129–139. doi: 10.1007/s12033-011-9480-9

Khan, J. A., and Dijkstra, J. (2006). *Handbook of plant virology*. New York, NY: Food Products Press, 282–284.

Kim, D., Lee, Y., Dreher, T., and Cho, T. (2018). Empty turnip yellow mosaic virus capsids as delivery vehicles to mammalian cells. *Virus Res.* 252, 13–21. doi: 10.1016/j.virusres.2018.05.004

Krishna, S., Hiremath, C., Munshi, S., Prahadeeswaran, D., Sastri, M., Savithri, H., et al. (1999). Three-dimensional structure of physalis mottle virus: Implications for the viral assembly. *J. Mol. Biol.* 289, 919–934. doi: 10.1006/jmbi.1999.2787

Krueger, C., Thoms, F., Keller, E., Leoratti, F., Vogel, M., and Bachmann, M. (2019). RNA and toll-like receptor 7 license the generation of superior secondary plasma cells at multiple levels in a B cell intrinsic fashion. *Front. Immunol.* 10:736. doi: 10.3389/fimmu.2019.00736

Kumar, P., van Son, M., Zheng, T., Valdink, D., Raap, J., Kros, A., et al. (2018). Coiled-coil formation of the membrane-fusion K/E peptides viewed by electron paramagnetic resonance. *PLoS One* 13:e0191197. doi: 10.1371/journal.pone.0191197

Larson, S., Lucas, R., Greenwood, A., and McPherson, A. (2005). The RNA of turnip yellow mosaic virus exhibits icosahedral order. *Virology* 334, 245–254. doi: 10.1016/j.virol.2005.01.036

Lebel, M., Chartrand, K., Leclerc, D., and Lamarre, A. (2015). Plant viruses as nanoparticle-based vaccines and adjuvants. *Vaccines* 3, 620–637. doi: 10.3390/vaccines3030620

Litowski, J., and Hodges, R. (2002). Designing heterodimeric two-stranded alpha-helical coiled-coils. Effects of hydrophobicity and alpha-helical propensity on protein folding, stability, and specificity. *J. Biol. Chem.* 277, 37272–37279. doi: 10.1074/jbc.M204257200

Martelli, G., Sabanadzovic, S., Abou-Ghanem Sabanadzovic, N., Edwards, M., and Dreher, T. (2002). The family Tymoviridae. *Arch. Virol.* 147, 1837–1846. doi: 10.1007/s007050200045

Masarapu, H., Patel, B., Chariou, P., Hu, H., Gulati, N., Carpenter, B., et al. (2017). Physalis mottle virus-like particles as nanocarriers for imaging reagents and drugs. *Biomacromolecules* 18, 4141–4153. doi: 10.1021/acs.biomac.7b01196

Matthews, R. (1960). Properties of nucleoprotein fractions isolated from turnip yellow mosaic virus preparations. *Virology* 12, 521–539. doi: 10.1016/0042-6822(60)90176-8

Michels, B., Leimkühler, M., Lechner, M., Adrian, M., Lorber, B., and Witz, J. (1999). Polymorphism of turnip yellow mosaic virus empty shells and evidence for conformational changes occurring after release of the viral RNA. A differential scanning calorimetric study. *Eur. J. Biochem.* 264, 965–972. doi: 10.1046/j.1432-1327.1999.00705.x

Minten, I. J., Hendriks, L. J., Nolte, R. J., and Cornelissen, J. J. (2009). Controlled encapsulation of multiple proteins in virus capsids. *J. Am. Chem. Soc.* 131, 17771–17773. doi: 10.1021/ja907843s

Mohsen, M., Augusto, G., and Bachmann, M. (2020). The 3Ds in virus-like particle based-vaccines: "Design, delivery and dynamics". *Immunol. Rev.* 296, 155–168. doi: 10.1111/imr.12863

Mohsen, M., Rothen, D., Balke, I., Martina, B., Zeltina, V., Inchakalody, V., et al. (2021). Neutralization of MERS coronavirus through a scalable nanoparticle vaccine. *NPJ Vaccines* 6:107. doi: 10.1038/s41541-021-00365-w

Mohsen, M., Zha, L., Cabral-Miranda, G., and Bachmann, M. (2017). Major findings and recent advances in virus-like particle (VLP)-based vaccines. *Semin. Immunol.* 34, 123–132. doi: 10.1016/j.smim.2017.08.014

Nimmerjahn, F., and Ravetch, J. (2008). Fcgamma receptors as regulators of immune responses. *Nat. Rev. Immunol.* 8, 34–47. doi: 10.1038/nri2206

Noorani, S., Bahrulolum, H., Hoseini, Z., Katalani, C., Hajizade, A., Easton, A., et al. (2021). Virus-like particles: Preparation, immunogenicity and their roles as nanovaccines and drug nanocarriers. *J. Nanobiotechnology* 19:59. doi: 10.1186/s12951-021-00806-7

Ogrina, A., Skrastina, D., Balke, I., Kalnciema, I., Jansons, J., Bachmann, M., et al. (2022). Comparison of bacterial expression systems based on potato virus Y-like particles for vaccine generation. *Vaccines* 10:485. doi: 10.3390/vaccines10040485

Osorio-Keese, M., Keese, P., and Gibbs, A. (1989). Nucleotide sequence of the genome of eggplant mosaic tymovirus. *Virology* 172, 547–554. doi: 10.1016/0042-6822(89)90197-9

Powell, J., Barbar, E., and Dreher, T. (2012). Turnip yellow mosaic virus forms infectious particles without the native beta-annulus structure and flexible coat protein N-terminus. *Virology* 422, 165–173. doi: 10.1016/j.virol.2011.10.019

Powell, J., and Dreher, T. (2022). The generation of empty Turnip yellow mosaic virus capsids through depletion of virion-associated divalent cations. *J. Virol. Methods* 309:114595. doi: 10.1016/j.jviromet.2022.114595

Reinke, A., Grant, R., and Keating, A. (2010). A synthetic coiled-coil interactome provides heterospecific modules for molecular engineering. *J. Am. Chem. Soc.* 132, 6025–6031. doi: 10.1021/ja907617a

Rothen, D., Krenger, P., Nonic, A., Balke, I., Vogt, A., Chang, X., et al. (2022). Intranasal administration of a virus like particles-based vaccine induces neutralizing antibodies against SARS-CoV-2 and variants of concern. *Allergy* 77, 2446–2458. doi: 10.1111/all.15311

Sahithi, K., Nancy, P., Vishnu Vardhan, G., Kumanan, K., Vijayarani, K., and Hema, M. (2019). Detection of infectious bursal disease virus (IBDV) antibodies using chimeric plant virus-like particles. *Vet. Microbiol.* 229, 20–27. doi: 10.1016/j.vetmic.2018.12.008

Sastri, M., Kekuda, R., Gopinath, K., Kumar, C., Jagath, J., and Savithri, H. (1997). Assembly of physalis mottle virus capsid protein in *Escherichia coli* and the role of amino and carboxy termini in the formation of the icosahedral particles. *J. Mol. Biol.* 272, 541–552. doi: 10.1006/jmbi.1997.1258

Sastri, M., Reddy, D., Krishna, S., Murthy, M., and Savithri, H. (1999). Identification of a discrete intermediate in the assembly/disassembly of physalis mottle tymovirus through mutational analysis. *J. Mol. Biol.* 289, 905–918. doi: 10.1006/jmbi.1999.2786

Savithri, H. S., Munshi, S. K., Suryanarayana, S., Divakar, S., and Murthy, M. R. N. (1987). Stability of belladonna mottle virus particles: The role of polyamines and calcium. *J. Gen. Virol.* 68, 1533–1542. doi: 10.1099/0022-1317-68-6-1533

Schmitz, N., Dietmeier, K., Bauer, M., Maudrich, M., Utzinger, S., Muntwiler, S., et al. (2009). Displaying Fel d1 on virus-like particles prevents reactogenicity despite greatly enhanced immunogenicity: A novel therapy for cat allergy. *J. Exp. Med.* 206, 1941–1955. doi: 10.1084/jem.20090199

Shahana, P., Das, D., Gontu, A., Chandran, D., and Maithal, K. (2015). Efficient production of Tymovirus like particles displaying immunodominant epitopes of Japanese Encephalitis Virus envelope protein. *Protein Expr. Purif.* 113, 35–43. doi: 10.1016/j.pep.2015.03.017

Shin, H., Chae, K., and Cho, T. (2013). Modification of Turnip yellow mosaic virus coat protein and its effect on virion assembly. *BMB Rep.* 46, 495–500. doi: 10.5483/bmbrep.2013.46.10.046

Shin, H., Kim, D., and Cho, T. (2018). Cysteine – added mutants of Turnip yellow mosaic virus. *J. Bacteriol. Virol.* 48:137. doi: 10.4167/jbv.2018.48.4.137

Storni, F., Zeltins, A., Balke, I., Heath, M., Kramer, M., Skinner, M., et al. (2019). Vaccine against peanut allergy based on engineered virus-like particles displaying single major peanut allergens. *J. Allergy Clin. Immunol.* 145, 1240–1253.e3. doi: 10.1016/j.jaci.2019.12.007

Tan, F., Kong, J., Ng, J., Alitheen, N., Wong, C., Yong, C., et al. (2021). Recombinant turnip yellow mosaic virus coat protein as a potential nanocarrier. *J. Appl. Microbiol.* 131, 2072–2080. doi: 10.1111/jam.15048

Tariq, H., Batool, S., Asif, S., Ali, M., and Abbasi, B. (2022). Virus-like particles: Revolutionary platforms for developing vaccines against emerging infectious diseases. *Front. Microbiol.* 12:790121. doi: 10.3389/fmicb.2021.790121

Thompson, K., Bashor, C., Lim, W., and Keating, A. (2012). SYNZIP protein interaction toolbox: In vitro and in vivo specifications of heterospecific coiled-coil interaction domains. *ACS Synth. Biol.* 1, 118–129. doi: 10.1021/sb200015u

Thoms, F., Haas, S., Erhart, A., Nett, C., Rüfenacht, S., Graf, N., et al. (2020). Immunization of cats against Fel d 1 results in reduced allergic symptoms of owners. *Viruses* 12:288. doi: 10.3390/v12030288

Thoms, F., Jennings, G. T., Maudrich, M., Vogel, M., Haas, S., Zeltins, A., et al. (2019). Immunization of cats to induce neutralizing antibodies against Fel d 1, the major feline allergen in human subjects. *J. Allergy Clin. Immunol.* 144, 193–203. doi: 10.1016/j.jaci.2019.01.050

van Roon, A., Bink, H., Plaisier, J., Pleij, C., Abrahams, J., and Panna, N. (2004). Crystal structure of an empty capsid of turnip yellow mosaic virus. *J. Mol. Biol.* 341, 1205–1214. doi: 10.1016/j.jmb.2004.06.085

Vasques, R., Correa, R., da Silva, L., Blawid, R., Nagata, T., Ribeiro, B., et al. (2019). Assembly of tomato blistering mosaic virus-like particles using a baculovirus expression vector system. *Arch. Virol.* 164, 1753–1760. doi: 10.1007/s00705-019-04262-5

Walker, A., Skamel, C., and Nassal, M. (2011). SplitCore: An exceptionally versatile viral nanoparticle for native whole protein display regardless of 3D structure. *Sci. Rep.* 1:5. doi: 10.1038/srep00005

Werner, S., Marillonnet, S., Hause, G., Klimyuk, V., and Gleba, Y. (2006). Immunoabsorbent nanoparticles based on a tobamovirus displaying protein A. *Proc. Natl. Acad. Sci. U.S.A.* 103, 17678–17683. doi: 10.1073/pnas.0608869103

Zeltins, A., West, J., Zabel, F., El Turabi, A., Balke, I., Haas, S., et al. (2017). Incorporation of tetanus-epitope into virus-like particles achieves vaccine responses even in older recipients in models of psoriasis, Alzheimer's and cat allergy. *NPJ Vaccines* 2:30. doi: 10.1038/s41541-017-0030-8

Zepeda-Cervantes, J., Ramírez-Jarquín, J., and Vaca, L. (2020). Interaction between virus-like particles (VLPs) and pattern recognition receptors (PRRs) from dendritic cells (DCs): Toward better engineering of VLPs. *Front. Immunol.* 11:1100. doi: 10.3389/fimmu.2020.01100

Zinkhan, S., Ogrina, A., Balke, I., Reseviča, G., Zeltins, A., de Brot, S., et al. (2021). The impact of size on particle drainage dynamics and antibody response. *J. Control. Release* 331, 296–308. doi: 10.1016/j.jconrel.2021.01.012

Zinkhan, S., Thoms, F., Augusto, G., Vogel, M., and Bachmann, M. (2022). On the role of allergen-specific IgG subclasses for blocking human basophil activation. *Front. Immunol.* 13:892631. doi: 10.3389/fimmu.2022.892631

4. DISCUSSION

Understanding the dynamics between immune cells and nanomaterials becomes crucial when considering the utilization of nanoparticles (NPs) for immunotherapy applications. The physicochemical attributes of NPs, such as size, morphology, surface charge, chemistry, and ligand concentration, can be manipulated to improve their biodistribution, enhance therapeutic cargo carriage, enable precise targeting, and modulate immunogenic responses (Fontana *et.al.,* 2019). NPs make up a diverse group of carriers, all sharing a common feature: their size falls between 1 and 1000 nm and the types of NPs employed in vaccines include VLPs, viral vectors, lipid nanoparticles (LNPs), liposomes, and positively charged polymers (Gomes *et.al.,* 2017).

Several compelling aspects about VLPs make them intriguing - they serve as a secure platform since they lack any genetic material that can replicate and their ability to stimulate the immune system mainly depends if the antigens are arranged in a repetitive manner, forming strong pathogen-associated structural patterns (PASPs). Additionally, VLPs are valuable tools because they can present a variety of epitopes on their surface and can encapsulate nucleic acids from their host expression systems or other chosen substances. This property enables them to activate TLRs on APCs (Mohsen *et.al.,* 2018). Furthermore, for most cases high yield of soluble VLPs can be produced in recombinant bacterial cells and plants following strict manufacturing rules (cGMP) when using well-optimized expression systems and cultivation conditions (Zeltins, 2013).

This study offers a substantial basis for designing novel and universally recognized plant VLP platforms based on viruses from Bromovirus, Potyvirus and Tymovirus groups, and their potential application in constructing new vaccines. In future, by incorporating specific antigens of interest, these platforms could be harnessed to address infections and various conditions, ranging from cancer to autoimmune diseases and allergies. The obtained data provides insight into how the size and morphology of VLPs, as well as the antigen presentation strategy, can contribute to their immunostimulatory potential.

This study involved the creation of twelve different plant VLP platforms, all of which were successfully expressed in the *E. coli* expression system. Subsequently, these systems were used for purification of VLPs containing the target antigens, preserving either filamentous or icosahedral structures, respectively.

In the case of CCMV VLPs, which are derived from a plant Bromovirus and produced directly in *E. coli* cells, the morphological architecture was influenced by the site of TT epitope insertion. To date, this study represents the initial exploration and comparison of how the same virus CP monomer can give rise to two distinct morphological forms – one forming nano-sized icosahedra ($CCMV_{TT}$ N-terminal mutant) and the other elongated rods in the micrometer range ($CCMV_{TT}$ C-terminal mutant), including the analysis of their drainage kinetics and immunogenicity in murine models.

Icosahedral viral capsids consist of chemically identical CP subunits organized into pentameric and hexameric conformations, enabling a single subunit to engage in both pentameric and hexameric interactions. The variations in $CCMV_{TT}$ morphology can be linked to the previously mentioned role of the CCMV CP gene's C-terminal end, which plays a role in stabilizing dimeric interactions. The insertion of an epitope into the C-terminus potentially disrupts the mechanism responsible for pentamer forming. In this case, intact hexamers arrange themselves into a tubular lattice that is enclosed by icosahedral caps at both ends, giving rise to bacilliform particles whose lengths correlate with the dimensions of the encapsulated RNA (Hull *et.al.,* 1970). A similar observation was noted in publications about morphological changes in bacteriophages (Rumnieks *et al.*, 2009) and in some plant sobemoviruses (Zeltins, 2018) after disassembly/reassembly experiments *in vitro*. The formation of rod-shaped $CCMV_{TT}$ VLPs consisting of hexameric units was confirmed through a cross-presentation experiment in which sera collected for ELISA assays were tested against VLPs coated with the opposite shape. In other words, sera obtained from mice vaccinated with round-shaped $CCMV_{TT}$ VLPs demonstrate a faster and more efficient recognition of rod-shaped $CCMV_{TT}$ VLPs compared to the reverse scenario. This phenomenon can be explained by the hypothesis that sera from round-shaped $CCMV_{TT}$ VLPs may contain antibodies capable of recognizing and binding to both pentamers and hexamers, whereas sera from rod-shaped $CCMV_{TT}$ VLPs predominantly target hexameric structures.

The size of VLPs is definitely among their crucial attributes affecting how they stimulate the immune system (Gomes *et.al.,* 2017). This study has confirmed that round-shaped $CCMV_{TT}$ VLPs, sharing the same genetic information as rod-shaped $CCMV_{TT}$ VLPs but displaying distinct morphology, exhibit enhanced drainage to secondary lymphoid organs and improved efficacy in activating APCs and B cells resulting in increased IgG and IgA titers. Previous studies have demonstrated that nano-sized particles can easily move to lymph nodes and are more likely to be taken up by DCs and macrophages residing in the lymph nodes which are considered being the most important APCs (Gomes *et.al.*, 2017). Furthermore, VLPs bigger than 200 nm have to be endocytosed

by APCs to be carried to the lymph nodes. This process could take about 24 hours and could impact the amount of antigen actually reaching the lymph nodes (Fontana *et.al.*, 2019).

Additionally, the presence of RNA carried by VLPs serves a dual role as both a structural component and an essential element in activating TLRs for effective immune response. The signaling through TLRs plays a pivotal role in shaping the characteristics of the immune response generated, making TLR ligands a central consideration in the design and development of VLP-based vaccines. To boost antibody responses and stimulate the production of protective IgG2a antibodies in mice and IgG1 antibodies in humans, vaccines should be administered alongside specific TLR ligands (Bachmann & Jennings, 2010). Throughout this study, we have emphasized the correlation between the presence of nucleic acid packed inside VLPs and the induced T cell response. VLPs containing more TLR ligands, as indicated by higher signal intensity in NAG, could indeed correlate with a more pronounced Th1 response.

Since both round and rod-CCMV$_{TT}$ VLPs contain a comparable amount of nucleic acid, which acts as TLR7/8 agonists, enhancing the efficacy of innate immune system stimulation, this study allowed to establish a correlation between the size of the VLP and the variations in induced IgG subclasses by removing the TLR7/8 ligand effect as a potential confounding variable. Hence, these findings imply that B cells are more proficient at engaging with and processing structures that are 30 nanometers in size, as opposed to larger micron-sized structures, resulting in class switching to IgG2a/b and IgA. Furthermore, calculated ratio between Th1 and Th2-associated IgG subclasses, revealed that the influence of Th1 is more pronounced when dealing with round-shaped CCMV.

To further explore these observations, two experimental designs employing a convenient model antigen Feld1 were conducted. As the CCMV VLPs are not suitable for introduction of large antigen sequences by genetic fusion we chose two other plant VLPs with different morphologies originating from the genera *Potyvirus* and *Tymovirus*, for the display the Fel d 1 antigen. As indicated above PVY CPs form filamentous VLPs whereas Tymovirus VLPs are icosahedrons, respectively. To evaluate the most effective antigen presentation method, we selected several strategies for displaying the antigen. These strategies involved widely used modifications, such as genetic fusions and chemical coupling, complemented by less common enzymatic and physical approaches. While SpyTag/SpyCatcher enzymatic conjugation partners and physical binding partners Ecoil/Kcoil have been successfully employed in studies seeking scaffolds for presenting epitopes for use in subunit vaccines (Tan *et.al.*, 2021b; Hassani-Mehraban *et.al.*, 2015), it is noteworthy that synthetic zipper pair

SZ18/17 in this context has been described for the first time. Furthermore, all enzymatic and physical partner binding processes were achieved by co-expressing both partners (modified VLPs and antigens) directly in the single *E. coli* culture, thereby bypassing the need for time-consuming separate expression and purification processes.

It was previously known that PVY can tolerate N- and C-terminal fusions while maintaining morphological integrity as filaments (Kalnciema *et.al.,* 2012). This research has validated these findings when filaments ranging from 400 to 800 nm either for direct or mosaic PVY CP VLPs were observed after Feld1 incorporation. Alternatively, directly in *E. coli* forming conjugation partners SpyT/SpyC2 and 3 formed shorter filaments around 200 – 400 nm whereas the same observation was much more pronounced for chemically coupled VLPs with sizes ranging from 100 to 200 nm, and even smaller ones, resulting in a more diverse range of particle sizes within the population. The reduction in size might be explained by the fact that chemical coupling has a negative effect on long particles which was also noted by groups working with Papaya Mosaic virus (PapMV; Rioux *et.al.*, 2012; Therien *et.al.,* 2017).

Nonetheless, majority of icosahedral tymovirus CP C-terminal fusions failed to assemble into VLPs. This work proves that the antigen sequence of Feld1 can successfully be incorporated at the C-terminal end of the EMV CP gene after a flexible G4S linker sequence which significantly improved chimeric VLP assembly. Furthermore, it has now been proven that VLPs derived from tymoviruses can tolerate the incorporation of the Feld1 antigen, which is approximately the same size as the tymovirus CP itself using either direct fusion or mosaic system. However, both purified VLPs appeared somewhat heterogeneous, suggesting that the size of the antigen still has a considerable impact on VLP integrity but can be improved with a simple improvement in flexibility.

One of the most important determinants for creating an effective immune response is antigen density, which can be expressed as the distance between one antigen and another on the viral surface. Furthermore, especially 5 – 10 nm distance between antigens are considered the most effective for B cell stimulation (Bachmann & Jennings, 2010). Improved antigen density leads to a decrease in the spacing between antigens on the particle's surface, therefore promotes the cross-linking of B cell receptors (BCRs), ultimately resulting in heightened B cell activation and more robust antibody responses (Jegerlehner *et.al.,* 2002). It's important to consider that the antigen density and, consequently, the antigen presentation capabilities can vary between filaments and icosahedral particles. Icosahedral particles typically maintain a more rigid structure, whereas filaments tend to

float in the solution and can adopt various bent positions. This variability in filament shape can complicate the precise setup of the required spacing for surface-exposed antigens.

In this study, we have also evaluated the density of incorporated Feld1 antigen in the constructed VLP vaccines by performing densitometric analysis on SDS-PAGE gel. Although we assumed that for EMV CP direct fusion each CP contains one Feld1 molecule resulting in 100% incorporation this might not be the case for PVY CP as it undergoes a proteolytic processing at the N-terminus of CP by *E. coli* trypsin-like enzymes (Kalnciema *et.al.,* 2012). Although processing occurs during the expression in *E. coli* and majority of truncated CPs are removed during purification steps, some of the remaining proteases can still truncate purified PVY CP appearing as additional band in SDS-PAGE gel analysis. It's worth noting that the presence of a proteolytic band was not as evident for PVY-Feld1 direct fusion, potentially because the elevated antigen density might have an impact on covering the region responsible for proteolytic cleavage. On the contrary, in purified samples of mosaic and both SpyT/SpyC conjugate VLPs, there might be mixed populations, with one population containing the preferred VLP-antigen fusions and complexes and another population consisting of cleaved Feld1 antigen aggregates altering the presentation of the antigen to the immune system.

All these things considered, the main criteria for selecting the most effective vaccination platform should be based on considerations of total anti-Feld1 IgG levels, antibody specificity or avidity, and the dominance of a Th1 immune response. Taking into account the first two requirements, cPVY-Feld1 with only 26% Feld1 incorporation has demonstrated the highest efficiency as an antigen presentation platform, although it has shown a notable Th2 signaling pathway activation. Indeed, chemical coupling offers numerous advantages over other expression platforms, beginning with the fact that each principal component (VLP and antigen) is purified separately, thus preserving their natural configuration and protein secondary structures. Moreover, the presence of relatively shorter particles in the case of cPVY-Feld1 may also enhance the previously described kinetics of drainage to the lymph nodes. In the meantime, it's noteworthy that the PVY-SpyT/SpyC3-Feld1 variant, which exhibited the strongest nucleic acid signal intensity, also led to a more balanced IgG1/IgG2a ratio against Feld1. This observation suggests that this approach could be particularly promising for TLR stimulation purposes.

Alternatively, the incorporation of Feld1 in EMV CP vaccines, as observed in SDS-PAGE, could be considered a more reliable parameter when addressing surface exposed antigen density issue. Despite the absence of structural analysis data for EMV CP, we have successfully shown the surface

exposure of the Feld1 antigen through the use of Feld1-derived monoclonal antibodies(mAb's). Mab's recognized all EMV-Feld1 vaccine candidates with high specificity, especially the EMV-Feld1 direct fusion, providing strong evidence of previously mentioned high structural similarity of recombinant Feld1 to the native antigen for this vaccine variant.

Certainly, EMV icosahedral particles indeed maintain a robust and repetitive surface antigen structure, which subsequently ensures the necessary spacing between antigens for optimal antibody responses. First, the previously mentioned ratio between Th1 and Th2-associated IgG subclasses, which showed a more balanced distribution, suggests that there has been co-stimulation of TLRs and B cells. This phenomenon may be attributed to the presence of packaged nucleic acid, which was notably observed in three constructs: SZ18/17, Ecoil/Kcoil, and cEMV-Feld1. Secondly, antibody avidity, which measures the strength of binding between antibodies and antigens, is believed to be linked to protection against infection. Furthermore, it is suggested that avidity data could be used alongside antibody titer data to identify biological factors associated with clinical protection against diseases (Bauer, 2021). Interestingly, three out of five EMV-Feld1 variants produced IgG antibodies with an avidity index of around 50%, while cEMV-Feld1 exhibited an even higher specificity with 63% specific antibody production. Furthermore, despite only 5.2% Feld1 antigen incorporation in the EMV-Ecoil/Kcoil-Feld1 vaccine variant, it exhibited an antibody specificity of 25%. This clearly demonstrates that antigen multiplicity is one of the key contributors to vaccine immunogenicity, as previously emphasized.

Based on the evaluation of these criteria, two of the vaccines derived from EMV CP and containing Feld1, SZ18/17 and cEMV-Feld1, emerged as the most promising candidates. They demonstrated very high levels of total IgGs, an avidity index exceeding 50%, and a pronounced Th1 response. Furthermore, antibodies formed against SZ18/17 variant, exhibited the highest recognition of nFeld1as the production of specific IgG antibodies against nFeld1 was considered an equally significant parameter for evaluating vaccine efficacy. Although, resolving excessive IgG production against the EMV carrier is crucial for exploring further application possibilities. Overall, this experimental data comparing two different VLPs with one Feld1 antigen, despite several expression platform choices, showed that the most promising platforms were once again icosahedral particles.

In conclusion, the physical properties of particles, which encompass aspects like size, surface charge, structure, flexibility, shape, surface chemistry, and hydrophobicity, hold a vital role in shaping how nanoparticles engage with cells. These interactions impact various factors, including how long

they stay in circulation, their ability to enter the lymphatic system, their distribution within tissues, and their capacity to engage with and be taken up by cells (Fontana *et al.,* 2019). To design effective nanoparticle-based vaccines, it's essential to analyze and optimize these parameters to achieve desired characteristics. This study clearly shows the significance of smaller nanoparticles (up to 200 nm) over larger ones when interacting with the immune system in complex scenarios, as evidenced by experiments involving preclinical animal models. Furthermore, the outcomes observed in the development and evaluation of EMV-Feld1 vaccine platforms indicate that the chosen construction approach can have a notable impact on both the progress and the specificity of the immune responses triggered. Consequently, it is advisable to explore multiple VLP carriers and antigen incorporation strategies for each novel VLP-based vaccine, aiming to identify the most optimal variant.

5. CONCLUSIONS

1. Insertion of a TT universal epitope into the N- terminal end of the CCMV CP results in the formation of icosahedral T=3 VLPs with a diameter of ~30 nm whereas insertion into C-terminal end results in rod-shaped VLPs, 1 µm in length and ~30 nm in width.
2. Round-shaped $CCMV_{TT}$ VLPs demonstrated improved migration towards secondary lymphoid organs, facilitating effective interactions with professional APCs and B cells which resulted in a notable induction of systemic IgA and IgG responses, accompanied by prominent formation of splenic germinal centers.
3. Round-shaped $CCMV_{TT}$ VLPs are capable of polarizing elicited T cell response toward the Th1 pathway.
4. By utilizing genetic methods, including both direct and mosaic fusion techniques, as well as SpyTag/SpyCatcher-mediated enzymatic coupling to the VLP carrier, the Feld1 antigen can be incorporated into the PVY CP without hindering the formation of filamentous VLPs when expressed in *E. coli* cells.
5. The Feld1 antigen can be incorporated into the EMV CP via genetic methods like direct and mosaic fusion, or a physical binding approach involving coiled-coil forming peptides Ecoil/Kcoil and the synthetic zipper pair SZ18/17, followed by expression in *E. coli* cells while preserving icosahedral T=3 particle formation.
6. The Feld1 antigen can be chemically coupled to either PVY or EMV VLPs using the SMPH crosslinker.
7. All constructed PVY-Feld1 and EMV-Feld1 vaccine variants exhibited enhanced immunogenicity, as evidenced by their recognition by two monoclonal Feld1 antibodies and their ability to induce elevated anti-Feld1 antibody titers in mouse models.
8. All developed EMV-Feld1 vaccines resulted in an antibody-antigen binding avidity exceeding 45%, while the most favorable PVY-Feld1 variant was observed in the chemically coupled version, demonstrating only 36% specificity.
9. Within both the PVY-Feld1 and EMV-Feld1 groups, IgG1 subclass antibodies were observed as the predominant class against all vaccine variants.
10. While antibodies produced by all PVY-Feld1 and EMV-Feld1 vaccine variants recognized nFeld1, the overall titers against nFeld1 were higher for PVY-Feld1 groups.

6. MAIN THESIS FOR DEFENCE

1. Plant VLPs with introduced antigens can be efficiently expressed and purified from E. coli host system which ensures the encapsulation of host nucleic acids during the expression procedure.
2. Icosahedral plant VLPs, with a size of approximately 30 nm, emerge as superior vaccination candidates due to their capacity for rapid trafficking into secondary lymphoid organs, leading to heightened immunogenicity when compared with larger filamentous VLPs measuring around 1 μm.
3. The chemical coupling approach possess characteristics that position it as the most efficient platform for facilitating immune cell recognition of the Feld1 antigen.
4. Icosahedral VLPs demonstrate an elevated production of protective Th1-associated IgG subclasses.

7. PUBLICATIONS

1. **“The impact of size on particle drainage dynamics and antibody response”**

   Simon Zinkhan, Anete Ogrina, Ina Balke, Gunta Reseviča, Andris Zeltins, Simone de Brot, Cyrill Lipp, Xinyue Chang, Lisha Zha, Monique Vogel, Martin F. Bachmann, Mona O. Mohsen. The impact of size on particle drainage dynamics and antibody response. J Control Release. 2021 Mar 10; 331:296-308. doi: 10.1016/j.jconrel.2021.01.012.

2. **“Comparison of bacterial expression systems basen on potato virus Y- like particles for vaccine generation”**

   Anete Ogrina, Dace Skrastina, Ina Balke, Ieva Kalnciema, Juris Jansons, Martin F. Bachmann, Andris Zeltins. Comparison of Bacterial Expression Systems Based on Potato Virus Y-like Particles for Vaccine Generation. Vaccines (Basel). 2022 Mar 22;10(4):485. doi: 10.3390/vaccines10040485.

3. **“Bacterial expression systems based on Tymovirus-like particles for the presentation of vaccine antigens”**

   Anete Ogrina, Ina Balke, Ieva Kalnciema, Dace Skrastina, Juris Jansons, Martin F. Bachmann, Andris Zeltins. Bacterial expression systems based on Tymovirus-like particles for the presentation of vaccine antigens. Front Microbiol. 2023 Mar 23; 14:1154990. doi: 10.3389/fmicb.2023.1154990.

8. APPROBATION OF THE RESEARCH

1. A. Ogrina, S. Zinkhan, I. Balke, G. Resevica, A. Zeltins, S. de Brot, C. Lipp, X. Chang, L. Zha, M. Vogel, M. F. Bachmann, M. O. Mohsen. 2020. g. LU 78. konference. "Modificētu Lopbarības pupiņas raibuma vīrusam līdzīgo daļiņu morfoloģijas ietekme uz imūnatbildi". Mutiska prezentācija.
2. A. Ogrina, S. Zinkhan, I. Balke, G. Resevica, A. Zeltins, S. de Brot, C. Lipp, X. Chang, L. Zha, M. Vogel, M. F. Bachmann, M. O. Mohsen. 2021. g. LU 79. konference. "Vīrusam līdzīgo daļiņu izmēru ietekme uz infiltrāciju limfmezglos un antivielu atbildi". Mutiska prezentācija.
3. A. Ogrina, D. Skrastina, I. Balke, I. Kalnciema, J. Jansons, M.F. Bachmann, A. Zeltins. 2022. g. LU 80. konference. "Dažādu uz kartupeļu vīrusa Y (PVY) vīrusveidīgo daļiņu balstītu bakteriālo sistēmu salīdzinājums vakcīnu izveidei". Mutiska prezentācija.
4. A. Ogrina, D. Skrastina, I. Balke, I. Kalnciema, J. Jansons, M.F. Bachmann, A. Zeltins. 2022. g. FEBS3+ starptautiskā zinātniskā conference Tallinā, Igaunijā. "Bacterial Expression Systems Based on Potato Virus Y-like Particles for Vaccine Generation". Stenda referāts.
5. A. Ogrina, I. Balke, I. Kalnciema, D. Skrastina, J. Jansons, M.F. Bachmann, A. Zeltins. 2023. g. LU 81. konference. "Uz jauna Tymovirus- līdzīgām daļiņām balstītas bakteriālās ekspresijas sistēmas vakcīnu antigēnu prezentēšanai". Mutiska prezentācija.
6. A. Ogrina, I. Balke, I. Kalnciema, D. Skrastina , J. Jansons, M.F. Bachmann, A. Zeltins. 2023. g. Virus-like particles & Nanoparticle Vaccines starptautiskā konference, Rīga, Latvija. "Bacterial expression systems based on plant – virus like particles for the presentation of vaccine antigens". Stenda referāts.

9. ACKNOWLEDGEMENTS

I would like to express my gratitude to my supervisor, Dr. biol. Andris Zeltiņš, for providing me with the opportunity to conduct my PhD research under his guidance and contribute to the fascinating vaccine research in his laboratory;

To my advisor, Dr. biol. Ina Baļķe, for her assistance throughout my period of study and research, especially providing guidance during the initial steps of my work in biotechnology;

To my laboratory team Ieva Kalnciema, Gunta Resevičа, Vilija Zeltiņa, Rebeka Ludviga, Jeļena Šapiro for the advices, support and encouragement.

To our collaboration partners from Prof. Martin Bachmann laboratory in University of Bern, Switzerland – especially Dr. biol. Mona O. Mohsen, Simon Zinkhan, Romano Josi and Prof. Martin Bachmann for their efforts and knowledge during our joint projects and my stay in Bern.

To Dr. biol. Dace Skrastiņa for her help with immunology experiments.

To Dr. biol. Juris Jansons for electron microscopy images.

To Jānis Bogans for DLS experiments.

To my reviewers for their thoughts and questions.

To all the amazing science teachers and professors throughout my years of study who made science so interesting;

And finally - to my family and my partner, Edgars, for their patience and unwavering support during my studies and research, and for always being there for me.

10. REFERENCES

Adolph K.W, Butler P.J. (1974). Studies on the assembly of a spherical plant virus. I. States of aggregation of the isolated protein. *J Mol Biol* **88**:327-41.

Adolph K.W., Butler P.J. (1976). Assembly of a spherical plant virus. *Philos Trans R Soc Lond B Biol Sci* **276:**113-22. doi: 10.1098/rstb.1976.0102.

Al-Barwani F., Donaldson B., Pelham S.J., Young S.L., Ward V.K. (2014). Antigen delivery by virus-like particles for immunotherapeutic vaccination. *Ther Deliv* **5**:1223-40. doi: 10.4155/tde.14.74.

Alexander J., Sidney J., Southwood S., Ruppert J., Oseroff C., Maewal A., Snoke K., Serra H.M., Kubo R. T, Sette A., et al. (1994). Development of high potency universal DR-restricted helper epitopes by modification of high affinity DR-blocking peptides. *Immunity* **1**:751-61. doi: 10.1016/s1074-7613(94)80017-0.

Ali A., Roossinck M.J. (2008). Rapid and efficient purification of Cowpea chlorotic mottle virus by sucrose cushion ultracentrifugation. *J Virol Methods*, **141**:84-6

Ali A., Shafiekhani M., Olsen J. (2011). Molecular charecterization of the complete genomes of two new field isolates of Cowpea Chlorotic mottle virus, and their phylogenetic analysis. *Virus Genes* **43**: 120 – 129.

Allison R. F., Janda M., Ahlquist P. (1988). Infectious In Vitro Transcripts from Cowpea Chlorotic Mottle Virus cDNA clones and exchange of individual RNA components with Brome Mosaic Virus. *J Virol* **62**: 3581-3588.

Almendárez-Rodriguez C., Solis-Andrade K.I., Govea-Alonso D.O., Comas-Garcia M., Rosales-Mendoza S. (2022). Production and characterization of chimeric SARS-CoV-2 antigens based on the capsid protein of cowpea chlorotic mottle virus. *Int J Biol Macromol* **213**:1007-1017. doi: 10.1016/j.ijbiomac.2022.06.021.

Andre F.E., Booy R., Bock H.L., Clemens J., SDatta S.K., John T.J., Lee B.W., Lolekha S., Peltola H., Ruff T.A., Santosham M., Schmitt H.J. (2008). Vaccination greatly reduces disease, disability, death and inequity worldwide. *Bull World Health Organ* **86**: 81–160;

Anindya R., Savithri H.S. (2003). Surface-exposed amino- and carboxy-terminal residues are crucial for the initiation of assembly in Pepper vein banding virus: a flexuous rod-shaped virus. *Virology* **316**:325-36. doi: 10.1016/s0042-6822(03)00593-2.

Atherton, J. (2009). Acid–base balance: maintenance of plasma pH. *Anaesthesia & Intensive Care Medicine*, Volume **10**, Issue 11, pp 557-561, ISSN 1472-0299, doi: 10.1016/j.mpaic.2009.08.005.

Azizgolshani O., Garmann R.F., Cadena-Nava R., Knobler C.M., Gelbart W.M. (2013). Reconstituted plant viral capsids can release genes to mammalian cells. *Virology* **441**:12-7. doi: 10.1016/j.virol.2013.03.001.

Bachmann M.F., Dyer M.R. (2004). Therapeutic vaccination for chronic diseases: A new class of drugs in sight. *Nature Reviews Drug* Discovery **3**, 81 – 88, doi: 10.1038/nrd1284.

Bachmann M.F., Jennings G.T. (2010). Vaccine delivery: a matter of size, geometry, kinetics and molecular patterns. *Nat Rev Immunol* **10**:787-96.

Bachmann M.F., Zingernagel R.M. (1997). Neutralizing antiviral B cell responses. *Annual Review of Immunology* **15**, 235 – 270.

Bachmann M.F., Zabel F. (2016). Immunology of Virus – Like Particles. In: *Viral Nanotechnology*. Y. E. Khudyakov, P. Pumpens, Eds., CRC Press: Boca Raton, Florida, USA, pp. 121-128.

Balke I., Zeltins A. (2020). Recent Advances in the Use of Plant Virus-Like Particles as Vaccines. *Viruses* **12**:270. doi: 10.3390/v12030270.

Balke I., Zeltins A. (2019). Use of plant viruses and virus-like particles for the creation of novel vaccines. *Adv Drug Deliv Rev* **145**:119-129. doi: 10.1016/j.addr.2018.08.007.

Bancroft J.B. (1970). The self-assembly of spherical plant viruses. *Adv Virus Res.* **16**:99-134. doi: 10.1016/s0065-3527(08)60022-6.

Bancroft J. B., Flack I.H. (1972). The behavior of cowpea chlorotic mottle virus in CsCl. *J GenVirol* **15:247 – 251**. doi: 10.1099/0022-1317-15-3-247

Bancroft, J.B., Hiebert.E. (1967). Formation of an infectious nucleoprotein from protein and nucleic acid isolated from a small spherical virus. *Virology* **32**:354–356. doi: 10.1016/0042-6822(67)90284-x.

Bancroft J.B, Rees M.W., Johnson M.W., Dawson J.R.O. (1973). A Salt – stable mutant of Cowpea Chlorotic mottle virus. *Journal of General Virology* **21**, 507 - 513. doi: 10.1099/0022-1317-21-3-507

Barnhill H.N., Reuther R., Ferguson P.L., Dreher T., Wang Q. (2007). Turnip yellow mosaic virus as a chemoaddressable bionanoparticle. *Bioconjug Chem* **18**:852-9. doi: 10.1021/bc060391s.

Bauer G. (2021). The potential significance of high avidity immunoglobulin G (IgG) for protective immunity towards SARS-CoV-2. *Int J Infect Dis* **106**:61-64. doi: 10.1016/j.ijid.2021.01.061.

Bienboire - Frosini C., Durairaj R., Pelosi P., Pageat P. (2020). The Major Cat Allergen Fel d 1 Binds Steroid and Fatty Acid Semiochemicals: A Combined In Silico and In Vitro Study. *Int J Mol Sci* **21**:1365. doi: 10.3390/ijms21041365.

Bonnet B., Messaoudi K., Jacomet F., Michaud E., Fauquert J.L., Caillaud D., Evrard B. (2018). An update on molecular cat allergens: Fel d 1 and what else? Chapter 1: Fel d 1, the major cat allergen. *Allergy Asthma Clin Immunol* **14**:14. doi: 10.1186/s13223-018-0239-8.

Bransom K.L., Weiland J.J., Tsai C.H., Dreher T.W. (1995). Coding density of the turnip yellow mosaic virus genome: roles of the overlapping coat protein and p206-readthrough coding regions. *Virology* **206**:403-12. doi: 10.1016/s0042-6822(95)80056-5.

Brenner S., Horne R.W. (1959). A negative staining method for high resolution electron microscopy of viruses. *Biochim Biophys Acta* **34**:103-10. doi: 10.1016/0006-3002(59)90237-9.

Brune K.D., Howarth M. (2018). New Routes and Opportunities for Modular Construction of Particulate Vaccines: Stick, Click, and Glue. *Front Immunol*; **9**:1432. doi: 10.3389/fimmu.2018.01432.

Bujarski J.J. (2021). Bromoviruses (*Bromoviridae*). Encyclopedia of Virology. **2021**:260–267. doi: 10.1016/B978-0-12-809633-8.21563-X.

Cadena-Nava R.D., Comas-Garcia M., Garmann R.F., Rao A.L., Knobler C.M., Gelbart W.M. (2012). Self-assembly of viral capsid protein and RNA molecules of different sizes: requirement for a specific high protein/RNA mass ratio. *J Virol* **86**:3318-26. doi: 10.1128/JVI.06566-11.

Canady M.A., Larson S.B., Day J., McPherson A. (1996). Crystal structure of turnip yellow mosaic virus. Nat Struct Biol **3**:771-81. doi: 10.1038/nsb0996-771.

Cerovská N., Hoffmeisterová H., Pecenková T., Moravec T., Synková H., Plchová H., Velemínský J. (2008). Transient expression of HPV16 E7 peptide (aa 44-60) and HPV16 L2 peptide (aa 108-120) on chimeric potyvirus-like particles using Potato virus X-based vector. *Protein Expr Purif* **58**:154-61. doi: 10.1016/j.pep.2007.09.006.

Chandran D., Shahana P.V., Rani G.S., Sugumar P., Shankar C.R., Srinivasan V.A. (2009). Display of neutralizing epitopes of Canine parvovirus and a T-cell epitope of the fusion protein of Canine distemper virus on chimeric tymovirus-like particles and its use as a vaccine candidate both against Canine parvo and Canine distemper. *Vaccine* **28**:132-9. doi: 10.1016/j.vaccine.2009.09.093.

Chen T.H., Chen T.H., Hu C.C., Liao J.T., Lee C.W., Liao J.W., Lin M.Y., Liu H.J., Wang M.Y., Lin N.S., Hsu Y.H. (2012). Induction of protective immunity in chickens immunized with

plant-made chimeric Bamboo mosaic virus particles expressing very virulent Infectious bursal disease virus antigen. *Virus Res* **166**:109-15. doi: 10.1016/j.virusres.2012.02.021.

Chen Q., Lai H. (2013). Plant – derived virus – like particles as vaccines. Hum. *Vaccin. Immunother.* **9**: 26 – 49.

Choudhury S., Kakkar V., Suman P., Chakrabarti K., Vrati S., Gupta S. K. (2009). Immunogenicity of zona pellucida glycoprotein-3 and spermatozoa YLP (12) peptides presented on Johnson grass mosaic virus-like particles. *Vaccine* **27**, 2948–2953.

Chung B.Y., Miller W.A., Atkins J.F., Firth A.E. (2008). An overlapping essential gene in the Potyviridae. *Proc Natl Acad Sci U S A* **105**:5897-902. doi: 10.1073/pnas.0800468105.

Cosslett V. E., Markham R. (1948) Structure of turnip yellow mosaic virus crystals in the electron microscope. *Nature* **161:**250-2. doi: 10.1038/161250a0.

Craig P.O., Alzogaray V., Goldbaum F.A. (2012). Polymeric Display of Proteins through High Affinity Leucine Zipper Peptide Adaptors. *Biomacromolecules* **13**:1112-21. doi: 10.1021/bm201875p.

de Assis Filho F. M., Paguio O. R., Sherwood J. L., Deom C. M. (2002). Symptom induction by Cowpea chlorotic mottle virus on Vigna unguiculata is determined by amino acid residue 151 in the coat protein. J Gen Virol 83, 879-883.

Cuesta, R., Yuste-Calvo, C., Gil-Cartón, D. Sánchez F, Ponz F, Valle M. (2019). Structure of Turnip mosaic virus and its viral-like particles. Sci Rep 9, 15396. doi: 10.1038/s41598-019-51823-4.

Donaldson B., Al-Barwani F., Young V., Scullion S., Ward V., Young S. (2014). Virus-Like Particles, a Versatile Subunit Vaccine Platform. Subunit Vaccine Delivery 9:159–80. doi: 10.1007/978-1-4939-1417-3_9.

Douglas T., Young M. (1998). Host–guest encapsulation of materials by assembled virus protein cages. Nature 393: 152–155. doi: 10.1038/30211

Edwards S.J., Hayden M.B., Hamilton R.C., Haynes J.A., Nisbet I.T., Jagadish M.N., (1994.) High level production of potyvirus-like particles in insect cells infected with recombinant baculovirus. *Arch Virol* **136**, 375–380. doi: 10.1007/BF01321065.

Fontana F., Figueiredo P., Santos H.A. (2019). Advanced nanovaccines for immunotherapy applications: From concept to animal tests. *Ther Bionanomaterials,* 231-260, doi: 10.1016/B978-0-12-815341-3.00010-9

Fox J., X. Zha, J. Speir, Young M. (1996). Analysis of a salt stable mutant of cowpea chlorotic mottle virus. *Virology*. **222**:115–122. doi: 10.1006/viro.1996.0402.

Fox J.M., Wang G., Speir J.A., Olson N.H., Johnson J.E., Baker T.S., Young M.J. (1998). Comparion of the native CCMV virion with in vitro assembled CCMV virions by Cryoelectron Microscopy and Image Reconstruction. *Virology* **244**: 212-218. doi: 10.1006/viro.1998.9107.

Fredsgaard L., Goksøyr L., Thrane S., Aves K.L., Theander T.G., Sander A.F. (2021). Head-to-Head Comparison of Modular Vaccines Developed Using Different Capsid Virus-Like Particle Backbones and Antigen Conjugation Systems. *Vaccines (Basel)* **9**:539. doi: 10.3390/vaccines9060539.

Gibbons M.M., Klug W.S. (2008). Influence of nonuniform geometry on nanoindentation of viral capsids. *Biophys* J **95**:3640-9. doi: 10.1529/biophysj.108.136176.

Gomes A.C., Mohsen M.O., Bachmann M.F. (2017). Harnessing Nanoparticles for Immunomodulation and Vaccines *Vaccines (Basel)* **5**:6. doi: 10.3390/vaccines5010006.

Hammond R., Abrahamian P. (2021). Tymoviruses (Tymoviridae), Editor(s): Dennis H. Bamford, Mark Zuckerman, Encyclopedia of Virology (Fourth Edition), Academic Press, pp 818-826, ISBN 9780128145166, doi: 10.1016/B978-0-12-809633-8.21305-8.

Hammond J.M., Sproat K.W., Wise T.G., Hyatt A.D., Jagadish M.N., Coupar B.E. (1998). Expression of the potyvirus coat protein mediated by recombinant vaccinia virus and assembly of potyvirus-like particles in mammalian cells. *Arch Virol.* **143**, 1433–1439.

Hanafi L.A., Bolduc M., Gagné M.E., Dufour F., Langelier Y., Boulassel M.R., Routy J.P., Leclerc D., Lapointe R. (2010). Two distinct chimeric potexviruses share antigenic cross-presentation properties of MHC class I epitopes. *Vaccine* **28**:5617-26. doi: 10.1016/j.vaccine.2010.06.024.

Hassani-Mehraban A., Creutzburg S., van Heereveld L., Kormelink R. (2015). Feasibility of Cowpea chlorotic mottle virus-like particles as scaffold for epitope presentations. *BMC Biotechnol* **15**:80. doi: 10.1186/s12896-015-0180-6.

Hayden C.M., Mackenzie A.M., Skotnicki M.L., Gibbs A. (1998). Turnip yellow mosaic virus isolates with experimentally produced recombinant virion proteins. *J Gen Virol* **79**:395-403. doi: 10.1099/0022-1317-79-2-395.

Hema M., Nagendrakumar S.B., Yamini R., Chandran D., Rajendra L., Thiagarajan D., Parida S., Paton D.J., Srinivasan V.A. (2007). Chimeric tymovirus-like particles displaying foot-and-mouth disease virus non-structural protein epitopes and its use for detection of FMDV-NSP antibodies. *Vaccine* **25**:4784-94. doi: 10.1016/j.vaccine.2007.04.023.

Hoffmeisterova H., Cerovska N., Moravec T., Plchova H., Folwarczna J., Veleminsky J. (2008). Transient expression of fusion gene coding for the HPV-16 epitopes fused to the sequence of potyvirus coat protein using different means of inoculation of Nicotiana benthamiana and Brassica rapa, cv. Rapa plants. *Plant Cell Tissue Organ Cult.* **94**, 261–267. doi: 10.1007/s11240-008-9370-4

Hu Y., Zandi R., Anavitarte A., Knobler C.M., Gelbart W.M. (2008). Packaging of a polymer by a viral capsid: the interplay between polymer length and capsid size. *Biophys J.* **94**:1428-36. doi: 10.1529/biophysj.107.117473.

Hull R. (1970). Studies on alfalfa mosaic virus. III. Reversible dissociation and reconstitution studies. *Virology* **40**, 34–47. doi: 10.1016/0042-6822(70)90376-4.

Jagadish M.N., Ward C.W., Gough K.H., Tulloch P.A., Whittaker L.A., Shukla D.D. (1991). Expression of potyvirus coat protein in Escherichia coli and yeast and its assembly into virus-like particles. *J Gen Virol* **72**, 1543–1550. doi: 10.1099/0022-1317-72-7-1543.

Jegerlehner A., Maurer P., Bessa J., Hinton H.J., Kopf M., Bachmann M.F. (2007). TLR9 signaling in B cells determines class switch recombination to IgG2a. *J Immunol* **178**:2415-20. doi: 10.4049/jimmunol.178.4.2415.

Jegerlehner A., Storni T., Lipowsky G., Schmid M., Pumpens P., Bachmann M.F. (2002). Regulation of IgG antibody responses by epitope density and CD21-mediated costimulation. *Eur J Immunol* **32**:3305-14. doi: 10.1002/1521-4141(200211)32:11<3305::AID-IMMU3305>3.0.CO;2-J.

Johnson J., Speir J. (1997). Quasi-equivalent viruses: a paradigm for protein assemblies. *J Mol Biol* **269**:665–675. doi: 10.1006/jmbi.1997.1068.

Kalnciema I., Skrastina D., Ose V., Pumpens P., Zeltins A. (2012). Potato virus Y-like particles as a new carrier for the presentation of foreign protein stretches. *Mol Biotechnol* **52**:129-39. doi: 10.1007/s12033-011-9480-9.

Kaumaya P.T., Kobs-Conrad S., Seo Y.H., Lee H., VanBuskirk A.M., Feng N., Sheridan J.F., Stevens V. (1993). Peptide vaccines incorporating a 'promiscuous' T-cell epitope bypass certain haplotype restricted immune responses and provide broad spectrum immunogenicity. *J Mol Recognit* **6**:81-94. doi: 10.1002/jmr.300060206.

Kerlan C., Moury B. (2008). Potato Virus Y, in: Granoff A., Webster R.G. (eds.) Encyclopedia of Virology, 3rd edn., pp. 287–96, New York: Academic Press.

Kezar A., Kavčič L., Polák M., Nováček J., Gutiérrez-Aguirre I., Žnidarič M.T., Coll A., Stare K., Gruden K., Ravnikar M., Pahovnik D., Žagar E., Merzel F., Anderluh G., Podobnik M.

(2019). Structural basis for the multitasking nature of the potato virus Y coat protein. *Sci Adv* **5**:eaaw3808. doi: 10.1126/sciadv.aaw3808.

Khan J. A., Dijkstra J. (2006). Handbook of Plant Virology. NY: Food Products Press. 311 – 312 pp.

Kinnear C., Moore T.L., Rodriguez-Lorenzo L., Rothen-Rutishauser B., Petri-Fink A. (2017). Form Follows Function: Nanoparticle Shape and Its Implications for Nanomedicine. *Chem Rev* **117**:11476-11521. doi: 10.1021/acs.chemrev.7b00194.

King A. M. Q., Adams M. J., Carstens E. B., Lefkowitz E. J. (2012). Virus Taxonomy. Ninth Report of the International Comitee on Taxonomy of Viruses. San Diego: Academic Press. 969 - 670 pp.

Klug W.S., Bruinsma R.F., Michel J., Knobler C.M., Ivanovska I.L., Schmidt C.F., Wuite G. (2006). Failure of Viral Shells, Phys. Rev. Lett. 97, 228101. doi: 10.1103/PhysRevLett.97.228101.

Koch K., Jones T., Badillo-Vargas I.E. (2020). Chapter 26 - Arthropod vectors of plant viruses, Editor(s): L.P. Awasthi, Applied Plant Virology, Academic Press, pp 349-379, ISBN 9780128186541, doi: 10.1016/B978-0-12-818654-1.00026-8.

Koho T., Ihalainen T.O., Stark M., Uusi-Kerttula H., Wieneke R., Rahikainen R., Blazevic V., Marjomäki V., Tampé R., Kulomaa M.S., Hytönen V.P. (2015). His-tagged norovirus-like particles: A versatile platform for cellular delivery and surface display. *Eur J Pharm Biopharm* **96**:22-31. doi: 10.1016/j.ejpb.2015.07.002.

Konstantinou G.N. (2017). T-Cell Epitope Prediction. Methods Mol Biol 1592:211-222. doi: 10.1007/978-1-4939-6925-8_17.

Kovacs-Nolan J., Mine Y. (2006). Tandem copies of a human rotavirus VP8 epitope can induce specific neutralizing antibodies in BALB/c mice. Biochim Biophys Acta 1760:1884-93. doi: 10.1016/j.bbagen.2006.07.015.

Krishna S.S., Hiremath C.N., Munshi S.K., Prahadeeswaran D., Sastri M., Savithri H.S., Murthy M.R. (1999). Three-dimensional structure of physalis mottle virus: implications for the viral assembly. *J Mol Biol* **289**:919-34. doi: 10.1006/jmbi.1999.2787.

Kroner P. A., Young B. M., Ahlquist P. (1990). Analysis of the role of brome mosaic virus 1a protein domains in RNA replication, using linker insertion mutagenesis. J Virol 64: 6110 – 6120. doi: 10.1128/JVI.64.12.6110-6120.1990.

Lam P., Steinmetz N.F. (2019). Delivery of siRNA therapeutics using cowpea chlorotic mottle virus-like particles. Biomater Sci 7:3138-3142. doi: 10.1039/c9bm00785g.

Laliberté-Gagné M.E., Bolduc M., Garneau C., Olivera-Ugarte S.M., Savard P., Leclerc D. (2021). Modulation of Antigen Display on PapMV Nanoparticles Influences Its Immunogenicity. Vaccines (Basel) 9:33. doi: 10.3390/vaccines9010033.

Lampinen V., Gröhn S., Soppela S., Blazevic V., Hytönen V.P., Hankaniemi M.M. (2023). SpyTag/SpyCatcher display of influenza M2e peptide on norovirus-like particle provides stronger immunization than direct genetic fusion. Front Cell Infect Microbiol 13:1216364. doi: 10.3389/fcimb.2023.1216364.

Larson S.B., Day J., Canady M.A., Greenwood A., McPherson A. (2000). Refined structure of desmodium yellow mottle tymovirus at 2.7 A resolution. J Mol Biol 301:625-42. doi: 10.1006/jmbi.2000.3983.

Larson S.B., Lucas R.W., Greenwood A., McPherson A. (2005). The RNA of turnip yellow mosaic virus exhibits icosahedral order. *Virology* **334**:245-54. doi: 10.1016/j.virol.2005.01.036.

Laubreton D., Bay S., Sedlik C., Artaud C., Ganneau C., Dériaud E., Viel S., Puaux A.L, Amigorena S., Gérard C., Lo-Man R., Leclerc C. (2016).The fully synthetic MAG-Tn3 therapeutic vaccine containing the tetanus toxoid-derived TT830-844 universal epitope provides anti-tumor immunity. *Cancer Immunol Immunother* **65**:315-25. doi: 10.1007/s00262-016-1802-0.

Lavelle L., Gingery M., Phillips M., Gelbart W.M., Knobler C.M., Cadena-Nava R.D., Vega-Acosta J.R., Pinedo-Torres L.A., Ruiz-Garcia J. (2009). Phase Diagram of Self assembled Viral Capsid Protein Polymorphs. *J Phys Chem B* **113**:3813 -3819.

Lavelle L., Michel J.P., Gingery M. (2007). The disassembly, reassembly and stability of CCMV protein capsids. *J Virol Methods* **146**:311-6. doi: 10.1016/j.jviromet.2007.07.020.

Le D.H., Lee K.L., Shukla S., Commandeur U., Steinmetz N.F. (2017). Potato virus X, a filamentous plant viral nanoparticle for doxorubicin delivery in cancer therapy. *Nanoscale* **9**:2348-2357. doi: 10.1039/c6nr09099k.

Le D.H., Méndez-López E., Wang C., Commandeur U., Aranda M.A., Steinmetz N.F. (2019). Biodistribution of Filamentous Plant Virus Nanoparticles: Pepino Mosaic Virus versus Potato Virus X. *Biomacromolecules* **20**:469-477. doi: 10.1021/acs.biomac.8b01365.

Lico C., Mancini C., Italiani P., Betti C., Boraschi D., Benvenuto E., Baschieri S. (2009). Plant-produced potato virus X chimeric particles displaying an influenza virus-derived peptide activate specific CD8+ T cells in mice. *Vaccine* **27**:5069-76. doi: 10.1016/j.vaccine.2009.06.045.

Liepold L., Anderson S., Willits D., Oltrogge L., Frank J.A., Douglas T., Young M. (2007). Viral capsids as MRI contrast agents. *Magn Reson Med* **58**:871-9. doi: 10.1002/mrm.21307.

Ligabue-Braun R., Sachett L.G., Pol-Fachin L., Verli H. (2015). The Calcium Goes Meow: Effects of Ions and Glycosylation on Fel d 1, the Major Cat Allergen. *PLoS One* **10**:e0132311. doi: 10.1371/journal.pone.0132311.

Liu F., Ge S., Li L., Wu X., Liu Z., Wang Z. (2012). Virus – like particles: Potential veterinary vaccine immunogens. *Research in Veterinary Science* **93**: 553 – 559. doi: 10.1016/j.rvsc.2011.10.018.

Lomonossoff G.P., Evans D.J. (2014). Applications of plant viruses in bionanotechnology. *Curr Top Microbiol Immunol* **375**:61-87. doi: 10.1007/82_2011_184.

Lund L.H., Andersson K., Zuber B., Karlsson A., Engström G., Hinkula J., Wahren B., Winberg G. (2003). Signal sequence deletion and fusion to tetanus toxoid epitope augment antitumor immune responses to a human carcinoembryonic antigen (CEA) plasmid DNA vaccine in a murine test system. Cancer Gene Ther 10:365-76. doi: 10.1038/sj.cgt.7700574.

Manolova V., Flace A., Bauer M., Schwarz K., Saudan P., Bachmann M.F. (2008). Nanoparticles target distinct dendritic cell populations according to their size. *Eur J Immunol* **38**:1404-13. doi: 10.1002/eji.200737984.

Martelli G.P., Sabanadzovic S., Abou-Ghanem Sabanadzovic N., Edwards M.C., Dreher T. (2002). The family Tymoviridae. *Arch Virol* **147**:1837-46. doi: 10.1007/s007050200045.

Martínez-Turiño S., García J.A. (2020). Potyviral coat protein and genomic RNA: A striking partnership leading virion assembly and more. *Adv Virus Res* **108**:165-211. doi: 10.1016/bs.aivir.2020.09.001.

McCormick A.A., Corbo T.A., Wykoff-Clary S., Nguyen L.V., Smith M.L., Palmer K.E., Pogue G.P. (2006). TMV-peptide fusion vaccines induce cell-mediated immune responses and tumor protection in two murine models. *Vaccine* **24**:6414-23. doi: 10.1016/j.vaccine.2006.06.003.

McDonald J.G., Bancroft, J.B. (1977). Assembly studies on Potato virus Y and its coat protein. *J Gen Virol* **35**, 251–263. doi: 10.1099/0022-1317-35-2-251

McDonald J.G., Beveridge, T.J., Bancroft, J.B. (1976). Self-assembly of protein from a flexuous virus. *Virology* **69**: 327–331. doi: 10.1016/0042-6822(76)90220-8

Michel J.P., Ivanovska I.L., Gibbons M.M., Klug W.S., Knobler C.M., Wuite G.J., Schmidt C.F. (2006). Nanoindentation studies of full and empty viral capsids and the effects of capsid

protein mutations on elasticity and strength. *Proc Natl Acad Sci U S A* **103**:6184-9. doi: 10.1073/pnas.0601744103.

Minten I.J., Hendriks L.J., Nolte R.J., Cornelissen J.J. (2009). Controlled encapsulation of multiple proteins in virus capsids. *J Am Chem Soc* **131**:17771-3. doi: 10.1021/ja907843s.

Mohsen M.O., Gomes A.C., Vogel M., Bachmann M.F. (2018). Interaction of Viral Capsid-Derived Virus-Like Particles (VLPs) with the Innate Immune System. *Vaccines (Basel)* **6**:37. doi: 10.3390/vaccines6030037.

Mohsen M.O., Heath M.D., Cabral-Miranda G., Lipp C., Zeltins A., Sande M., Stein J.V., Riether C., Roesti E., Zha L., Engeroff P., El-Turabi A., Kundig T.M., Vogel M., Skinner M.A., Speiser D.E., Knuth A., Kramer M.F., Bachmann M.F. (2019). Vaccination with nanoparticles combined with micro-adjuvants protects against cancer. *J Immunother Cancer* **7**:114. doi: 10.1186/s40425-019-0587-z. Erratum in: J Immunother Cancer. 2019 May 23;7(1):137.

Obeng E.M., Fulcher A.J., Wagstaff K.M. (2023). Harnessing sortase A transpeptidation for advanced targeted therapeutics and vaccine engineering. *Biotechnol Adv* **64**:108108. doi: 10.1016/j.biotechadv.2023.108108.

Panina-Bordignon P., Tan A., Termijtelen A., Demotz S., Corradin G., Lanzavecchia A. (1989). Universally immunogenic T cell epitopes: promiscuous binding to human MHC class II and promiscuous recognition by T cells. *Eur J Immunol* **19**:2237-42. doi: 10.1002/eji.1830191209.

Parvizpour S., Pourseif M.M., Razmara J., Rafi M.A., Omidi Y. (2020). Epitope-based vaccine design: a comprehensive overview of bioinformatics approaches. *Drug Discov Today* **25**:1034-1042. doi: 10.1016/j.drudis.2020.03.006.

Pazos-Castro D., Margain C., Gonzalez-Klein Z., Amores-Borge M., Yuste-Calvo C., Garrido-Arandia M., Zurita L., Esteban V., Tome-Amat J., Diaz-Perales A., Ponz F. (2022). Suitability of potyviral recombinant virus-like particles bearing a complete food allergen for immunotherapy vaccines. *Front Immunol* **13**:986823. doi: 10.3389/fimmu.2022.986823.

Pomwised R., Intamaso U., Teintze M., Young M., Pincus S.H. (2016). Coupling Peptide Antigens to Virus-Like Particles or to Protein Carriers Influences the Th1/Th2 Polarity of the Resulting Immune Response. *Vaccines (Basel)* **4**:15. doi: 10.3390/vaccines4020015.

Powell J.D., Barbar E., Dreher T.W. (2012). Turnip yellow mosaic virus forms infectious particles without the native beta-annulus structure and flexible coat protein N-terminus. *Virology* **422**:165-73. doi: 10.1016/j.virol.2011.10.019.

Pumpens P., Pushko P. (2022). Virus – like particles. A comprehensive guide. Boca Raton, FL: CRC press.

Pushko P., Pumpens P., Grens E. (2013). Development of virus-like particle technology from small highly symmetric to large complex virus-like particle structures. *Intervirology* **56**: 141–165. doi: 10.1159/000346773.

Revers F., García J.A. (2015). Molecular biology of potyviruses. *Adv Virus Res* **92**:101-99. doi: 10.1016/bs.aivir.2014.11.006.

Rioux G., Babin C., Majeau N., Leclerc D. (2012). Engineering of Papaya Mosaic Virus (PapMV) Nanoparticles through Fusion of the HA11 Peptide to Several Putative Surface-Exposed Sites. *PLoS ONE* **7**: e31925. doi: 10.1371/journal.pone.0031925.

Riechmann J.L., Laín S., García J.A. (1992). Highlights and prospects of potyvirus molecular biology. *J Gen Virol* **73**:1-16. doi: 10.1099/0022-1317-73-1-1.

Roberts I.M., Wang D., Findlay K., Maule A.J. (1998). Ultrastructural and temporal observations of the potyvirus cylindrical inclusions (Cls) show that the Cl protein acts transiently in aiding virus movement. *Virology* **245**:173-81. doi: 10.1006/viro.1998.9132.

van Roon A.M., Bink H.H., Plaisier J.R., Pleij C.W., Abrahams J.P., Pannu N.S. (2004). Crystal structure of an empty capsid of turnip yellow mosaic virus. *J Mol Biol* **341**:1205-14. doi: 10.1016/j.jmb.2004.06.085.

Roossinck M.J., Martin D.P., Roumagnac P. (2015). Plant Virus Metagenomics: Advances in Virus Discovery. Phytopathology **105**:716-27. doi: 10.1094/PHYTO-12-14-0356-RVW.

Ruedl C., Schwarz K., Jegerlehner A., Storni T., Manolova V., Bachmann M.F. (2005). Virus-like particles as carriers for T-cell epitopes: limited inhibition of T-cell priming by carrier-specific antibodies. *J Virol* **79**:717-24. doi: 10.1128/JVI.79.2.717-724.2005.

Rumnieks J., Ose V., Tars K., Dislers A., Strods A., Cielens I., Renhofa R. (2009). Assembly of mixed rod-like and spherical particles from group I and II RNA bacteriophage coat proteins. Virology 391:187-94.

Sabharwal P., Sushmitha C., Amritha C.K., Natraj U., Murthy M.R.N. Savithri, H.S. (2020). Development of pepper vein banding virus chimeric virus-like particles for potential diagnostic and therapeutic applications. Arch Virol 165: 1163–1176. doi: 10.1016/j.virol.2009.06.023.

Sahithi K.D., Nancy P.A., Vishnu Vardhan G.P., Kumanan K., Vijayarani K., Hema M. (2019). Detection of infectious bursal disease virus (IBDV) antibodies using chimeric plant virus-like particles. Vet Microbiol 229:20-27. doi: 10.1016/j.vetmic.2018.12.008.

Saini M., Vrati S. (2003). A Japanese encephalitis virus peptide present on Johnson grass mosaic virus-like particles induce virus-neutralizing antibodies and protects mice against lethal challenge. J. Virol. 77, 3487–3494. doi: 10.1128/jvi.77.6.3487-3494.2003.

Sastri M., Kekuda R., Gopinath K., Kumar C.T., Jagath J.R., Savithri H.S. (1997). Assembly of physalis mottle virus capsid protein in Escherichia coli and the role of amino and carboxy termini in the formation of the icosahedral particles. J Mol Biol 272:541-52. doi: 10.1006/jmbi.1997.1258.

Sastri M., Reddy D.S., Krishna S.S., Murthy M.R., Savithri H.S. (1999). Identification of a discrete intermediate in the assembly/disassembly of physalis mottle tymovirus through mutational analysis. J Mol Biol 289:905-18. doi: 10.1006/jmbi.1999.2786.

Schneider W.L., Greene A.E., Allison R.F. (1997). The carboxyl terminal two-thirds of the cowpea chlorotic mottle bromovirus capsid protein is incapable of virion formation yet supports systemic movement. Journal of Virology 71:4862-4865.

Schoonen L., Maassen S., Nolte E.J.M., van Hest J.C.M. (2017). Stabilization of a Virus-Like Particle and Its Application as a Nanoreactor at Physiological Conditions. Biomacromolecules 18: 3492- 3497. doi: 10.1021/acs.biomac.7b00640

Shahana P.V., Das D., Gontu A., Chandran D., Maithal K. (2015). Efficient production of Tymovirus like particles displaying immunodominant epitopes of Japanese Encephalitis Virus envelope protein. Protein Expr Purif 113:35-43. doi: 10.1016/j.pep.2015.03.017.

Shin H.I., Chae K.H., Cho T.J. (2013). Modification of Turnip yellow mosaic virus coat protein and its effect on virion assembly. BMB Rep 46:495-500. doi: 10.5483/bmbrep.2013.46.10.046.

Shin H.I., Kim D., Cho T.J. (2018). Cysteine – added Mutants of Turnip Yellow Mosaic Virus. Journal of Bacteriology and Virology 48:137 - 146. doi: 10.4167/jbv.2018.48.4.137.

Shukla S., Ablack A. L., Wen A. M., Lee K. L., Lewis J. D., Steinmetz N. F. (2013). Increased Tumor Homing and Tissue Penetration of the Filamentous Plant Viral Nanoparticle Potato Virus X. Mol. Pharm 10: 33-42. doi: 10.1021/mp300240m.

Shukla S., Dickmeis C., Nagarajan A. S., Fischer R., Commandeur U., Steinmetz N. F. (2014). Molecular Farming of Fluorescent Virus-Based Nanoparticles for Optical Imaging in Plants, Human Cells and Mouse Models. Biomater Sci 2: 784-797.

Shukla D.D., Strike P.M., Tracy S.L., Gough K.H., Ward C.W. (1988). The N and C termini of the coat proteins of Potyviruses are surface – located and the N terminus contains the major virus – specific epitopes. J Gen Virol 69: 1497 – 1508. doi: 10.1099/0022-1317-69-7-1497.

Shukla D.D., Ward C.W. (1989). Structure of potyvirus coat proteins and its application in the taxonomy of the potyvirus group. Adv Vir Res 36: 273–314. doi: 10.1016/s0065-3527(08)60588-6.

Smith K.M. (1931) Composite nature of certain potato viruses of the mosaic group as revealed by the use of plant indicator. Proc R So Londo, Ser B: Biol. Sci 109: 251–267.

Smith T.J., Chase E., Schmidt T., Perry K.L. (2000). The structure of cucumber mosaic virus and comparison to cowpea chlorotic mottle virus. J Virol 74:7578-86. doi: 10.1128/jvi.74.16.7578-7586.2000.

Speir J.A., Munshi S., Wang G., Baker T.S., Johnson J.E. (1995). Structures of the native and swollen forms of cowpea chlorotic mottle virus determined by X-ray crystallography and cryo-electron microscopy. Structure 3: 63-78. doi: 10.1016/s0969-2126(01)00135-6.

Suci P.A., Berglund D.L., Liepold L., Brumfield S., Pitts B., Davison W., Oltrogge L., Hoyt K.O., Codd S., Stewart P.S., Young M., Douglas T. (2007). High-density targeting of a viral multifunctional nanoplatform to a pathogenic, biofilm-forming bacterium. Chem Biol 14:387-98. doi: 10.1016/j.chembiol.2007.02.006.

Tan F.H., Kong J.C., Ng J.F., Alitheen N.B., Wong C.L., Yong C.Y., Lee K.W. (2021). Recombinant turnip yellow mosaic virus coat protein as a potential nanocarrier. J Appl Microbiol 131:2072-2080. doi: 10.1111/jam.15048.

Tan T.K., Rijal P., Rahikainen R., Keeble A.H., Schimanski L., Hussain S., Harvey R., Hayes J.W.P., Edwards J.C., McLean R.K., Martini V., Pedrera M., Thakur N., Conceicao C., Dietrich I., Shelton H., Ludi A., Wilsden G., Browning C., Zagrajek A.K., Bialy D., Bhat S., Stevenson-Leggett P., Hollinghurst P., Tully M., Moffat K., Chiu C., Waters R., Gray A., Azhar M., Mioulet V., Newman J., Asfor A.S., Burman A., Crossley S., Hammond J.A., Tchilian E., Charleston B., Bailey D., Tuthill T.J., Graham S.P., Duyvesteyn H.M.E., Malinauskas T., Huo J., Tree J.A., Buttigieg K.R., Owens R.J., Carroll M.W., Daniels R.S., McCauley J.W., Stuart D.I., Huang K.A., Howarth M., Townsend A.R. (2021). A COVID-19 vaccine candidate using SpyCatcher multimerization of the SARS-CoV-2 spike protein receptor-binding domain induces potent neutralising antibody responses. Nat Commun 12:542. doi: 10.1038/s41467-020-20654-7.

Tang J., Johnson J.M., Dryden K.A., Young M.J., Zlotnick A., Johnson J.E. (2006). The role of subunit hinges and molecular "switches" in the control of viral capsid polymorphism. J Struct Biol 154:59-67. doi: 10.1016/j.jsb.2005.10.013.

Thérien A., Bédard M., Carignan D., Rioux G., Gauthier-Landry L., Laliberté-Gagné M., Bolduc M., Savard P., Leclerc D. (2017). A versatile papaya mosaic virus (PapMV) vaccine platform based on sortase-mediated antigen coupling. J Nanobiotechnol 15: 54. doi:10.1186/s12951-017-0289-y.

Thoms F., Haas S., Erhart A., Nett C.S., Rüfenacht S., Graf N., Strods A., Patil G., Leenadevi T., Fontaine M.C., Toon L.A., Jennings G.T., Senti G., Kündig T.M., Bachmann M.F. (2020). Immunization of Cats against Fel d 1 Results in Reduced Allergic Symptoms of Owners. Viruses 12:288. doi: 10.3390/v12030288.

Thoms F., Jennings G.T., Maudrich M., Vogel M., Haas S., Zeltins A., Hofmann-Lehmann R., Riond B., Grossmann J., Hunziker P., Fettelschoss-Gabriel A., Senti G., Kündig T.M., Bachmann M.F. (2019). Immunization of cats to induce neutralizing antibodies against Fel d 1, the major feline allergen in human subjects. J Allergy Clin Immunol 144:193-203. doi: 10.1016/j.jaci.2019.01.050.

Thrane S., Janitzek C.M., Agerbæk M.Ø., Ditlev S.B., Resende M., Nielsen M.A., Theander T.G., Salanti A., Sander A.F. (2015). A Novel Virus-Like Particle Based Vaccine Platform Displaying the Placental Malaria Antigen VAR2CSA. PLoS One 10: e0143071. doi: 10.1371/journal.pone.0143071.

Toy R., Peiris P. M., Ghaghada K. B., Karathanasis E. (2014). Shaping Cancer Nanomedicine: The Effect of Particle Shape on the in Vivo Journey of Nanoparticles. Nanomedicine (Lond) 9: 121-134. doi: 10.2217/nnm.13.191.

Traynor P., Young B. M., Ahlquist P. (1991). Deletion analysis of brome mosaic virus 2a protein: effects on RNA replication and systemic spread. J Virol 65: 2807. doi: 10.1128/JVI.65.6.2807-2815.1991.

Utterström J., Naeimipour S., Selegård R., Aili D. (2021). Coiled coil-based therapeutics and drug delivery systems. Adv Drug Deliv Rev 170:26-43. doi: 10.1016/j.addr.2020.12.012.

Vailes L.D., Sun A.W., Ichikawa K., Wu Z., Sulahian T.H., Chapman M.D., Guyre P.M. (2002). High-level expression of immunoreactive recombinant cat allergen (Fel d 1): Targeting to antigen-presenting cells. J Allergy Clin Immunol 110:757-62. doi: 10.1067/mai.2002.129035.

Välimäki S., Liu Q., Schoonen L., Vervoort D.F.M., Nonappa, Linko V., Nolte R.J.M., van Hest J.C.M., Kostiainen M.A. (2021). Engineered protein cages for selective heparin encapsulation. J Mater Chem B 9:1272-1276. doi: 10.1039/d0tb02541k.

Valkonen J.P.T. (2007). Viruses: Economical Losses and Biotechnological Potential in Potato Biology and Biotechnology, Chapter 28, Elsevier Science B.V., Pages 619-641, doi: 10.1016/B978-044451018-1/50070-1.

Vasques R.M., Correa R.F..T, da Silva L.A., Blawid R., Nagata T., Ribeiro B.M., Ardisson-Araújo D.M.P. (2019). Assembly of tomato blistering mosaic virus-like particles using a baculovirus expression vector system. Arch Virol 164:1753-1760. doi: 10.1007/s00705-019-04262-5.

Visser J.C., Bellstedt D.U., Pirie M.D. (2012). The recent recombinant evolution of a major crop pathogen, potato virus Y. PLoS One 7: e50631. doi: 10.1371/journal.pone.0050631.

Vriend G., Verduin B.J., Hemminga M.A. (1986). Role of the N-terminal part of the coat protein in the assembly of cowpea chlorotic mottle virus. A 500 MHz proton nuclear magnetic resonance study and structural calculations. J Mol. Biol 191:453–60. doi: 10.1016/0022-2836(86)90140-3.

Xu-Amano J., Kiyono H., Jackson R.J., Staats H.F., Fujihashi K., Burrows P.D., Elson C.O., Pillai S., McGhee J.R. (1993). Helper T cell subsets for immunoglobulin A responses: oral immunization with tetanus toxoid and cholera toxin as adjuvant selectively induces Th2 cells in mucosa associated tissues. J Exp Med 178:1309-20. doi: 10.1084/jem.178.4.1309.

Yildiz I., Shukla S., Steinmetz N.F. (2011). Applications of viral nanoparticles in medicine. Curr Opin Biotechnol 22:901-8. doi: 10.1016/j.copbio.2011.04.020.

Zeltins A. (2013). Construction and characterization of virus-like particles: a review. Molecular Biotechnology 53: 92 – 107. doi: 10.1007/s12033-012-9598-4.

Zeltins A. (2018). Protein Complexes and Virus-Like Particle Technology. Subcell Biochem 88:379-405. doi: 10.1007/978-981-10-8456-0_16.

Zeltins A. (2016). Viral Nanoparticles: Principles of Construction and Characterization. In: Viral Nanotechnology. Y. E. Khudyakov, P. Pumpens; Eds., CRC Press: Boca Raton, Florida, USA, pp. 93-119.

Zeltins A., West J., Zabel F., El Turabi A., Balke I., Haas S., Maudrich M., Storni F., Engeroff P., Jennings G.T., Kotecha A., Stuart D.I., Foerster J., Bachmann M.F. (2017). Incorporation of tetanus-epitope into virus-like particles achieves vaccine responses even in older

recipients in models of psoriasis, Alzheimer's and cat allergy. NPJ Vaccines 2:30. doi: 10.1038/s41541-017-0030-8.

Zhang Y., Dong Y.X., Zhou J.H., Li X., Wang F. (2018). Application of Plant Viruses as a Biotemplate for Nanomaterial Fabrication. Molecules 23:2311. doi: 10.3390/molecules23092311.

Zhao H.L., Yao X.Q., Xue C., Wang Y., Xiong X.H., Liu Z.M. (1995). Increasing the homogeneity, stability and activity of human serum albumin and interferon-alpha2b fusion protein by linker engineering. Protein expr Purif 61:73-7. doi: 10.1016/j.pep.2008.04.013.

Zlotnick A., Aldrich R., Johnson J.M., Ceres P., Young M.J. (2000). Mechanism of capsid assembly for an icosahedral plant virus. Virology 277:450–456. doi: 10.1006/viro.2000.0619.

Wen X., Wen K., Cao D., Li G., Jones R.W., Li J., Szu S., Hoshino Y., Yuan L. (2014). Inclusion of a universal tetanus toxoid CD4(+) T cell epitope P2 significantly enhanced the immunogenicity of recombinant rotavirus ΔVP8* subunit parenteral vaccines. Vaccine 32:4420-4427. doi: 10.1016/j.vaccine.2014.06.060.

Wyatt S.D., Kuhn C.W. (1980). Derivation of a new stain of cowpea chlorotic mottle virus from resistant cowpeas. J GenVirol 49:289-296. doi: 10.1099/0022-1317-49-2-289.

Wylie S.J., Adams M., Chalam C., Kreuze J., López-Moya J.J., Ohshima K., Praveen S., Rabenstein F., Stenger D., Wang A., Zerbini F.M. Ictv Report Consortium. ICTV Virus Taxonomy Profile: Potyviridae. J Gen Virol 98:352-354. doi: 10.1099/jgv.0.000740.